Towards Practical Design of Impulse Radio Ultrawideband Systems: Parameter Estimation and Adaptation, Interference Mitigation, and Performance Analysis

by

İsmail Güvenç

A dissertation submitted in partial fulfillment
of the requirements for the degree of
Doctor of Philosophy
Department of Electrical Engineering
College of Engineering
University of South Florida

Major Professor: Hüseyin Arslan, Ph.D.
Ravi Sankar, Ph.D.
Thomas Weller, Ph.D.
Miguel Labrador, Ph.D.
Frederick Martin, Ph.D.

Date of Approval:
March 31, 2006

Keywords: Channel estimation, energy detector, multiuser detection, ranging and localization, sub-Nyquist sampling, timing jitter.

DEDICATION

To my beloved wife Zeynep ...

ACKNOWLEDGEMENTS

The foremost, I would like to thank my advisor, Dr. Huseyin Arslan. His help, support, encouragement, and guidance made this dissertation possible. I have learned a lot from him; how to come up with ideas that can lead to good research, how to be persistent on a research topic, how to write technical papers in a good flow, how to present your ideas, and most important of all, how to study hard. His continuous pushing and high expectations put me under a lot of stress many times through the course of this dissertation, but this was for my own good; and hey, who said it was going to be easy!

I would also like to thank to Dr. Ravi Sankar, Dr. Thomas Weller, Dr. Miguel Labrador, and Dr. Frederick Martin for serving in my committee, for reviewing my dissertation, and for their valuable time, feedback and suggestions; and to Dr. Aydin Sunol for chairing my defense. Dr. Paris Wiley, Dr. Don Morel, Gayla Montgamery, Irene Wiley, Becky Brenner, and Norma Paz from the Electrical Engineering administration and staff definitely deserve many thanks for helping out in numerous issues over the past years.

I owe a lot to the people of Mitsubishi Electric Research Labs (MERL) where I spent 7 months of my Ph.D. as an intern. I would especially like to thank to Dr. Zafer Sahinoglu for providing me the opportunity to work at MERL on some real research projects. I enjoyed my time working with him; he was always very supportive and helpful. I also enjoyed fruitful discussions with Dr. Philip Orlik and Dr. Andreas Molisch; it was a great opportunity to work together with them and I tried to benefit as much as I can from their invaluable knowledge and experience. Sincere thanks go to our group manager Dr. Jinyun Zhang for her support.

I would like to thank a lot to my colleagues at USF. I am grateful to my room-mate Tevfik Yucek with whom I stayed with for the first two years of my Ph.D., and to my friends Mustafa Emin Sahin and Hasari Celebi, all of whom I owe a lot. Many thanks go to my other colleagues Kemal Ozdemir (thank you for the teas!), Serhan Yarkan, Hisham Mahmoud, Sadia Ahmed, Fabian Aranda, Oscar V. Gonzales, Omer Dedeoglu, Sriraj Manavalan, Jiang Liu, Nigel Brown, Sharath Reddy, and others. We shared many things together, including long group meetings, conference travels, and fruitful discussions; I wish all of you the best in your future careers and lives. I would also like to thank to my friend and ex-class mate Sinan Gezici from Princeton University; I was

lucky that we were working on the same topic, and I learned a lot from him on UWB through messenger/phone conversations.

Special thanks go to the Turkish community at Tampa for their continuous support outside the university environment, for gatherings, picnics, weekly soccer and basketball games. I would like to thank Murat abi for being there in case we need something (and for bringing us free pizza), to Salih abi for helping us out if we have a trouble with our cars, and to other numerous people for their friendship and support.

My deepest gratitude goes to my wife for her encouragement and patience. You were there to share joys and disapointments, and to provide hope and motivation at times I started losing them. I know that it was very difficult to be the wife of a Ph.D. student, and I will always remember your understanding and support; I am a very lucky husband.

The last but not the least, I would like to express my utmost appreciation to my parents Mehmet and Hatice, and to my dear brother Oguz, all of whom made a lot of sacrifices for bringing me up to this point. I will be forever indebted to them for all they have done.

TABLE OF CONTENTS

LIST OF TABLES

LIST OF FIGURES

TOWARDS PRACTICAL DESIGN OF IMPULSE RADIO ULTRAWIDEBAND SYSTEMS: PARAMETER ESTIMATION AND ADAPTATION, INTERFERENCE MITIGATION, AND PERFORMANCE ANALYSIS

İsmail Güvenç

ABSTRACT

Ultrawideband (UWB) is one of the promising technologies for future short-range high data rate communications (e.g. for wireless personal area networks) and longer range low data rate communications (e.g. wireless sensor networks). Despite its various advantages and potentials (e.g. low-cost circuitry, unlicensed reuse of licensed spectrum, precision ranging capability etc.), UWB also has its own challenges. The goal of this dissertation is to identify and address some of those challenges, and provide a framework for *practical* UWB transceiver design.

In this dissertation, various modulation options for UWB systems are reviewed in terms of their bit error rate (BER) performances, spectral characteristics, modem and hardware complexities, and data rates. Time hopping (TH) code designs for both synchronous (introduced an adaptive code assignment technique) and asynchronous UWB impulse radio (IR) systems are studied. An adaptive assignment of two different multiple access parameters (number of pulses per symbol and number of pulse positions per frame) is investigated again considering both synchronous and asynchronous scenarios, and a mathematical framework is developed using Gaussian approximations of interference statistics for different scenarios. Channel estimation algorithms for multiuser UWB communication systems using symbol-spaced (proposed a technique that decreases the training size), frame-spaced (proposed a pulse-discarding algorithm for enhanced estimation performance), and chip-spaced (using least squares (LS) estimation) sampling are analyzed. A comprehensive review on multiple accessing and interference avoidance/cancellation for IR-UWB systems is presented.

BER performances of different UWB modulation schemes in the presence of timing jitter are evaluated and compared in static and multipath fading channels, and finger estimation error, effects

of jitter distribution, and effects of pulse shape are investigated. A unified performance analysis approach for different IR-UWB transceiver types (stored-reference, transmitted-reference, and energy detector) employing various modulation options and operating at sub-Nyquist sampling rates is presented. The time-of-arrival (TOA) estimation performance of different searchback schemes under optimal and suboptimal threshold settings are analyzed both for additive white Gaussian noise (AWGN) and multipath channels.

CHAPTER 1

INTRODUCTION

Together with the enormous research and developments within the last decade, wireless communications have penetrated into various aspects of our daily lives. Continuously increasing demand on high data rate services require novel technologies that are capable of supporting broadband applications. As more and more devices go wireless, future technologies will face spectral crowding, and the coexistence of wireless devices will be a major issue. Often, new wireless devices operate in one of the Industrial, Scientific, and Medical (ISM) bands (900MHz, 2.4GHz, 5.8GHz), or Unlicensed National Information Infrastructure (UNII) band (5.2GHz). Spectral crowding in these bands suggest either new unlicensed bands for future wireless devices, or innovative technologies that can coexist with devices operating at the same frequency bands.

Ultrawideband (UWB) is a recent technology that brings attractive solutions for future wireless broadband applications. First Report and Order released by Federal Communications Commissions (FCC) in 2002 defines UWB transmissions to have a fractional bandwidth greater than 20%, or a transmission bandwidth of at least 500 MHz. The use of ultra wide bandwidth promises very high data rates implied by the Shannon's capacity theorem. Since the power spectrum of UWB devices overlaps with various other technologies, transmission power is restricted by a spectral mask released by FCC. Although quiet conservative, this mask ensures the coexistence of UWB systems with the other technologies sharing the same spectrum.

Impulse radio (IR) is a popular implementation of UWB systems; although conceptually not very new, UWB-IR is recently becoming popular for wireless communications. It is realized by transmission of extremely short duration (usually sub-nanosecond) pulses. Rather than sending a single pulse, a number of pulses determined by the processing gain of the system are transmitted per symbol. The processing gain serves as a parameter to flexibly adjust the data rate, bit error rate (BER), and coverage area of transmission.

However, impulse radio is not the only approach to UWB, and any system that has a bandwidth larger than 500MHz is considered as UWB by FCC definition. Orthogonal frequency division (OFDM) based UWB is another implementation of *non-impulse radio* UWB scheme. By using 128 sub-carriers modulated with quadrature phase shift keying (QPSK), the composite signal occupies 528MHz , meeting the FCC definition for UWB [1].

In order to understand the importance of UWB the wireless research community, it is sufficient to have a look at the conferences and special issues organized on UWB. Within the last couple of years, there have been numerous conferences specifically on UWB systems[1], not to mention the various workshops and sessions on UWB in many communications related conferences. Moreover, many of the prestigious journals have prepared special issues on UWB[2]. There have been two different standardization activities for high-rate (IEEE 802.15.3a) and low-rate (IEEE 802.15.4a) UWB technology[3], and around 10 books were published (or are in press) on UWB only within the last few years. These facts underline the significant interest of the wireless research community in UWB systems.

In this introductory chapter, unique aspects, promises, and challenges of UWB systems are outlined. Some of the important problems in UWB system design are emphasized, and why we selected to focus on these problems in this dissertation is discussed. Then, a brief outline of the dissertation is presented.

1.1 Unique Aspects and Promises of UWB

1.1.1 Underlay Spectrum Usage

Probably one of the most attractive features of UWB systems is *unlicensed reuse of the licensed spectrum*, as long as power and bandwidth restrictions are adhered to. Due to high fractional bandwidth of UWB signals, transmission power is very low, thus resulting in insignificant interference to other licensed or unlicensed narrowband wireless technologies operating within the same band.

[1] To count few; IEEE UWBST (May 2002, Baltimore, MD), IEEE UWBST (Nov. 2003, Reston, VA), IEEE UWBST (May 2004, Kyoto, Japan), IEEE ICU (Sep. 2005, Zurich, Switzerland), IEEE ICUWB (Sep. 2006, Waltham, MA) etc.

[2] To count few; IEEE Journal on Selected areas on Communications (Dec. 2002, and 2nd quarter of 2006), IEEE Transactions on Vehicular Technology (Sep. 2005), IEEE Transactions on Microwave Theory and Techniques (Apr. 2006), IEE Proceedings on Communications (Jan. 2006), Journal on Communications and Networks (Dec. 2003), Eurasip Journal on Wireless Communications and Networking (3rd quarter of 2006), Eurasip Journal on Applied Signal Processing (Mar. 2005), Wiley Wireless Communications and Mobile Computing (Aug. 2005), Elsevier Signal Processing Journal (4th quarter of 2005) etc.

[3] The high-rate standardization working group was recently disbanded due to not being able to agree on one of the two competing proposals.

For example, in United states, an UWB device may operate anywhere within the frequency range 3.1GHz−10.6GHz as long as the effective isotropic radiated power (EIRP) is less than −41dBm/MHz. Another license-free band in US and Japan is between 57GHz-63GHz (known as 60GHz band), which offers higher data rates at shorter distances.

Considering the crowding of ISM bands, the promise of UWB for underlay usage of the available spectrum implies significant spectrum utilization which is a distinct issue when compared with other wireless technologies[4]. As more and more devices go wireless, importance of UWB and cognitive radio will increase considerably.

1.1.2 UWB Channels

Due to extremely large bandwidths of UWB signals, the transmitted UWB signal duration is very small. This implies that a large number of distinct multipath replicas of the received signal can be *observed* at the receiver[5].

The unique channel structure of UWB systems have many implications. The high temporal resolution of UWB signals results in lower fading margins and robustness against multipath[6]. On the other hand, Rake receivers are essential for coherent signal detection; the receiver has to lock on these multipath components to collect the energy. As this may considerably increase the complexity, alternative lower-complexity receiver types are possible.

As of now, there are two standardized channel models that describe the UWB channel characteristics. The IEEE 802.15.3a channel model includes description of 4 different scenarios (one line of sight (LOS), three non-line of sight (NLOS)) [2]. A more comprehensive channel model is introduced by IEEE 802.15.4a working group, which models 9 different environments (LOS and NLOS), and includes issues such as frequency dependency, soft onset of power delay profile etc. [3].

1.1.3 Potential Data Rates and Operating Ranges

Extremely large bandwidths of UWB signals imply data rates on the order of Gigabits per second. A data of 667Mbit/s was demonstrated by Pulse-Link, Inc in early 2005, which was measured after

[4]Note that cognitive radio and opportunistic spectrum usage has recently gained significant attention as another possible solution to spectral crowding problem. Nevertheless, opportunistic usage of the spectrum complements underlay spectrum usage rather than competing with it.

[5]On the other hand, in narrowband technologies, since the symbol duration is very long, many of the multipath components come within the symbol duration. The receiver therefore observes only a single (or few) multipath components each of which has a large fading margin.

[6]In fact, the earlier multipath components have much lower fading margins (named as specular components) and the later multipath components have higher fading margins (referred as diffuse components).

forward error correction error applied to the data [4]. The over-the-air data rate of the company's wireless devices at present is said to be 1.3Gbit/s. The goal is to take these to much higher data rates.

It should be noted that such high data rates are achieved only at short distances (on the order of few meters) due to the spectral masks (i.e. transmitted power limitations) of regulatory agencies. If longer ranges are targeted such as in wireless sensor networks, the number of pulses to be transmitted per symbol (i.e. the processing gain) will increase, implying much lower data rates[7].

1.1.4 Ranging With UWB

Due to ultra wide bandwidth signal transmission of UWB systems, sub-decimeter ranging and positioning becomes possible. This unique characteristic of UWB makes it very attractive for numerous applications that use position information. The most important challenge for ranging in UWB systems is to identify the first arriving multipath component, which does not have to be the strongest. Upon accurate detection of the time of arrival of a received signal, localization can be achieved using standard triangulation techniques.

One of the first wireless localization companies that was certified by FCC in 2004 was Ubisense; the company develops tracking systems that use UWB RFID technology to create indoor, real-time location positioning systems. The Ubisense devices use active tags operating in the frequency band from 5.8 to 7.2GHz [5].

Another ranging technology that is currently in the market is *Sapphire DART Ultra wideband Precision Asset Location System*$^{\text{TM}}$ by Multispectral Solutions [6]. The Sapphire technology is capable of covering ranges of 200 meters with a resolution and accuracy of better than 30 cm, and a battery life times in excess of 5 years. In [6], the physical sizes of two localization devices were compared, where the UWB tag size was shown to be less than quarter the size of the spread-spectrum tag.

1.1.5 Low Cost, Small Size, Low-Power

For pulse based UWB systems, transceiver circuitry are low-cost and simple, since no frequency translation, carrier recovery or power amplifiers are employed [7]. Transmitted power level is also

[7] In other words, rather than transmitting at high power levels, inherent repetition coding of UWB is used to reach longer distances (and at the same time keep the transmitted power within the spectral mask).

extremely low. These features make UWB an attractive technology to be used in, for example, PDAs or cell phones [8]. They are also very suitable for wireless sensor devices or RF tags which are typically manufactured in large quantities and need to be very inexpensive.

Some of the early low-cost, low-complexity UWB products in the market were by Cellonics, Inc. [9], and by Freescale Semiconductors, Inc. [10].

1.2 Challenges for UWB System Design

1.2.1 Difficulty of Energy Capture Using Rake Receivers

The number of multipath components observed by a UWB receiver can be on the order of hundreds depending on the dispersiveness of the channel and the operating bandwidth. In order to have a good performance, the receiver has to collect the energy from different multipath components. This can be achieved using multiple cross-correlators that lock at different multipath replicas, which is commonly referred as a Rake receiver. Rake receivers typically require the estimation of the timings, amplitudes/phases, and the pulse shapes at individual multipath arrivals[8]. To have satisfactory energy capture, the number of Rake fingers required may be large in a dispersive UWB channel, which may considerably increase the receiver complexity.

1.2.2 Sampling Rate Requirements

Typical bandwidths for transmitted UWB signals are on the order of Gigahertz. For a receiver that samples the signal at above Nyquist rate for all-digital implementation, this implies sampling rates much larger than the sampling rates used in narrowband receivers. Therefore, the receiver complexity and cost increases considerably if all-digital implementation is targeted[9].

Alternatively, UWB signals can be sampled after some analog front-end processing. Even though it yields suboptimal performance, this approach is more practical and less costly, since it decreases the sampling rate requirements.

[8] Suboptimal implementations of Rake receivers may have relaxed *a-priori* knowledge requirements as will be discussed in Chapter 8.

[9] It is worth to note that despite the difficulty of practical low-cost implementation of such high-rate UWB receivers, a good percentage of the literature assumes above Nyquist-rate sampling. However, implementation of many of the proposed algorithms in the literature becomes very difficult and/or costly due to sampling rate issues.

1.2.3 Synchronization Requirements

The time duration of the pulses transmitted by a UWB device are typically less than a nanosecond. The received pulses are then correlated with a template at the receiver which ideally matches with the pulse both in time and shape. Due to the short duration of the pulses, any small timing mismatch (e.g. on the order of fraction of a nanosecond) between the received pulse and the correlator template yields significant degradation in the correlation value, and therefore the detection performance.

In order to have satisfactory performance, accurate synchronization algorithms that consider the the unique channel characteristics of UWB signaling are required. Also, accurate synchronization naturally depends on (and is limited by) the capability of the sampling device used at the receiver.

1.2.4 Multiple Accessing

Multiple accessing is an essential part of UWB systems to accommodate many users within the same channel. Time division multiple access (TDMA), frequency division multiple access (FDMA), code division multiple access (CDMA), and carrier-sense multiple access (CSMA) are all possible multiple access options for UWB networks. Time-hopping and direct-sequence UWB are popular CDMA based approaches that are applicable to UWB systems.

Transmission of the signals around noise level and extremely dispersive nature of the received signals impose many challenges on practical implementation of multiuser UWB-IR systems. Estimation and mitigation of multiuser interference may be extremely difficult as it becomes challenging to sense and handle it. Fortunately, unique signaling of time hopping IR systems characterized by the processing gain and sparse pulsing enables efficient and low complexity multiuser transceiver designs (different than direct-sequence DS-CDMA techniques).

1.2.5 Channel Parameter Estimation

Channel parameter estimation is essential for accurate demodulation of the received UWB symbols. For coherent receivers (e.g. the Rake receivers), channel parameters include arrival times, amplitudes, phases, and pulse shapes of the received multipath components. Having estimated these, Rake fingers can lock on different multipath components to collect the energy from multiple taps. However, as discussed before, since the number of multipath components may be extremely large in

a dispersive UWB channel, estimation of parameters for a large number of multipath components may be very costly.

For differentially-coherent and non-coherent receivers, estimation of such parameters might not be required; however, at least, start and end points of the integration region has to be estimated for optimal (or close to optimal) performance. For ranging and localization techniques, accurate estimation of the time of arrival (TOA) of the first multipath component is extremely important and can be considered under the scope of channel parameter estimation. While such a sensitive estimation of the leading edge path may not be that important for symbol demodulation, it is a critical step for localization accuracy.

1.3 Dissertation Outline

1.3.1 Towards Practical Design of Impulse Radio Ultrawideband Systems: Parameter Estimation/Adaptation, Interference Mitigation, and Performance Analysis

In this dissertation, based on the preliminary discussion in the previous sections, we try to identify and address certain challenges related to practical UWB transceiver design. In the literature, many aspects of UWB systems have been analyzed under ideal scenarios. However, for example, sampling rate limitations were rarely considered even though it becomes an important issue when it comes to practical implementation. Therefore, for practical purposes, we consider sub-Nyquist sampling rates in chapters 5, 8, and 9 when analyzing channel estimation, different transceiver types, and ranging, respectively. Timing jitter is another practical limitation, and we analyze its effects in Chapter 7. Finally, multiple access interference is considered as a practical case in many of the chapters and techniques to dealy with it are presented.

Even though Rake receivers are the optimal UWB receivers with perfect channel parameter knowledge, they are often very complex and costly to implement. Transmitted-reference and energy detector receivers are two other *practical* transceiver types, which we consider in Chapter 8. Various modulation alternatives that may be applicable to different transceivers are discussed in Chapter 2, where we also provide prelimenary knowledge regarding diffirent topics.

While channel parameter estimation is an *a-priori* step required for demodulation (or for ranging), parameter adaptation makes it possible for a wireless device adapt to changes in the environment for enhanced performance. Channel parameter estimation issues are handled in Chapter 5, and in

part in Chapter 8. Also, estimation of the TOA parameter, which is an essential step in time-based UWB localization technologies, is treated in Chapter 9. Adaptation of two kinds of multiple access parameters (i.e. the number of pulses per symbol, and number of pulse positions per frame) for the purpose of coping with interference in the system is investigated in Chapter 4. An adaptive time hopping sequence assignment algorithm was proposed in Chapter 3 for a centralized scheme.

Multiple accessing helps separating the users in time, frequency, or code domains. However, such a multiuser separation may not always be possible for decentralized scenarios, or under severe multipath. This introduces the problem of multiuser interference. An extensive review of multiuser interference (MUI) mitigation techniques is presented in Chapter 6. Also, a simple chip-discarding receiver is proposed in Chapter 5 to mitigate MUI effects *prior to* channel estimation step. Multiple access parameter adaptation (Chapter 4) and adaptive assignment of time hopping sequences (Chapter 3) can also be seen as different approaches to deal with interference.

The performances of different algorithms and techniques discussed above are analyzed with closed form expressions and/or simulations. In the rest of this chapter, we will provide more details regarding the content of these upcoming individual chapters.

1.3.2 Chapter 2: Modulation Options

In Chapter 2, we introduce the signaling model of UWB systems, and review possible modulation options from various aspects. Spectral characteristics and BER performances of the binary and higher order modulation types are investigated, and effects of multipath, multiuser interference, and timing jitter are discussed.[10]

1.3.3 Chapter 3: Time Hopping Sequence Design

Chapter 3 is on the multiple accessing options and time hopping sequence design for UWB systems. Various possible multiple access formats are discussed, and time-hopping sequence constructions for synchronous and asynchronous systems are analyzed. A new sequence construction for synchronous multiple access (e.g. the downlink) is proposed that accounts for the multipath effects. For asynchronous channels, correlation characteristics of different TH codes are investigated.[11]

[10] Certain parts of the content in this chapter were published in [11, 12].
[11] Certain parts of the content in this chapter were published in [13, 14].

1.3.4 Chapter 4: Adaptation of Multiple Access Parameters

In Chapter 4, an adaptive assignment of multiple access parameters in cluster based wireless sensor networks is investigated both for synchronous and asynchronous systems. In particular, number of pulses and the code cardinality (i.e. the number of possible pulse positions per frame) are used as two means of adapting to the interference level in the environment to keep up with the quality of service requirements. Two cases are investigated in detail; *fixed frame duration*, where the goal is to increase the average throughput, and the other with *fixed symbol duration*, where the goal is to increase the network lifetime.[12]

1.3.5 Chapter 5: Channel Estimation at Different Sampling Rates

Channel estimation with three different sampling rate options are discussed in Chapter 5. For symbol rate sampling, a low-complexity absolute value based channel estimator is proposed; it is shown that multiple access interference can be mitigated during channel estimation stage using a simple pulse discarding technique using frame-rate samples; and a least-squares channel estimation model is discussed when a chip-spaced sampling is applied.[13]

1.3.6 Chapter 6: Review of Multiple Access Interference Mitigation Techniques

Having discussed the effects of multiple access interference on channel estimation in Chapter 5, in Chapter 6, we present a comprehensive review on multiuser interference cancellation techniques for UWB systems. Unique characteristics of UWB that allow novel interference cancellation schemes are emphasized, and various interference cancellation techniques in the literature are classified appropriately.[14]

1.3.7 Chapter 7: Timing Jitter Effects

The impact of timing mismatch and effects of timing jitter on the performance of UWB systems are discussed in Chapter 7. First, the BER performances for each case are derived for a fixed value of timing jitter. Later, a uniform distribution of jitter is assumed to evaluate the performance of the

[12] Certain parts of the content in this chapter were published in [15, 16].
[13] Certain parts of the content in this chapter were published in [17, 18].
[14] Certain parts of the content in this chapter will be submitted to [19].

system, and the theoretical results are verified by computer simulations. It is concluded that even a small amount of timing mismatch can yield significant performance losses in a UWB system.[15]

1.3.8 Chapter 8: Performances of Different Transceiver Types at Sub-Nyquist Sampling

The complexity of coherent UWB receivers using Rake reception motivates the lower-complexity alternatives such as transmitted-reference receivers and energy detectors. Even though matched filtering is the optimal signal detection technique with Nyquist rate sampling, differentially coherent and non-coherent transceiver architectures may be favorable at lower rate samples. In Chapter 8, we present a unified performance analysis approach for different IR-UWB transceiver types employing various modulation options and operating at sub-Nyquist sampling rates. The captured low-rate energy histograms of different transceiver types as well as different combining schemes are used towards a semi-analytic performance evaluation. These results are then verified via simulations using 802.15.4a channel models.[16]

1.3.9 Chapter 9: TOA Estimation and Ranging with UWB

Ranging in impulse radio ultrawideband (IR-UWB) systems can be achieved by searching the paths prior to the strongest path in order to identify the leading edge path. The accuracy of such a method greatly depends on the threshold selection, which is a difficult task considering the unknown channel parameters. In Chapter 9, we analyze the TOA estimation performance under optimal threshold settings (with the assumption of full knowledge of channel parameters), and compare its performance when the threshold is set based only on the noise statistics. First, an additive white Gaussian noise (AWGN) scenario is considered and the optimal threshold that maximizes the probability of detection of the arriving signal is investigated. Then, realistic multipath situations are analyzed and the threshold selection criteria is changed so as to minimize the mean absolute error in TOA estimate. The IEEE802.15.4a channel models are used to compare the performances of different approaches.[17]

[15] Certain parts of the content in this chapter were published in [20, 21].
[16] Certain parts of the content in this chapter were published in [22], and are submitted to [23].
[17] Certain parts of the content in this chapter were published in [24], and are submitted to [25].

1.3.10 Other Work Done

Apart from the work discussed above, there were some other work that did not get into this dissertation[18]. During my internship at Mitsubishi Electric Research Labs, I have worked significantly on time of arrival estimation for UWB systems[19]. Also, I have co-authored papers with my colleagues at USF[20]. Some other research results were also presented in Wireless and Microwave Conference (WAMICON).[21]

[18] There were few different reasons for not including these in the dissertation. Some of the research were protected by patent submissions (from the internship), and it was not appropriate to include them in the manuscript. In some other work, I was not the main author, and/or my contribution was rather minor. Also, I wanted to keep the integrity of the manuscript and have the topics in a good flow.

[19] I have worked on multi-scale energy products and normalized threshold selection for ranging in IR-UWB [26]-[29], ranging with different signaling waveforms [30, 31], comparison of different transceiver types for ranging [32, 33], and energy image analysis for mitigation of multiuser interference in time of arrival estimation [34, 35]. I also have IEEE standard contributions [36, 37] and patent applications [38]-[41] on some of these topics.

[20] I have worked on optimization of energy detectors with Mustafa Emin Sahin [42, 43], on ranging related channel statistics with Hasari Celebi [44], on opportunistic spectrum usage in wireless communication systems with Serhan Yarkan [45], and on UWB testbed design with Nigel Brown and James Tucker [46].

[21] See poster presentations [47]-[49]

CHAPTER 2

UWB MODULATION OPTIONS

2.1 Introduction

A major challenge when designing UWB systems is the selection of the appropriate modulation scheme. Data rate, transceiver complexity, BER performance, spectral characteristics of the transmitted signal, and robustness against impairments and interference are all related with the employed modulation type. Determining the right modulation for a given application is thus crucial.

Although various UWB modulations have been individually investigated in the past [50]-[53], the primary concern has often been the BER performance with the assumption of ideal conditions. Welborn analyzed pulse amplitude modulation (PAM), on-off keying (OOK), pulse position modulation (PPM), and binary phase shift keying (BPSK) modulations [54]. Effects of multipath [55]-[57], multiple access interference [50], [55], [59], narrowband interference [55], [60], [61], and timing jitter [20], [62], [63] on the UWB performance has been investigated, but analysis were specific for the modulation schemes chosen.

In spite of its significance, a unique reference analyzing possible UWB modulation options considering the overall system efficiency and practical conditions is not available to the best knowledge of the authors. In this work, the goal is to cover commonly used UWB modulation schemes in a single compact reference and to analyze their performances in practical conditions such as multipath, multiple access interference, narrowband interference, and timing jitter.

The chapter is organized as follows. First, a generic system model is given. Then commonly used UWB modulation schemes are reviewed in terms of their BER performances, spectral characteristics, and transceiver complexities. Later, the performances of different modulations under practical conditions are analyzed and simulations for specific scenarios are presented. The last section concludes the chapter.

2.2 System Model

The generic transmitted signal $s^{(k)}(t)$ and received signal $r^{(k)}(t)$ by user k in a single-path, and single-user environment can be written as[1]

$$s^{(k)}(t) = \sum_{j=-\infty}^{\infty} A_{tx}^{(k)} a_j^{(k)} b_{\lfloor j/N_s \rfloor}^{(k)} \omega_{tr}(t - jT_f - c_j^{(k)} T_h - \delta \alpha_{\lfloor j/N_s \rfloor}^{(k)}) \ , \tag{2.1}$$

$$r^{(k)}(t) = \sum_{j=-\infty}^{\infty} A^{(k)} a_j^{(k)} b_{\lfloor j/N_s \rfloor}^{(k)} \omega_{rec}(t - jT_f - c_j^{(k)} T_h - \delta \alpha_{\lfloor j/N_s \rfloor}^{(k)} + \epsilon_j) + n(t) \ , \tag{2.2}$$

where T_f is the nominal interval between two pulses, N_s is the number of pulses per symbol, and δ is the modulation index if the modulation is PPM. T_h is the chip duration which is equal to pulse width T_c for antipodal modulation schemes and larger than T_c for PPM. Decimal codes $c_j^{(k)} \in \{0, 1, \cdots, N_h\}$ (where N_h denotes the number of pulse positions per frame[2]), and binary codes $a_j^{(k)}$ are pseudo-random codes unique to user k, and are used to employ time hopping (TH) UWB or direct sequence (DS) UWB multiple access schemes, respectively[3]. The timing jitter for the jth pulse, ϵ_j, is a zero-mean random variable. The transmitted and received pulse amplitudes for user k are represented by $A_{tx}^{(k)}$ and $A^{(k)}$, respectively, and $n(t)$ is the additive white Gaussian noise (AWGN) with double-sided spectrum of $\frac{N_0}{2}$. With $b_{\lfloor j/N_s \rfloor}^{(k)}$ changing the amplitudes of the pulses (OOK, BPSK, positive PAM, M-ary PAM) or $\delta \alpha_{\lfloor j/N_s \rfloor}^{(k)}$ varying the time positions of the pulses (PPM, M-ary PPM), UWB signals can be modulated in different ways as shown in Table 2.1.[4]

The transmitted *monopulse* is represented by ω_{tr}. Due to the differentiation effects of the antennas, received signal ω_{rec} is modeled as the derivative of the *monopulse* [50]

$$\omega_{rec}(t) = [1 - 4\pi(\frac{t}{\tau})^2] e^{-2\pi(\frac{t}{\tau})^2} \ , \tag{2.3}$$

[1] This signal model will be used as a generic signal model in the subsequent chapters. However, slightly modified versions of this signal model will be presented in Chapters 8 and 9 in order to account for specific issues in those chapters.

[2] The relation between N_s, N_h and data rate R_s is given as $R_s = \frac{1}{T_s} = \frac{1}{N_s T_f} \leq \frac{1}{N_s N_h T_c} sec^{-1}$, where $N_h T_c \leq T_f$.

[3] The codes $a_j^{(k)}$ are also commonly referred as random polarity codes where $a_j^{(k)}$ and $a_i^{(l)}$ are independent for $(k, j) \neq (l, i)$ [64].

[4] $\delta_{opt} = \underset{\delta}{\text{argmax}}\{R(0) - R(\delta)\}, \ \tilde{m} = 0, 1, ..., (M-1), \ \psi = \log_2 M$.

Table 2.1 UWB modulation options and BER/SER performances.

Binary Schemes	$b^{(k)}_{\lfloor j/N_s \rfloor}$	$\delta\alpha^{(k)}_{\lfloor j/N_s \rfloor}$	BER
Orthogonal PPM	1	$0, T_c$	$Q\left(\sqrt{\frac{N_s A E_p}{N_0}}\right)$
Optimum PPM	1	$0, \delta_{opt}$	$Q\left(\sqrt{\frac{N_s A E_p}{N_0}(R(0) - R(\delta_{opt}))}\right)$
BPSK	± 1	0	$Q\left(\sqrt{\frac{2N_s A E_p}{N_0}}\right)$
PAM	a_1, a_2	0	$Q\left(\sqrt{\frac{(a_2-a_1)^2 N_s A E_p}{2N_0}}\right)$
OOK	$0, a$	0	$Q\left(\sqrt{\frac{a^2 N_s A E_p}{2N_0}}\right)$
M-ary Schemes	$b^{(k)}_{\lfloor j/N_s \rfloor}$	$\delta\alpha^{(k)}_{\lfloor j/N_s \rfloor}$	**SER**
M-ary PPM [52]	1	$\tilde{m}T_c$,	$\frac{1}{\sqrt{2\pi}}\int_{-\infty}^{+\infty}[1-(1-Q(x))^{M-1}]$ $\times e^{-(x-\sqrt{\frac{2\psi N_s A E_p}{N_0}})^2/2}dx$
M-ary PAM [52]	$2m-1-M$, $m = 1, 2..., M$	0	$\frac{2(M-1)}{M}Q\left(\sqrt{\frac{6\psi N_s A E_{pav}}{(M^2-1)N_0}}\right)$, $E_{pav} = \frac{(M^2-1)E_p}{3}$

where τ is used to adjust the pulse width, T_c. The autocorrelation function, and the total energy of the received pulse are expressed as[5]

$$R(\Delta t) = \frac{\int_{-\infty}^{\infty} \omega_{rec}(t)\omega_{rec}(t-\Delta t)dt}{\int_{-\infty}^{\infty} \omega_{rec}^2(t)} \tag{2.4}$$

$$= \left[1 - 4\pi(\frac{\Delta t}{\tau})^2 + \frac{4\pi^2}{3}(\frac{\Delta t}{\tau})^4\right] e^{-\pi(\frac{\Delta t}{\tau})^2} , \tag{2.5}$$

$$E_p = \int_{-\infty}^{\infty} \omega_{rec}^2(t)dt , \tag{2.6}$$

and the received energy per bit is given by $E_b = N_s A E_p$.

2.3 Evaluation of Modulation Options

The major criteria to evaluate the efficiency of a particular modulation scheme are its BER performance, spectral shape, data rate, and transceiver complexity. In this section different modulation options from these aspects will be evaluated, followed by a brief discussion of other pronounced UWB modulation schemes.

[5] Upon incorporating the amplitudes of the pulses, we can also represent the transmitted and received pulse energies for user k by $E_{tp}^{(k)}$ and $E_{rp}^{(k)}$, respectively.

2.3.1 BER Performances

For any binary modulation, BER can be calculated using the Euclidean distance d_{12} between two symbols as given in [52]

$$P_b = Q\left(\sqrt{\frac{d_{12}^2}{2N_0}}\right) \quad . \tag{2.7}$$

The Euclidean distance between the two symbols is $\sqrt{2E_p}$ for orthogonal PPM, $2\sqrt{E_p}$ for BPSK, $a\sqrt{E_p}$ for OOK, and $(a_1 - a_2)\sqrt{E_p}$ for PAM. Plugging these values in (2.7) and considering the effects of processing gain N_s and pulse amplitude A, BER performances of binary modulations are obtained as summarized in Table 2.1.

Theoretical plots for binary modulations in AWGN and Rayleigh fading channels using $N_s = 1$ and $A = 1$ are depicted in Fig. 2.1. It is seen that orthogonal PPM and OOK modulations have the same BER performance when the average transmitted pulse energies are the same ($a = \sqrt{2}$). BPSK is 3dB more power efficient than both OOK and orthogonal PPM. For the case of $T_c = 0.8$ns, δ_{opt} is evaluated as $0.16ns$ and $R(\delta_{opt})$ as -0.6, which makes optimum PPM $1dB$ power inefficient than BPSK. Performance plots in Fig. 2.1 for Rayleigh fading channel show that similar degradation is observed in all modulation schemes.

Fig. 2.2 compares the symbol error rate (SER) performances of *M-ary* PPM and *M-ary* PAM for various modulation orders, M. It is seen that as M increases, SER performance of *M-ary* PPM gets better due to the increased dimensionality of the *Euclidean space*, while the SER performance of *M-ary* PAM gets worse because of the decreased Euclidean distance between the symbols. For M larger than 4, power efficiency of *M-ary* PPM is better than BPSK (binary PAM). The performance improvement in *M-ary* PPM comes in the expense of increased transceiver complexity and bounded data rate, since the larger symbol duration limits the pulse repetition frequency (PRF). For example, instead of using 8-ary PPM to transmit 3 bits, BPSK can be used in the same time interval to transmit 8 bits. Spectrally efficient *M-ary* PAM can be considered to achieve higher data rates with a moderate power efficiency.

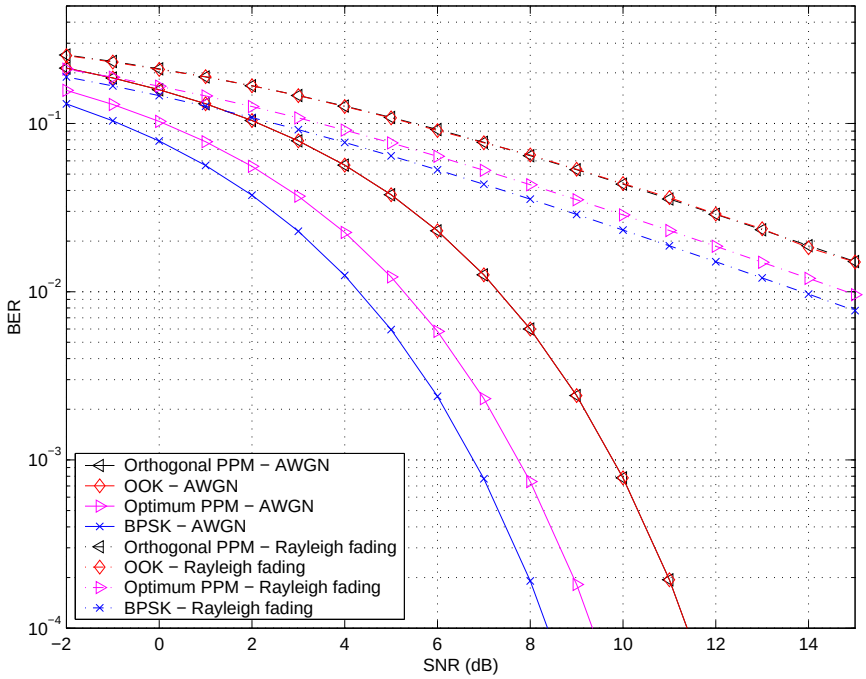

Figure 2.1 BER performances in AWGN and Rayleigh fading channels.

2.3.2 Spectral Characteristics

Spectral characteristics of different modulation schemes carry significant importance due to interference effects on the other technologies. Power spectral density (PSD) of the modulated UWB waveform must be within the spectral mask specified by the regulating agencies. For example, in United States (US), Federal Communications Commission (FCC) allows $-41dBm/MHz$ power levels for the frequency band of $3.1 - 10.6GHz$. Beyond this band, power levels are extremely low.

Spectra of transmitted signals when employing different modulations are investigated in [54, 65]. Due to the periodicity of the pulses, OOK, positive PAM, and PPM have discrete spectral lines in the signal PSD. This forces a reduction in the overall transmitted power to fit within the required spectral mask. Methods such as pulse dithering [50], which randomly changes the pulse-to-pulse intervals, and polarity randomization [65], which randomly changes pulse polarities, are proposed to smooth the spectrum. On the other hand, antipodal modulation schemes (BPSK and M-ary PAM) inherently offer a smooth PSD due to random polarities of the modulated pulses.

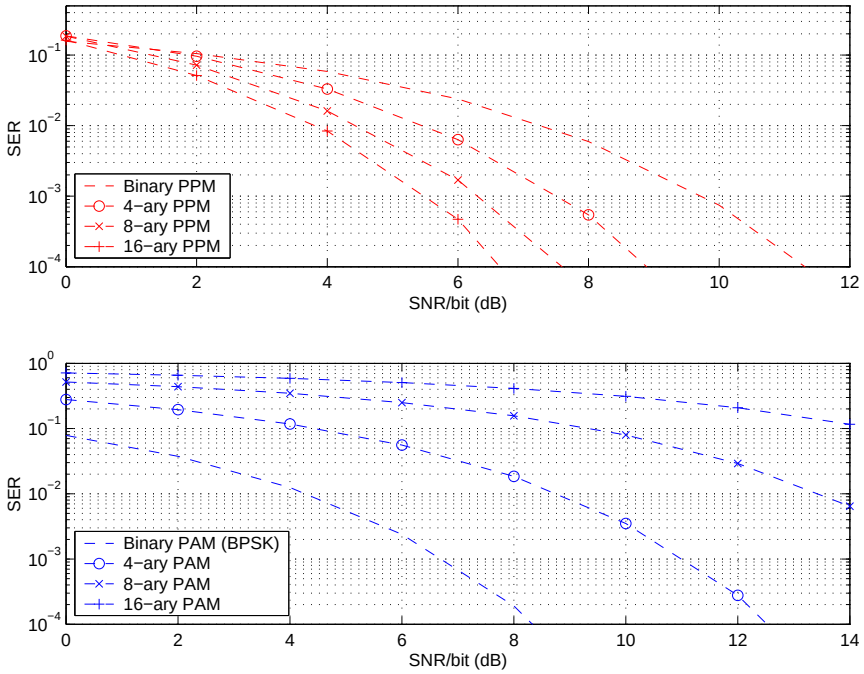

Figure 2.2 SER performances of *M-ary* PPM and *M-ary* PAM.

Table 2.2 Power Spectral Densities of various UWB modulations.

Modulation	Power Spectral Density
PAM	$\frac{\sigma_a^2}{T_f}\left\|\Omega(f)\right\|^2 + \frac{\mu_a^2}{T_f^2}\sum_{\lambda=-\infty}^{\infty}\left\|\Omega(\frac{\lambda}{T_f})\right\|^2\delta_D(f-\frac{\lambda}{T_f})$
OOK	$\frac{1}{T_f}\left\|\Omega(f)\right\|^2 + \frac{1}{T_f^2}\sum_{\lambda=-\infty}^{\infty}\left\|\Omega(\frac{\lambda}{T_f})\right\|^2\delta_D(f-\frac{\lambda}{T_f})$
BPSK	$\frac{1}{T_f}\left\|\Omega(f)\right\|^2$

In Table 2.2, power spectral densities of different modulation formats are summarized [54], where $\Omega(f)$ denotes the Fourier transform of $\omega_{tr}(t)$, $\delta_D(t)$ is the Dirac delta function, and σ_a^2, μ_a^2 are the variance and mean-square of the weight-sequence, respectively (uniform pulse spacing in TH-UWB is assumed with no polarity randomization).

2.3.3 Transceiver Complexity

Non-coherent demodulation, such as envelope detection or square-law detection, is commonly used to decrease the complexity [54] and cost [66] of the receivers. Therefore, if the transceiver complexity and cost are the primary concerns, a scheme that enables non-coherent demodulation (OOK, positive PAM, PPM, and *M-ary* PPM) should be considered. On the other hand, BPSK

and *M-ary* PAM require coherent demodulation since the information is embedded in the polarities of the pulses. Number of cross-correlators is another issue that increases the receiver complexity, and *M-ary* orthogonal schemes must be carefully designed considering the complexity/performance trade-off.

2.3.4 Other Modulation Alternatives

Some of the other modulation schemes that are pronounced for UWB technology but not included in Table 2.1 are pulse interval modulation (PIM), bi-orthogonal signaling, and orthogonal pulse modulation (OPM). Although multiband scheme is not a modulation option, it is included in the analysis since it enables quadrature phase shift keying (QPSK) modulation because of the used pulse shapes.

PIM: Information is represented by changing the pulse-to-pulse intervals. Although it has better spectral efficiency than PPM scheme, it is power inefficient [67].

Bi-orthogonal Signaling: To construct a set of M waveforms, $\frac{M}{2}$ orthogonal waveforms and their negatives are used. Compared with *M-ary* PPM, *M-ary* bi-orthogonal signaling has simpler receiver structure since half the number of correlators are employed [52]. Another advantage of this scheme is that it combines the power efficiency of *M-ary* PPM with the smooth power spectrum of M-ary PAM [68].

OPM: Modified Hermite polynomials are used to construct orthogonal pulses to represent different symbols [63]. Pulses of different orders can be used for multiple access purposes or to construct an *M-ary* scheme.

Multiband Scheme: UWB spectrum is divided into a number of frequency bands by using a different pulse shape at each band. Depending on the desired data rate, one or more of the bands can be used in communication. Pulses at different bands do not cause interference to each other since they are orthogonal per *Parsavel's Theorem*[6].

2.4 Modulation Performances in Practical Conditions

The modulation options in previous section are evaluated assuming ideal conditions. In order to make a fair analysis of modulation schemes, practical conditions such as multipath, multiple access,

[6] $\int_{-\infty}^{\infty} x(t)y^*(t)dt = \int_{-\infty}^{\infty} X(f)Y^*(f)df$

narrowband interference, and timing jitter should be taken into account. In this section, UWB modulation schemes under such practical scenarios are evaluated.

2.4.1 Multipath

Due to reflection, diffraction and scattering effects, the transmitted signal arrives at the receiver through multiple paths with different delays. The received signal from a channel with N taps can be written as follows

$$r_{mp}(t) = \sum_{l=1}^{N} \gamma_l s^{(k)}(t - \tau_l) + n(t) \ , \tag{2.8}$$

where γ_l is the tap gain for the lth tap arriving at time τ_l and $s^{(k)}(t)$ is the transmitted signal from (2.1).

By using Rake receivers, it is possible to collect the energy at the delayed taps. *All-Rake*, *selective Rake*, or *partial Rake* receivers are all feasible approaches to collect all, strongest, or first arriving resolvable multipath components, respectively [69]. Optimal combining of the multipath components is achieved by maximal ratio combining (MRC), where the finger weights are designed based on the channel tap weights to maximize the output SNR. A reduced complexity combining technique that does not require the estimates of the fading amplitudes is equal gain combining (EGC), where all the multipath components are weighted equally.

When the time delays τ_l between the signal taps are on the order of PPM modulation index δ, the delayed taps behave as data modulation and the performance of PPM is degraded [56, 57]. The degradation in *M-ary* PPM is worse due to the large time frame that a symbol can occupy and consequently higher probability of data modulation effect. Computer simulations are performed to see the data modulation effect of multipath on PPM. A two tap static channel is assumed with tap weights $\gamma_1 = 0.82, \gamma_2 = 0.57$ and tap delay randomly changing between T_c and $2T_c$ for each bit. Fig. 2.3 shows that when no Rake receiver is used, more degradation is observed in PPM compared to BPSK. For higher SNRs, the gap between orthogonal PPM with and without Rake receivers widens. It is also seen that due to modulation effect, Rake receiver is not as effective for orthogonal PPM as it is for BPSK.

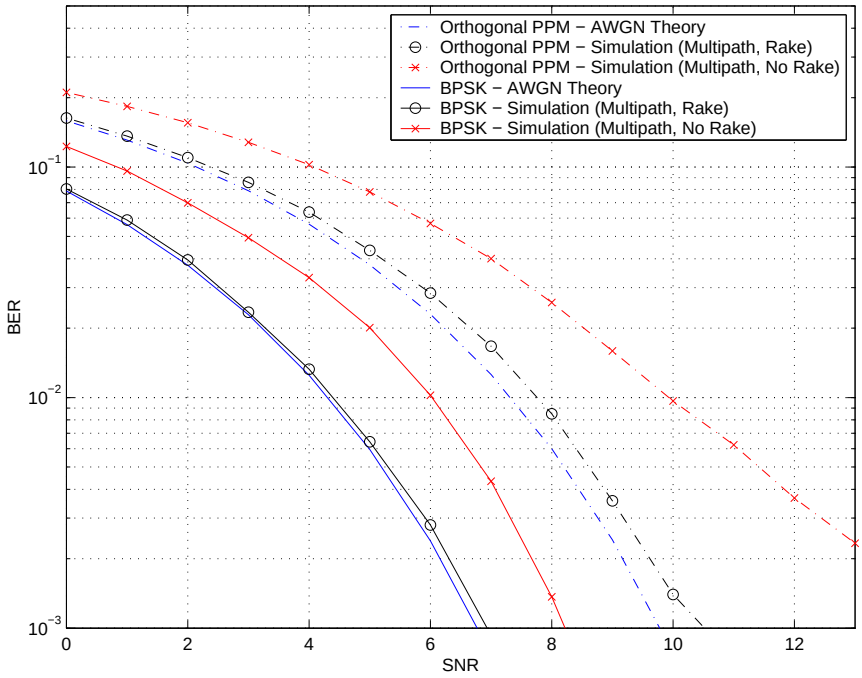

Figure 2.3 Comparison of BPSK and orthogonal PPM modulations in a two tap multipath channel.

2.4.2 Multiple Access Interference

Two multiple access schemes are commonly discussed for sharing the channel in a UWB network: TH-UWB and DS-UWB. TH-UWB [50] makes use of unique time hopping codes $c_j^{(k)}$ to position each of the N_s pulses within time frames jT_f of a particular bit. Alternatively, DS-UWB [55] uses binary codewords $a_j^{(k)}$ for determining the polarities of each of the N_s pulses that represent a bit. Unlike TH-UWB, no timing gap is left between the transmitted pulses when using DS-UWB to maximize the data rate. Although this approach is more appropriate for ad-hoc networks where transmission of each user is asynchronous [58], it does not combat multipath and narrowband interference as well as TH-UWB does [55].

A multiple access scheme can either be synchronous or asynchronous depending whether the symbols from different users are aligned or not. Both of these scenarios will be discussed in more detail in upcoming chapters, but here we provide an introductory discussion.

2.4.2.1 Synchronous Communications

For synchronous systems, circularly-shifted orthogonal PN codes $c_j^{(k)}$ can be constructed as follows [59, 13]

$$c_j^{(k)} = [(k+j-1) \mod N_h] \ , \quad 0 \leq j \leq N_h - 1, \ 1 \leq k \leq N_h \ . \tag{2.9}$$

Since these sequences are orthogonal to each other, the BER will be constant up to N_h users.

Computer simulations were performed to compare the performances of orthogonal PPM and BPSK modulations in a synchronous multi-user environment. It is assumed that a base station randomly assigns a codeword obtained by (2.9) to each user. The performance of the first user is analyzed and $N_h = 50$, $N_s = 50$, and $SNR = -10dB$ were selected, where the large value of the processing gain N_s increases the power efficiency by $17dB$ at the expense of decrease in the data rate. A chip duration of $T_h = T_c = 0.8ns$ was employed for both schemes to analyze the performances at the same data rates, which yields a bit duration of $2\mu sec$ and a data rate of $0.5Mbps$. Results in Fig. 2.4 verify that BPSK has invariant BER up to N_h users, while a degradation is observed upon arrival of two particular users for PPM. This is because of the larger symbol duration of orthogonal PPM ($2T_c$) that yields a collision with the codes of two other users. The problem can be prevented by halving either the data rate or the number of users when using orthogonal PPM.

2.4.2.2 Asynchronous Communications

In an asynchronous multiuser channel, the composite received signal from N_u users is given by

$$r(t) = \sum_{k=1}^{N_u} \gamma^{(k)} s^{(k)}\left(t - \tau^{(k)}\right) + n(t) \ , \tag{2.10}$$

where $\gamma^{(k)}$ and $\tau^{(k)}$ are the attenuation and the delay of the kth user. Once this signal is sampled at the desired user's receiver, the matched filter output is given by (considering initially BPSK modulation)

$$Y = b^{(\xi)}\sqrt{E_b^{(\xi)} N_s} + M + N \ , \tag{2.11}$$

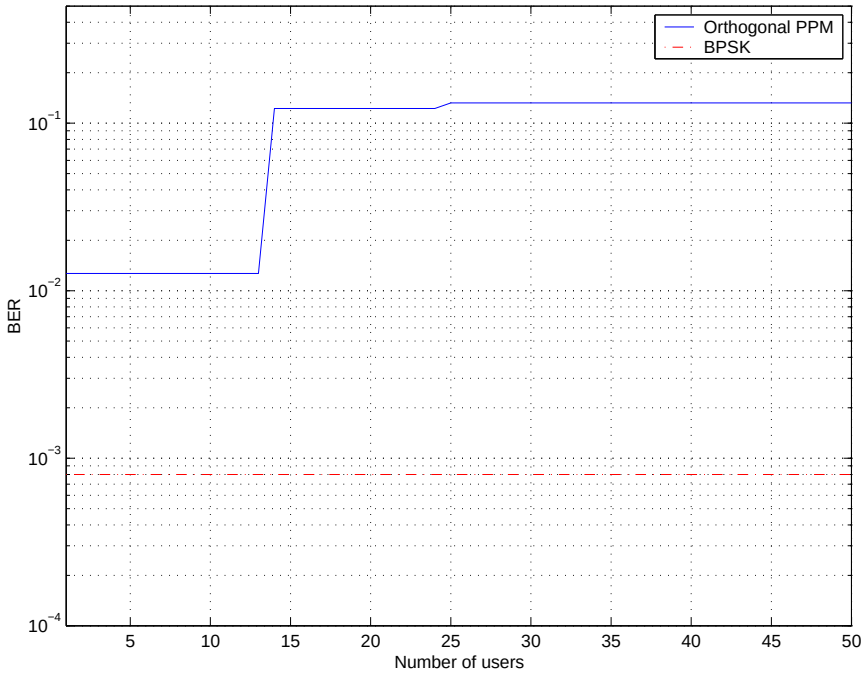

Figure 2.4 Performances of orthogonal PPM and BPSK modulations in a synchronous multiple user environment with $T_f = T_c$.

where ξ refers to the desired user, $b^{(\xi)}$ is the desired users's symbol, $N \sim \mathcal{N}(0\,,\,\sigma^2)$ is the output noise and M is the total MAI, which is the sum of interference terms from the interfering users:

$$M = \sum_{k=1,k\neq\xi}^{N_u} M_k \ , \tag{2.12}$$

where M_k is the MAI from user k. Similar to the approach in [70], when random polarity codes are used for each pulse, we can approximate the MAI from user k by the following Gaussian random variable, when the number of pulses per information symbol for user ξ, N_s, is large:

$$M_k \sim \mathcal{N}\left(0\,,\,\frac{E_{rp}^{(k)}}{N_h}\right), \tag{2.13}$$

where $E_{rp}^{(k)}$ is the energy of a received pulse from user k.

Then, we can express the *signal to interference plus noise ratio* (SINR) of the system for user ξ as

$$\text{SINR} \approx \frac{N_s E_{rp}^{(\xi)}}{\sigma_n^2 + \frac{1}{N_h} \sum_{\substack{k=1 \\ k \neq \xi}}^{N_u} E_{rp}^{(k)}} \ , \tag{2.14}$$

which can be directly inserted into Q(.) function as $\text{Q}(\sqrt{SINR})$ to evaluate the BER for BPSK. Similar approaches can be repeated to calculate BER to be $\text{Q}(\sqrt{SINR/2})$ for PPM (due to doubled noise effects in both pulse positions [52]) and OOK.

To demonstrate the performance differences of different modulation schemes (orthogonal PPM, BPSK) in such an asynchronous multiuser environment, we have done simple computer simulations, and compared them with the theoretical expressions. The parameters are selected as $N_s = 1$, $T_c = 0.8ns$, $SNR = 7dB$, $N_u = 100$, and $T_f = 20T_c$. Time delays τ_ψ of each user are selected randomly between 0-19T_c as multiples of pulse duration T_c. It is observed from Fig. 2.5 that BPSK outperforms PPM for all different possible values of number of users. Also, Gaussian approximation is seen to show some deviation for small number of users, while showing a good agreement when the number of users is large.

2.4.3 Narrowband Interference

Since the transmission occurs over an ultra-wide frequency range, UWB spectrum overlaps with various other narrowband technologies. Assuming static channel and single user case, received signal in the presence of interference is given by

$$r_{nbi}(t) = s^{(j)}(t) + I(t) + n(t) \ , \tag{2.15}$$

where $I(t)$ represents the narrowband interference term.

Performances of different modulation schemes under NBI have been investigated in the past [60]. The effect of NBI on the UWB performance is more related with the amount of overlap of interferer spectrum with the UWB spectrum than the employed modulation scheme. If the operating frequency of narrowband interferer is closer to the central frequency of the UWB system, performance degradation of UWB will be worse. Multiband scheme is widely proposed to cancel the NBI by dynamically or statically not transmitting at the band/bands that are occupied by other narrow-

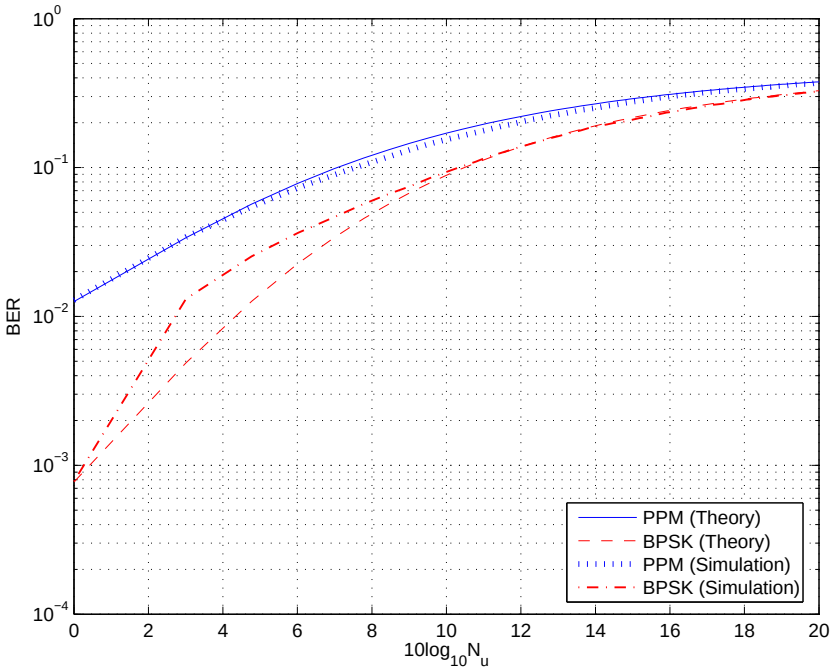

Figure 2.5 Theoretical and simulated BER performances of BPSK and PPM in an asynchronous multiple access channel.

band technologies [71]. Another method to mitigate NBI is placing a notch at the interferer band by properly designing TH codes [72].

2.4.4 Timing Jitter

Due to the transceiver clock instabilities, timing mismatches occur between the correlator template and the received pulse, and this decreases the effective SNR at correlator output. Such timing jitter is typically on the order of 10ps with the current transistor technology and is usually modeled by a Gaussian or uniform distribution [20, 62].

Theoretical analysis for the effect of timing jitter on different modulation schemes is given in [20] and summarized in Table 7.1 for a certain amount of jitter. The performance results in Fig. 2.6 for $SNR = 10dB$ show that the degradation in BPSK and PPM are similar, while OOK performs worse for large jitter. BER equation in Table 7.1 for OOK implies that timing jitter does not affect the *false alarm rate*, but increases the *missed detection rate*, yielding biased decisions towards zero. The problem will be more pronounced in M-ary PAM, which also uses threshold detection. Jitter

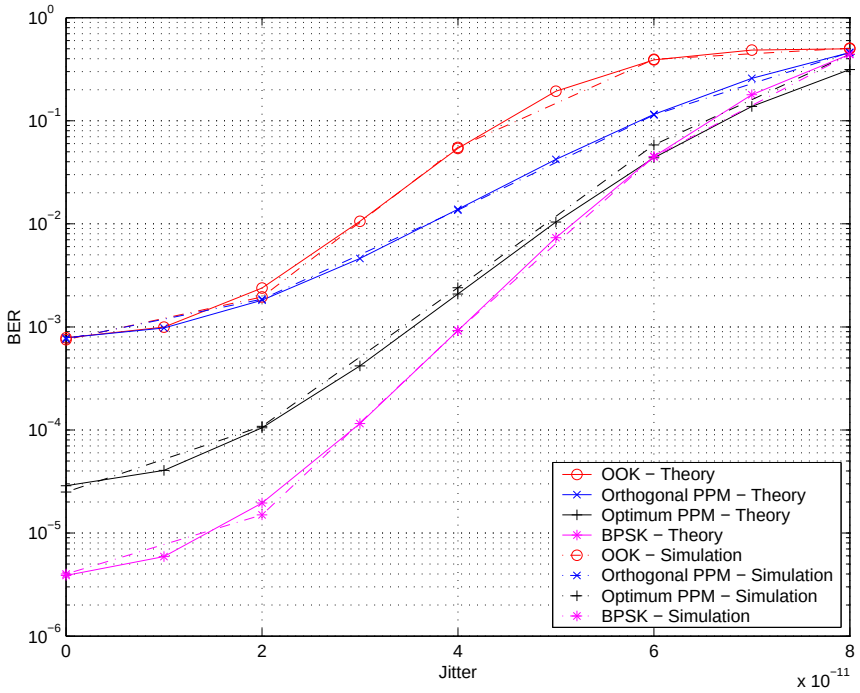

Figure 2.6 Effect of timing jitter on BER performances (SNR=10dB).

becomes a serious problem for multiband scheme as well, since the autocorrelation functions of the pulses used in higher order bands decay much faster than the autocorrelation function of the *monopulse*. The topic will be discussed in more detail and relevant derivations will be provided in Chapter 7.

2.5 Conclusion

In this chapter, the BER performances, spectral characteristics, and transceiver complexities of possible UWB modulation schemes are revisited. Effects of multipath, multiple access, narrowband interference, and timing jitter are analyzed and verified via simulations. It is shown that PPM performance degrades in multipath and multi-user environments since symbols occupy larger time durations. Compared to other modulations, OOK and *M-ary* PAM are more susceptible against timing jitter. Although multiband scheme provides interference mitigation and flexibility of data rate, it is more susceptible against timing jitter especially at the higher frequency bands. In summary, BPSK can be preferred for its high power efficiency and smooth spectrum; OOK for its simple

transceiver structure; M-ary PPM for its improved power efficiency; and M-ary PAM for higher data rates.

CHAPTER 3

TIME-HOPPING MULTIPLE ACCESS FOR IR-UWB

3.1 Introduction

Multiple accessing for UWB-IR makes it possible to accommodate multiple users on the same UWB channel. Time hopping (TH) [73], direct sequence (DS) [74], and frequency hopping (FH) [75] approaches are the most common multiple access options for UWB-IR systems. In order to reduce/avoid multiuser interference (MUI), pseudo random codes are often used as in code division multiple access (CDMA) systems. However, designing codes with optimal autocorrelation and cross-correlation properties is not possible.

Careful design of the TH codes minimizes the effects of multipath and multiuser interference (MUI), controls the power spectrum for good coexistence with other technologies, and improves synchronization between the transmitter and the receiver. Earlier research on DS and FH multiple access sequence design can be applied to TH-IR networks, with some modifications. For example, DS codes (such as m-sequences and Gold sequences) can be converted into decimal values before applying to TH-IR [76]-[79]. FH sequences [80]-[84] can be used directly with TH-IR, but their autocorrelation and crosscorrelation characteristics will be different. Correlation properties of TH codes are derived in terms of those of FH codes in [85] and it is shown that maximum number of hits in correlation functions of TH sequences is twice that of FH sequences. In [86]-[89], implementation of FH sequences (such as linear congruence codes (LCCs), hyperbolic congruence codes (HCCs), permutation sequences) to TH-IR were presented. A novel TH code design for synchronous CDMA systems is presented in [90], which yields bounded collisions and can be successfully applied to UWB-IR. One-coincidence FH sequence construction that has a specified distance between adjacent symbols has been proposed in [91], and a similar approach can be considered for TH-IR to minimize the inter-frame interference from the user's own pulses due to multipath.

In this chapter, first, an overview of multiple accessing options for UWB systems is presented. Then, TH code design for both synchronous and asynchronous UWB-IR systems are considered.

For synchronous systems, a novel code assignment algorithm that depends on the number of users and the delay spread of the channel is proposed. The proposed codes are also extended to quasi-synchronous scenarios. Afterwards, TH code design for asynchronous transmission is studied. FH codes obtained by finite field theory are applied to TH-IR, and their autocorrelation and cross-correlation characteristics are investigated. For different codes, histograms for number of hits are generated through computer simulations. These histograms provide a better measure for the code efficiency than the maximum number of hits, and make it possible to develop mathematical models for multiuser performance analysis.

3.2 Multiple Accessing Options for UWB

In order to effectively share the available spectrum between different users, multiple accessing carries importance in wireless communication systems. Among other multiple accessing options, time division multiple access (TDMA), frequency division multiple access (FDMA), and CDMA are the most popular multi-access techniques for wireless systems.

3.2.1 TDMA

In TDMA systems, each user transmits over disjoint time intervals. Based on the length of the time slots with respect to the symbol duration, TDMA systems can be divided into two groups: long time slot TDMA, and interleaved TDMA [92]. Time slots in long time slot TDMA are fixed and sweep many symbol durations (i.e. in Fig.3.1-(c), $T_{slot} > T_s$, where T_s is the symbol duration). Usually, a central node handles the assignment of the time slots to each user, and maintains the synchronization. However, when the architecture is decentralized, synchronization of the users is not possible. Instead, in such architectures, each user may employ a contention based random access approach to get hold of the channel, which can also be interpreted as a form of TDMA. For example, in carrier sense multiple access (CSMA) systems, a node senses at random times if the channel is busy or not; if it is free, the user accesses the channel for a specific time. CSMA is not very efficient for UWB systems, as very low transmission power requirement of UWB makes it extremely inefficient to sense whether the channel is busy or not [92].

Time slot durations in Fig. 3.1-(c) may also be much smaller than the symbol duration as in interleaved TDMA ($T_{slot} < T_s$). For example, pulsed UWB approaches usually transmit many low duty cycle pulses to represent a bit (i.e. $T_{slot} = T_c$ for chip interleaved case, where T_c is the chip

duration), where the number of pulses is determined by the processing gain of the system. The *off-time* between two consecutive pulses implies a second type of processing gain, and other users may transmit in the gaps between these pulses. On the other hand, rather than a constant pulse-to-pulse interval, a user specific TH code can be used to identify the timing positions of the pulses. This helps the channelization of the system, while smoothing the power spectral density.

3.2.2 FDMA

Another option of sharing the channel between different users is FDMA, where each user may transmit simultaneously over different frequency bands. Multiband UWB is a popular pulse based UWB scheme which can be interpreted as a form of FDMA. As opposed to conventional FDMA systems, which use carriers to allocate the bands, in multiband UWB, usually, frequency domain sharing of the channel is achieved by pulse shaping. By appropriately designing the pulses, the central frequencies of the bands can be adjusted. Also, multiband UWB offers the flexibility to coexist with narrowband interferers and to comply with the local regulations by dynamically turning off certain sub-bands. On the other hand, conventional FDMA (with mixers) can also be employed if desired; however, this increases the size and complexity of the transceiver.

Note that multiple bands can also be employed by the same user to increase the data rate. On the other hand, large number of narrowband signals can be transmitted simultaneously within the same band to comply with the 500 MHz FCC requirement for UWB systems. Orthogonal frequency division multiplexing (OFDM) is a *non-pulse based* approach to UWB, which is realized by simultaneously transmitting many overlapping narrowband signals (modulated with different symbols) at orthogonal sub-carriers. In contrast to IR, OFDM systems combat multipath effects by increasing the symbol duration and by adding a cyclic prefix which is larger than the maximum excess delay of the channel.

Rather than a fixed allocation of bands for each user, alternatively, frequency hopping can be realized by hopping from one band to another. This brings the benefits of frequency diversity, and the channelization of the system with user-specific frequency hopping codes. For example in multiband OFDM, multiple bands with at least 500 MHz wide are employed, where users employ frequency hopping over these bands to share the channel. Fast frequency hopping ($T_{hop} < T_s$) and slow frequency hopping ($T_{hop} > T_s$) are two different versions of frequency hopping systems.

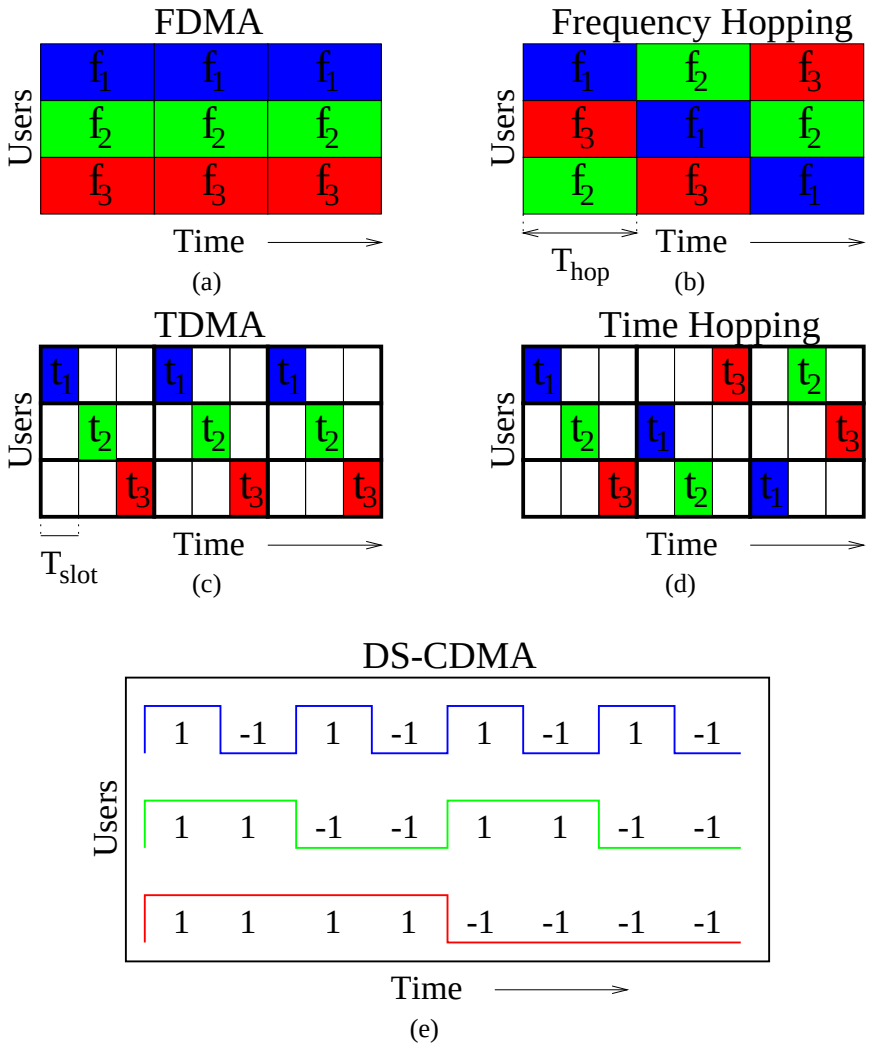

Figure 3.1 Multiple access options for UWB.

FDMA approach to UWB multiple access have certain limitations. By partitioning the whole UWB spectrum into narrower bands, time resolution of the transmitted UWB signal decreases. Therefore, the benefits of UWB such as multipath immunity, precise positioning etc. are somewhat diminished by using FDMA [92].

3.2.3 CDMA

Another popular multiple access scheme that is used in many wireless communication technologies is DS-CDMA. In DS-CDMA, the users can simultaneously occupy the same wide channel. The users are multiplexed to the channel by spreading the users' narrower bandwidth signals with a binary

± 1 pseudo-noise (PN) sequence. Direct sequence approach to UWB is based on transmission of impulsive pulses within consecutive chips. It is very similar to traditional DS-CDMA systems, however, the bandwidth of the transmitted signal is much larger. In addition, pulse shaping is crucial not to violate the regulatory spectral masks.

As mentioned before, TH and FH can be seen as forms of TDMA and FDMA, respectively. These approaches can also be considered as forms of CDMA systems. Since user specific multiple access *codes* are used in both approaches, it can be argued that multiple accessing is achieved in code domain. As will be discussed in the latter sections, many of the multiuser algorithms used in DS-CDMA systems can be directly applied to TH-IR, which further motivates this interpretation. All these five multiple accessing approaches to UWB are depicted in Fig. 3.1.

Combinations of these different multiple access options are also possible. For example, time-frequency hopping hops both over time and frequency domains, which mitigates for the multipath by allowing time intervals between the pulses in the same band [1]. On the other hand, in conjunction with time hopping, polarity coding as in DS-CDMA systems can be used, which increases the system capacity, and smoothes the power spectrum.

3.3 Signal Model and Code Correlation Function

Consider the received multiuser signal in (2.10), where each user may arrive at the receiver with different delays $\tau^{(k)}$. Then, depending on the relative delays τ (see Fig. 3.2) between different users in a multiuser UWB-IR system, three possible transmission scenarios can be considered:

- *Synchronous Transmission:* $\tau^{(1)} = \tau^{(2)} = \cdots = \tau^{(N_u)}$,
- *Quasi-Synchronous Transmission:* $|\tau^{(k_m)} - \tau^{(k_n)}| \leq \xi$,
- *Asynchronous Transmission:* $0 < \tau < N_s N_h T_c$,

where (k_m, k_n) are any pairs of users, and ξ is a very small value compared to the symbol duration.

3.3.1 Code Correlation Function

Ideally, the sequences employed by different users are required to be orthogonal to avoid interference. Two TH codes are orthogonal if for all time frames j, there is no pulse overlap between

different users, *i.e.* for a synchronous scheme, and any two users k_m, k_n ,

$$c_j^{(k_m)} \neq c_j^{(k_n)} \ . \tag{3.1}$$

This orthogonality can not be maintained for certain cases, such as in the presence of multipath or in the absence of synchronism. Hence, a number of pulses from different users may collide, resulting in a performance degradation. A performance measure that is commonly used for the evaluation of the code characteristics is the code correlation function (known as Hamming correlation function in FH literature), defined as [85, 89] [1]

$$\begin{aligned} C_{k_m k_n}(\tau) = & \sum_{j=0}^{N_s-1} h\left[jN_h + c_{mod(j+a,N_s)}^{(k_m)}, jN_h + c_j^{(k_n)} + b\right] \\ & + \sum_{j=0}^{N_s-1} h\left[(j+1)N_h + c_{mod(j+a+1,N_s)}^{(k_m)}, jN_h + c_j^{(k_n)} + b\right] \ , \end{aligned} \tag{3.2}$$

where the function $h[c_A, c_B]$ for any two integers c_A, c_B is given by

$$h[c_A, c_B] = \begin{cases} 0, & \text{if } [c_A \neq c_B] \ \ mod(N_s N_h) \\ 1, & \text{if } [c_A = c_B] \ \ mod(N_s N_h) \end{cases} \tag{3.3}$$

Note that chip synchronism is assumed between different users' signals, which yields a worst case performance bound. The time delay is defined as $\tau = aN_h + b$, where a is the integer number of time frames within the delay duration, and b is the remaining number of chip durations. The code correlation function in (3.2) shows the number of hits between two different TH sequences with some relative delay with respect to each other, or between the delayed versions of the same TH sequence. Note that (3.2) consists of two disjoint terms, first summation corresponding to the case when $c_j^{(k_n)} + b < N_h$ (see h_1 in Fig. 3.2), and the second summation corresponding to the case when $c_j^{(k_n)} + b \geq N_h$ (see h_2 in Fig. 3.2). Note also that (3.2) is periodic due to the involved modular operations, and considers the collisions from the neighboring bits.

[1] The terms $mod(a_1, a_2)$, and $[a_1] \ mod(a_2)$ are used interchangeably throughout the text to represent the modulo of a_1 with respect to a_2.

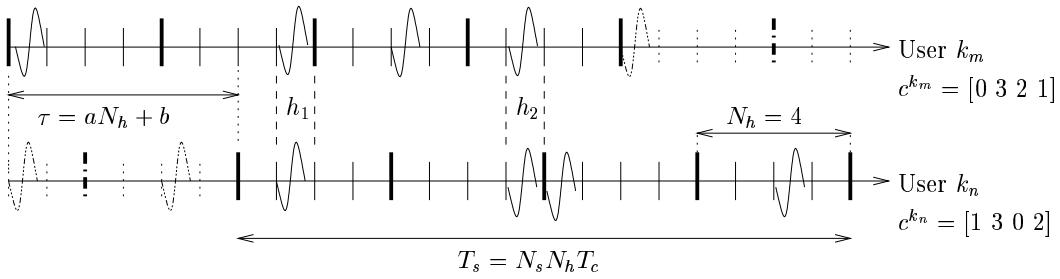

Figure 3.2 Asynchronous UWB transmission ($a = 1$, $b = 2$, $N_h = 4$, $N_s = 4$).

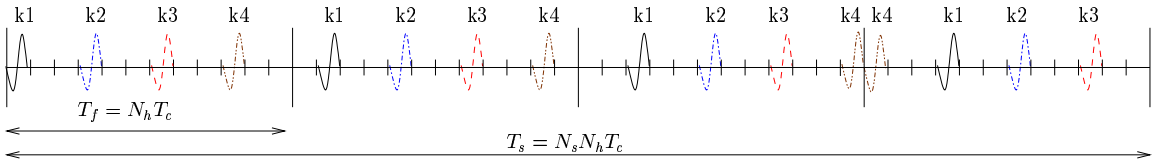

Figure 3.3 Proposed codes for the first four users ($N_h = 12$, $N_s = 4$, $D = 3$).

3.4 Adaptive TH Sequence Design for Synchronous UWB Systems

For synchronous systems, the time delay τ between different users is zero, and there are many possible orthogonal code constructions for flat fading channels (such as *any* of the codes given in Table 3.2, or Gold codes). For example, a variant of linear congruence codes is given by [86]

$$c_j^{(k)} = [k + j - 1] \ \ mod(N_h), \tag{3.4}$$

where $0 < j \leq N_s - 1$ and $1 < k \leq N_h$. These circularly shifted codes assure that codes for different users are orthogonal as indicated in (3.1). Therefore, as long as $N_u \leq N_h$, addition of new users to the system does not affect the performance, yielding an invariant bit error rate (BER). Signal-to-noise ratio (SNR) in this case is given by

$$SNR = \frac{(N_s m_p)^2}{\sigma_{rec}^2}\ , \tag{3.5}$$

which is independent of the number of users. Polarization codes as in CDMA can also be used to assign orthogonal ± 1 sequences to each user that have the same TH code, and hence increasing the number of orthogonal codes to $N_h N_s$ [93].

In dispersive channels, the multipath components of a certain user's signal collide with other users' signals, and the codes in (3.4) are no longer orthogonal. To solve this problem, a code

construction scheme which adaptively assigns codes to the users for the purpose of minimizing the degradation due to multipath is proposed. The code construction is a function of number of users present in the system, and maximum excess delay of the channel, both of which are assumed to be known by the central node (such as a base station in cellular systems, or an access point in wireless local area networks). The proposed codes are given by

$$c_j^{(k)} = [(k-1)D + j + \lfloor \frac{k-1}{N_s} \rfloor] \ \ mod(N_h), \tag{3.6}$$

For this proposed code construction, the processing gain N_s is selected to allow the multipath components to die away as follows

$$N_s = \frac{N_h}{D} \ . \tag{3.7}$$

Using (3.6), a minimum difference of D is assured between $c_j^{(k)}$ and $c_j^{(k+1)}$ (i.e. the consecutive user's hopping code within the same time frame), and it is given by

$$D = \lceil \frac{\tau_d}{T_c} + 1 \rceil \ , \tag{3.8}$$

with τ_d being the maximum excess delay of the channel and $\lceil . \rceil$ representing the ceiling operation. This allows the delayed taps to die away, and assures the orthogonality of the codes for $N_u \leq N_s$ despite the multipath components. For $N_u > N_s$, $\lfloor \frac{k-1}{N_s} \rfloor$ is used to shift the codes to construct a new group of orthogonal codes. By this way, D code groups are constructed, each having N_s orthogonal sequences. Any pairs of sequences within the same group satisfy

$$C_{k_m k_n}(\tau) = 0 \ , \ 0 \leq \tau < D \ , \tag{3.9}$$

implying that there is no collision with the multipath components of the other users within the group. An example set of proposed codes for $N_s = 4$, $N_u = N_h = 12$, and $D = 3$ are presented in Table 3.1, with each column containing a group of orthogonal codes, and Fig. (3.3) depicts the transmitted pulses for the corresponding first four users. Note that if the maximum excess delay decreases, base station can adaptively regroup the available codes, so that the number of orthogonal codes in a certain group increases and the overall system performance improves.

Table 3.1 Numerical example for the proposed time-hopping codes ($N_s = 4, N_h = 12, D = 3$).

User #	TH (Group 1)				User #	TH (Group 2)				User #	TH (Group 3)			
1	0	1	2	3	5	1	2	3	4	9	2	3	4	5
2	3	4	5	6	6	4	5	6	7	10	5	6	7	8
3	6	7	8	9	7	7	8	9	10	11	8	9	10	11
4	9	10	11	0	8	10	11	0	1	12	11	0	1	2

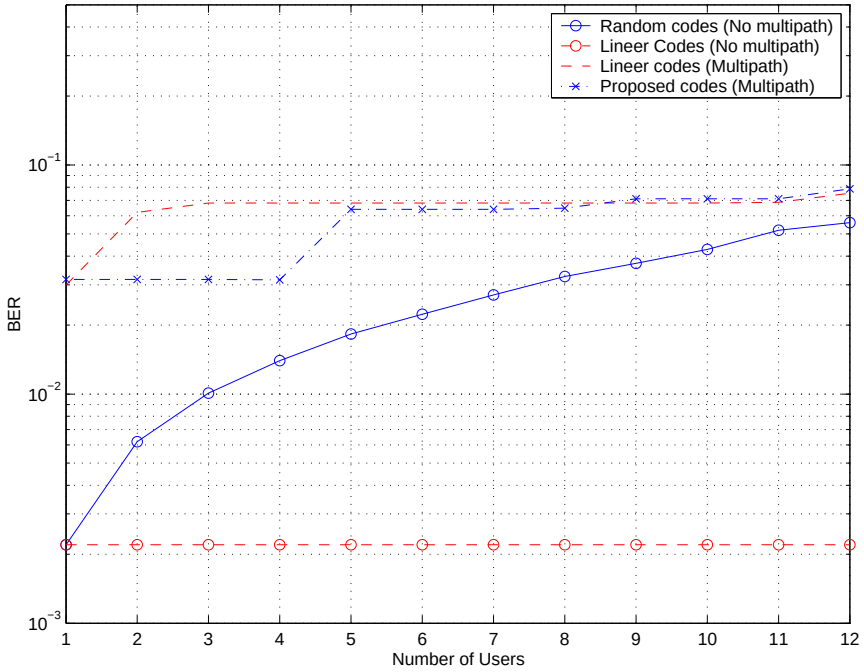

Figure 3.4 Comparison of random, linear, and proposed codes in static and dispersive channels (SNR=0 dB, $N_s = 4$, $N_h = 12$, $D = 3$).

In Fig. 3.4, performances of the random codes, linear codes in (3.4), and proposed codes in (3.6) (as presented in Table 3.1) are compared in static and dispersive channels. It is observed that as opposed to random codes, it is possible to avoid multiple access interference using orthogonal codes in static channels. For the multipath channel, a Rayleigh fading channel with 3 taps and exponential tap weights are assumed, with each tap arriving at multiples of T_c $(D = 3)$[2]. The performance of the first user ($k = 1$), which uses maximal ratio combining (MRC) Rake receiver is investigated. The decrease in the overall performance due to fading is obvious. It is seen that the effect of multipath for number of users up to N_s is successfully mitigated using the codes in Table 3.1. For number of users larger than N_s, the BER performance gradually degrades with the inclusion of certain users

[2]Although a very simple channel model was assumed for ease of explanation, it is possible to extend the code construction to more realistic channel models [94].

to the system. For example for user 1, the interference comes from the users 5 and 8 in group 2, and from users 9 and 12 in group 3, whose multipath components collide with certain Rake fingers of user 1. Similarly for user 2, the interference comes from the users 5 and 6 in group 2, and from users 9 and 10 in group 3. This structured form of the interference results in a staircase type of degradation in the BER performance.

Since the TH sequences and received power levels of all the users are known by the base station in a cellular scenario, the performance degradation can be handled further with interference cancellation algorithms (such as successive interference cancellation, maximum-likelihood detection, etc...). Instead of processing all the users' signals, only the users who interfere with each other can be considered in these algorithms, which will considerably decrease the system complexity. In the downlink, or in asynchronous systems, where neither the hopping sequences nor the amplitudes of other users are known, blind multiuser detection schemes can be implemented [73].

Another design parameter that needs to be considered for TH sequence construction is the power spectral density (PSD) of the UWB pulse train. The codes proposed in (3.6) have periodic pulse-to-pulse durations, thus yielding spectral lines in the transmitted signal PSD. This can be prevented by randomly shuffling the columns of the codeword matrix presented in Table 3.1, which still ensures a timing gap of D between the different users' codes and smoothes the power spectrum.

The inter-frame interference from the user's own pulses or from other users' pulses is another source of performance degradation. This happens when the multipath components of a pulse positioned closer to the end of a time frame affect the pulses positioned earlier in the next time frame. For example in Fig. 3.3, the pulses of user $k4$ in third time frame causes self interference to its own pulse in the fourth time frame. This can be prevented by choosing $N_h T_c \leq T_f$ to let the multipath components die away between each frame.

3.4.1 TH Sequence Design for Quasi-Synchronous Transmission

Achieving perfect synchronization of the users, which assures the orthogonality between these users' multiple access codes, is a difficult task. Therefore, non-orthogonality of the codes due to access timing errors will yield performance degradation. In order to solve this problem in quasi-synchronous systems, the multiple access sequences can be designed so that they allow a certain amount of access timing error. Such sequences have a zero correlation zone (ZCZ) within an IFW of size $\tilde{D}$, or low correlation zones (LCZ) within a similar window. Therefore, the code correlation

functions for these schemes satisfy

$$C_{k_m k_n}(\tau) = \begin{cases} 0, & \text{if } 0 < \tau < \tilde{D} \quad \text{(ZCZ)} \\ \epsilon, & \text{if } 0 < \tau < \tilde{D} \quad \text{(LCZ)} \end{cases} \tag{3.10}$$

where ϵ is a negligibly small correlation value. Note that (3.10) has to be satisfied for the autocorrelation function to improve the performance in multipath, as well as for the crosscorrelation function to improve the performance in multiuser environment. Algorithms to obtain such codes have been developed for DS schemes [95], and for FH schemes [96] in the past. In this subsection, a Lemma that applies to certain TH code constructions will be presented, and application of the proposed codes in (3.6) to quasi-synchronous scenarios will be explained.

***Definition** 1.* Full code is a code whose placement operator is a permutation of the Galois field [80] (such as the construction given in (3.6), LCCs, and HCCs).

***Definition** 2.* A Galois field $GF(p)$ is a finite field with elements $0, 1, 2, \cdots, p-1$, where p is a prime number.

***Lemma** 1.* Assume that a TH code construction yields full codes, and c_j^k with with j fixed is also a permutation of the Galois field (such as the case in the proposed codes in (3.6), LCCs, and HCCs). Then, it is not possible that *each* pair selected from the set of *all* possible codes will have ZCZ of size $\tilde{D} \geq 1$.

Proof: The proof is complete if it is shown that for $\tau = 1$, *i.e.* for $a = 0$ and $b = 1$, there exists two users k_m, k_n for which $C_{k_m k_n}(\tau) > 0$. Therefore, from (3.2) the following needs to be satisfied

$$c_{j+1}^{(k_n)} = c_j^{(k_m)} , \tag{3.11}$$

Since a full code is a permutation of the Galois field, there will always be two sequences that will satisfy (3.11), and therefore the proof is valid by definition.

Although for full codes it is not possible to design the codes with ZCZs as described above, the codes for different users can be grouped so that they have ZCZs within the group. This can be

realized by using the code construction proposed in (3.6). Based on the number of users in the system, the base station can adaptively select the codes so that the length of the IFW is maximized. As the number of users increases, length of the IFW is decreased to support larger number of users. Nevertheless, time hoping sequence construction for quasi-synchronous systems with ZCZ and LCZ are open research issues, and require further investigation.

3.5 TH Sequence Design for Asynchronous UWB-IR Systems

When the transmission is asynchronous, user delays τ are totally random, and it is no longer possible to design the codes that give interference free communication. However, it is still possible to design codes in a way that number of hits between two codes (determined by the Hamming correlation in (3.2)) for any value of τ is bounded, thanks to the properties of Galois fields and finite field theory [84]. In this section, autocorrelation and crosscorrelation characteristics of various FH code constructions obtained using finite field theory are studied, and their performances when used in TH-IR are investigated. Hit histograms for different code families are generated, and these are then used to develop mathematical models for multi user performance analysis.

3.5.1 Code Constructions and Correlation Properties

Code constructions, the conditions for hit, and maximum number of hits in code correlation functions for some of the most common FH code constructions are summarized in Table 3.2. Note that while LCC and HCC yield full codes, quadratic congruence codes (QCC) and cubic congruence codes (CCC) do not. A hit between two FH codes occurs when the following is satisfied

$$c_{j+a}^{k_m} = c_j^{k_n} + b \; mod(p) \; . \tag{3.12}$$

The maximum number of hits is calculated by finding the number of solutions for (3.12), which is the order of the polynomial from Langrange's Theorem [80]. If $k_m = k_n$, the maximum number of hits corresponds to the peak value of the sidelobes of the autocorrelation function (ACF). On the other hand, for two distinct users k_m and k_n, maximum number of hits corresponds to the maximum value of the crosscorrelation function (CCF). Unfortunately, it is not possible to minimize both correlation functions at the same time, and there is a trade off in preferring one construction to the other. Plugging different code constructions in (3.12), maximum number of hits for a certain

Table 3.2 FH code constructions and maximum number of hits in aperiodic correlation functions for FH and TH implementations (all operations are done in $GF(p)$).

	LCC	QCC	CCC	HCC
Code Construction	$[kj]$	$[kj^2]$	$[kj^3]$	$[k/j]$
Hit condition (FH codes, ACF)	$k_m(j+a) = k_m j + b$	$k_m(j+a)^2 = k_m j^2 + b$	$k_m(j+a)^3 = k_m j^3 + b$	$\frac{k_m}{j+a} = \frac{k_m}{j} + b$
# of hits (ACF)	FH:p-1, TH:p-1	FH:1, TH:2	FH:2, TH:4	FH:2, TH:4
Hit condition (FH codes, CCF)	$k_m(j+a) = k_n j + b$	$k_m(j+a)^2 = k_n j^2 + b$	$k_m(j+a)^3 = k_n j^3 + b$	$\frac{k_m}{j+a} = \frac{k_n}{j} + b$
# of hits (CCF)	FH:1, TH:2	FH:2, TH:4	FH:3, TH:6	FH:2, TH:4

code construction can be easily evaluated, as shown in Table 3.2. Note that the number of hits for TH codes is twice the number of hits for FH codes, which is due to the second summation term in (3.2).

Having smaller sidelobes in the ACF yields improved performance in multipath environments, as well as better synchronization. On the other hand, the CCF of the codes must be minimized to improve robustness against MUI. It is observed in Table 3.2 that linear congruence codes have 2 hits at maximum in their CCFs, but have poor autocorrelation characteristics. Quadratic congruence codes have optimum combination of autocorrelation (2 hits) and crosscorrelation (4 hits) characteristics.

3.5.2 Modeling of MUI Based on Code CCF

Although the maximum number of hits in the correlation functions gives information about code performances, a more realistic approach would be to use the probability distribution functions of the hits to evaluate the code efficiency. In order to test the performances of the codes in Table 3.2, computer simulations are done, and the histograms for the number of hits between two code sequences are produced. For a particular construction, correlation (i.e. the number of hits) of a certain user's code with all the other users' codes and all possible time shifts τ are calculated, and aggregate number of hits are taken into account when evaluating the histograms. It is observed that maximum number of hits in Tables 3.3, 3.4 for aperiodic ACF and CCF are consistent with the theoretical results given in Table 3.2.

Aperiodic CCF does not consider the correlation effects from the neighboring bits. In order to take this into account, periodic CCF are obtained by circularly shifting the whole symbol chip by chip, and getting the correlation with other users' signals. It is observed in Table 3.5 that the

Table 3.3 Hit percentages (aperiodic ACF).

	0	1	2	3	4	5	6	7-30
RC	62.7	28.68	6.34	1.89	0.33	0	0	0
LCC	96.72	0.11	0.11	0.11	0.11	0.11	0.11	2.64
QCC	56.41	38.76	4.78	0	0	0	0	0
CCC	76.18	1.55	20.99	0.11	1.11	0	0	0
HCC	75.51	1.55	22.32	0.11	0.44	0	0	0

Table 3.4 Hit percentages (aperiodic CCF).

	0	1	2	3	4	5	6	7-30
RC	62.56	27.39	7.98	0.3	0.03	0.01	0	0
LCC	50.03	49.97	0	0	0	0	0	0
QCC	64.72	21.98	12.07	1.07	0.16	0	0	0
CCC	63.31	26.77	7.02	2.5	0.34	0.04	0.02	0
HCC	63.48	24.46	10.79	1.18	0.1	0	0	0

Table 3.5 Hit percentages (periodic CCF).

	0	1	2	3	4	5	6	7-30
RC	36.24	37.44	18.41	6.21	1.42	0.25	0.02	0.01
LCC	18.15	63.77	18.09	0	0	0	0	0
QCC	39.37	29.34	24.54	5.54	1.13	0.06	0.01	0
CCC	36.89	37.12	17.19	7.1	1.4	0.25	0.05	0
HCC	37.29	33.5	22.31	5.87	0.94	0.07	0.02	0

maximum number of hits is larger compared to the aperiodic case as expected, since the collisions from the neighboring symbols are included.

When p is further increased, maximum number of hits in the aperiodic correlation functions increases for random codes (RC), while they remain the same for the other code constructions using congruence equations (as long as p is prime). This implies that since the maximum number of hits when using the mathematical code constructions are bounded, they are better suited for systems with larger processing gains N_s, than the random time hopping codes. For the periodic CCF, the maximum number of hits increases for all code constructions with increasing p.

Using the produced hit histograms, it is possible to obtain the probability distribution function (PDF) of the MUI, which can be used to evaluate the BER performance in multiple access channel. Assuming BPSK modulation is used, and the polarity of each hit is independent[3], a mapping from the hit histogram to the interference PDF can be generated. If the number of hits h between two

[3]Note that although this is not always the case for a system with small number of users, usage of polarization codes and larger number of users in the system justifies this assumption.

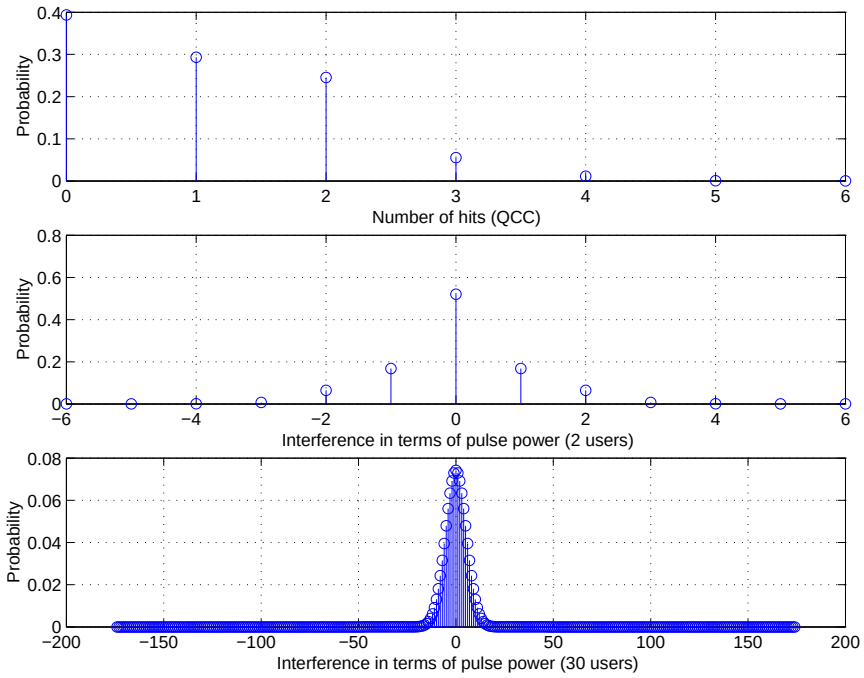

Figure 3.5 Histogram of number of hits, and the corresponding PDFs for MUI for 2 and 30 users.

codes is even ($h \in 0, 2, 4 \cdots$), the PDF of the MUI is derived as

$$P_I(\pm h\sqrt{E_p}) = \sum_{k=\frac{h}{2}}^{M/2} \binom{2k}{k-\frac{h}{2}} \frac{1}{2^{2k}} P_{hit}(2k) \ , \tag{3.13}$$

and if h is odd ($h \in 1, 3, 5 \cdots$), MUI-PDF is derived as

$$P_I(\pm h\sqrt{E_p}) = \sum_{k=\frac{h+1}{2}}^{M/2} \binom{2k-1}{k-\frac{h-1}{2}} \frac{1}{2^{2k-1}} P_{hit}(2k-1) \ , \tag{3.14}$$

where P_{hit} denotes the histogram of the code sequences given in Table 3.2, M is the maximum number of hits, and $\sqrt{E_p}$ is the energy per pulse. P_I is the interference PDF when there are 2 users in the system, and cumulative interference PDF for N_u users can be evaluated by $N_u - 1$ fold convolution of P_I by itself. The BER equation for BPSK can then be conditioned on the MUI-PDF, and the performance in MUI can be evaluated [97]. The hit histogram (periodic CCF) for QCC, and the interference in terms of pulse power for 2 and 30 users are depicted in Fig. 3.5. It is seen that as the number of users increases, the PDF of MUI converges to a Gaussian distribution, making it possible to model the MUI with Gaussian approximation.

3.6 Conclusion

In this chapter, code constructions for synchronous, quasi-synchronous, and asynchronous transmission schemes are analyzed. For the synchronous transmission, an adaptive code construction algorithm is proposed to minimize the degradation in dispersive channels. The proposed codes are extended to quasi-synchronous scenarios to obtain IFWs for a group of users. Possible asynchronous TH code constructions are analyzed, and it is proposed to use the code histograms as a performance measure, rather than the maximum number of hits in the correlation functions. It is demonstrated via computer simulations that it is possible to generate sequences with better correlation properties than random sequences. The hit histograms are mapped into MUI-PDFs using certain transformations, which enables the performance evaluation of UWB-IR schemes in multiuser environments.

CHAPTER 4

ADAPTATION OF MULTIPLE ACCESS PARAMETERS FOR IR-UWB

4.1 Introduction

Together with recent advances in integrated circuits, the evolution of wireless sensor networks (WSNs) towards inexpensive, low-power, and small-size implementations has gained incredible momentum. WSNs can be implemented in a variety of areas, such as military, telemedicine, telemetry, robotics, fault detection, consumer electronics, and security. Depending on the requirements of a specific application, the number of nodes in a WSN may range from a few nodes to thousands of nodes. In large WSNs, it is essential to have energy efficient communications to increase the network lifetime.

Ultrawideband impulse radio (UWB-IR) is a highly promising physical layer technology for WSNs due to its unique characteristics such as low power transmission, low cost and low complexity transceiver circuitry, flexibility to transmit within a large unlicensed spectrum (as long as complying with regulatory power requirements), precise location capability, and secure transmission due to employed multiple access sequences. In a UWB-IR system, time-hopping (TH) codes are employed as a multiple access method [98]. By appropriately designing the TH codes, it is possible to control multiple access interference in UWB systems to a certain extent [13, 15]. TH multiple access can provide interference free communications in synchronous systems. Even in an asynchronous system, excessive interference can be avoided due to low duty cycle and large processing gain of UWB-IR pulse transmission. Even if some of the pulses are corrupted, the rest of the pulses will be sufficient to extract the information. In addition, low complexity multiuser receivers, such as chip discriminators [99], can be used to discard the corrupted pulses, and implement adaptive rate control algorithms based on the interference level.

Adaptation of wireless communication systems allows better exploitation of the system resources based on the estimation of wireless link quality [100]. The link quality is often measured by the signal-to-interference plus noise ratio (SINR) of the received signal. For example, adaptive coding [101, 102]

schemes can achieve higher throughput when the channel quality is good by decreasing the amount of redundancy transmitted. On the other hand, when the link quality is poor, reliable transmission can be insured by increasing the coding power (amount of redundancy). Similarly, the modulation scheme can be adaptively changed in order to better exploit the link quality [103]. For M-ary pulse position modulation (PPM), even though the data rate is increased by $\log_2 M$, increasing the modulation order M increases the effective time spanned by a single pulse by M. The good news is that the power efficiency is improved for higher order M-ary PPM schemes, i.e. less power is required to assure the same bit error rate (BER). On the other hand, higher order M-ary pulse amplitude modulation (PAM) levels have worse power efficiency (compared to lower order M-ary PAM schemes), but the data rate improves by $\log_2 M$ with the pulses spanning the same time duration. These characteristics of both higher order modulation schemes can be used to adapt to the changes in the link quality. Assigning multiple codes to the users, changing the pulse shape [104] and duration, and changing the transmitted pulse power [105] as in conventional schemes are other forms of adaptation in UWB systems to better exploit the system resources.

Adaptation of multiple access parameters in UWB-IR systems (i.e. the number of pulses per symbol, and the frame duration) is another flexible mean of exploiting system resources efficiently. Increasing the number of pulses per symbol increases the SINR, which can be considered as a power control approach in the time domain without changing pulse amplitudes. Increasing the frame duration (which is related with the cardinality of the code) again improves the SINR in a multiuser environment, as it becomes less likely that the pulses will receive hits. However, these improvements come at the expense of a decrease in data rate. By measuring the link quality (which depends on the channel, multiuser interference etc.), it is possible to improve the data rate by modifying both of the multi-access parameters, while satisfying a minimum BER requirement (which is set by quality of service (QoS) requirements). Alternatively, if a certain data rate is required by the system, the transmission power can be reduced to improve the network lifetime, when the link quality is good.

Adaptive rate and power allocation has been well studied for code division multiple access (CDMA) systems in the past [106]-[109]. Optimal assignment of number of pulses per symbol and the frame duration for UWB systems in range limited and multiuser interference limited environments were analyzed in [110], where the Gaussian approximation is used to characterize the link quality and assess data rate gains for asynchronous communications. In [111], use of the standard Gaussian approximation (SGA) to capture the multiple access interference (MAI) in power unbal-

anced scenarios was investigated, and it was shown to be applicable to densely deployed networks. Another Gaussian approximation of MAI for chip synchronous and chip asynchronous scenarios was derived in [70] for a system with fixed number of pulses per symbol and fixed frame duration. Although adaptation of frame duration and number of pulses per symbol was analyzed in [112] in the context of medium access control (MAC) for UWB ad hoc networks, a mathematical framework for the MAI has not been developed. In [113] and [114], the radio resource allocation problem was analyzed as a theoretical constraint optimization problem for ad hoc networks, where the system throughput is maximized considering a UWB physical layer, traffic patterns, and system topology. Both reserved bandwidth (QoS) and dynamic bandwidth (best effort) scenarios are considered, and admission policies of new users to the system are presented.

In this chapter, adaptation of multiple access parameters is investigated in both synchronous and asynchronous environments for cluster based WSNs, and theoretical performance analysis to characterize the link quality is presented for different scenarios. For synchronous communications (downlink), an orthogonal TH sequence construction approach is proposed, which resembles the orthogonal variable spreading factor (OVSF) codes in CDMA systems [115]. For asynchronous communications, multiuser interference is modeled by a Gaussian approximation approach for two communication scenarios: *fixed frame duration*, where the goal is to maximize the overall data rate, and *fixed symbol duration*, where the goal is to have an identical data rate for all the users, and improve the network lifetime. For the fixed symbol duration case, the required symbol energy to meet the BER requirement is calculated, and the number of pulses to transmit is evaluated (which implies joint assignment of both the number of pulses per symbol and the frame duration, as the symbol duration is constant). Extension of the analysis to multipath channels is performed for both cases. Also, the validity of the Gaussian approximation for different parameters is evaluated using the Kullback-Leibler (KL) distance metric, and its effects on the BER is analyzed for different parameters and SINRs. Improvements in the data rate and power consumption for the adaptation schemes are demonstrated with computer simulations for fixed and mobile cluster head scenarios.

The chapter is organized as follows. Section 4.2 gives the system model for the UWB signaling and the sensor network. Adaptation schemes for synchronous and asynchronous communications systems are analyzed in Section 4.3 and Section 4.4, respectively. Extensions to multipath channels are provided in Section 4.5. The validity of Gaussian approximation is investigated in Section 4.6,

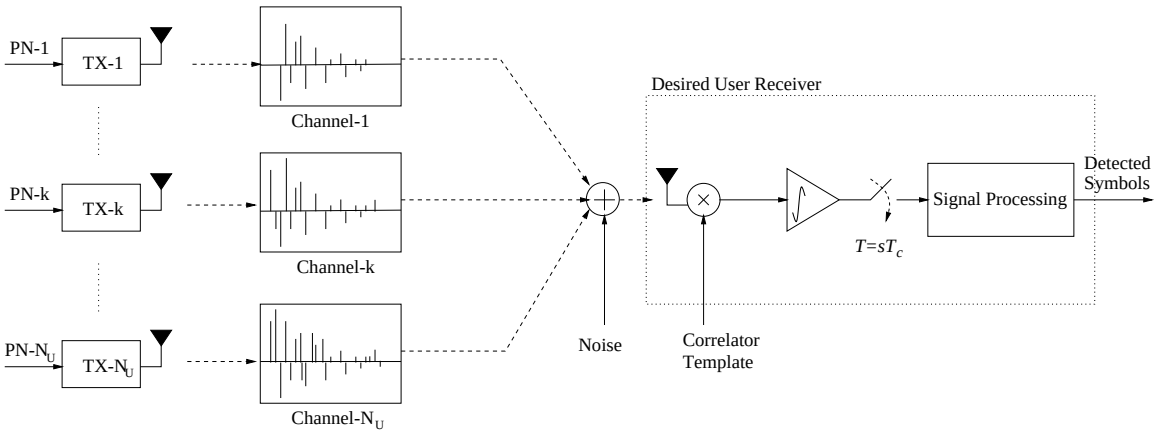

Figure 4.1 The received signals from multiple users and the correlator receiver.

which is followed by the simulation results in Section 4.7. Finally, some concluding remarks are made.

4.2 System Model

4.2.1 UWB Matched Filter Receiver for Variable Multiple Access Parameters

Consider the multiuser received signal model in (2.10), however with variable multiple access parameters $N_s^{(k)}$ and $N_h^{(k)}$. Then, we may design a MF receiver (see Fig. 4.1) with the following template signal for the zeroth bit of user ξ ($b_0^{(\xi)}$ without loss of generality):

$$s_{temp}^{(\xi)}(t) = \frac{1}{\sqrt{N_s^{(\xi)}}} \sum_{j=0}^{N_s^{(\xi)}-1} a_j^{(\xi)} \omega_{rx}(t - jT_f^{(\xi)} - c_j^{(\xi)} T_c - \tau_\xi) \ . \tag{4.1}$$

The output of the MF is then given by

$$Y = b_0^{(\xi)} \sqrt{E_{rp}^{(\xi)} N_s^{(\xi)}} + M + N \ , \tag{4.2}$$

where $N \sim \mathcal{N}(0\,,\,\sigma_n^2)$ is the output noise and M is the total MAI, which is given by

$$M = \sum_{k=1, k\neq\xi}^{N_u} M_k \ , \tag{4.3}$$

where M_k is the MAI from user k. The statistics of M will be analyzed in Section 4.4.

4.2.2 Sensor Network Model and BER Evaluation

A cluster based WSN is considered, where the cluster head has more complex circuitry, and therefore higher processing capabilities compared to the sensor nodes. Note that from robustness, self configurability, and an overall network lifetime perspective it is more appropriate that each node can have the capability to be the cluster head. However, this increases the overall cost of the nodes, as being a cluster head has considerably larger complexity, and in particular for UWB systems, requires a bank of correlators at each sensor node. Therefore, the former approach is taken for the rest of the chapter. The communication happens in rounds as in [116], where, after each round, the cluster head may update the multiple access parameters. Consider a cluster of N_u sensors, with each node having a transmitted pulse energy of $E_{tp}^{(k)}$ to communicate with the cluster head, which transmits the information to a remote base station. The received pulse energy for user k at the cluster head is given by

$$E_{rp}^{(k)} = E_{tp}^{(k)} \frac{\alpha_k}{d_k^n} \ , \tag{4.4}$$

where n denotes the path loss exponent, d_k is the distance between the kth sensor node and the cluster head, and α_k is the fading coefficient for user k. When there is no MAI, the probability of error for user k which employs binary phase shift keying (BPSK) modulation is given by

$$P_b^{(k)} = Q\left(\sqrt{\mathrm{SNR}_k}\right) = Q\left(\sqrt{\frac{N_s^{(k)} E_{rp}^{(k)}}{\sigma_n^2}}\right) \ , \tag{4.5}$$

where, energy per symbol (bit) of user k is given by $E_{rs}^{(k)} = N_s^{(k)} E_{rp}^{(k)}$, $Q(x)$ is given by $\frac{1}{2}\mathrm{erfc}(\frac{x}{\sqrt{2}})$, and SNR denotes the signal-to-noise ratio (interference effects will be considered later). Conventional UWB networks use the same number of pulses per symbol, and the same frame duration for each user, ensuring reliable communications with the furthest away user. If the minimum BER required by the system is given by P_b, the processing gain assigned to each user is given by

$$N_s = \frac{\left[Q^{-1}(P_b)\right]^2 \sigma_n^2}{E_{rp}^{min}} \ . \tag{4.6}$$

where E_{rp}^{min} denotes the minimum received pulse energy, which is from the furthest away user in an ideal environment. The raw data rate for each user is then given by $\frac{1}{N_s N_h T_c}$.

In order to better exploit the system resources, it is possible to change the number of pulses ($N_s^{(k)}$), and number of chips per frame ($N_h^{(k)}$), for each user based on the channel quality, the distance of the user from the cluster head, the long and short term fading effects, and the interference level in the system. In the following sections, first, synchronous communications will be considered, where the orthogonal construction of TH sequences allows interference-free communications, such as in the downlink. Then, adaptation of $N_s^{(k)}$ and $N_h^{(k)}$ in asynchronous systems is analyzed under a BER constraint and for two different cases: fixed frame duration (to maximize the data rate), and fixed symbol duration (to maximize the network lifetime). Later, extension to multipath scenarios will be covered, followed by the analysis of validity of Gaussian approximation for different multiple access parameters.

Table 4.1 Code construction algorithm for synchronous communications.

```
for k = 1 : N_u
  c^k = rand(S, N_s^(k))
  S = S − c^k
end
```

4.3 Synchronous Communications

In synchronous communications, it is possible to design the TH codes orthogonally to avoid MAI. In this mode of operation, the cluster head may assign just enough number of pulses to each sensor node k to ensure the desired BER P_b

$$N_s^{(k)} = \left\lceil \frac{\left[Q^{-1}(P_b)\right]^2 d_k^n \sigma_n^2}{E_{tp}^{(k)} \alpha^k} \right\rceil \ , \tag{4.7}$$

where $\lceil x \rceil$ is the smallest integer greater than or equal to x. The orthogonal construction of the codes with different processing gains is carried out as follows. Let N_c denote the number of chip positions within the symbol period. After each round, each sensor can report the observed SNR, and using (4.7), the cluster head can evaluate N_c prior to constructing a new set of time hopping codes as follows:

$$N_c = \sum_{k=1}^{N_u} N_s^{(k)} \ . \tag{4.8}$$

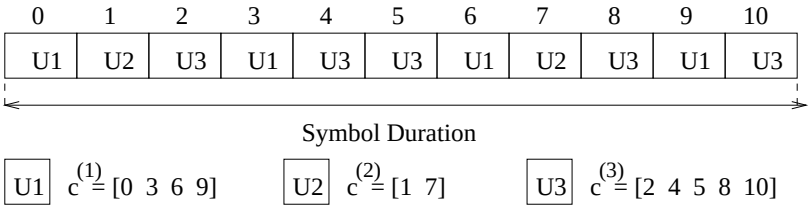

Figure 4.2 An example code construction for three users with different processing gains.

Note that N_c is a just enough number of chips per symbol, and determines the data rate common to all sensor nodes. In addition to changes in channel quality due to movements/deaths of the nodes or a movement of the cluster head, the distances may change, which may change the value of N_c after each round. After calculating N_c, the cluster head constructs the orthogonal codes as in Table 4.1, where $\mathbf{S}$ is the set of integers ranging from 1 to N_c, rand$(\mathbf{S}, N_s^{(k)})$ denotes $N_s^{(k)}$ random integers chosen from set $\mathbf{S}$, and the operator "$-$" excludes the set of numbers on the right of the operator from the set on the left of the operator. Note that conventional frame-based code and signal notation in (2.10) is not used here, where the sequence $\mathbf{c^k}$ for user k points to the locations of the pulses within the symbol, rather than within the frame (i.e. there are no frames, and the common symbol duration for all the nodes is N_cT_c). In Fig. 4.2, a simple example for the downlink TH sequences of 3 users employing different processing gains is presented in order to depict the construction of the TH codes, and clarify the distinctions between the signaling structures for synchronous and asynchronous cases. In a sense, the proposed construction is similar to the OVSF codes in CDMA systems [115]; however, our construction is more flexible, as the length of a particular code does not need to be a multiple of the length of any of the shorter length codes. For the sake of simplicity, the codes are constructed in a random manner, which works well for single tap (flat fading) channels. For dispersive channels, more sophisticated code designs can be used [13], where a larger pulse duration may be presumed to compensate for the channel effects.

The average data rate with the proposed scheme will improve since the average number of pulses per symbol decreases. The ratio of the data rates for the proposed and conventional approaches is

$$\frac{R_{prop}}{R_{conv}} = \frac{N_u T_s \max_k(N_s^{(k)})}{N_c T_s} = \frac{N_u \max_k(N_s^{(k)})}{\sum_{k=1}^{N_u} N_s^{(k)}} , \tag{4.9}$$

where R_{prop} and R_{conv} are the data rates for the proposed and conventional approaches, respectively. On the other hand, the total transmitted power for any round is fixed for all cases, and individual user powers are adapted indirectly through changing number of pulses per symbol. The proposed method also improves the energy consumption (per symbol), as less aggregate energy will be used per symbol.

4.4 Asynchronous Communications

In the previous section, it is assumed that the UWB system is completely synchronized. This requires compensation of delays in various multipath arrivals, which is not generally feasible in the uplink, but may be considered for downlink communications. Therefore, uplink transmission is usually assumed to be asynchronous, and multiple access interference degrades the system performance. For analytical purposes, we approximate an asynchronous UWB system by a chip-synchronous system, where the misalignment between the symbols of the users are integer multiples of the chip interval T_c. Assuming without loss of generality that the delay of the desired user is zero ($\tau_\xi = 0$), we assume that $\tau_k = \Delta_k T_c$ for $k \neq \xi$, where $\Delta_k \in \{0, 1, \ldots, N_h^{(k)} N_s^{(k)} - 1\}$ with equal probability. As studied in [70], the chip-synchronous assumption usually results in over-estimating the error probability, and hence the system design based on this approximation will be on the safe side.

In order to calculate the BER of the desired user in the presence of multiple users with random time hopping codes, we will employ Gaussian approximations for large number of pulses per information symbol. This is similar to the Gaussian approximations employed in [70] and [64]. However, we derive a more general formula in the case of different number of pulses per symbol in the fixed throughput case in Section 4.4.2.

4.4.1 Case 1: Fixed Frame Duration

In this case, the frame durations of all the users are the same. Hence, N_h is common for all of them (see for example Fig. 4.3a, where $N_s^{(1)} = 4$, $N_s^{(2)} = 3$, $N_s^{(3)} = 2$, and $N_h^{(k)} = 3$ for all k). The aim is to meet the BER requirement for all users in the system.

In order to satisfy a certain BER threshold, we adapt the number of pulses per symbol so that we can maximize the overall data rate of the system [110].

Similar to the approach in [70], we can approximate the MAI from user k by the following Gaussian random variable, when the number of pulses per information symbol for user ξ, $N_s^{(\xi)}$, is

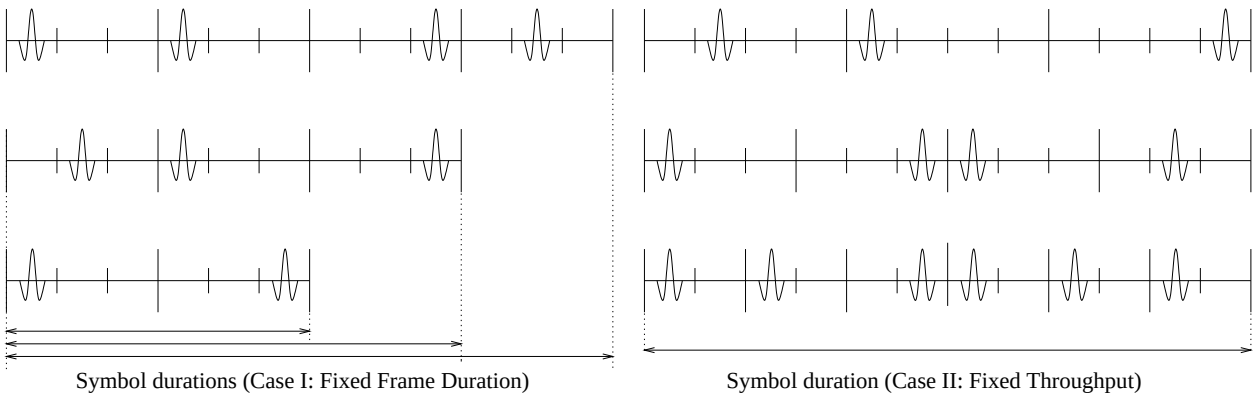

Figure 4.3 Example transmitted signals for a) Fixed frame duration, and b) Fixed throughput.

large:

$$M_k \sim \mathcal{N}\left(0\,,\,\frac{E_{rp}^{(k)}}{N_h}\right), \tag{4.10}$$

where $E_{rp}^{(k)}$ is the energy of a received pulse from user k.

Then, we can express, using (4.2) and (4.3), the SINR of the system for user ξ as

$$\text{SINR} \approx \frac{N_s^{(\xi)} E_{rp}^{(\xi)}}{\sigma_n^2 + \frac{1}{N_h}\sum_{\substack{k=1\\k\neq\xi}}^{N_u} E_{rp}^{(k)}}\,, \tag{4.11}$$

from which the value of $N_s^{(\xi)}$ can be obtained as

$$N_s^{(\xi)} = \left\lceil \frac{\text{SINR}}{E_{rp}^{(\xi)}} \left(\sigma_n^2 + \frac{1}{N_h} \sum_{\substack{k=1\\k\neq\xi}}^{N_u} E_{rp}^{(k)} \right) \right\rceil \quad . \tag{4.12}$$

In other words, by setting the value of $N_s^{(\xi)}$ according to (4.12), we transmit just enough number of pulses per symbol to meet the BER requirement. This is contrary to conventional systems, where the worst case parameters are used for all users, hence a lower overall data rate is obtained. Note that all the users transmit with the same power over a block, however, for a given transmit power, the bit rate will depend on the link quality.

4.4.2 Case 2: Fixed Throughput

Now consider the case where a fixed throughput is to be assigned to all users. Hence, we consider a common symbol time and BER in this scenario. In other words, the total processing gain defined by $N_c = N_s^{(k)} N_h^{(k)}$ is constant in this case (see Fig. 4.3b, where $(N_s^{(1)}, N_h^{(1)}) = (3,4)$, $(N_s^{(2)}, N_h^{(2)}) = (4,3)$, and $(N_s^{(3)}, N_h^{(3)}) = (6,2)$). Therefore, we can change the number of pulses per symbol and the frame duration as long as their multiplication is fixed. In this case, we employ the following lemma to approximate the MAI from user k:

Lemma 1: In a chip-synchronous scenario, the distribution of the MAI from user k converges to the following Gaussian random variable

$$M_k \sim \mathcal{N}\left(0\,,\,\frac{E_{rp}^{(k)}}{N_h^{(k)}}\right)\ , \tag{4.13}$$

as $\min\{N_s^{(\xi)}, N_s^{(k)}\} \longrightarrow \infty$.

Proof: See Appendix of [16].

In other words, for large values of $N_s^{(\xi)}$ and $N_s^{(k)}$, the MAI from user k converges to a zero mean Gaussian random variable.

From (4.13), the total MAI can be approximated as

$$M \sim \mathcal{N}\left(0\,,\,\sum_{k=1,k\neq\xi}^{N_u}\frac{E_{rp}^{(k)}}{N_h^{(k)}}\right)\ . \tag{4.14}$$

Then, the SINR of the system can be obtained as

$$\text{SINR} = \frac{N_s^{(\xi)} E_{rp}^{(\xi)}}{\sigma_n^2 + \sum_{\substack{k=1\\k\neq\xi}}^{N_u}\frac{E_{rp}^{(k)}}{N_h^{(k)}}}\ , \tag{4.15}$$

which can be expressed as

$$\text{SINR} = \frac{E_{rs}^{(\xi)}}{\sigma_n^2 + \frac{1}{N_c}\sum_{\substack{k=1\\k\neq\xi}}^{N_u} E_{rs}^{(k)}}\ , \tag{4.16}$$

by the defining the received *symbol* energy of the kth user by $E_{rs}^{(k)} = N_s^{(k)} E_{rp}^{(k)}$ for $k = 1, \ldots, N_u$.

When we assign the same SINR values to all the users, they have the same BER, hence the same throughput since they have the same symbol time. Hence, from (4.16), we see that we can choose the same received symbol energy to achieve the same BER for all users. Denoting that common energy by E_{rs}, we obtain from (4.16) that

$$E_{rs} = \frac{\sigma_n^2 \, \text{SINR}}{1 - \left(\frac{N_u - 1}{N_c}\right) \text{SINR}} \, . \tag{4.17}$$

In other words, for a desired SINR value, we can calculate the required received symbol energy of the users. Since the symbol energy is the multiplication of the number of pulses per symbol and the pulse energy, the received symbol energy can be expressed as

$$E_{rs} = E_{ts}^{(k)} \frac{\alpha_k}{d_k^n} = N_s^{(k)} E_{tp}^{(k)} \frac{\alpha_k}{d_k^n} \, . \tag{4.18}$$

Therefore, the users can use different number of pulses per symbol and/or different pulse energy depending on the channel state and their location. In a practical setting, the cluster head can calculate the SINR for each of the users and feedback them how to scale their symbol energy in order to achieve the desired SINR. Note that when a user is very far away from the cluster head or its channel is in a deep fade, the transmitted symbol energy needs to be increased considerably, which might violate the FCC's regulations [117]. Therefore, multi-hopping might be necessary in some cases.

The received signal energy in (4.18) implies that given the fading coefficient and distance of user k, the energy can be set by changing $N_s^{(k)}$ and/or $E_{tp}^{(k)}$. In other words, there is a flexibility in adjusting the symbol energy. Note that this is different from the reserved bandwidth (RB) case in [113], since $N_s^{(k)}$ and $N_h^{(k)}$ are both variable (their multiplication is constant) in our case. In [113], the RB case assumes $N_s^{(k)}$ is fixed (implying that $N_h^{(k)}$ is fixed as the data rate is fixed), and therefore the adaptation is acquired by only scaling $E_{tp}^{(k)}$.

Even though there is a flexibility in adjusting the received power, there are a few issues to consider when setting the symbol energy. First, the FCC's restriction on the peak-to-average signal ratio can restrict the use of very small $N_s^{(k)}$ values. Secondly, the inter-frame interference (IFI) can be an issue in a multipath environment when choosing the number of frames per symbol, where choosing larger frames reduces the effects of the IFI.

4.5 Extension to Multipath Channels

[1]Due to extremely short duration pulses employed, it is likely to observe individual multipath components (even though not being very dispersive) even in low-power and very short-range communications in densely deployed sensor networks. Longer-range communications may yield much severe and dispersive channel impulse responses, where the maximum excess delay of the channel may be on the order of hundreds of nanoseconds. Therefore, it becomes very crucial to consider the effects of multipath, since it has significant effect on the performance. Consider transmission over frequency selective channels, where the channel for user k is modeled as

$$h^{(k)}(t) = \sum_{l=1}^{L} \alpha_l^{(k)} \delta(t - (l-1)T_c - \tau_k) \ , \tag{4.19}$$

where $\alpha_l^{(k)}$ and τ_k are the fading coefficient of the lth path and the delay of user k, respectively, and L is the total number of received taps. We assume $\tau_1 = 0$, and $\sum_{l=1}^{L} |\alpha_l^{(k)}|^2 = 1$ without loss of generality.

From (2.1) and (4.19), the received signal can be expressed as

$$r(t) = \sum_{k=1}^{N_u} \sqrt{E_{rp}^{(k)}} \sum_{j=-\infty}^{\infty} a_j^{(k)} \, b_{\lfloor j/N_f \rfloor}^{(k)} u^{(k)} \left(t - jT_f^{(k)} - c_j^{(k)} T_c - \tau_k \right) + \sigma_n n(t) \ , \tag{4.20}$$

where

$$u^{(k)}(t) = \sum_{l=1}^{L} \alpha_l^{(k)} \omega_{rx} \left(t - (l-1)T_c \right) \ . \tag{4.21}$$

Consider a RAKE receiver for the ξth user, which has the following template signal for the 0th information bit:

$$s_{temp}^{(\xi)}(t) = \frac{1}{\sqrt{N_s^{(\xi)}}} \sum_{j=0}^{N_s^{(\xi)}-1} a_j^{(\xi)} v(t - jT_f^{(\xi)} - c_j^{(\xi)} T_c) \ , \tag{4.22}$$

where

$$v(t) = \sum_{l=1}^{L} \beta_l \omega_{rx} \left(t - (l-1)T_c \right) \ , \tag{4.23}$$

[1]This section was mostly contributed by Sinan Gezici, and is included here for completeness.

with $\boldsymbol{\beta} = [\beta_1, ..., \beta_L]$ being the RAKE combining weights. As considered in [118], the template signal given by (4.22) and (4.23) can represent different multipath diversity combining schemes by appropriate choices of the weighting vector $\boldsymbol{\beta}$.

From (4.20)-(4.23), the output of the Rake receiver can be expressed as follows:

$$Y = \int r(t) s_{temp}^{(\xi)}(t) dt = b_0^{(\xi)} \sqrt{N_s^{(\xi)} E_{rp}^{(\xi)}} \sum_{l=1}^{L} \alpha_l^{(\xi)} \beta_l + M + N, \tag{4.24}$$

where the first term is the desired signal part, M is the MAI from other users and N is the output noise, which is approximately distributed as $N \sim \mathcal{N}\left(0\,,\, \sigma_n^2 \sum_{l=1}^{L} \beta_l^2\right)$ for large $N_s^{(\xi)}$ [118]. We assume $N_h^{(\xi)} \gg (L-1)$ so that the IFI and the inter-symbol interference (ISI) are negligible [119].

The MAI term in (4.24) can be expressed as in (4.3); that is, as the sum of MAI terms from other users.

For the fixed frame duration case, the result in [118] can be directly applied to this case by observing that the polarity codes make the distribution of the MAI terms independent of the information bits. In this case, we obtain

$$M_k \sim \mathcal{N}\left(0\,,\, \frac{E_{rp}^{(k)}}{N_h}\left[\sum_{j=1}^{L}\left(\sum_{l=1}^{j} \beta_l \alpha_{l+L-j}^{(k)}\right)^2 + \sum_{j=1}^{L-1}\left(\sum_{l=1}^{j} \alpha_l^{(k)} \beta_{l+L-j}\right)^2\right]\right) \tag{4.25}$$

for large $N_s^{(\xi)}$ [118].

For the fixed symbol interval case, we have the following result:

Lemma 2: In a chip-synchronous scenario, the distribution of the MAI from user k converges to the following Gaussian random variable

$$M_k \sim \mathcal{N}\left(0\,,\, \frac{E_{rp}^{(k)}}{N_h^{(k)}}\left[\sum_{j=1}^{L}\left(\sum_{l=1}^{j} \beta_l \alpha_{l+L-j}^{(k)}\right)^2 + \sum_{j=1}^{L-1}\left(\sum_{l=1}^{j} \alpha_l^{(k)} \beta_{l+L-j}\right)^2\right]\right), \tag{4.26}$$

as $\min\{N_s^{(\xi)}, N_s^{(k)}\} \longrightarrow \infty$.

Proof: See Appendix of [16].

From (4.25) and (4.26), it is observed that the MAI from an interfering user converges, as $N_s^{(\xi)}$ and $N_s^{(k)}$ go to infinity, to Gaussian random variables with zero mean, similar to the ones in (4.10) and (4.13), with the only difference being scaling factors to the variance terms, which purely depend on the multipath channel of the interfering user and the finger assignment of the RAKE receiver. In

other words, the same dependence on the received pulse energy and the processing gain parameters (N_s and N_h) is preserved as in the AWGN case.

4.6 Validity of Gaussian Approximation

In the previous sections, Gaussian approximations were used to model the multiuser interference in an asynchronous environment. In this section, the dependence of the accuracy of Gaussian approximation on the multiple access parameters is analyzed using the KL distance [120]. Moreover, the accuracy of the Gaussian approximation is evaluated for different SNR values.

4.6.1 KL Distance Between the Approximate and Actual MAI Distributions

Consider the equations (4.10) and (4.13) for *case 1* and *case 2*, respectively, where the interference from a second user was approximated using a Gaussian distribution with its variance depending on the parameters $N_s^{(\xi)}$, $N_h^{(k)}$, and $E_{rp}^{(k)}$ ($N_h^{(k)}$ is constant for *case 1*). In order to see how well the approximation captures the actual interference probability density function (PDF), the theoretical Gaussian PDF and the MAI PDF obtained from simulations can be compared for different ranges of multiple access parameters. The KL distance (or relative entropy) is commonly used to characterize the similarity between two distributions. Let $f_{theo}^{N_s^{(\xi)},N_h^{(k)}}$ denote the PDF of the interference corresponding to a set of parameters $N_s^{(\xi)}$, $N_h^{(k)}$; and let $f_{sim}^{N_s^{(\xi)},N_h^{(k)}}$ denote the PDF of the interference generated using simulations and corresponding to the same set of parameters. Then, the KL distance between two distributions is given by

$$K\left(f_{theo}^{N_s^{(\xi)},N_h^{(k)}} || f_{sim}^{N_s^{(\xi)},N_h^{(k)}}\right) = \sum_{i=-\infty}^{\infty} f_{theo}^{N_s^{(\xi)},N_h^{(k)}}(i) \times \ln \frac{f_{theo}^{N_s^{(\xi)},N_h^{(k)}}(i)}{f_{sim}^{N_s^{(\xi)},N_h^{(k)}}(i)} \,. \tag{4.27}$$

The larger the KL distance, the less would be the similarity between the two PDFs. As the KL distance metric is not symmetric, the average of the two KL distances (i.e. $K(f_{theo}||f_{sim})$ and $K(f_{sim}||f_{theo})$) is used in this chapter to evaluate the similarity between the two distributions.

Note that while the interference distribution lies between $(-\sqrt{E_{rp}^{(\xi)}N_s^{(\xi)}}, \sqrt{E_{rp}^{(\xi)}N_s^{(\xi)}})$, the support of the theoretical Gaussian distribution is $(-\infty, \infty)$. Analyzing (4.27) under this fact implies that KL distance may converge to infinity if not properly treated. Therefore, as an approximation, we truncate the theoretical Gaussian distribution to lie within the support of the interference dis-

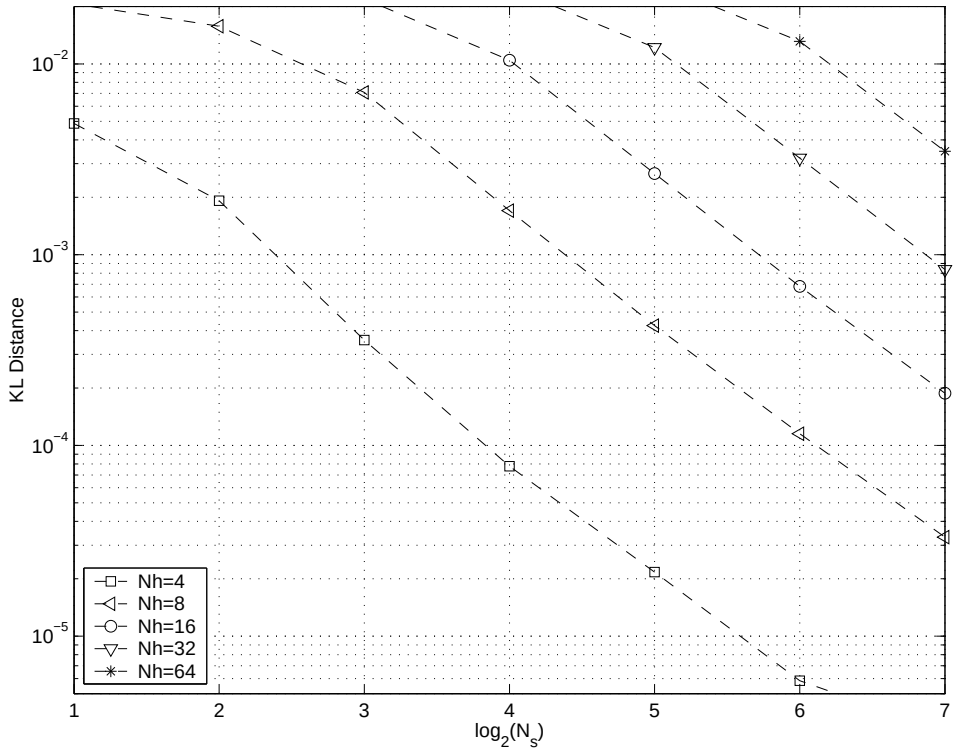

Figure 4.4 KL distances for case-1 with respect to $N_s^{(\xi)}$ and $N_h^{(k)}$. Only two users with equal power are considered.

tribution, and the area under the (omitted) tails of the Gaussian distribution are included as delta functions at the edges of the truncated Gaussian distribution.

In Fig. 4.4, simulation results for *case 1* are presented for various values of frame durations and processing gains. Two users with equal power levels are considered, and the KL distances are computed for different values of $N_s^{(\xi)}$ and $N_h^{(k)}$. It is observed that the MAI converges to a Gaussian distribution for larger values of $N_s^{(\xi)}$, and for smaller values of $N_h^{(k)}$ (2.10^7 bits are used in simulations). Similar simulations are repeated for *case 2*, where similar results are observed.

4.6.2 BER Performances Using the GA and the Actual MAI Distribution

Even though the KL distance characterizes the accuracy of Gaussian approximation for different set of parameters (relative to another set of parameters), how much this will affect the BER is also dependent on SNR. For example, if the noise variance is large, inaccuracy of the Gaussian approximation may not yield significant deviations from the actual BER. On the other hand, BER

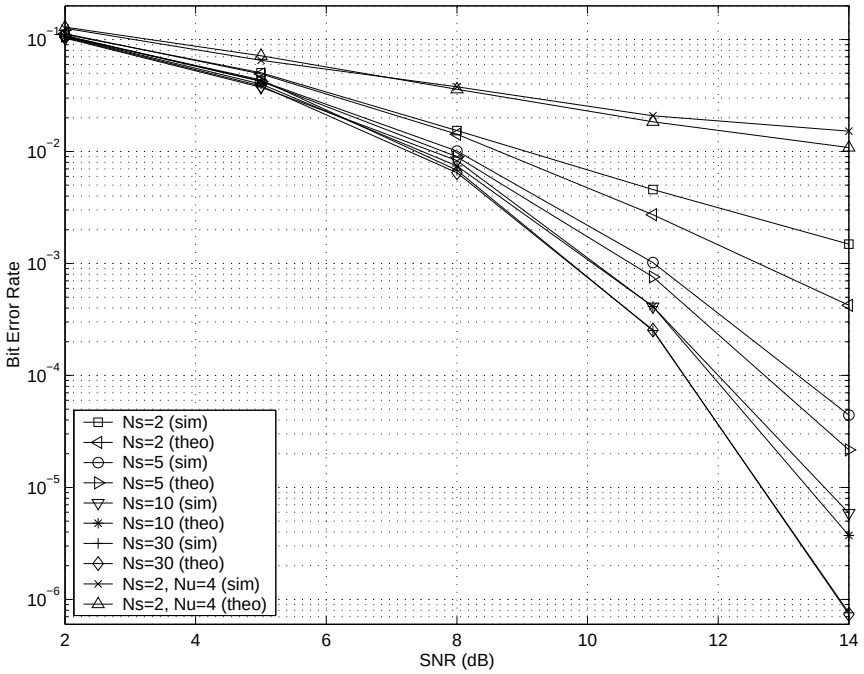

Figure 4.5 Comparison of theoretical and simulation BERs for *case 1*. Only two users with equal power are considered ($N_h = 10$).

of the systems operating at high SNR environments may be very sensitive against inaccuracies in the Gaussian approximation.

In Fig. 4.5, the BER vs. SNR curves for *case 1* and for different multiple access parameters are presented, which are obtained using the simulations and the Gaussian approximation. It is observed that the larger values of N_s increases the accuracy of Gaussian approximation. It is also seen that as the SNR increases, the deviation between the BERs obtained using the Gaussian approximation and the simulations increases. The theoretical and simulation BER results for four users were also presented for comparison purposes, where it can be observed that Gaussian approximation provides a tighter bound.

4.7 Simulation Results

Computer simulations are performed to demonstrate the improvements in the data rate and reductions in power consumption for synchronous and asynchronous scenarios. Only a *single cluster* of a WSN is considered in the simulations, and 100 sensor nodes are randomly distributed over a 25×25 meters field. The results can also be generalized for multiple clusters, where sensor nodes

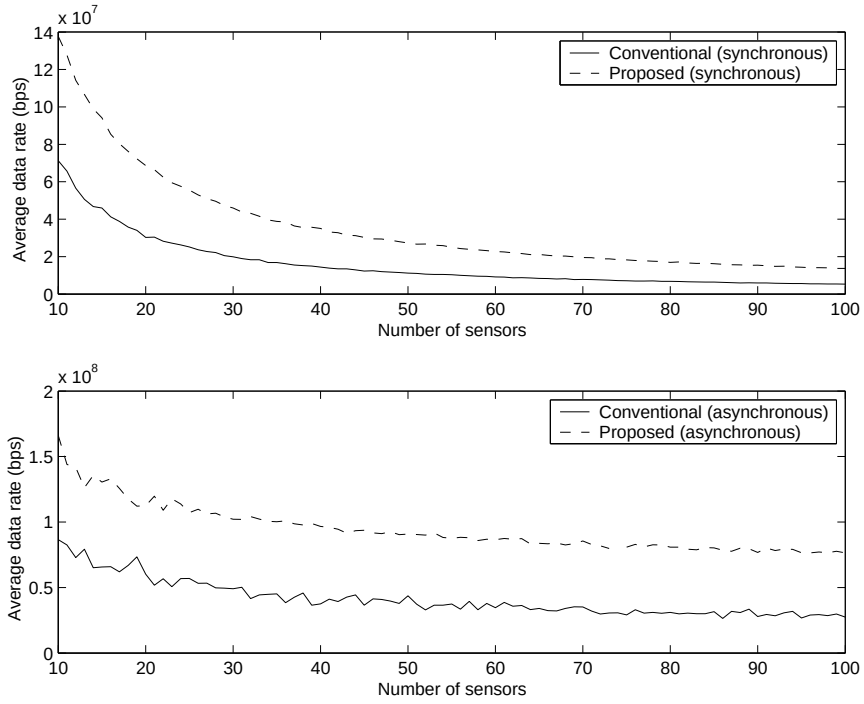

Figure 4.6 Data rate improvements using the adaptive approach in synchronous and asynchronous scenarios.

in each cluster communicate adaptively with the cluster head, and the cluster heads (which form another upper-level cluster within themselves) communicate adaptively with the sink. Corresponding to a BER of 10^{-4} for BPSK modulation, SNR = 8.39dB is targeted. The path loss exponent is taken to be $n = 2.4$, the pulse width is set to $T_c = 0.3$ns, and the chip synchronous case is considered in all scenarios. It is assumed that the transmitted pulse occupies the whole 7.5GHz of bandwidth in between 3.1GHz – 10.6GHz. Since the FCC mask allows a maximum transmission power of -41dBm/MHz within this frequency range, the maximum transmit energy per second can be calculated to be 0.562mW. This is the maximum power that any sensor can transmit within the limits of FCC regulations, which might restrict the selection of optimum N_h and N_s even if SINR is appropriate.

For synchronous communications, the data rate improvement with respect to the number of users is evaluated when optimum $N_s^{(k)}$ is used to construct orthogonal sequences for each user (equations (4.6) and (4.7)), and it is averaged over 100 realizations of the sensor distributions. The noise variance is taken to be 20dB weaker than the energy per transmitted pulse. Two schemes are

analyzed: the conventional approach, where the worst case processing gain is used for all the users; and the adaptive approach, where just enough processing gain is assigned to each user. Results in the first part of Fig. 4.6 show that the average data rate for the synchronous communications with the proposed method is at least twice that of the conventional approach. Note that Fig. 4.6 does not demonstrate the gains obtained due to deaths and mobilities of the sensors, which are exploited periodically to update the codes and increase the data rate. Furthermore, a straightforward analysis can be repeated to demonstrate the additional savings in power consumption due to the decrease in the average processing gain used per symbol.

For asynchronous communications, *case 1* and *case 2* are analyzed separately. For *case 1*, the Gaussian approximation is used to evaluate the data rates for conventional and proposed methods in an MAI-limited environment. The simulation results in the second part of Fig. 4.6 imply that increasing the number of sensors does not affect the data rate significantly as much as it affects the synchronous communications. This is because a fixed frame duration is used for different number of users, and the number of pulses per symbol is the only term that determines the data rate. In the conventional method, the data rate is lower-bounded by the data rate of the furthest away user, which does not change significantly with the number of users. For adaptive implementation, since fewer pulses are used for closer sensors, and higher aggregate data rates are achieved.

Simulation results for *case 2* are presented in Figs. 4.7 and 4.8, where the data rates are identical for all the users: $(N_c T_c)^{-1} = (10^4 \times 0.3 \times 10^{-9})^{-1} = 33$kbps. Continuous transmission of all the sensors, and very low initial battery energy assignments (1mJ) for each node are assumed for simulation purposes. The parameters are updated after each round of 300μsec to adapt to the Rayleigh fading channel and possibly changed distances, and the energy consumption in 5×10^4 rounds is analyzed. Simulation results indicate substantial gains in network lifetime when using adaptive assignment of processing gain (PG)[2]. Also, the effects of mobility of the cluster head (CH) is analyzed, which may be considered, for example, for rescue-robot applications where the robot acts as a cluster head to communicate with various sensors, and although the power consumption of the robot is not very crucial, we would like to maximize the network lifetime of the sensors. It is observed in Figs. 4.7 and 4.8 that if the cluster head randomly moves in the network, the network lifetime shortens seriously. On the other hand, the movement of the cluster head after each round to an optimal location (which is the expected value of the locations of the *alive* sensor nodes,

[2]Adaptive PG implies adaptation of N_s based on the distance between the transmitter and the receiver, while fixed PG implies fixed N_s regardless of the distance.

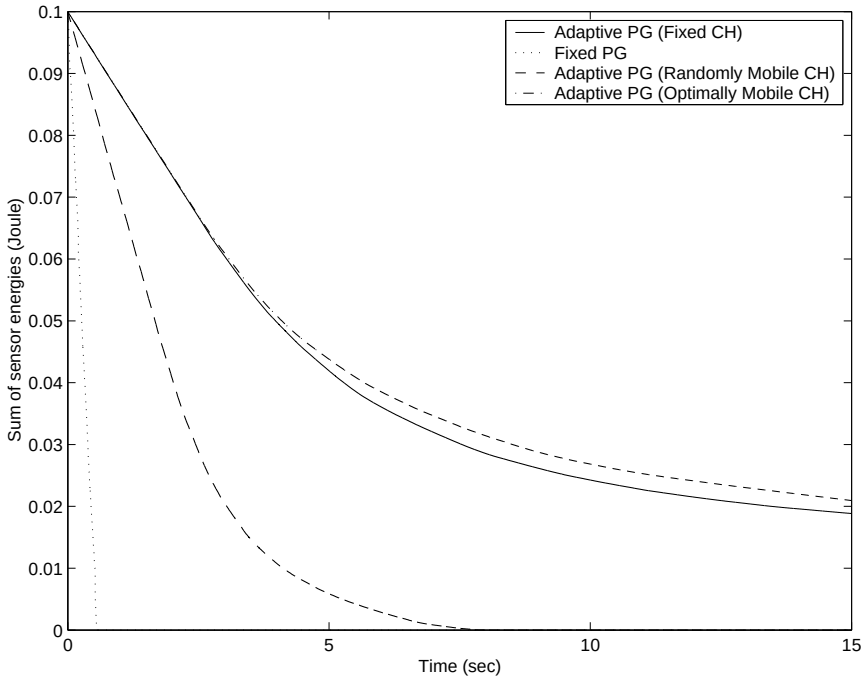

Figure 4.7 Remaining aggregate energy in the network with respect to time.

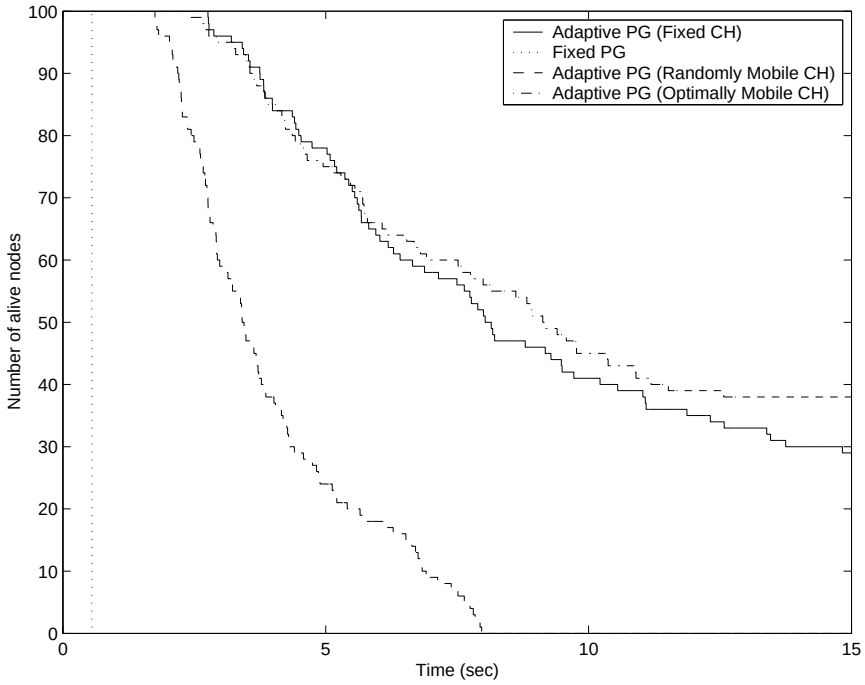

Figure 4.8 Number of alive nodes in the network with respect to time.

i.e. $E[x_s, y_s]$, where (x_s, y_s) are the coordinates of each sensor node) slightly increases the network lifetime compared to the case when the cluster head is motionless and located at the center of the network.

4.8 Conclusion

In this chapter, adaptation of multiple access parameters in cluster based UWB-IR WSNs has been analyzed for both synchronous and asynchronous communications systems. For synchronous communications, an orthogonal sequence construction scheme has been presented, which assigns variable processing gains to the sensors, and acquires the desired BER requirement at each sensor. For asynchronous communications systems, a Gaussian approximation method has been employed to adapt the transmission powers and the processing gains of the sensors, and a mathematical framework has been developed for the analysis of MAI when the users employ different numbers of pulses per symbol and different frame durations. The main contribution of the chapter is on the analysis of variable frame duration case, both in AWGN and in multipath channels. Also, the accuracy of the Gaussian approximation has been investigated and quantified using the KL distance based on the parameters (N_s, N_h) in a way not addressed in the literature before. It has been shown to be accurate for populated networks with large N_s, small N_h, and low SNR values. Simulation results outline the potential improvements in power savings and/or throughput using adaptive system design based on the two parameters.

Many of the analysis discussed in the chapter can also be extended to other centralized architectures (not necessarily cluster-based) that employ UWB signals, where a central node controls the assignment of TH codes to the other nodes. The main motivation behind considering UWB systems for WSNs is due to its uniquely fitting characteristics, including low-complexity transceiver circuitry, low-power transmission, and flexible bandwidth allocation.

CHAPTER 5

CHANNEL ESTIMATION FOR IR-UWB UNDER MULTIPLE ACCESS INTERFERENCE

5.1 Introduction

Accurate estimation of the channel is essential for successful detection of the transmitted symbols in UWB communication systems. However, accurate channel estimation is a difficult task in realistic multipath and multiple access environments.

Sampling the received signals at Nyquist rate gives enormous signal processing capabilities at the receiver for channel estimation. However, due to extremely short duration of pulses, Nyquist rate sampling of UWB signals is not practical. Instead, the signal can be sampled after analog front-end processing (such as analog filtering and correlation). Symbol-spaced, frame-spaced, and chip-spaced sampling are some possible sampling options. Symbol-spaced sampling of the received signal allows estimation of the channel based on white-noise assumption over all the pulses (all pulses are equivalently affected). However, often, multiuser UWB systems can be impaired by multi-access and multipath interference that only affects certain pulses. Frame-spaced sampling allows to estimate the noise variance over each pulse position, and discard heavily corrupted pulses before the channel estimation. Further increasing the sampling rate (e.g. chip-spaced channel estimation) allows implementation of all-Rake (*ARake*) receivers by only using a single analog correlator.

5.1.1 Prior Art on UWB Channel Estimation

Maximum likelihood (ML) data aided and non-data aided channel estimation techniques for UWB systems were considered in [121] in the presence of white noise to find both the delays and fading coefficients of the multipath components. Other ML based channel estimators were presented in [94, 122], and Cramer-Rao Lower Bounds (CRLB) for ML channel estimation in UWB systems were derived in [123]. Optimization of pilot symbol assisted modulation (PSAM) type of channel estimation was discussed in [124], iterative UWB channel estimation techniques were proposed

in [125]-[127], frequency-domain channel estimation schemes were considered in [128]-[130], and a space alternating expectation maximization (SAGE) algorithm was used towards UWB channel estimation in [131].

The computational complexities of the above techniques (especially ML based channel estimators) are usually high, especially if Nyquist rate sampling rates are required (e.g. [121, 94]). Some lower complexity UWB channel estimation techniques include semi-blind algorithms [132], subspace-based techniques [133], power of R (with R denoting the data covariance matrix) algorithm [134], blind algorithms using cyclostationarity of the UWB signaling with PPM [135], channel estimators with lower sampling rate requirements (ML channel estimator using swept sampling [136] and orthogonal sinusoidal correlation receiver (OSCR) based channel estimator [137]), and other non-training based algorithms [138]-[140]. A clustered low-complexity channel estimation technique was presented in [141], which uses a 2-stage approach. The first step estimates the nominal location and dispersion of a cluster (using ML or LS based techniques), and a second step concentrates around the estimated nominal parameters to reduce the complexity.

Mitigation of multiuser interference effects prior to channel estimation is also an important issue which was not investigated in detail in the literature. Chip discrimination [142] and blinking receiver [143] were proposed to improve the symbol detection performance when the noise is not white simply by discarding the strongly corrupted pulses. However, this requires the knowledge of either the signal to noise ratio (SNR) estimate on each pulse position of the desired user, or the time hopping (TH) sequences and delays of the other active users.

5.1.2 Work Done

Analysis and evaluation of UWB channel estimation schemes for different sampling rates have not been performed to the best knowledge of the authors. In this chapter, training based UWB channel estimation is analyzed for symbol spaced sampling, and a semi-blind approach is proposed to improve the spectral efficiency. For frame-spaced sampling, we propose a pulse-discarding receiver *prior to* the channel estimation (as opposed to previous pulse discarding receivers that require channel information). Also, a chip-spaced channel estimator is presented, which enables low-complexity collection of the available energy in various multipath components. Before all, prior art on UWB channel estimation will be briefly reviewed. Some of the notations used in the chapter are as follows:

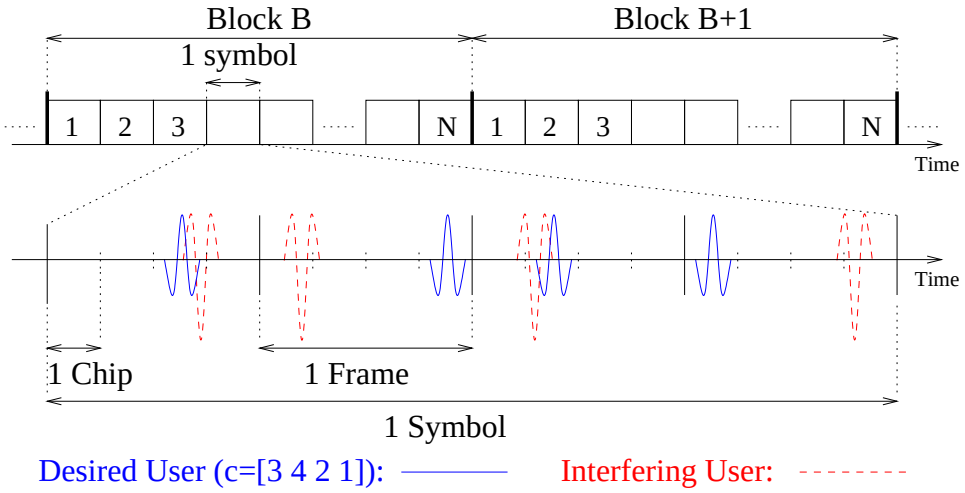

Figure 5.1 TH-UWB-IR signaling structure.

the Binomial and Gaussian distributions are represented with $\mathcal{B}$ and $\mathcal{N}$, respectively, $\delta_D(.)$ denotes the Dirac delta function, and $(.)^T$ is the transpose of a matrix/vector.

5.2 System Model

Consider a modification of the multiuser received signal model in (2.1) as follows to account the multipath effects

$$r(t) = \sum_{k=1}^{N_u} \sum_{l=1}^{L_k} \gamma_{kl} r_l^{(k)}\left(t - \tau_{kl}\right) \ , \tag{5.1}$$

where $r_l^{(k)}(t)$ represents the signal from the lth multipath component of the kth user, γ_{kl}, τ_{kl} are the fading coefficients and delays of the lth multipath component of the kth user, respectively, and the channel impulse response (CIR) of the kth user can be represented as

$$h_k(t) = \sum_{l=1}^{L_k} \gamma_{kl} \delta_D(t - \tau_{kl}) \ , \ \sum_{l=1}^{L_k} \left|\gamma_{kl}\right|^2 = 1 \text{ forall } k \ . \tag{5.2}$$

Also let (5.1) be observed over a block of N symbols where the channel is assumed stationary (n denotes the symbol index); for notational simplicity, we use E_k for the received symbol energy of the kth user, and b_{kn} for the nth bit of the kth user. Block, symbol, frame, and chip notations in a TH-UWB-IR system are summarized in Fig. 5.1, where it is also shown that multiple access

interference only affects certain pulses of the desired user. Note that the interfering user's pulses do not need to be chip aligned with the desired user's pulses, and the channels (τ_{kl} and γ_{kl}) of all users are assumed constant and independent at each block.

After the matched filter, the continuous signal in (5.1) can be sampled at symbol-spaced, frame-spaced, and chip-spaced rates (determined by the sampling rate s in Fig. 4.1, where channel estimation and symbol detection are achieved in 'Signal Processing' block). Consider initially a *frame-spaced sampled* signal over N symbols, where the correlator consists of unit-energy pulses matched to the received pulse shape. Assuming the desired user is the first user without loss of generality, we have

$$\mathbf{Y}_N^{(l)} = \mathbf{S}^{(l)}\mathbf{D}_N + \mathbf{Z}_N \ , \tag{5.3}$$

where $\mathbf{Y}_N^{(l)}$ is an $N_s \times N$ matrix of (frame-spaced) matched filter outputs (matched to desired user's signal) of the lth tap, $\mathbf{Z}_N$ is an $N_s \times N$ noise matrix with each element distributed with $\mathcal{N}(0, \frac{N_0}{2})$, $\mathbf{D}_N$ is a $N_u \times N$ data matrix of bits b_{kn}, and $\mathbf{S}^{(l)}$ is an $N_s \times N_u$ matrix where the elements s_{jk} characterizes the correlation of interfering users with the lth tap of user of interest. With desired user being the first user, we have $s_{j1} = \sqrt{\frac{E_1}{N_s}}\gamma_{1l}$, and (for $k \neq 1$)

$$s_{jk} = \begin{cases} 0 & , j\text{th pulse non-corrupted} \\ \sqrt{\frac{E_k}{N_s}}\tilde{b}_k\tilde{\gamma}_k R_{kj} & , j\text{th pulse corrupted by user } k \end{cases} \tag{5.4}$$

where R_{kj} identifies the correlation of the jth pulse of the desired user's template, and the kth user's pulse that interferes with the jth pulse of the template. Interfering bit and corresponding fading coefficient for the kth user are denoted by $\tilde{b}_k$ and $\tilde{\gamma}_k$, respectively. Note that neither the delays nor the fading amplitudes of the interferer pulses are known to the desired user's receiver in practice. For analytical purposes, consider a chip synchronous scenario, where we have

$$P_{s_{jk}}(x) = P_{nohit}\delta_D(x) + 0.5P_{hit}\delta_D\big(x - \sqrt{E_k/N_s}\big) + 0.5P_{hit}\delta_D\big(x + \sqrt{E_k/N_s}\big) \ , \tag{5.5}$$

and

$$P_{nohit} = \big(1 - \frac{1}{N_h}\big), \ P_{hit} = 1 - P_{nohit} \ . \tag{5.6}$$

The mathematical model for *symbol-spaced sampling* can be easily obtained from (5.3) as

$$\mathbf{y}_N^{(l)} = \mathbf{1}_{N_s} \mathbf{Y}_N^{(l)} \ , \tag{5.7}$$

where $\mathbf{y}_N^{(l)}$ is an $1 \times N$ vector of symbol-spaced samples for the lth tap, and $\mathbf{1}_{N_s}$ is an $1 \times N_s$ vector of ones.

In order to represent *chip-spaced samples*, we will transform each codeword entry $c_j^{(k)}$ into a vector $\tilde{\mathbf{c}}_j^{(k)}$, where $\tilde{\mathbf{c}}_j^{(k)}$ is a zero vector of $1 \times N_h$, with only the entry $c_j^{(k)}$ being 1. Also denote $\mathbf{C}^{(k)} = \left[\tilde{\mathbf{c}}_1^{(k)} \ \tilde{\mathbf{c}}_2^{(k)} \ \cdots \ \tilde{\mathbf{c}}_{N_s}^{(k)} \ 0 \ 0 \cdots \ 0\right]$ to be a vector of length $1 \times N_h N_s + L - 1$, where $L-1$ zeros are concatenated to incorporate a chip-spaced channel of length L. Furthermore, let $\mathbf{C}_l^{(k)}$ represent $\mathbf{C}^{(k)}$ circularly-shifted by $l-1$ in the positive direction, $\tilde{\mathbf{C}}^{(k)} = \left[(\mathbf{C}_0^{(k)})^T \ (\mathbf{C}_1^{(k)})^T \ \cdots \ (\mathbf{C}_{L-1}^{(k)})^T\right]$ denote a codeword matrix of size $N_c \times L$ (where $N_c = N_s N_h + L - 1$), and $\mathbf{h}_k = [\gamma_{k1} \ \gamma_{k2} \cdots \ \gamma_{kL}]$ denote the chip-spaced *hypothesized* channel model. Then, the chip-spaced received signal model is given by (assuming first-user w.l.o.g.)

$$\bar{\mathbf{Y}}_N = \tilde{\mathbf{C}}^{(1)} \mathbf{h}_1 b_N^{(1)} + \bar{\mathbf{Z}}_N \ , \tag{5.8}$$

where $\bar{\mathbf{Y}}_N$ and $\bar{\mathbf{Z}}_N$ are $N_c \times N$ chip-spaced signal and noise matrices (note that noise samples have the same statistics as in $\mathbf{Z}_N$, and MAI can be also further folded into noise), respectively, and $b_N^{(1)}$ is an $1 \times N$ vector of bits for the desired user.

5.3 Channel Estimation

Channel estimation in UWB systems is the task of estimating timing (τ_l), fading coefficient (γ_l), and pulse shape (ω_l) of each individual multipath component l that will be used in the detection process. In this chapter, we assume perfect knowledge of the path delays and pulse shapes (except for the chip-spaced sampling, where a chip-spaced CIR is hypothesized), and try to estimate the fading coefficients from the matched filter outputs. Accurate estimation of fading coefficients is especially crucial for accurate detection of symbols in (coherent) binary/M-ary pulse amplitude modulation schemes, for selective Rake (*SRake*) receivers to order the taps, and for maximum ratio combining (MRC) of the channel taps for the purpose of maximizing the SNR.

5.3.1 Symbol-Spaced Channel Estimation

Symbol-spaced channel estimation can be achieved by transmission of training (non-data) bits which are known both to transmitter and receiver. In a multiuser environment, interference from other users can severely degrade the channel estimation. Even if the interference is only over a single pulse, this can degrade the channel estimation and yield large mean square error (MSE) if the interferer's power is dominant with respect to the processing gain of the desired user. Let N_T denote the number of training symbols transmitted; then, the channel estimate for the desired user is given as

$$\hat{\gamma}_{1l}^{(tr)} = \frac{1}{\sqrt{E_1/N_s}N_T N_s}\mathbf{1}_{N_s}\mathbf{Y}_{N_T}^{(l)}(\mathbf{b}_{N_T}^{(1)})^T \ , \tag{5.9}$$

where $\hat{\gamma}_{1l}^{(tr)}$ and $b_{N_T}^{(1)}$ are the training-based channel estimate of the lth tap, and $1 \times N_T$ vector of training bits of the desired user, respectively (where the data to training ratio is given by $\frac{N-N_T}{N_T}$). Note that multiple channel estimates for different l can be achieved for Rake reception, which can be implemented by using multiple sets of training symbols with different offsets (still using symbol-spaced sampling). Inserting (5.3) into above yields

$$\hat{\gamma}_{l1}^{(tr)} = \frac{1}{\sqrt{E_1/N_s}N_T N_s}\mathbf{1}_{N_s}\mathbf{S}^{(l)}\tilde{\mathbf{D}}^T + \tilde{z} \ , \tag{5.10}$$

where $\tilde{\mathbf{D}} = \begin{bmatrix} N_T & d_2 & d_3 & \cdots & d_{N_u} \end{bmatrix}$ is an $1 \times N_u$ vector, $d_k = 2\bar{d} - N_T$, $\bar{d} \sim \mathcal{B}(N_T, 0.5)$, and $\tilde{z}$ denotes the noise after the channel estimator. Upon further processing, we obtain

$$\hat{\gamma}_{1l}^{(tr)} = \gamma_{1l} + \tilde{m} + \tilde{z} \ , \tag{5.11}$$

where $\bar{m}$ is the multiple access interference (MAI), and is given by

$$\bar{m} = \frac{1}{\sqrt{E_1/N_s}N_T N_s}\sum_{j=1}^{N_s}\sum_{k=2}^{N_u} s_{jk}d_k \ . \tag{5.12}$$

From central limit theorem, for large N_s and N_u, $\bar{m}$ approaches a Gaussian distribution, and the corresponding MSE can be calculated.

The training based channel estimation discussed above does not exploit the information in the data bits. By processing the data bits, the data-to-training symbol ratio can be improved considerably, increasing the spectral efficiency. In this chapter, we propose to estimate the amplitudes of each fading coefficient from solely the data symbols, and estimate the phase by transmitting few training symbols. For M-ary modulation schemes, expectation maximization (EM) algorithm can be used to estimate the cluster centers, from which phase can be easily estimated. For BPSK modulation considered in this chapter, due to the complexity of EM algorithm, we propose to use a simple absolute value-based (AVB) algorithm to estimate the amplitudes of the fading coefficients, followed by the polarity estimation. The channel estimate after the first step is calculated as

$$\tilde{\gamma}_{1l}^{(avb)} = \pm \frac{1}{\sqrt{E_1/N_s} N N_s} \left| \mathbf{1}_{N_s} \mathbf{Y}_N^{(l)} \right| \mathbf{1}_N^T \ , \tag{5.13}$$

where $\tilde{\gamma}_{1l}^{(avb)}$ denotes the channel estimate of the lth tap of desired user with $e^{\pm j\pi}$ phase ambiguity. The phase can then be resolved by transmission of few training symbols, and the channel estimate is given by

$$\hat{\gamma}_{1l}^{(avb)} = \underset{\tilde{\gamma}_{1l}^{(avb)}}{\operatorname{argmin}} \left| \tilde{\gamma}_{1l}^{(avb)} - \hat{\gamma}_{1l}^{(tr)} \right| \ , \tag{5.14}$$

where $\hat{\gamma}_{1l}^{(tr)}$ is the channel estimate using few training bits (solely for phase estimation purposes). Using simple probability theory techniques, and when the phase is exactly known, the eventual distribution of AVB channel estimate can be easily calculated as

$$P_{\tilde{\gamma}_{1l}^{(avb)}}(x|x>0) = \frac{1}{\sqrt{2\pi\sigma_z^2}} \left(e^{-\frac{(x-\gamma_{1l})^2}{2\sigma_z^2}} + e^{-\frac{(-x-\gamma_{1l})^2}{2\sigma_z^2}} \right) \ , \tag{5.15}$$

and $P_{\tilde{\gamma}_{1l}^{(avb)}}(x|x<0) = 0$. Note that this approach will yield a better MSE than training based channel estimation if the perfect phase knowledge is assumed. After incorporating the phase estimation error, final channel estimate is given by

$$\hat{\gamma}_{1l}^{(avb)} = E\left[\tilde{\gamma}_{1l}^{(avb)}\right] P_{\hat{\gamma}_{1l}^{(tr)}}(x>0) - E\left[\tilde{\gamma}_{1l}^{(avb)}\right] P_{\hat{\gamma}_{1l}^{(tr)}}(x<0) \ , \tag{5.16}$$

from which the MSE can be evaluated.

5.3.2 Frame-Spaced Channel Estimation

In the previous section, it was assumed that we do not have high enough sampling rate to sample the received signal at frame rate, which limits the signal processing capability to improve the performance of our channel estimator. As discussed in the previous sections, interference from other users can severely degrade the channel estimation, as well as accurate detection of the transmitted symbols. If frame-spaced samples are available, they can be processed to implement low-complexity pulse discarding algorithms. Conventional pulse discarding methods proposed for enhanced detection of symbols in multiuser scenarios assume either the perfect knowledge of the channel and set a pulse-discarding threshold after correlator that optimizes the BER [142], or, assume the perfect knowledge of the time hopping sequences to determine the corrupted pulses [143]. However, in practice, neither of these are available to the receiver, and channel estimation itself can be improved by discarding the pulses appropriately.

Note that special care needs to be taken when discarding the pulses, as they will be also used in the detection process. If a pulse is not corrupted significantly, it may be better not to discard it. Interference due to corrupted pulses from far users can be folded into Gaussian noise, which is a valid assumption for large N_s [143]. However, for near user interference, some of the pulses can be significantly affected compared to others. Especially when the signal to interference ratio (SIR) is very low (which may be as small as -40dB), this may severely prevent the detection of the transmitted bits. In this chapter, we propose a threshold based on the second order statistics of frame-spaced matched filter outputs (i.e. elements y_{jn} of $\mathbf{Y}_N^{(l)}$), which after evaluating over N bits is given by

$$\Sigma_j = E\big[(b_{1n}\gamma_{1l} + I_{jn} + z_{jn})^2\big] = (\gamma_{1l})^2 + E\big[I_{jn}^2\big] + \sigma_z^2 \ , \tag{5.17}$$

and where $\Sigma_j = E\big[y_{jn}^2\big]$. The term I_{jn} represents the total interference over jth pulse, which is the only frame-dependent component in the second order statistics. As in a well-designed UWB system, very few of the pulses will be corrupted, and Σ_j will be similar for different pulse positions, except the ones that are significantly corrupted. We propose here a threshold that accounts the mean and minimal points of the histogram of Σ_j, which is given by

$$\xi = 2E\big[\Sigma_j\big] - \min\big(\Sigma_j\big) \ , \tag{5.18}$$

where the pulses with $\Sigma_j > \xi$ are discarded prior to channel estimation and symbol detection. Note that this is different than both [142, 143], as neither the channel estimates nor the TH sequences are known *a priori*. Note also that the threshold given above can be further optimized by optimizing the detection SNR; however, in here, we only consider the channel estimation aspects.

5.3.3 Chip-Spaced Channel Estimation

Symbol and frame spaced models in previous sections assume that the desired user is already synchronized to the particular taps, and we would like to estimate their fading coefficients for better reception. However, synchronization process itself can require higher sampling rates; for symbol/frame spaced sampling, multiple sampling devices can be used to lock into particular strong multipath components. When chip-spaced sampling is used, the receiver hypothesizes a multipath component at each chip-spaced sample, and using a single-correlator, the channel observed by the receiver can be estimated. Although the matched filtering is achieved in analog domain, different Rake reception schemes (*ARake, SRake, PRake* etc.), and different combining schemes (MRC, EGC etc.) can be implemented in digital domain. Using the chip spaced model previously discussed, the least squares (LS) channel estimate is evaluated as

$$\mathbf{h}_1 = \frac{1}{N_T}\big((\tilde{\mathbf{C}}^{(1)})^T\tilde{\mathbf{C}}^{(1)}\big)^{-1}(\tilde{\mathbf{C}}^{(1)})^T\bar{\mathbf{Y}}_{N_T}(b_{N_T}^{(1)})^T \ . \tag{5.19}$$

Note that the channel order L is assumed to be known *a priori* to the receiver in order to construct the matrix $\tilde{\mathbf{C}}^{(1)}$. Also, the received signal energies are folded into channel estimates.

5.4 Simulation Results and Discussion

Computer simulations are performed to evaluate the performances of the channel estimation algorithms in single and multiuser scenarios and at different sampling rates. The frame duration, number of pulses per bit, block length, and number of users are set to $N_h = 5, N_s = 20, N = 40$, and $N_u = 5$, respectively. In Fig. 5.2, MSE of training based channel estimator (CE) with $N_T = 10$ training bits is compared with the AVB CE with $N_T = 10, 5, 3$ bits, where remaining bits in the block for all cases are used as data bits. The simulation results show that exploiting the information in the data bits considerably improves the performance for high SNR region. When the SNR is low, phase estimation error increases, and the performance of semi-blind channel estimator suffers.

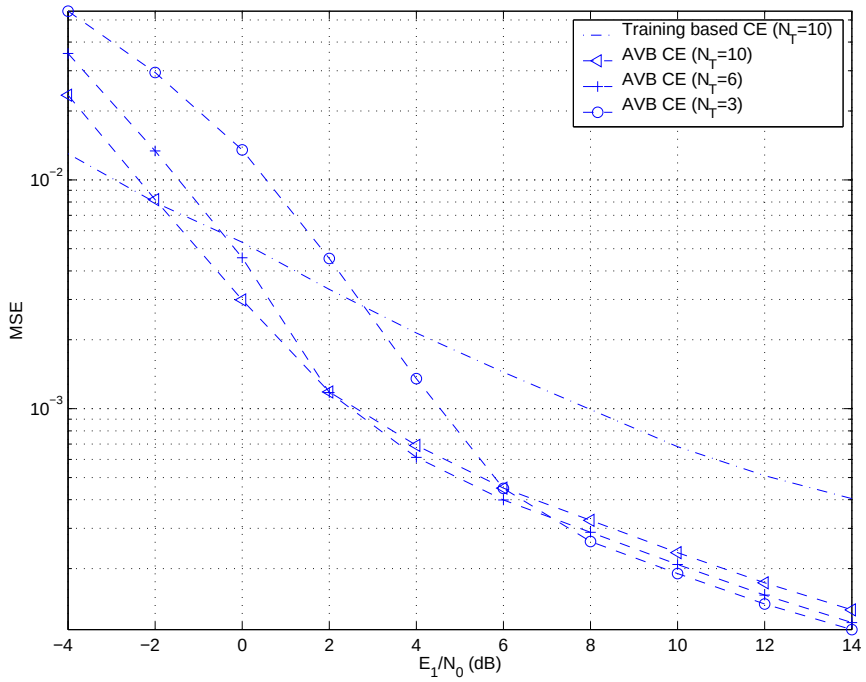

Figure 5.2 Comparison of training based and AVB channel estimation algorithms.

Transferring more training bits at low SNR region is more preferable for semi-blind case, while on the other hand larger number of data bits yields a better channel estimator at high SNR region. Note that the information in the training bits can be also used to assist estimation of the channel amplitudes, which would yield a better MSE.

Performance improvement in frame-spaced channel estimation due to pulse discarding is demonstrated in Fig. 5.3. Single user and 10 user cases are evaluated. For 10 user case, 8 users have identical powers with the desired user, and two different cases where the last user's received power is 10db and 20dB stronger than the desired user are considered, and results are averaged over 10^4 trials, where at each trial the TH codes of users are randomly generated. It is observed that discarding the pulses slightly increases the MSE for the single user case. However, for multiple access channels, there are considerable gains, especially in the presence of a user that has significantly larger received signal power than the desired signal.

Finally, we have investigated what portion of the energy can be captured using chip spaced sampling. The channel models of [2] are used, where arrival times are Poisson distributed as in Fig. 5.4a. Each channel realization is sampled at chip-space of 0.8ns using a template of $N_s = 4$

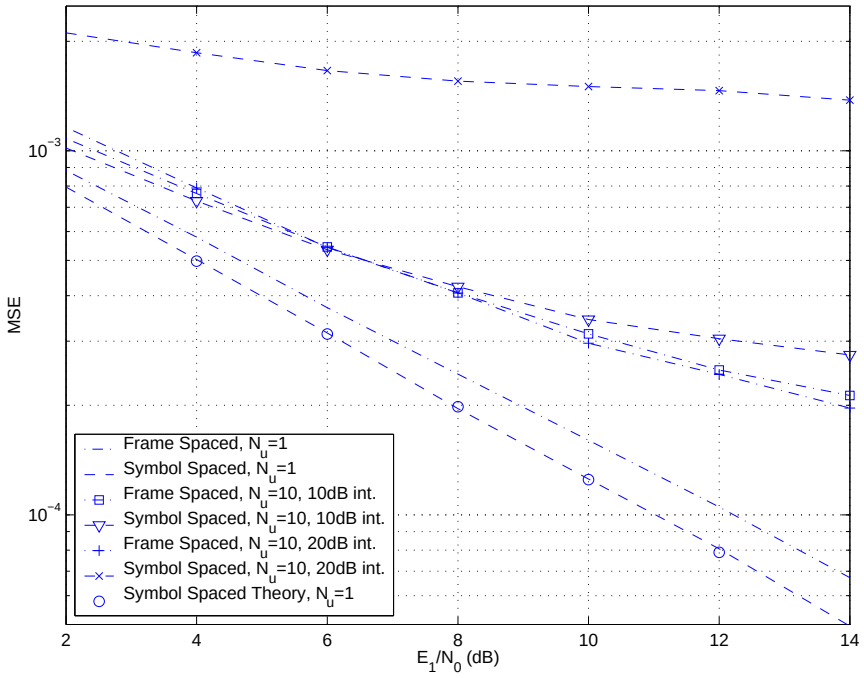

Figure 5.3 Performance of pulse discarding algorithm.

pulses per symbol, and the energy in *the channel observed by the receiver at chip-spaced sampling (Fig. 5.4b)* is averaged over 500 channel realizations. Note that certain multipath components look larger in chip-spaced observed channel; this is due to two consecutive channel taps appearing very close to each other (smaller than chip duration) in actual channel realization. Also, the channel that the receiver observes depends on the bandwidth, and will change for different chip durations. The average energies captured by chip-spaced sampling, and that captured by the strongest multipath component are obtained as $(0.324, 0.079)$ for CM1, $(0.264, 0.071)$ for CM2, $(0.296, 0.034)$ for CM3, and $(0.299, 0.016)$ for CM4 (with respect to a normalized total available energy of 1). This implies that chip-spaced sampling can be effectively used to implement *ARake* reception with low complexity.

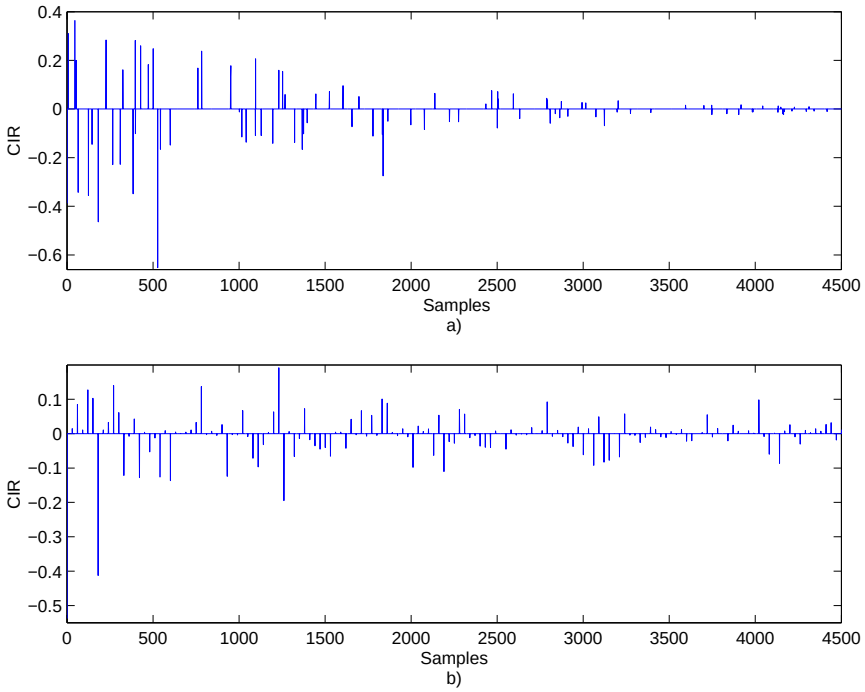

Figure 5.4 Channel realizations from CM1: a) Actual realization, b) Chip-spaced observed realization.

CHAPTER 6

A REVIEW ON MULTIUSER INTERFERENCE AVOIDANCE AND CANCELLATION FOR UWB SYSTEMS

6.1 Introduction

Multiple accessing is an essential part of UWB systems to accommodate many users within the same channel. Multiuser aspects of other wireless technologies such as direct sequence (DS) code division multiple access (CDMA) systems have been studied extensively in the past. However, a complete study on the multiple access capabilities of UWB-IR systems is required. Transmission of the signals around noise level and extremely dispersive nature of the received signals impose many challenges on practical implementation of multiuser UWB-IR systems. On the other hand, unique signaling of time hopping (TH) IR systems characterized by the processing gain and sparse pulsing enables efficient and low complexity multiuser transceiver designs (different than DS-CDMA techniques), and requires further research.

In this chapter, a comprehensive overview of multiple accessing, transmitter-side multiuser interference mitigation, and receiver-side multiuser interference cancellation techniques for IR-UWB systems will be presented. The chapter is organized as follows. First, the signaling and receiver sampling models (both uplink and downlink) for TH and DS IR-UWB systems are presented in Section 6.2.

Multiple access sequence design and multiuser interference are related issues. For example, by appropriately designing the multiple access sequences for each user, it is possible to reduce the multiuser interference to some extent. In Section 6.3, transmitter-side multiuser interference mitigation techniques in the literature for both synchronous and asynchronous communications are covered.

Although multiuser interference can be decreased to some extent at the transmitter side, usually, it can not be totally prevented, and some receiver processing is required for interference cancellation. Almost all of the multiuser interference cancellation algorithms used in DS-CDMA systems can be

directly applied to IR-UWB; however, the signaling structure of IR-UWB can be exploited to design lower complexity and efficient multiuser receivers (see e.g. [142]-[146]). Section 6.4 is a discussion on some multiple access interference (MAI) cancellation issues related specifically to IR-UWB. The rest of the sections are reviews of different multiuser interference cancellation classes; Section 6.5 is on maximum likelihood (ML) multiuser receivers, Section 6.6 is on linear multiuser receivers, Section 6.7 is on subtractive/iterative multiuser receivers, Section 6.8 is on subspace techniques for MAI cancellation, and Section 6.9 is on other techniques that does not fall within the discussed categories. The various related references in the literature are classified and tabulized and some concluding remarks are presented in Section 6.10.

6.2 Sampled Signal Models for Time Hopping Impulse Radio

Time hopping is a popular multiple access option for IR applicable to both short and long range communications. An example for the signaling structure of TH-IR systems was depicted in Fig. 5.1 for three users employing BPSK modulation, where multipath effects are not shown. User-1 and user-2 are synchronized to each other and employ orthogonal sequences, while user-3 is fully asynchronous with the other two users, and causes interference. It is observed that two of the pulses of user-1 are corrupted by the pulses of user-3 (i.e. the number of hits between multiple access sequences of the two users is 2). This causes multiuser interference, and can be handled using appropriate receiver algorithms. Moreover, it is fair to assume that the statistics (i.e. the channels, corrupted pulses etc.) of the users are constant over a block of N symbols, which will be used to design unique interference cancellation techniques later in the chapter.

The multiuser received signal model for TH-IR-UWB was presented in (2.10). When the signal in (2.10) arrives at the receiver, sampling-rate carries significant importance for the capability of the receiver to optimally detect the desired user's signal under interference. In below, we will present two different sampled-signal models which can be considered for different multiuser scenarios

- *Downlink scenario:* The receiver would like to demodulate only the desired user's signal. Therefore, only the interference from the other users' signals to the desired user's signal is important; the system model does not have to capture the correlations between the signals of all the users, and capturing the interference from other users to desired user is sufficient.

- *Uplink scenario:* The receiver (e.g. the base station) would like to jointly demodulate all the users' signals. Therefore, the system model must capture the correlation between any pair of users.

Since only the desired user's signal is detected in the first case, we will call it single user detection with interference cancellation (SUD/IC) in the sequel. On the other hand, all the users signals are jointly detected for the second case, which we will call multiuser detection (MUD).

6.2.1 Sampled Signal Model for Downlink (for SUD/IC)

With the assumption of perfect synchronism, frame-spaced samples provide sufficient statistics for the optimal detection of received signals of desired user [147][1]. Assuming that the receiver is already synchronized to one of the multipath components of the desired user, the correlator output can be sampled once per frame, yielding N_s samples per symbol. Further stacking outputs of N symbols in a matrix, we can represent the samples as follows

$$\mathbf{Y} = \underbrace{\begin{bmatrix} y_{1,1} & y_{1,2} & \cdots & y_{1,N} \\ y_{2,1} & y_{2,2} & \cdots & y_{2,N} \\ \vdots & \vdots & \ddots & \vdots \\ y_{N_s,1} & \cdots & \cdots & y_{N_s,N} \end{bmatrix}}_{N_s \times N} \tag{6.1}$$

In a multiuser environment, correlator output at a pulse position will also include the interference effects from the other users whose pulses collide with that particular pulse. Then, the correlations

[1] However, generally, much higher sampling rates are required for synchronization and channel estimation purposes.

$$\underbrace{\mathbf{Y}}_{N_s \times N} = \underbrace{\begin{bmatrix} A^1\gamma_l^1 & s_{1,2} & \cdots & s_{1,N_u} \\ A^1\gamma_l^1 & s_{2,2} & \cdots & s_{2,N_u} \\ \vdots & \vdots & \ddots & \vdots \\ A^1\gamma_l^1 & \cdots & \cdots & s_{N_s,N_u} \end{bmatrix}}_{\mathbf{S},\ N_s \times N_u} \underbrace{\begin{bmatrix} d_{1,1} & d_{1,2} & \cdots & d_{1,N} \\ d_{2,1} & d_{2,2} & \cdots & s_{2,N} \\ \vdots & \vdots & \ddots & \vdots \\ d_{N_u,1} & \cdots & \cdots & d_{N_u,N} \end{bmatrix}}_{\mathbf{D},\ N_u \times N} + \underbrace{\mathbf{Z}}_{N_s \times\ N} \tag{6.4}$$

---

from other users can be expressed as

$$\mathbf{S}^{(1)} = \underbrace{\begin{bmatrix} A^1\gamma_l^1 & s_{1,2} & \cdots & s_{1,N_u} \\ A^1\gamma_l^1 & s_{2,2} & \cdots & s_{2,N_u} \\ \vdots & \vdots & \ddots & \vdots \\ A^1\gamma_l^1 & \cdots & \cdots & s_{N_s,N_u} \end{bmatrix}}_{N_s \times N_u} \tag{6.2}$$

$$s_{j,k} = \begin{cases} 0, & \text{if } j\text{th pulse non-corrupted;} \\ A^1 b^{(k)} \gamma^{(k)} R_j^{(k)}, & \text{if } j\text{th pulse corrupted;} \end{cases} \tag{6.3}$$

where $R_j^{(k)}$ characterizes the interference from the kth user to the jth pulse of the desired user. Note that the above equation considers only the interference of the other users on the desired user, which was chosen to be user $k = 1$ without loss of generality (we will use the same assumption throughout the chapter). Observing the correlator outputs over a block of N symbols yields the equation (6.4), where $\mathbf{Z}$ is a noise matrix, and it is assumed the statistics of the users (hit locations, channels) does not change over the block.

The conventional receiver *equally* weights the N_s matched filter outputs per symbol to make bit decisions as follows

$$\hat{\mathbf{b}}^{(1)} = \text{sgn}(\mathbf{1}_{N_s}\mathbf{Y}) \ , \tag{6.5}$$

where $\hat{\mathbf{b}}$ is a N vector of estimated bits for user-1, and $\text{sgn}(x) = x/|x|$ gives the sign of variable x. More sophisticated approaches to process these statistics are possible for SUD/IC as will be discussed in the upcoming sections. These approaches typically require some *a-priori* information about the correlation matrix $\mathbf{S}$, which may be provided by a feedback message, or can be estimated blindly from the matrix $\mathbf{Y}$ (which requires processing power and memory).

If only a single bit is considered, (6.4) boils down to

$$\mathbf{r_1} = \mathbf{SAb} + \mathbf{n} \ , \tag{6.6}$$

where $\mathbf{r}_1$ is an $N_s \times 1$ vector of frame-spaced samples for user-1, $\mathbf{b}$ is $N_u \times 1$ vector of bits from different users, $\mathbf{A}$ is an $N_u \times N_u$ diagonal matrix of user amplitudes (assume all the amplitudes in (6.3) are folded into this matrix), and $\mathbf{n}$ is a $N_s \times 1$ noise vector.

6.2.2 Sampled Signal Model for Uplink (for MUD)

While the system model in (6.4) captures the interference from other users to desired user, it fails to characterize the mutual interference between different users. This is because the information is collected with the spreading codes of the desired user only; in order to characterize the mutual interference, the received signal has to be sampled at higher rates (e.g. the chip rate). Then, the following well-known model can be used as a sampled system model in the uplink [147]

$$\mathbf{y} = \mathbf{RAb} + \tilde{\mathbf{n}} \ , \tag{6.7}$$

where this time $\mathbf{y}$ is an $N_u \times 1$ vector of symbol-samples, and the $N_u \times N_u$ matrix $\mathbf{R}$ characterizes the cross-correlations between the spreading sequences of different users. Various MUD techniques are possible that optimally/suboptimally detects the symbols of different users based on the characteristics of the cross-correlation matrix $\mathbf{R}$.

6.3 Transmitter-Side Interference Mitigation Techniques

The interference level in a multiuser wireless communication system can be controlled to some extent at the transmitter side. For example, the multiuser interference is determined by the correlation characteristics of the multiple access sequences employed by different users. In a TH-IR system, by properly designing the TH sequences, it may be possible to avoid/reduce the multiple access interference. In this section, various possible techniques in the literature that attempt to avoid the interference using transmitter-side mitigation techniques will be reviewed. Both synchronous and asynchronous communications are considered.

6.3.1 Synchronous Communications (Downlink)

6.3.1.1 Multipath-Aware TH Sequence Design

In a fully synchronous (i.e. $\tau^{(k)}$ of all the users are identical) and non-dispersive channel, it is possible to design the TH codes orthogonally so that there is no interference among the users. In such a system, the number of users that can communicate without interfering each other is limited to N_h. For example, Fig. 5.1 implies that four synchronous users can communicate with no multiuser interference. One way of increasing the capacity is to use ± 1 polarity coding (as in DS-CDMA systems) in parallel with time hoping, which increases the number of users that can communicate without causing interference to each other to $N_s N_h$.

It is well known that UWB receivers *observe* extremely dispersive channels. Due to the very short duration pulses used in communication, the number of resolvable paths arriving at the receiver may be on the order of hundreds. Therefore, even for a synchronous transmission with users employing orthogonal TH sequences, channel dispersion will introduce multiple access interference, and limit the capacity of TH-IR. Fortunately, it is possible to tackle this problem in the downlink by appropriately assigning the TH sequences. By knowing the number of users, and the maximum excess delay of the channel, a central node can intelligently assign the codes to the users so that the interference due to multipath is minimized. This is achieved by introducing sufficiently long *gaps* between the pulses of the users at transmission [13, 14]. The code construction is given by

$$c_j^{(k)} = \left((k-1)D + j + \left\lfloor \frac{k-1}{N_s} \right\rfloor \right) \bmod(N_h) \ , \tag{6.8}$$

where $j \in \{0, 1, \cdots, N_s - 1\}$, $k \in \{1, 2, \cdots, N_h\}$, $D = \lceil \tau_d / T_c + 1 \rceil$, τ_d is the maximum excess delay of the channel, and $\lfloor . \rfloor$, $\lceil . \rceil$ denote the integer floor, and integer ceiling operations, respectively. The number of pulses per symbol is selected as $N_s = N_h / D$, so that multipath components do not destroy orthogonal code construction for $N_u \leq N_s$.

As the number of users increases, the TH codes assigned by the central node to the new users are chosen to introduce minimal interference (for $K > N_s$, new group of mutually orthogonal codes are obtained by shifting the previous set by $\lfloor (k-1)/N_s \rfloor$). Note that the interference will affect only certain users, and knowing the interferer's TH codes and channels, simple interference cancellation routines can be employed. In Fig. 3.3, a simple example for the downlink transmission of a central node to 4 users is presented, where the maximum excess delay is assumed to sweep 3 chip intervals.

Since the gaps between the pulses are larger then the maximum excess delay, multiuser interference is prevented. On the other hand, if the number of users exceeds 4, the new users' signals will occupy these gaps, resulting in multiuser interference. By periodically estimating and tracking the maximum excess delay and total number of users, the central node can dynamically assign the optimal codes to the users to minimize the multipath and interference effects.

6.3.1.2 Multistage Block Spreading

A detailed analysis of downlink signal transmission was presented in [148] in the context of multistage block spreading (MSBS). The authors show that a TH-UWB system that uses polarity coding supports up to $N_s N_h$ orthogonal waveforms (users) as opposed to N_h users when no polarity coding is implemented.

In order to preserve the mutual orthogonality of the users even in multipath channels, the transmitter first spreads a block of symbols, which is followed by chip interleaving. At the receiver side, the received signal is despread by a linear filtering stage. This in essence reduces the multiple access channel into a set of single-user ISI channels; an equalizer can be then conveniently used for symbol detection without any need for some other multiuser signal processing algorithm.

6.3.1.3 Adaptive Processing Gain Assignment

The processing gain in a TH-UWB system can be adjusted based on the data rate, bit error rate (BER), and range requirements [15]. Knowing the link qualities of the users, a central node can determine the processing gain $N_s^{(k)}$ to be assigned to user k to guarantee reliable communication. For synchronous (downlink) communications, orthogonal code constructions with variable processing gains for different users can be developed to increase the aggregate data rate as a result of optimal choice of $N_s^{(k)}$ for each user.

The BER in a TH-IR communication system using orthogonal modulation (like orthogonal PPM[2]) is given by the following well-known equation

$$BER = Q\left(\sqrt{\frac{N_s^{(k)} E_{rx}^{(k)}}{N_0}}\right) \tag{6.9}$$

[2]Note that overlapping PPM is also possible, which can be designed to have optimum performance.

where $E_{rx}^{(k)}$ is the received energy per pulse of user k, $N_s^{(k)}$ is the processing gain used in communication with the kth user, and $Q(x)$ is given by $\frac{1}{2}\text{erfc}(\frac{x}{\sqrt{2}})$. In order to meet the BER requirements for users with different link qualities, (6.9) implies that the central unit needs to use larger number of pulses for weak links. On the other hand, the TH sequences of the users can still be constructed orthogonally. This requires periodically calculating the *common* symbol durations of the users in terms of the chip duration, which is given by $N_h' = \sum_{k=1}^{N_u} N_s^{(k)}$. Later, the sequences of the users can be constructed orthogonally[3] using a simple algorithm as given in Table 4.1, where N_u is the number of users, $\mathbf{S}$ is the set of integers ranging from 1 to N_h', $\text{rand}(\mathbf{M}, m)$ chooses m random integers from the set of integers $\mathbf{M}$, and "$-$" excludes the set on the right of the operator from the set on the left of the operator[4]. Note that conventional TH-IR notation as in (2.1) is not used here, i.e. the TH codes identify the positions of the pulses within the symbol duration, and there are no frames. Since the locations and the link qualities of the users may change with time, the TH codes need to be updated periodically.

In Fig. 4.2, a simple example for the downlink TH sequences of 3 users employing different processing gains is presented. Note that the proposed codes are similar to orthogonal variable spreading factor (OVSF) codes in CDMA systems, but has better flexibility as the sequence length does not have to be powers of 2.

6.3.1.4 Pre-Rake and MUI Mitigation Filtering

A transmitter-based channel equalization and MAI suppression approach was presented in [150]. The authors first present an overview of Pre-rake architecture. To summarize, Pre-rake receivers use the knowledge of the channel impulse response to transmit the time-reversed form of the signal after multipath. This enables usage of simple matched filter receivers at the receiver rather than conventional all-Rake receivers (i.e. the complexity is shifted from the receiver to transmitter). Even though Pre-rake mitigates multipath effects, it does not combat with the leftover inter-symbol interference (ISI) effects. In [150], the authors first propose a zero-forcing pre-equalization scheme at the transmitter so that ISI effects are mitigated. In particular, the transmitter filter ensures that the composite channel impulse response at the receiver is an ideal delta function.

[3]The multipath effects may also be mitigated as discussed before.

[4]Another approach that designs orthogonal code constructions using an exhaustive search for conventional TH-UWB systems was discussed in [149].

In order to further mitigate the multiuser effects, a MUI mitigation filter is further applied to the summation of the transmitted signals from all the users (using pre-Rake filter for each user). The MUI mitigation filter ensures that the composite channel impulse response at the receiver in the presence of MUI interference is a delta function. The drawback of the proposed approaches is that the transmitter has to know the channels of the users.

6.3.2 Asynchronous Communications (Uplink)

In the uplink communications, or in decentralized architectures, the signals from different users arrive at the receiver with arbitrary delays (see Fig. 6.1). This implies that the TH sequences can not be constructed orthogonally, and it is not possible to have interference-free communications. On the other hand, each user is still separated by their specific TH sequences in a *quasi-orthogonal* way; as more and more users join the system, the interference level increases, which degrades the overall link qualities of the users.

Even in asynchronous scenarios, it may be possible to have multiuser interference mitigation at the transmitter side to some extent, and different possible techniques will be discussed below.

6.3.2.1 Sequence Design Using Congruence Equations

Use of TH sequences with good autocorrelation and crosscorrelation characteristics may decrease the interference in a multiuser environment. The correlation functions of the sequences characterize how much the signals are affected from multipath and multiuser interference. With the assumption of chip synchronism that yields a worst case analysis for the interference, the correlation between two TH sequences is measured by the number of hits between these sequences. Having large number of hits in autocorrelation of a sequence may imply that degradation due to multipath may be severe (i.e. when the pulse-to-pulse duration is smaller than the maximum excess delay). One other implication of comparatively larger autocorrelation sidelobes is that it may be harder to achieve synchronization. On the other hand, larger number of hits in the crosscorrelation function of two sequences implies that the sequences are more susceptible against multiuser interference.

Ideally, the autocorrelation function (ACF) of a sequence is desired to be $N_s\delta(\tau_c)$, where the delay τ_c ranges from $-N_s+1$ to N_s-1, and the crosscorrelation function (CCF) of two sequences is desired to be zero regardless of the delay between the sequences. However, no such perfect sequences exist. In Fig. 6.1, correlations and number of hits of the TH sequences for the first two users in

Table 6.1 Sequence constructions and maximum number of hits in aperiodic correlation functions for FH and TH.

	LCC	QCC	CCC	HCC
Code Construction $f(k,j)$	$[kj]$	$[kj^2]$	$[kj^3]$	$[k/j]$
Max. # of hits (FH-ACF)	p-1	1	2	2
Max. # of hits (TH-ACF)	p-1	2	4	4
Max. # of hits (FH-CCF)	1	2	3	2
Max. # of hits (TH-CCF)	2	4	6	4

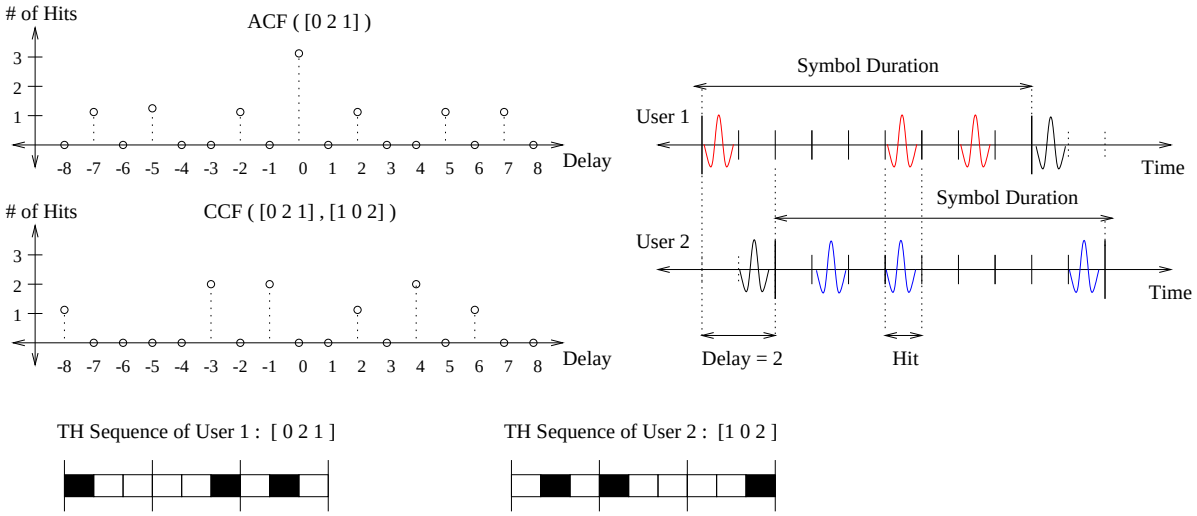

Figure 6.1 Autocorrelation and crosscorrelation functions of the TH codes for the first two users in Fig. 3.1 ($N_s = 3, N_h = 3$).

Fig. 3.1 are analyzed. It is seen that the maximum value of the ACF sidelobes is 1, while the CCF can be as large as 2 for certain delays.

Even though it is not possible to generate sequences with optimal correlation characteristics, thanks to finite field theory, it is possible to generate sequences whose correlation functions are upper-bounded. Such sequences have been well investigated in the past for frequency hopping communication systems [83], and can be also applied to TH-IR. A good review of application of such sequences to TH-UWB systems can be found in [89, 86]. In particular, linear, quadratic, cubic, and hyperbolic congruence codes (LCC, QCC, CCC, HCC) are some of the sequence constructions that have been analyzed before for FH systems. Table 6.1 summarizes these sequence constructions, and gives the maximum values of the ACFs and CCFs for both FH and TH systems. Given the sequence construction by the function $f(k,j)$, where k is the user index, j is the frame index, and the delay being represented in terms of frame and chip durations, i.e. $\tau_c = aN_h + b$, the following

needs to be satisfied for a collision to occur between the delayed versions of the FH sequences [151]

$$\begin{cases} f(k_m, j+a) = f(k_m, j) + b, & \text{if ACF} \\ f(k_m, j+a) = f(k_n, j) + b, & \text{if CCF} \end{cases} \tag{6.10}$$

where k_m and k_n denote different users. By plugging the constructions from Table 6.1, rearranging the terms, and using the Langrange's theorem which says that maximum number of solutions of a polynomial in the finite field is equal to the power of that polynomial [83], the maximum values of the ACFs and CCFs (i.e. the maximum number of hits for any delay and any user) for each construction can be easily evaluated. As a result, as long as the constructions are realized in Galois Field[5] $GF(p)$, regardless of the sequence length, the maximum number of hits between *"any"* two sequences of the same construction will be constant. Note that this is not true for random sequences, where the maximum number of hits increases with the sequence length. However, this is valid only for aperiodic correlations, i.e. the hits from consecutive symbols are not considered, and the maximum number of hits for the periodic correlations may be larger [151].

It is observed in Table 6.1 that the maximum value of the correlation function for TH systems is twice that of FH case, which is due to the fact that for a particular sequence, a hit may come from any two consecutive frames of one another sequence. Although linear congruence codes are seen to have excellent crosscorrelation characteristics, they have very poor autocorrelation characteristics, making them very susceptible against multipath. On the other hand, quadratic congruence codes have optimum combination of autocorrelation and cross-correlation characteristics.

The probability distribution of the number of hits (or usually the maximum number of hits which may be easy to evaluate as discussed), and the number of interfering users determine the multiuser interference to the desired signal. For small number of users, and for large frame size N_h, the probability distribution of the interference is more impulsive [92], i.e. most of the time there will not be any hits and therefore there will not be any interference. As the number of users increases, from central limit theorem, the probability distribution of the multiple access interference approaches to a Gaussian distribution. Knowing certain *a priori* information about the sequences (such as the location of hits), it may be possible to develop efficient multiuser interference cancellation algorithms, which will be discussed in the next sections.

[5] A Galois Field $GF(p)$ is a finite field with elements $0, 1, 2, \cdots, p-1$, where p is a prime number.

6.3.2.2 Pseudo-Chaotic Time Hopping

A pseudo-chaotic time hopping (PCTH) approach was presented in [152], where TH sequences with random distribution of inter-pulse arrivals are generated. The generated TH sequences are driven by the binary information sequence, and therefore yielding an aperiodic sequence. A sequence of M bits are used in an M-bit shift register, where the transmitted pulses can reside in any $N_f = 2^M$ positions within a symbol. The transmitted signal model for PCTH is so that each user transmits its pulses within one frame as opposed to one pulse per frame as in conventional TH-UWB.

The advantage of PCTH is that the random inter-pulse arrivals yield a smooth spectrum. On the other hand, the main disadvantage is the inter-pulse interference due to multipath components from previous pulses and all pulses being transmitted in the same frame.

6.3.2.3 Asynchronous Block Spreading and Zero-Correlation Zones

As discussed in previous sections, in order to achieve MAI-free reception, MSBS was proposed in [148]. However, MSBS is only possible in synchronous channels, which is very difficult to achieve in high-speed UWB systems. In [153], an asynchronous block spreading technique with a zero correlation zone (ZCZ) was presented, which completely removes the MAI and maintains the code orthogonality even with asynchronous users. The authors first present the construction of sequences with a ZCZ, which allow MAI free reception up to a certain asynchronism between the users. Later, since the multiuser interference is completely removed using the ZCZ code characteristics, a Fast Fourier Transform (FFT) based channel equalization scheme is proposed to mitigate the inter-symbol interference of the desired user.

Apart from [153], there are other papers that present code constructions with a zero correlation zone for TH-UWB [154, 85], DS-UWB [155], and DS-CDMA [156, 157, 95] systems. Note that the general idea for ZCZ code construction in all these references is to design the sequences in a way that up to a certain time shift between any pairs of sequences, the cross-correlation function of the sequences becomes zero. Such systems are also commonly referred as "quasi-synchronous" systems, since synchronization is assumed to be maintained within a certain margin.

6.4 Issues Related to Multiple Access Interference Cancellation for IR-UWB

Although it is possible to decrease the multiple access interference to a certain extent at the transmitter side, often, it is not possible to have interference-free communications. However, multiuser detection and interference cancellation algorithms at the receiver make it possible to improve the system performance.

Since DS-CDMA and TH-IR both employ user-specific multiple access sequences to share the spectrum, almost all of the multiuser interference cancellation methods used in DS-CDMA (such as the ones in [147]) can be considered for TH-IR (see e.g. [158]). However, DS-CDMA and TH-IR have different signaling structure. As there is no off-time for the transmission of DS-CDMA signals, all the users that are transmitting simultaneously interfere with each other. This implies that the interference canceler needs to consider the signals received from all the users, which considerably increases the system complexity. For instance, for maximum-likelihood (ML) receivers, the receiver complexity, $O(2^{N_u})$, increases exponentially with the number of total users N_u, which makes it impossible to be implemented in practice in a system with large number of users. Similarly, decorrelator and minimum mean square error (MMSE) type of receivers require a matrix inversion $\left(\text{implying a complexity of } O(N_u^3)\right)$, where the matrix size grows with the number of total users.

Fortunately, unique signaling scheme of TH-IR systems enables the efficient implementation of low complexity interference cancellation methods. The key point that makes TH-IR architectures different from that of DS multiple access schemes is that not all the users interfere with each other, thanks to the sparse signaling scheme. If there is interference from a certain user, it only affects certain pulses, but not all the pulses of the desired user. This fact implies that it may be sufficient to consider only certain users and certain pulses when designing the interference canceler, which considerably decreases the complexity of the receiver.

There are some issues that need to be mentioned before the discussion of specific multiuser detection methods:

- TH-IR signals may be sampled at different rates at the receiver. Sampling the signal with Nyquist rate right after the antenna may imply more efficient receiver algorithms, as the signal can be perfectly reconstructed. However, due to the extremely large bandwidth of UWB signals, Nyquist rate sampling is not usually practical. In addition, it requires a large buffer to store the samples. Often, the signal is sampled after the correlator, where chip-spaced, frame-

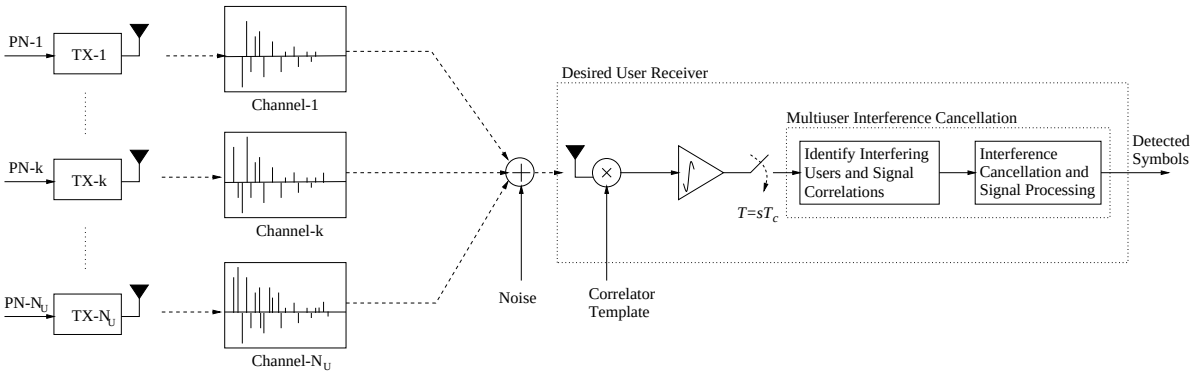

Figure 6.2 Multiple access TH-IR and interference cancellation receiver.

spaced, and symbol-spaced sampling can be implemented (requiring $N_h N_s$, N_s, 1 samples per symbol, respectively). If Rake receivers are implemented, it is also required to sample the signal at multipath arrivals of the desired user's signal. In Fig. 6.2, sampling of the correlator output at chip rate is demonstrated.

- Certain *a priori* information may be available to the receiver for use in MAI cancellation. For example in a centralized scenario, a central node may know or estimate the TH sequences, delays, amplitudes, and channels of the users. Then, these information may be used to obtain the signal correlations, and cancel the interference. Signal correlations can be also estimated by processing and averaging the matched filter outputs over a number of symbols. However, knowledge of such *a priori* information and/or estimating them may not be an easy task for UWB due to low power and dispersive nature of the received signals.

- The receiver may be interested in demodulating only one user (such as in the downlink), rather than making individually optimum decisions (such as in the uplink) [147], which relaxes the requirements on *a priori* information knowledge or estimation.

- Complexity/performance trade-offs need to be well evaluated considering the application characteristics and requirements. For example, in cases where near/far effect is dominant, substantial performance gains may be obtained using very low complexity chip discriminators.

- Some receivers may require buffering of the correlator outputs over many symbols for post-processing, which requires memory and increases the receiver complexity. Also, this introduces delays in detecting the symbols, which is not appropriate for delay-sensitive applications.

- Many wireless communication systems operate in dynamic environments, where the channel quality continuously changes, and the users enter/leave the system. Therefore, especially in the downlink, the employed interference cancellation technique needs to be adaptive. As the calculation of the interference correlation matrix is often very costly, low complexity (decision directed or blind) tracking algorithms (such as reduced rank techniques to decrease the size of the correlation matrix) are required.

6.5 Maximum Likelihood Detectors

It is well known that the optimal receiver that minimizes the probability of detection error for all users is the maximum-likelihood sequence detection. The ML receiver optimizes the decisions of all the users by jointly estimating the sequence of bits that have the closest distance to the received signal in the Euclidean space [147]. This requires a complexity of $O(M^{N_u})$, where M represents the number of constellation points per user. It is a centralized algorithm, and the amplitude and TH-sequence information for all the users in the system are required.

The ML receiver has been considered for UWB systems in [159] for MUD, which includes all the active users in the system to optimize the performance. In particular, the bit sequence estimate is given by

$$\hat{\mathbf{b}} = \underset{\mathbf{b}}{\operatorname{argmin}} \left\{ \mathbf{y} - \mathbf{RAb} \right\} , \tag{6.11}$$

where correlation matrix $\mathbf{R}$ is $N_u \times N_u$. The search for $\mathbf{b}$ is a combinatorial optimization problem, and the algorithm becomes impractical for large N_u. Alternative and/or lower complexity implementations of ML algorithm will be discussed below, which make use of specific characteristics of IR-UWB systems.

6.5.1 Alternative and/or Lower-Complexity ML Techniques for UWB

6.5.1.1 Quasi-ML Receiver

In [144], a lower complexity quasi-ML algorithm is introduced for SUD/IC, which utilizes the fact that not all the users in the system interfere with each other. The bit decisions using the quasi-ML

detector are achieved by considering only the users whose pulses are colliding with the desired user

$$\hat{b}^{(1)} = \underset{b_1 \in \{-1,+1\}}{\operatorname{argmin}} \underset{\sum_{\mathbf{b} \in \{-1,+1\}^{N'_u}}}{} ||\mathbf{r}_1 - \mathbf{S}^{(k)}[b_1 \mathbf{b}]^T||^2 \ , \tag{6.12}$$

where N'_u is the number of users whose at least one pulse collides with one of the pulses of the desired user. Although this decreases the complexity, the characteristic of sparse transmission of pulses is not fully exploited.

6.5.1.2 Low-Complexity Joint ML Detection

Another lower-complexity ML algorithm for SUD/IC is introduced in [73] which assumes that in a well designed UWB system very few of the other users' pulses will collide with a certain pulse of the desired user. The proposed algorithm does not require the *a-priori* information of TH sequences or channels of the other users (as opposed to [144]), or any kind of synchronism. On the other hand, in order to obtain reliable statistics for different pulse positions, sufficiently large number of training symbols are required. The assumptions are that the number of colliding pulses over a certain pulse position is at most one, the channel is constant over a block of symbols, and the processing gain is sufficiently small (as opposed to pulse discarding receivers to be discussed). The algorithm exploits the SNR estimates over each pulse position to estimate the channels of the desired and interfering users (with a phase ambiguity for the interfering users' channels). Then, the following joint ML metric is used to detect the bits of the desired user

$$\begin{aligned} ML_j^{joint}(n) &= \left| R_j^{(k)}(n) - b_H^{(k)}(n)\hat{\gamma}^{(k)}(n) - b_H^{(i)}\tilde{\gamma}_j^{(i)} \right|^2 , \\ ML_j^{single}(n) &= \left| R_j^{(k)}(n) - b_H^{(k)}(n)\hat{\gamma}^{(k)}(n) \right|^2 , \\ ML^{total}(n) &= \sum_{j \subset colliding} ML_j^{joint} + \sum_{i \subset non-colliding} ML_i^{single} \ , \end{aligned} \tag{6.13}$$

where n is the bit number, $R_j^{(k)}(n)$ is the correlator output for the jth pulse of the kth user's nth bit, $b_H^{(k)}$ and $b_H^{(i)}$ are the bit hypothesis corresponding to the desired and any interfering users, $\hat{\gamma}^{(k)}(n)$ is the channel estimate of the desired user that takes pulse amplitude and pulse correlation into account, and $\tilde{\gamma}_j^{(i)}$ is any interfering user's channel that takes pulse mis-alignment factor, pulse

amplitude and correlations into account[6]. The ML metric for the corrupted pulses is denoted by ML^{joint}, and for the non-corrupted pulses by ML^{single}; the optimum bit sequence is the one that minimizes the total metric $ML^{total}(n)$. The complexity of the algorithm increases with the total number of colliding symbols (from different users), but not all the users in the system.

6.5.1.3 Recursive Convex Relaxation

A recursive ML detection algorithm was proposed by Zhang *et. al.* in [160], where the authors decrease the computational complexity by relaxing the system model. This allows application of quadratic programming (QP) techniques, whose global solution can be found with polynomial time computational complexity. In particular, the authors formulate the ML detection as an optimization problem as follows

$$\text{minimize } \mathbf{x}^T\mathbf{H}\mathbf{x} + \mathbf{x}^T\mathbf{p} \tag{6.14}$$

$$\text{subject to : } x_i \in \{-1, +1\} \text{ for } i = 1, 2, \cdots, N_u \ , \tag{6.15}$$

where $\mathbf{H} = \mathbf{ARA}$, $\mathbf{p} = 2\mathbf{Ay}$, and x_i is the ith element of $\mathbf{x}$. By relaxing the above optimization problem as follows

$$\text{minimize } \mathbf{x}^T\mathbf{H}\mathbf{x} + \mathbf{x}^T\mathbf{p} \tag{6.16}$$

$$\text{subject to : } -1 \leq x_i \leq +1 \text{ for } i = 1, 2, \cdots, N_u \ , \tag{6.17}$$

and applying recursive QP techniques, very close performances to conventional ML detection can be obtained with substantial gains in the computational complexity.

6.5.1.4 Signal Pre-treatment Prior to ML Detection

In [161], a three-stage multiuser detection algorithm is proposed. At the first step (data pre-treatment), wavelet packet transformation is applied to multiuser received signal. This suppresses adverse effects of Gaussian noise to improve the ML detection performance. Second step uses a wide-band space-time spectrum estimator which recognizes the number of users and realizes distance/angle super-resolution of signal sources; the knowledge regarding the users decreases the computational

[6]While the desired user's channel is the same for all the pulse positions within the bit, interfering signal's channel estimate will be different for each pulse position as different users might interfere with different pulse positions.

complexity of the algorithm. Finally, a robust M-detector as in [159] is applied to the resulting signal to achieve multiuser detection.

6.5.1.5 Frequency-Domain ML Detection

A frequency-domain ML detection approach that exploits the frequency-correlation of the multiple access interference is proposed in [162] for DS-UWB signals. The authors derive the following frequency domain log-likelihood function

$$\Lambda(\{\hat{b}_n\}) = -\sum_{n=-\infty}^{\infty}\sum_{j=-\infty}^{\infty}\left[\mathbf{Y}_n - \hat{b}_n\mathbf{G}_{EQ}\right]^{\dagger} \times \mathbf{R}^{-1}(n,j) \times \left[\mathbf{Y}_n - \hat{b}_n\mathbf{G}_{EQ}\right] , \tag{6.18}$$

where $\dagger$ denotes the conjugate-transpose operator, j is the chip index, n is the symbol index, $\mathbf{R}(n,j)$ is the time-frequency correlation matrix of the frequency-domain noise-plus-interference signal, and $\mathbf{Y}_n$ and $\mathbf{G}_{EQ}$ are the matrices that capture the Fast Fourier Transforms (FFTs) of the received signal (after modulation) and the unmodulated signal, respectively. The ML solution is given by the sequence of bits $\{\hat{\mathbf{b}}\}$ that maximizes the likelihood function in (6.18). Also, a lower-complexity algorithm was presented which neglects the temporal correlation of the interference , i.e. $\mathbf{R}(n,j) = 0$ for $n \neq j$, therefore simplifying the log-likelihood function to

$$\Lambda(\{\hat{b}_n\}) \sim \hat{b}_n \times \mathrm{Re}\Big\{\mathbf{G}_{EQ}^{\dagger}\mathbf{R}^{-1}(n,n)\mathbf{Y}_n\Big\} . \tag{6.19}$$

6.6 Linear Receivers and Pulse Combining Techniques

Due to the high complexity of ML type of multiuser receivers, linear multiuser receivers are more practical (even though sub-optimal) [163, 164, 165, 166]. The basic idea behind linear multiuser detection algorithms is to fit a suboptimal linear model to the received signal in order to obtain the initial soft bit values, and then use these values to map into the actual symbols which belong to a finite alphabet (such as using the *sign* operator to map into ± 1 for BPSK modulation). A general model that demonstrates how a linear multiuser detector $\mathbf{L}$ operates on the matched filter

outputs (6.7) or (6.3) to make a bit decision is given as follows

$$\hat{\mathbf{b}} = \begin{cases} \text{sgn}\left(\mathbf{Lr}\right), & \text{if SUD/IC;} \\ \text{sgn}\left(\mathbf{Ly}\right), & \text{if MUD.} \end{cases} \tag{6.20}$$

The two popular methods of selecting the linear multiuser detector $\mathbf{L}$ are decorrelator and MMSE receiver.

It is worth to emphasize here that the vectors that linear receivers operate on are different for the uplink (i.e. for MUD) and for the downlink (i.e. SUD/IC). In the uplink, the linear receivers operate on $N_u \times 1$ vector of signal samples from different users, i.e. on (6.7); the correlation matrix here has the role of characterizing the correlations between different users. On the other hand, for downlink, the linear receivers work on the $N_s \times 1$ vector of frame-spaced samples in (6.6). In other words, the receiver's goal is to optimally combine the N_s pulses using the interference correlation characteristics over different pulses.

6.6.1 Decorrelator

For the MUD algorithms (i.e. the uplink), the decorrelator receiver operates on (6.7) by applying the inverse of the correlation matrix

$$\mathbf{L}_{Dec} = \mathbf{R}^{-1} \, . \tag{6.21}$$

In the absence of noise, the decorrelator completely cancels the interference from the other users. It has much lower complexity then the optimum ML algorithm, does not require the knowledge of the amplitudes of the users, and can be easily implemented in a decentralized manner (one-by-one detection of the users). Two disadvantages of decorrelator detector are that it amplifies the noise, and a matrix inversion operation is required to get the inverse of $\mathbf{R}$, which increases the complexity. It might be required to recompute $\mathbf{R}$ at each bit (if the code sequences are changing from time to time, or after the activation of new users), and the research is directed on developing algorithms that decrease the cost of recomputation by adaptive algorithms that update the decorrelator coefficients.

6.6.1.1 Quasi-Decorrelator

A low complexity quasi-decorrelator has been applied for UWB in [144] for SUD/IC, which considers the interference from only the colliding users to decrease the complexity. The estimated bit using the proposed low-complexity algorithm (due to considering only the corrupted pulses) is given by

$$\hat{b}^{(1)} = \text{sgn}\left(\left((\mathbf{S}^{(1)})^T\mathbf{S}^{(1)}\right)^{-1}(\mathbf{S}^{(1)})^T\mathbf{r}_1\right) \ , \tag{6.22}$$

where correlation matrix $\mathbf{S}^{(1)}$ captures the interference from only the colliding users, but not all the users in the system.

6.6.1.2 Iterative Decorrelator

While matrix inversion operation in (6.21) is costly, lower-complexity techniques are desirable[7]. In [167], an iterative decorrelator approach is presented for MUD, which avoids matrix inversion. More specifically, in order to solve a linear equation of the form

$$\mathbf{Rx} = \mathbf{y} \ , \tag{6.23}$$

the authors propose to use an iterative procedure described by

$$D(\mathbf{x}_i) = \mathbf{x}_i + \gamma(\mathbf{y} - \mathbf{R}\mathbf{x}_i) = \mathbf{x}_{i+1} \ , \tag{6.24}$$

where γ is a critical (constant) parameter that determines the convergence characteristics of the algorithm, and $i \in \{0, 1, 2, \cdots\}$ is the iteration count. When $\hat{\mathbf{x}}$ is the solution of (6.23), $\hat{\mathbf{x}}$ satisfies $D(\hat{\mathbf{x}}) = \hat{\mathbf{x}}$. The authors derive that the optimal value of γ that yields fastest convergence is given by $\gamma_{opt} = (\lambda_{max} + \lambda_{min})^{-1}$, where λ_{max} and λ_{min} are the maximum and minimum eigenvalues of $\mathbf{R}$, respectively.

[7] Computational complexity of matrix inversion is a big problem for both decorrelator and MMSE receivers. A polynomial expansion detector was proposed in [164] to decrease the computational complexity in DS-CDMA that arises due to matrix inversion (see the Appendix of [19] for a brief overview of the algorithm).

6.6.2 MMSE Receivers

The decorrelator receiver has close to optimum performance for high SNR environments, but may have worse performance than the conventional detector if all the interferers are very weak. It is possible to incorporate the knowledge of the received signal powers and the noise variance, and improve the performance of the decorrelator using MMSE detector. The linear MMSE detector is chosen so as to minimize the expectation of the decision error, i.e.

$$\mathbf{L} = \underset{\mathbf{L}}{\operatorname{argmin}} \, \mathrm{E}\left[||\mathbf{b} - \mathbf{L}\mathbf{y}||^2\right] \ . \tag{6.25}$$

It can be easily verified that the MMSE receiver that minimizes the above equation is given by [147]

$$\mathbf{L}_{MMSE} = \left[\mathbf{R} + (N_0/2)\mathbf{A}^{-2}\right]^{-1} \ . \tag{6.26}$$

Note that MMSE detector depends on the noise variance and signal powers only through the SNR. For high SNR, the second matrix terms are negligible, the correlation matrix $\mathbf{R}$ becomes dominant term, and the performance of MMSE detector approaches to that of decorrelator. For low SNR, the second term dominates, and the performance of MMSE detector converges to that of conventional receiver.

The performance of MMSE detector was analyzed in detail under various asymptotic conditions in [168]; it is proved that for a simple two-user case, the BER of MMSE detector is better than that of decorrelating linear detector for all values of normalized crosscorrelations smaller than 0.9659.

In the next sections, we present different applications of MMSE receivers to UWB systems.

6.6.2.1 Quasi-MMSE Receivers

In [144], a lower complexity MMSE receiver was proposed for TH-UWB systems, where only the users whose pulses collide with the desired user are considered. The bit decision is given by

$$\hat{b}^{(1)} = \mathrm{sgn}\left(\frac{1}{\mathbf{A}}\left((\mathbf{S}^{(1)})^T\mathbf{S}^{(1)} + \sigma^2(\mathbf{A})^{-2}\right)^{-1}(\mathbf{S}^{(1)})^T\mathbf{r}_1\right) \ . \tag{6.27}$$

where σ^2 is the noise variance, and correlation matrix $\mathbf{S}^{(1)}$ captures the interference from only the colliding users.

6.6.2.2 MMSE Pulse and/or Finger Combining Receivers in Multipath Channels

The quasi-decorrelator receiver in (6.22) and the quasi-MMSE receiver in (6.27) are in fact two different pulse combining approaches in the presence of interference. Other work on MMSE combining of paths and/or fingers for UWB can be found in [169]-[172].

In [169, 170], for a DS-UWB system, the authors derive the optimal MMSE combining coefficients for the multipath components in the presence of multiuser and narrowband interference (e.g. wireless local area networks that use orthogonal frequency division multiplexing). The tap weights for the multipath components are adjusted adaptively using LMS or recursive least squares (RLS) algorithms. It is shown via simulations that while conventional Rake receivers fail to reject strong interference, adaptive MMSE receivers successfully mitigate interference effects.

A more comprehensive approach that considers both frame combining and/or multipath combining is presented in [171] which accounts both inter-frame interference and MAI. It is shown that the optimum MMSE receiver combines all the multipath components corresponding to all N_s pulses per symbol. Two sub-optimum receivers that have lower complexity are also presented. Optimal frame combining (OFC) is achieved by 1) Maximum ratio combining (MRC) of the multipath components at each frame, and 2) MMSE combining of the combined multipath components. On the other hand, optimum multipath combining (OMC) is achieved by 1) MMSE combining of the multipath components, and 2) Equal gain combining (EGC) of the contributions from different frames. All three proposed schemes are shown to perform better than conventional Rake receivers using simulations. Performances of conventional pulse combining, blinking receiver (see Section 6.6.3.1), and MMSE pulse combining are compared in [143]. Since the optimum finger selection problem is NP-hard, a lower-complexity finger selection algorithm based on Genetic algorithms is proposed in [172], which aims to maximize the SINR of the received signal using an iterative approach.

6.6.2.3 Iterative LMS algorithm for Determination of MMSE Combining Coefficients in TR Systems

In [173], an multiuser (and inter-symbol) interference suppression algorithm for TR systems is proposed which relies on optimal weighting of the collected samples. In particular, optimal weighting

coefficients $\mathbf{w}$ which minimize the following mean square error (MSE)

$$\text{MSE} = \min_{\mathbf{b}} \text{E}\left[(d^{(1)}[i] - \mathbf{w}^T\hat{\mathbf{y}}[i])^2\right] , \tag{6.28}$$

are calculated using a low-complexity iterative LMS algorithm, where i denotes the training symbol index, $d^{(1)}[i]$ is the ith transmitted training symbol for user-1, and $\hat{\mathbf{y}}[i]$ is a vector of delay-and-correlate outputs over N_s pulses and N_t training symbols. The iterative LMS algorithm to calculate the weighting vector is as follows

$$\mathbf{w}[i] = \mathbf{w}[i-1] + \mu[i-1]e[i-1]\hat{\mathbf{y}}[i-1] , \tag{6.29}$$

$$e[i-1] = d^{(1)} - \mathbf{w}^T[i-1]\hat{\mathbf{y}}[i-1] , \tag{6.30}$$

where the step size is given by $\mu[i] = \mu_{const}/||\hat{\mathbf{y}}[i]||$, and the algorithm stops when the end of the training samples is reached. The resulting combining coefficients are optimum in the MMSE sense, and the decision variable is given by $\hat{z}^{opt}[i] = \mathbf{w}_{opt}^T\hat{\mathbf{y}}[i]$.

6.6.2.4 Random-Sign Repetition for MMSE Detection

The performance of the multiuser receiver depends on the characteristics of the matrix $\mathbf{S}$; if it is rank-deficient (i.e. if it is not full-rank), the performance of the MMSE receiver may be poor. In [174, 175], a random sign repetition is included in the transmitted signal model to increase the chances of the matrix $\mathbf{S}$ being full-rank. When the MMSE receivers with and without sign repetition are considered, the simulation results for the proposed technique show on the order of 5dB gain at a BER of 10^{-3}.

6.6.2.5 Frequency-Domain MMSE Receivers

Similar to application of ML techniques in frequency domain, MMSE detection can also be achieved in frequency domain.

Frequency domain multiuser detection for TH-UWB-IR with PPM and in flat fading channels has been analyzed in [176]. Initially, the Fourier transform of the received signal is taken by correlating the received signal with sinusoidal waveforms of different central frequencies. When using PPM, the information is embedded in the timing delay of the pulses, which is interpreted as phase

delay in the frequency domain. Therefore, delay demodulation in time domain converts to phase demodulation in frequency domain; while the former model is non-linear, the latter model becomes linear. Having manipulated the received signal to a linear model, MMSE and ZF receivers can be used for demodulation of the received bits. Note that with this approach, the performance of the symbol detection depends on the selected frequency, and it is desired to choose the frequencies that yields the maximum signal power.

Another paper that uses ZF and MMSE receivers in the frequency domain is [177], where as opposed to [176], multipath effects were also considered. It is shown via simulations that ZF and MMSE receivers are less than only 5dB worse compared to AWGN performance, while conventional Rake receivers hit an early error floor especially when the number of users is large. Also, MMSE receiver starts to outperform ZF receiver as the number of users increases.

6.6.3 Pulse Discarding Receivers and Hard Pulse Combining

In terms of the receiver complexity, probably the most practical multiuser interference cancellation approach for TH-IR systems are pulse discarding receivers. The basic idea behind these type of receivers is simply to discard the pulses which are corrupted, and demodulate the information using the uncorrupted pulses. These receivers work well if the number of pulses per symbol, N_s, is large, and the number of corrupted pulses is relatively low. Two such receivers discussed in the literature are blinking receiver and chip discriminator. Hard pulse combining is another approach to combat severe interference without discarding the pulses.

6.6.3.1 Blinking Receiver

Blinking receiver [144] is a very low complexity receiver based on the discarding the pulses which are corrupted. It is designed for a centralized system, where the base station knows the TH codes of all the users, and can identify the corrupted pulses. Regardless of the the strength of the interferer, a pulse is discarded if it is corrupted, and the bit decision is performed based on the remaining pulses. The estimate of the k^{th} user's bit using Blinking receiver is given by the following linear model

$$\hat{b}^{(1)} = \text{sgn}\left(\mathbf{w}^T \mathbf{r}_1\right) \ , \tag{6.31}$$

where the elements of weighting vector $\mathbf{w} = [w_1, w_2, \cdots, w_{N_s}]^T$ are given by

$$w_j = \begin{cases} 1 & \text{if } [\mathbf{S}^{(1)}]_{j,2} = [\mathbf{S}^{(1)}]_{j,3} = \cdots = [\mathbf{S}^{(1)}]_{j,N_u'} = 0 \\ 0 & \text{otherwise} \end{cases} \tag{6.32}$$

which means that jth pulse will be used in the detection only if it is not corrupted at all. In practice, due to the highly dispersive nature of UWB channels yielding large number of hits from multipath components of other users, this receiver may perform poorly.

6.6.3.2 Chip Discriminator

If the number of collisions is large, or the interferers are weak, the blinking receiver is not efficient, since it discards a large portion of the useful information. Instead, chip discriminator [142], which is primarily designed to compensate for near/far effects in a power-unbalanced UWB network, provides more efficient results. In such near/far scenarios, there will be many *far* users that will have similar power levels at the receiver, while the power received from the *near* users which are colocated with the receiver will be comparatively huge. If the pulses received from such users collide with the desired user's pulses, the processing gain of the desired user might not be able to compensate for the interference. The idea behind chip discrimination is to detect such strong interferers by setting a threshold, and discard the pulses corrupted by these interferers in the demodulation. The bit estimate for the k^{th} user employing the chip discriminator is given by

$$\hat{b}^{(1)} = \text{sgn}\left(\mathbf{w}^T \mathbf{r}_1\right) \ , \tag{6.33}$$

where the elements of weighting vector $\mathbf{w} = [w_1, w_2, \cdots, w_{N_s}]^T$ are given by

$$w_j = \begin{cases} 1 & \text{if } [\mathbf{S}^{(1)}]_{j,k'} < T_\Delta \ , \qquad \forall k', \ 2 < k' < N_u' \\ 0 & \text{otherwise} \end{cases} \tag{6.34}$$

where $\mathbf{S}$ contains the channels and amplitudes of the colliding users, as well as their pulse location information. The threshold T_Δ is used to detect the pulses which are strongly corrupted and needs to be discarded in the demodulation. Note that chip discriminator does not need to know the TH sequences of the interfering users; however, channel estimate is required to be able to calculate the threshold.

Another pulse discarding receiver that works *prior to* channel estimation stage is discussed in [18]. The authors use the second order statistics of the matched-filter outputs, i.e. $\Sigma_j = \mathrm{E}[y_{jn}^2]$, and propose to use a threshold given by $\xi = 2\mathrm{E}[\Sigma_j] - \min(\Sigma_j)$, where the pulses with $\Sigma_j > \xi$ are discarded.

6.6.3.3 Hard Pulse Combining vs. Soft Pulse Combining

Conventional soft-combining of all the pulses within a symbol is achieved by (6.5). However, if one or few of the pulses are significantly corrupted, they may bias the bit decision. The basic idea behind the hard combiner is to combine the hard information (± 1) from the pulses, which will prevent the degradation due to the pulses which are corrupted by strong interferers. The bit estimate using the hard combiner is given by

$$\hat{b}^{(1)} = \mathrm{sgn}\left(\sum_{j=1}^{N_s} \mathrm{sgn}\left(r_{j1}\right)\right) \ , \tag{6.35}$$

where r_{j1} is the correlator output from the jth pulse of the desired user. The hard combining method gives satisfactory results *if* there is severe near/far problem in the system.

In [178], a hard combining of the pulses in a severe near/far scenario was shown to be efficient compared to soft pulse combining with no blanking (discarding the corrupted pulses), and to be comparable (1 dB worse) with soft decision when blanking is applied.

An adaptive receiver that can switch between hard-combining and soft-combining depending on the MAI level is introduced in [179]. For interference mitigation purposes, an adaptive coding/decoding scheme is proposed; the Hamming distances between different codewords employed by different users are used by a control unit at the receiver to decide hard or soft decoding of the received signal.

6.7 Iterative and/or Subtractive Interference Cancellation

An alternative non-linear group of multiuser receivers can be classified as iterative and/or subtractive interference cancellation receivers. Subtractive interference cancellation receivers rely on estimation, regeneration, and subtraction of the MAI at the receiver; an excellent review of such receivers can be found in [164]. The popular implementations of subtractive interference cancellation receivers are successive interference cancellation, parallel interference cancellation, and zero-

forcing decision feedback detectors (see the Appendix of [19] for a brief summary of these algorithms from [164]). Simulation comparison of successive and parallel interference cancellation, decorrelating decision feedback receiver, as well as MMSE and decorrelator receivers can be found in [166]. A direct application of the successive and parallel interference cancellation receivers to UWB systems can be found in [158, 180].

Another type of iterative detection algorithms are the iterative Turbo receivers. Such receivers work by iterating between two different decision algorithms (exchanging soft information about tentative decisions): 1) Soft MUD stage, and 2) Soft channel decoding stage [181]. Further information about the Turbo principle can be found in the following excellent tutorial papers [181, 182, 183].

For the rest of the section, we will review the application of iterative receivers to UWB systems.

6.7.1 Iterative Interference Cancellation for Convolutionally Coded UWB

Iterative interference cancellation that uses convolutional codes has been considered for UWB systems in [184]. Their proposed model is similar to the Iterative-Turbo model described above, and the algorithm iterates between two stages: 1) The multiuser detection is implemented at soft interference canceler likelihood calculation (SICLC) stage, and the output is fed into a soft-input soft-output (SISO) convolutional decoder in the form of a log-likelihood ratio, and 2) The SISO convolutional decoder processes the output of the SICLC (i.e. the *a-priori* information about the coded bits). The decoded soft information is fed back to the SICLC stage, and few iterations of algorithm substantially cancels the MAI.

In the SICLC stage, the parallel interference canceler (as described in Appendix of [19]) subtracts the total (soft) MAI from the desired user's signal, and later calculates the expectation of the desired user's bit as follows

$$\tilde{b^{(k)}} = E[b^{(k)}] = 1 \times p(b^{(k)} = 1) - 1 \times p(b^{(k)} = -1) \ . \tag{6.36}$$

Using the soft information that comes from the SISO decoder, (6.36) can be easily written as follows using the log-likelihood-ratios $L_{21}(b)$ of the bit b (see [183] for details)

$$\tilde{b}^{(k)} = \frac{e^{L_{21}(b^{(k)})} - 1}{1 + e^{L_{21}(b^{(k)})}} = \tanh\left(\frac{1}{2} L_{21}(b^{(k)})\right) \ . \tag{6.37}$$

The above soft information about the detected bit is passed back to the SISO decoder, which uses this soft information as an *a priori* information to calculate the *a posterior* soft bit value. Iteration continues until convergence.

This application of iterative Turbo method as above is very similar to its implementation in CDMA literature, and does not exploit the characteristics of UWB. Another approach that exploits the signaling scheme of UWB will be discussed in next.

6.7.2 Turbo Iterative Multiuser Detection Using the Inherent Repetition Code of UWB Systems

An approach that benefits from the sparse signaling of TH-IR (and therefore considers only interfering users) is the iterative-Turbo method, where the inherent repetition coding (processing gain) of TH-IR enables implementation with no additional coding [144, 145]. Instead of a specific convolutional code as in the previous case, pulse repetition code is used to update the *a priori* information. The proposed detector is composed of two parts: pulse detector, and the symbol detector.

6.7.2.1 Pulse Detector

The pulse detector computes the *a posteriori* log-likelihood ratio (LLR) of b_j^k, where b_j^k is the information carried on the j^{th} pulse of user k. Note that pulse detector assumes that uncorrelated information is carried on each pulse of the same symbol. The LLR of b_j^k is given by as in (6.38), where $\lambda_1^n(b_j^k)$ is the extrinsic information that is passed to the symbol detector, $\lambda_2^{n-1}(b_j^k)$ is the *a priori* information about b_j^k, and $f_j^k(g)$ are the locations of the corrupted pulses. Note that the a priori information $\lambda_2^{n-1}(b_j^k)$ (which is used in both numerator end denominator terms of $\lambda_1^n(b_j^k)$) is initially $\frac{1}{2}$, and is updated iteratively by the symbol detector.

6.7.2.2 Symbol Detector

The symbol detector makes use of the information that all the pulses within the same bit carry the same information, and calculates the a posteriori LLR of the transmitted information given the a priori LLR from all the N_s pulse detectors as in (6.39). Note that $\lambda_1^n(b_l^k)$ was used at the last step to evaluate $\lambda_2^n(b_j^k)$, which will be iteratively used in the pulse detector as the a priori information. After two iterations, simulation results demonstrate that single user performance is obtained.

$$
\begin{aligned}
L_1^n(b_j^k) &= \log\frac{Pr(b_j^k=1|y)}{Pr(b_j^k=-1|y)} = \log\frac{f(y|b_j^k=1)}{f(y|b_j^k=-1)} + \log\frac{Pr(b_j^k=1)}{Pr(b_j^k=-1)} \\
&= \log\frac{\sum_{\mathbf{b}\in\{\pm1\}^{N_u'}} e^{\frac{(y-\mathbf{A}_k^j[1\,\mathbf{b}]^T)}{2\sigma^2}} p(\mathbf{b})}{\sum_{\mathbf{b}\in\{\pm1\}^{N_u'}} e^{\frac{(y-\mathbf{A}_k^j[-1\,\mathbf{b}]^T)}{2\sigma^2}} p(\mathbf{b})} + \lambda_2^{n-1}(b_j^k) \\
&= \log\frac{\sum_{\mathbf{b}\in\{\pm1\}^{N_u'}} e^{\frac{(y-\mathbf{A}_k^j[1\,\mathbf{b}]^T)}{2\sigma^2}} \prod_{g=1}^{N_u'} 1+[\mathbf{b}]_g \tanh\left(\frac{1}{2}\lambda_2^{n-1}(b_j^{f_j^k(g)})\right)}{\sum_{\mathbf{b}\in\{\pm1\}^{N_u'}} e^{\frac{(y-\mathbf{A}_k^j[-1\,\mathbf{b}]^T)}{2\sigma^2}} \prod_{g=1}^{N_u'} 1+[\mathbf{b}]_g \tanh\left(\frac{1}{2}\lambda_2^{n-1}(b_j^{f_j^k(g)})\right)} + \lambda_2^{n-1}(b_j^k) \\
&= \lambda_1^n(b_j^k) + \lambda_2^{n-1}(b_j^k)\ , \qquad (6.38) \\
L_2^n(b_j^k) &= \log\frac{Pr\left(b_j^k=1|\lambda_1^n(b_j^k),\ j=1,\cdots,N_s\right)}{Pr\left(b_j^k=-1|\lambda_1^n(b_j^k),\ j=1,\cdots,N_s\right)} = \sum_{l=1,l\neq j}^{N_s} \log\frac{Pr\left(b_l^k=1|\lambda_1^n(b_l^k)\right)}{Pr\left(b_l^k=-1|\lambda_1^n(b_l^k)\right)} + \lambda_1^n(b_j^k) \\
&= \sum_{l=1,l\neq j}^{N_s} \lambda_1^n(b_l^k) + \lambda_1^n(b_j^k) = \lambda_2^n(b_j^k) + \lambda_1^n(b_j^k)\ . \qquad (6.39)
\end{aligned}
$$

6.7.3 Low Complexity Extrinsic Information Generation for Turbo Multiuser Detection Method

Due to high complexity of calculating the extrinsic information in the pulse detector stage[8], two lower-complexity approaches were discussed in [145]: 1) Gaussian approximation and 1) soft interference cancellation.

The Gaussian approximation method only considers the users that are significantly strong power levels (detected using an appropriate threshold), and folds rest of the interference into Gaussian noise. As a result, the number of interfering users need to be processed by the pulse-detector decreases, and an approximate *a-priori* LLR is generated by the pulse detector instead of the exact *a-priori* LLR. This implies a low-complexity implementation with slight performance losses.

The complexity after the Gaussian approximation can be still high if the number of strong interferers is large (e.g. in strong near/far scenarios), and an even lower-complexity approach is desirable. The soft cancellation method first generates the soft estimates of $\mathbf{b_j}^{(k)}$ by

$$
\left[\tilde{\mathbf{b}}_j^{(k)}\right]_i = \left[E\left\{b_j^{(1)}|\lambda_2(b_j^{(1)})\right\}\right]_i\ . \qquad (6.40)
$$

[8]The computation of $\lambda_1(b_j^k)$ is exponential in the number of pulses arriving at the receiver at the same time as the jth pulse of the kth user [145].

Using this soft soft information regarding the desired bit, the desired user's signal is regenerated, and then subtracted from the total received signal. The residual is the MAI signal, which is modeled using a Gaussian approximation, i.e.

$$\text{MAI} \sim \mathcal{N}\big(\mu_j^{(k)}, (\sigma_j^2)^{(k)}\big) \ . \tag{6.41}$$

At the pulse detector, the approximate *a priori* log-likelihood of the residual is calculated using (6.41) instead of the exact LLR. This decreases the complexity substantially; this is because regardless of the number of users, the residual is approximated by a single Gaussian distribution. Note that the soft information $\lambda_2(b_j^{(1)})$ (which is used to regenerate the desired user's signal and than the residual MAI) should be reliable to have good performance.

6.7.4 Low-Complexity Implementation of Fishler's Turbo Receiver

Another work that targets to decrease the computational complexity at the pulse detection step of Turbo-iterative detector is [185], which uses interference cancellation and an MMSE filter. In particular, given the *a-priori* LLR $\lambda_2^n(b_k^j)$, the the soft estimates of the transmitted interfering symbols are given by

$$\hat{b}_k^j = \text{E}\{b_k^j\} = \tanh\left(\frac{\lambda_2^n(b_k^j)}{2}\right) \ . \tag{6.42}$$

This soft estimate is subtracted from the received signal to obtain the interference-cancelled signal $\hat{r}_{l(j,k)}$ (similar to discussed before in Section 6.7.3). In addition to that, the linear MMSE filter for the jth pulse of the kth user can then be selected as follows to minimize the MSE

$$w_{k,j} = \underset{w}{\text{argmin}}\ \text{E}\Big\{\big|w^\dagger r_{l(k,j)} - b_k^j\big|^2\Big\} \ . \tag{6.43}$$

The output of the MMSE filter can be modeled with a Gaussian approximation, and the resulting expression can be used to obtain the desired soft output values $\lambda_1^n(b_k^j)$ to be used in the symbol detector.

6.7.5 Successive Interference Cancellation With Partial Rake Reception

In [186], a successive interference cancellation scheme is proposed for UWB systems. The idea is similar to the successive interference cancellation summarized in Appendix of [19]; the users are ranked according to their post-detection SNRs, and subtracted one by one (starting from the strongest user) from the received signal. However, a partial-Rake (PRake) receiver is used to collect the energies from different multipath components.

Another work that uses subtractive interference cancellation with PRake reception is [187]. In order to regenerate the interfering signals, a low-complexity PRake receiver (rather than an all-Rake receiver is used). After regeneration of the interference and subtraction from the received signal, the desired user's signal can be detected using an all-Rake receiver.

6.8 Blind/Adaptive Multiuser Detection Techniques

Due to the dynamic nature of the multiple access channel (i.e. the users entering/leaving the system, the power levels of the received signals changing depending on the changes in the environment etc.), the correlation matrix (for MMSE or decorrelator receivers) and the noise variance estimate (for MMSE receivers) have to be updated every once in a while. Using training sequences [188, 189], it is possible to obtain such adaptive implementations of MMSE receivers, where the goal is to find the optimum value of $\mathbf{L}$ that will minimize (6.25). An application of MMSE multiuser detection with hidden training sequences (i.e. part of the information sequence is used for adaptation) for the purpose of estimating the correlation matrix $\mathbf{R}$ is [190].

The simplest adaptive implementation of multiuser receivers is the gradient descent algorithm, which updates $\mathbf{L}$ so that the cost function (6.25) is gradually minimized [191]. Some of the more complex but faster algorithms are recursive least squares, and lattice structures. Other references on the adaptation of the MMSE algorithm with varying levels of complexity and performance can be found in [191].

On the other hand, the correlation matrix can also be updated without using any training sequences, i.e. in a blind way [192]. Blind techniques assume the knowledge of the signature waveform and the timing of only the desired user. and can be implemented using subspace based techniques. Subspace techniques, Wiener filters, minimum variance, and power-of-R algorithms are

some of the other blind MUD approaches. For the rest of this section, we will look at some important groups of adaptive MUD algorithms, and discuss available applications for UWB systems.

6.8.1 Subspace Techniques and Principal Components Method

Reduced-rank techniques, which rely on decreasing the rank of a correlation matrix in some way[9], are commonly used for interference cancellation in DS-CDMA systems [193]. A popular class of reduced-rank techniques is the subspace techniques, which use only the principal components (eigenvalues) to obtain the correlation matrix (and therefore are based on zeroing insignificant eigenvalues). The key benefit of subspace methods is the reduction of the interference correlation matrix size (whose size is normally $O(N_h N_s)$ for IR-UWB systems with chip-spaced sampling) by projecting the received vector onto a lower dimensional signal subspace. Therefore, they are appropriate for TH-IR-UWB systems where the processing gain (which identifies the received signal space) is typically much larger than the number of users (which determines the dimensionality of the lower-rank subspace where the received vector is to be projected).

A downside of subspace techniques is that the computational complexity of singular value decomposition (SVD), which is an integral part of subspace methods, is very large. Instead, subspace tracking algorithms may be used in dynamic channels, which are based on updating (with a low-complexity technique) the singular values and vectors once they are initially evaluated [194, 195].

Subspace based methods make it possible other detectors (such as decorrelator and the MMSE detector) to operate blindly, i.e. only with the information of the signature waveform and the timing of the desired user (without the need of training symbols). An excellent reference on subspace techniques for blind multiuser detection is [192] (see Appendix of [19] for a brief summary of MMSE and decorrelator receivers that use subspace techniques).

A subspace based multiuser detector has been proposed for TH-UWB-IR (with M-ary PPM) in [146, 196]. In the proposed receiver, first, the channel is estimated using the subspace method; this is achieved by first finding the covariance of the received signal, dividing this into signal and noise subspaces, using Eigenvalue decomposition to further process the signal, and then minimizing the resulting metric to estimate the channel. Later, knowing the estimate of the channel, different types of receivers can be used (Rake, ZF, MMSE, Subspace MMSE). Subspace MMSE and ZF receivers are shown to have similar and best performance.

[9]Thus, reduced-rank techniques are most appropriate if the processing gain is much larger then the signal dimensionality, so that rank reduction yields significant gains.

6.8.2 Multistage Wiener Filters

As discussed in the previous section, projection of the received signal vector onto a lower dimensional signal subspace decreases the complexity, and improves the tracking performance. However, this is correct if the dimensionality (i.e. $N_s \times N_h$ for chip-spaced sampling, and N_s for frame-spaced sampling) is much larger than the signal subspace (determined by the number of users). Therefore, for heavily loaded scenarios, principal component methods may not be appropriate, requiring alternative approaches [193]. As opposed to principal component methods, MSWF does not explicitly generate the signal subspace. The reduced-rank MSWF achieves close to full-rank MMSE performance with filter rank (determined by the number of applied stages) much smaller than the signal space. A good discussion on the details of MSWF can be found in [193].

A multistage Wiener filter (MSWF) has been considered for TH-IR in [197] to implement a reduced-rank MMSE filter. The chip-spaced sampling of the matched filter implies a correlation matrix with size $O(N_h N_s)$. However, the interference dimension is much lower, which can be exploited using low rank approximation of the correlation matrix. Consequently, as the number of required samples reduces, the tracking performance of the receiver substantially improves in a dynamic channel, where the value of the correlation matrix changes due to users entering and leaving the system [197]. The authors show that the output SINR of the system for $N_u = 100$, $N_h = 125$, $N_s = 4$, and $E_b/N_0 = 20$dB is around 18dB for the full-rank scheme (i.e. for rank being $N_s \times N_h = 500$); on the other hand, the same SINR can be obtained using as low as 10 stages in the MSWF.

Reduced-rank Wiener filters were also considered with frame-spaced sampling in [198] for TH-IR-UWB systems. Frame-rate sampling implies N_s samples per symbol rather than $N_s \times N_h$ samples per symbol, therefore yielding significant reduction in the detection complexity. The authors use the vector conjugate gradient (V-CG) method which generates a rank-m approximation of the full-rank Wiener filter after following iterations

$$\gamma_{m-1} = ||\mathbf{r}_{m-1}||^2/(\mathbf{d}_{m-1}^T \mathbf{R}_{yy} \mathbf{d}_{m-1}) \ , \tag{6.44}$$

$$\mathbf{L}_m = \mathbf{L}_{m-1} + \gamma_{m-1} \mathbf{d}_{m-1} \ , \tag{6.45}$$

$$\mathbf{r}_m = \mathbf{c}_1 - \mathbf{R}_{yy} \mathbf{L}_m \ , \tag{6.46}$$

$$\mathbf{d}_m = \mathbf{r}_m + \mathbf{d}_{m-1}(||\mathbf{r}_m||^2/||\mathbf{r}_{m-1}||^2) \ , \tag{6.47}$$

where the linear MMSE receiver is given by $\mathbf{L} = \mathbf{R}_{yy}^{-1}\mathbf{c}_1$, $\mathbf{L}_m$ is the rank-m approximation to the MMSE filter, $\mathbf{R}_{yy}$ is the data covariance matrix, $\mathbf{c}_1$ is the codeword vector for the desired user, $\mathbf{L}_0 = \mathbf{c}_1$, initial search direction is $\mathbf{d}_0 = \mathbf{r}_0$, and $\mathbf{r}_0 = \mathbf{c}_1\mathbf{L}_0$. Note that the reduced-rank V-CG filter converges to the full-rank Wiener filter in at most M steps, where $M \leq N_u$ is the number of distinct eigenvalues of $\mathbf{R}_{yy}$ [198].

6.8.3 Minimum Variance and Power of R Methods

Two other blind interference cancellation techniques which do not require training symbols are the minimum variance (MV) method and power of R (POR) method. The motivation behind MV blind receivers is to minimize the output variance of the receiver with respect to a certain code-based constraint, so that while canceling the multiuser interference, the desired user's signal is preserved [199]. While the TH sequences and timings of all the users are required for subspace techniques, MV technique requires only the knowledge of the desired user parameters. However, it is known that MV methods are very sensitive to signature mismatch and multipath effects due to signal cancellation, and therefore special care needs to be taken for TH-IR systems.

On the other hand, power of R (POR) technique is a *soft decision* blind method which falls in between subspace and MV methods. It raises the data covariance matrix $\mathbf{R}$ to a power m to virtually increase the SNR [200]. As $m \to \infty$, the POR method becomes identical to subspace methods, and MV is a special case of POR for $m = 1$. Note that POR technique outperforms the subspace based methods in systems with dense multipath or heavy loading, and therefore may be very appropriate for UWB systems which observe an extremely dispersive channel.

6.9 Other Approaches

Various other multiuser interference cancellation approaches have also been proposed for UWB, DS-CDMA, and multi-carrier (MC) CDMA systems in the literature which may not necessarily fall in the categories discussed in the previous sections. Kalman filters, Genetic algorithms, neural networks, sequential expectation maximization (EM) methods, frequency domain methods, and per-survivor processing are few of these approaches. In this section, some of these algorithms will be discussed; note that certain classes of MUD algorithms are not analyzed in detail yet for UWB systems; further research is required to evaluate the appropriateness and feasibility of these algorithms for practical UWB applications.

6.9.1 Frequency-Domain Techniques

Frequency domain multiuser detection techniques were considered for DS-CDMA systems in the past [201, 202]. As discussed in more detail in previous sections, frequency-domain multiuser detection algorithms were also applied to TH-UWB and DS-UWB systems; frequency-domain ML detection was analyzed in [162], while frequency domain ZF and MMSE receivers were investigated in [176, 177]. An FFT based multiuser detection algorithm for asynchronous block-spreading DS-UWB was presented in [153].

6.9.2 Kalman Filters

Kalman filters based multiuser detection schemes have been considered for *asynchronous* CDMA systems in the past [203, 204]. It was shown that among possible linear MMSE receivers, Kalman filter, which is a linear *recursive* MMSE receiver, is the best linear MMSE detector for a given detection delay [203].

A recent paper that uses Kalman filters for MUD in CDMA systems is [205], where pseudo random independence of the codes is exploited to generate separate Kalman filters for different users. The signal model to be used for the Kalman Filter and for a particular user k is given by

$$y^{(k)}(t) = s^{(k)}(t)a^{(k)}(t)b^{(k)}(t) + v(t) \ , \tag{6.48}$$

where $y(t)$ is the received signal, $s(t)$ is the spreading code, $b(t)$ is the transmitted bit, and $v(t)$ is the noise plus MAI with unknown variance, given by $\frac{1}{2}\sigma_v^2(t)$[10]. If we represent $x(t) = a(t)b(t)$ (dropped the user coefficient k for notation simplicity), state equations are written as follows

$$x(t+1) = \Phi(t)x(t) + w(t) \tag{6.49}$$

$$y(t) = s(t)x(t) + v(t) \tag{6.50}$$

where state transition matrix Φ is equal to 1 as long as the consecutive symbols are the same, and 0 otherwise. Similarly, the state noise $w(t)$ is zero as long as consecutive bits are the same, and its variance when there is a symbol change is given by $Q(t) = E[a(t)a(t)]$. Based on the state equations,

[10]Note here that Kalman filter is a blind model which does not use the spreading sequences of other users, and try to minimize overall noise by approximating the MAI with Gaussian approximation

the Riccati equations (which identify the updates of covariance matrices) and state update equations can be easily written.

Kalman filters were also considered for MUD in DS-UWB systems in a realistic UWB indoor channel [206]. First, a robust Kalman filter is used to estimate the channel parameters. Then, with the consideration of the channel estimation errors in the tracking mode, an adaptive multiuser decision feedback equalizer (based on the proposed robust Kalman filter) is developed, which suppresses both the MAI and ISI. The simulation results show that the MUD with robust Kalman filter outperforms conventional rake receivers and 1-stage parallel interference cancellation receivers.

6.9.3 Neural Networks

Neural networks are interconnected networks of parallel-operating perceptrons (simple processing units), which are commonly used to many complex problems such as classification problems, speech recognition, and scene analysis [207]. Based on the desired problem to be solved, the learning problem can be formulated so that a desired cost function is minimized by changing the internal structure of the network.

Application of neural networks for synchronous and asynchronous multiuser detection systems has been considered in [207]-[210]. The motivation behind Neural network type multiuser receivers is, similar to the other suboptimal receivers, the high degradation in conventional receiver under near/far problem, and optimum receiver being too complex to resolve the issue.

In the Neural network approach presented in [207], a back-propagation algorithm[11] is used to train the network for demodulation of signals. It is shown that Neural networks can be successfully applied both synchronous and asynchronous CDMA systems for the purpose of either SUD/IC or MUD. The authors show via simulations that for the 2-user channels that have strong near/far effect and at the desired SNR range of interest, the BER of Neural network receiver is few orders of magnitude better than that of the conventional receiver, and is independent of the powers of other users.

[11] Back-propagation algorithm is a training algorithm; it is applied to many classification problems in the literature, is an iterative gradient-descent algorithm that aims to minimize a cost function [207].

6.9.4 Genetic Algorithms

Genetic algorithm (GA) is another iterative optimization approach to obtain approximate solutions to NP-hard problems (which is the optimal ML multiuser detector in this case). They yield much faster solutions compared to exhaustive point-by-point search. For the optimization purposes, they use the genes (which correspond to vectors of bits) from a pool, and perform reproduction (randomly mate two vectors from the pool), crossover (exchange certain parts between the vector pairs) and mutatation (exchange of a single-bit from -1 to 1, or vice versa) operations until a good generation is obtained.

Genetic algorithm were applied to CDMA systems for MUD in synchronous [210, 211, 212] and asynchronous [213, 214] networks.

The authors propose a new modified Genetic algorithm technique in [210] for MUD purposes, where the number of required populations and generations are less than the previously proposed techniques. While the classical GA hits a floor at high SNR, the proposed GA has performance close to optimum ML detection with much lower complexity. The performance of the algorithm was also compared with three-layer perceptron Neural networks, conventional decorrelator and multistage detectors, and it was shown to outperform them all (however requiring higher complexity).

In [211], it was discussed that a good initial guess is required to prevent saturation effects (due to getting stuck at local optima rather than finding the global optimum solution) and have good detection performance; therefore, sub-optimum detectors such as decorrelator receivers can be used to obtain an initial guess before applying genetic algorithms.

In [212], the authors show via simulations that the MUD performance may be improved considerably by increasing pool-size, which introduces a compromise between the performance and computational complexity. Note that using larger pool sizes may improve the local-optima problem discussed above, since a more diverse population of genes are available that can help to get away from the local optima.

In [213], GAs were applied to asynchronous CDMA systems, where both the desired bits and so called "edge bits" (due to asynchronism of the users) within the observation window are estimated. The role of the GA is to search for the particular bit sequence that optimizes a log-likelihood function.

In another work, GA is used in the first step of a two-step MUD algorithm, where the second step is a multistage detector [214]. Motivation for such a hybrid approach is to decrease the computational complexity, and improve the convergence time of the algorithm.

As discussed before, Genetic algorithms can also be used to optimize the performance for MMSE pulse/finger combining [172].

6.9.5 Per-Survivor Processing

Per-survivor processing (PSP) algorithm is a tree-search based detection algorithm initially proposed in [215]. As it has been discussed, joint ML detector is the optimum algorithm with complexity $O(2^{N_u})$, and the PSP tree search algorithm with recursive least squares decrease the complexity to $O(K^2)$ with very close performance, and without the transmission of any training bits (i.e. the signal powers and phases are extracted adaptively).

The optimum joint ML algorithm can be implemented by an exhaustive tree search algorithm which constructs a tree with 2^{N_u} end points (corresponding to the composite symbol hypothesis). At the n^{th} step of the tree, there are 2^n end nodes corresponding to the composite symbol hypothesis of n bits. PSP tree search algorithm implements a much less complexity subtree algorithm, which still contains the ML path algorithm with high probability. This is achieved by choosing the paths that minimize a certain cost function.

The PSP multiuser detection algorithm was applied to multicarrier (MC) DS-CDMA systems in [216]; the branch metric in conventional single-carrier systems was modified to detect MC-DS-CDMA. In [217] was used as the MUD stage of a Turbo-iterative receiver in a convolutionally-coded CDMA system; the PSP based MUD generates soft outputs, which are then used by convolutional decoders.

6.10 Conclusion

In this chapter, multiple access sequence design and interference cancellation techniques for TH-UWB, DS-UWB, and CDMA systems are analyzed, giving emphasis on unique signaling aspects of TH/DS UWB systems. By appropriately designing the multiple access sequences in an IR-UWB system, multiuser interference can be reduced. Both synchronous and asynchronous channels are considered, and appropriate sequence constructions for each case are reviewed.

Although sequence design helps to reduce multiple access interference, usually, it can not be totally prevented. Unique signaling scheme of IR-UWB systems allow low complexity implementations of the interference cancellation methods used in CDMA based systems, as well as other unique algorithms.

Table 6.2 Overview of interference avoidance and cancellation techniques for multiuser IR-UWB systems.

		TH-UWB References	DS-UWB References	CDMA/General References
Interference Avoidance	Synchronous Systems	[151, 154, 85, 218, 15, 148, 150, 149]	[155]	[156, 157, 95]
	Asynchronous Systems	[151, 86, 89, 152]	[153]	[83]
ML Receivers		[144, 158, 159, 162, 73]	[160, 161]	[147]
Linear Receivers	Pulse Discarding Receivers	[144, 142, 18, 178, 179]		
	Decorrelator	[144, 158]	[167]	[163, 147, 164, 165]
	MMSE	[144, 158, 149]	[173, 175, 190]	[163, 147, 164, 165, 168]
	Pulse Combining Receivers	[171, 143, 172]	[169, 170]	
Iterative Receivers	Turbo MUD	[145, 185, 184]		[181, 182, 183]
	Successive and parallel IC	[158, 186, 187]	[180]	[147, 164, 165]
Blind/Adaptive Techniques	Subspace Methods	[146, 196]		[194, 195]
	Wiener Filters	[198, 197]		[193]
	MV and POR	[199]		[200]
Other	Frequency Domain Techniques	[153, 162, 176, 177]		[201, 202]
	Kalman Filters		[206]	[203, 204, 205]
	Neural Networks			[209, 210, 207, 208]
	Genetic Algorithms	[172]		[210, 211, 212, 213, 214]
	Per-survivor Processing			[215, 216, 217]

Even though high performance gains can be obtained using certain algorithms, their practical implementation for IR is still a big challenge. Further research is required to develop efficient and practical interference cancellation algorithms that consider transmission power limitations and realistic UWB channels; the author believes this chapter will serve as a good resource to derive potential research directions in the area and enhance the capabilities of IR-UWB in multiuser channels.

CHAPTER 7

SENSITIVITY OF IR-UWB TO TIMING MISMATCH AND EFFECTS OF TIMING JITTER

7.1 Introduction

Due to extremely short duration of pulses used, UWB systems require high sensitivity against timing errors for proper demodulation of the received signal. Ideally, transmitted pulses in a digital communication system arrive at the receiver at integer multiples of sampling times. In real systems, pulses are received at times that are different from integer multiples of sampling times, which is named as timing jitter [219]. The traditional way to measure the timing jitter is using the *eye pattern* observed in an oscilloscope, which is the synchronized and superimposed possible realizations of the received signal viewed within a particular signaling interval [220]. The thickness of the eye edges gives an idea about the range of the timing jitter.

According to the sources of timing jitter, it can be examined in two categories: random jitter and deterministic jitter [221]-[223]. Random jitter is assumed to be Gaussian in nature, and is caused by the accumulation of thermal noise sources [223]. Generally, deterministic jitter is bounded and non-Gaussian. Some examples for deterministic jitter are duty-cycle distortion, *e.g.* from asymmetric rise/fall times; inter-symbol interference, *e.g.* from channel dispersion or filtering; sinusoidal, *e.g.* from power supply feed-through; and uncorrelated, *e.g.* crosstalk by other signals [223]. The total jitter thus can have both random and deterministic components, and its PDF can be obtained by the convolution of the PDFs of the random jitter and the deterministic jitter [222]. Deterministic jitter can be reduced or eliminated once its source is determined [221]. Using the eye pattern technique, or the histogram technique in an oscilloscope, it is possible to distinguish between the random and deterministic components of the total jitter.

Effects of timing jitter on the performances of different technologies have been investigated in the past [224]-[226], and various methods are proposed to model the jitter distribution [222], [227]-[229]. Effect of timing jitter on the signal power spectral density (PSD) in a multipath environment has

been analyzed in [230]. Surveys and books have been written to clarify the relationships between different jitter aspects and measurement techniques [219], [231], [232].

New UWB radios are capable of precisely positioning the sub-nanosecond pulses with a Gaussian distributed root-mean-squared (RMS) jitter of $10ps$ and within a $50ns$ time window [233]. Even if the transceiver clocks are very stable and introduce very little jitter, other issues such as timing tracking and relative velocities between transmitter and receiver introduce additional degradation in synchronization [62].

Although timing jitter has a significant effect on the BER performance of UWB systems, theoretical performance analyses for UWB systems in the presence of timing jitter have not been done to the best knowledge of the authors. Especially, accurate mathematical modeling and theoretical BER analysis of the effect of timing jitter is required. Performance analysis of UWB modulation schemes in ideal conditions [51] and in other practical scenarios such as multipath [56], multiple access interference [234] and narrowband interference [60] have been done in the past. The effect of timing jitter on the PSD of UWB signals has been analyzed in [235]-[237] and it was concluded that jitter in fact helped to *smooth* the PSD due to the introduced randomness. The effect of uniformly distributed timing jitter on the UWB performance were simulated in [238] for optimum pulse position modulation (PPM) and in [239] for Hermite polynomial pulses. Lovelace *et. al.* analyze the performance degradation in the multiple access capability of the UWB system in the presence of Gaussian distributed timing jitter for binary and M-ary PPM schemes [62].

The focus of this chapter is the theoretical performance anaysis of UWB systems in the presence of timing jitter. The effects of timing jitter on the performances of orthogonal-PPM, optimum-PPM, on-off keying (OOK), and binary phase shift keying (BPSK) modulations are investigated. Theoretical BER equations for static and Rayleigh fading channels in the presence of timing jitter are derived and compared with simulations. For Rayleigh fading channels, flat and dispersive channel models are used. Based on [224], a worst case jitter distribution that can serve as an upper bound on the system performance is presented, and the effect of the pulse shape is analyzed.

The chapter is organized as follows. Section 7.2 gives a generic UWB system model for PPM and BPSK modulations. BER formulations under timing jitter are presented and compared with simulations in Section 7.3. In Section 7.4, the effect of timing jitter PDF on system performance is analyzed, and the PDF for jitter due to finger estimation error is presented. Section 7.5 analyzes

the effect of pulse shape on system performance when there is jitter, and the last section concludes the chapter.

7.2 System Model

7.2.1 Signal Model

Consider the equations (2.1) and (2.2) for the transmitted and received signals in Chapter 2. At the receiver, the received signal is correlated with a template and a decision is made based on the detection algorithm. The correlator template used for PPM is given by

$$v(t) = \omega_{rec}(t) - \omega_{rec}(t - \delta) \ . \tag{7.1}$$

Note that δ is larger than T_c for orthogonal PPM and smaller than T_c for overlapped PPM. Optimum PPM is achieved by selecting δ that minimizes $R(\delta)$, or maximizes $1 - R(\delta)$. For BPSK and OOK, ω_{rec} itself is used as the template. Templates used for BPSK and optimum PPM, and the received pulse with jitter when transmitting *zero* are depicted in Fig. 7.1. Output of the correlator is found by multiplying and integrating the received pulse with the receiver template

$$U = \int_{-\infty}^{\infty} r^{(1)}(t)v(t)dt \ . \tag{7.2}$$

This value can then be used to make a binary decision for BPSK and PPM as follows

$$b = \begin{cases} 0 & \text{if } U \geq 0 \\ 1 & \text{if } U < 0 \end{cases} \tag{7.3}$$

where b denotes the detected bit. For OOK, U is compared with a threshold T to make a decision

$$b = \begin{cases} 0 & \text{if } U \leq T \\ 1 & \text{if } U > T \end{cases} \tag{7.4}$$

Normalized correlation functions of the received pulse with the templates used in BPSK and optimum PPM schemes are depicted in Fig. 7.2. Notice that correlation functions, and therefore the SNRs after the correlator become zero when the timing jitter is around $80ps$, which determines a jitter budget for a typical UWB system employing the pulse shape in Fig. 7.1.

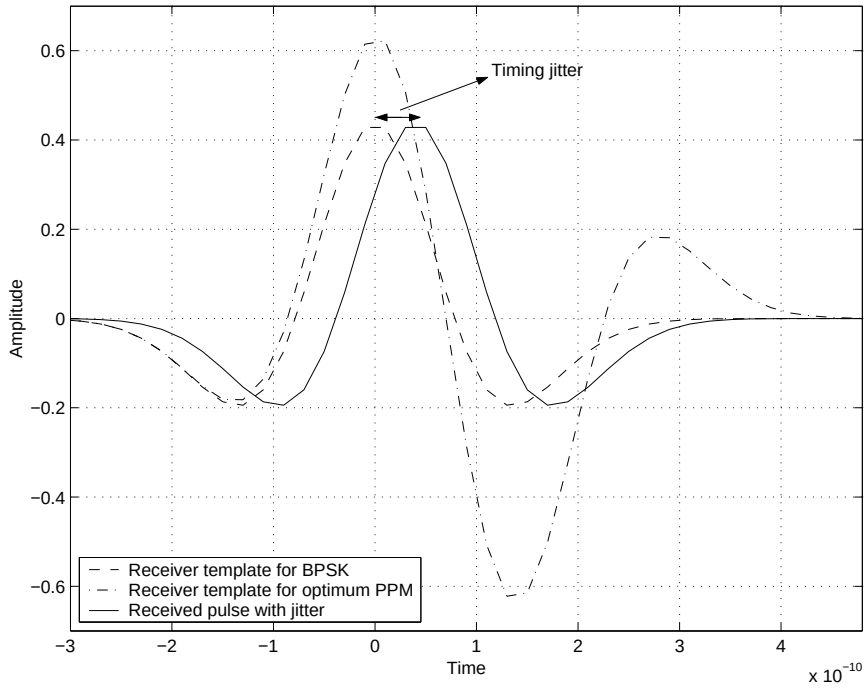

Figure 7.1 Templates used at the correlator for BPSK and optimum PPM, and the received pulse with jitter ($\tau = 0.277ns$).

7.2.2 BER Performance Analysis

In order to evaluate the BER performances, it is required to analyze the correlator outputs of signal and noise separately. When PPM is used, correlation of the received pulse with the template, m_p, and the variance of the correlation of the noise with the template, σ^2_{corr}, can be respectively evaluated as follows [50]

$$m_p = \int_{-\infty}^{\infty} \omega_{rec}(t)v(t)dt = E_p\left[1 - R(\delta)\right] \ , \tag{7.5}$$

$$\begin{aligned}\sigma^2_{corr} &= E\left[\left(\int_{-\infty}^{\infty} \tilde{n}(t)v(t)dt\right)^2\right] \\ &= \int_{-\infty}^{\infty}\int_{-\infty}^{\infty} v(t_1)v(t_2)E\left[\tilde{n}(t_1)\tilde{n}(t_2)\right]dt_1 dt_2 \\ &= N_0E_p\left[1 - R(\delta)\right] \ .\end{aligned} \tag{7.6}$$

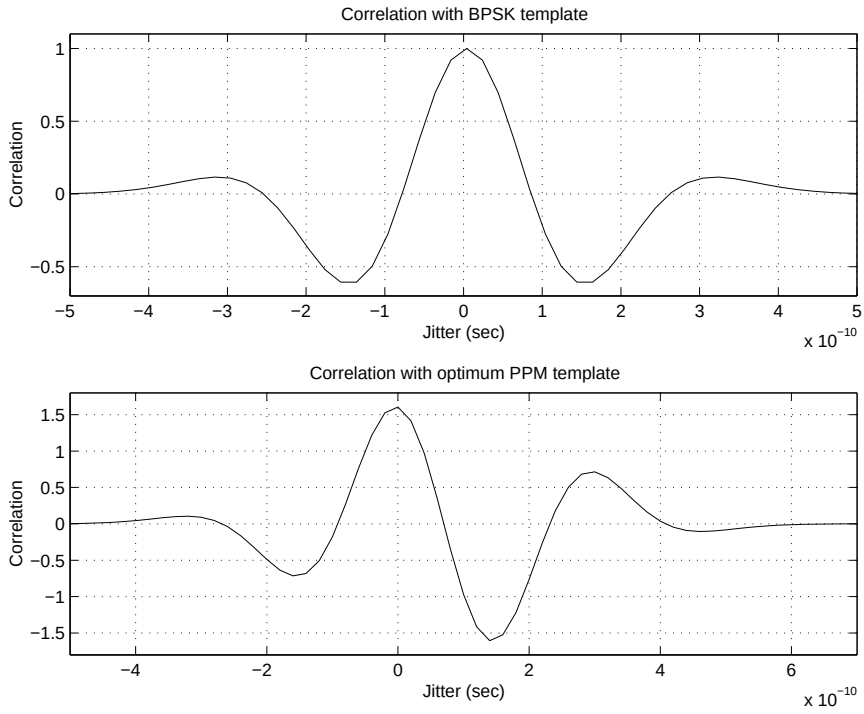

Figure 7.2 Correlation functions of the received pulse with the templates used for BPSK and optimum PPM ($\tau = 0.277ns$).

The SNR after the correlator considering the pulse amplitude and the processing gain is calculated as

$$SNR = \frac{(N_s\sqrt{A}m_p)^2}{N_s\sigma_{corr}^2} \ . \tag{7.7}$$

Using (7.5) and (7.6) in (7.7),

$$SNR = \frac{N_s A E_p}{N_0}(1 - R(\delta)) \ . \tag{7.8}$$

Following a similar approach for other modulation schemes and using the standard techniques [51, 52, 11], BER performances for the four binary modulation schemes can be derived as was shown in Table 2.1.

7.3 Effect of Timing Jitter on BER Performances

When there is timing jitter in the UWB signals, a deviation from its ideal timing position is observed in the received signal. This degrades the performance since jitter decreases m_p, the correlation of the received pulse with the receiver template. This section will cover the theoretical performance evaluation of different modulation schemes in the presence of timing jitter assuming that PDF of timing jitter is known. Uniform timing jitter is assumed throughout the section for simulation purposes[1], and the next section compares the performances for different distributions that have the same variance. BER performances in AWGN, single-tap Rayleigh fading and dispersive channels are derived initially for a fixed value of the timing jitter, and averaged over the PDF of timing jitter to find the expected performance. Obtained theoretical findings are then verified by simulation results.

7.3.1 BER Performances in Static Channel

For a fixed value of the timing jitter, there is ϵ_j amount of timing difference between the actual and the ideal positions of the receiver template. Correlation values with the signal and the noise for PPM with a fixed value of timing jitter are calculated as

$$m_p = \int_{-\infty}^{\infty} \omega_{rec}(t+\epsilon_j)v(t)dt = E_p\left[R(\epsilon_j) - R(\delta-\epsilon_j)\right] \ , \tag{7.9}$$

$$\begin{aligned}\sigma_{corr}^2 &= E\left[\left(\int_{-\infty}^{\infty} \tilde{n}(t+\epsilon_j)v(t)dt\right)^2\right] \\ &= \int_{-\infty}^{\infty}\int_{-\infty}^{\infty} v(t_1)v(t_2).E\left[\tilde{n}(t_1+\epsilon_j)\tilde{n}(t_2+\epsilon_j)\right]dt_1dt_2 \\ &= N_0E_p\left[1-R(\delta)\right] \ .\end{aligned} \tag{7.10}$$

Plugging (7.9) and (7.10) in (7.7), SNR for PPM for a fixed value of timing jitter is evaluated as follows

$$SNR = \frac{N_sAE_p}{N_0}\left[\frac{(R(\epsilon_j)-R(\delta-\epsilon_j))^2}{1-R(\delta)}\right] \ . \tag{7.11}$$

[1]Recall that although random jitter is assumed to be Gaussian, the total jitter, which is the sum of the random jitter and the deterministic jitter, can have different distributions.

Table 7.1 BER performances of UWB modulation schemes in AWGN channel and in the presence of timing jitter.

Modulation	BER
Orthogonal PPM	$Q\left(\sqrt{\frac{N_s A E_p}{N_0} R^2(\epsilon_j)}\right)$
Optimum PPM	$Q\left(\sqrt{\frac{N_s A E_p}{N_0} \frac{[R(\epsilon_j) - R(\delta_{opt} - \epsilon_j)]^2}{1 - R(\delta_{opt})}}\right)$
BPSK	$Q\left(\sqrt{\frac{2N_s A E_p}{N_0} R^2(\epsilon_j)}\right)$
OOK	$\frac{1}{2}\left[Q\left(\sqrt{\frac{N_s A E_p}{N_0}}\right) + Q\left(\sqrt{\frac{N_s A E_p}{N_0}[2R(\epsilon_j) - 1]^2}\right)\right]$

Note that in order to multiply the SNR with the processing gain N_s, it is assumed that all N_s pulses are subject to same amount of timing jitter. For orthogonal PPM, $R(\delta)$ becomes zero and the above equation reduces to

$$SNR = \frac{N_s A E_p}{N_0} R^2(\epsilon_j) \ . \tag{7.12}$$

For BPSK, using ω_{rec} as the receiver template and proceeding with a similar analysis yields

$$SNR = \frac{2N_s A E_p}{N_0} R^2(\epsilon_j) \ . \tag{7.13}$$

Note that the effect of timing jitter on the system performance is the attenuation of the SNR with the corresponding correlation terms that depend on the employed pulse shape and modulation scheme.

For OOK modulation, reception of *zero*s are not affected by timing jitter since no pulse is sent for the transmission of *zero*s. Reception of *one*s will be degraded severely due to employed detection algorithm that compares the correlator output with a certain threshold. The resulting BER equation can be evaluated to be the sum of the *false alarm rate* and the *missed detection rate* using standard tools, which is shown in Table 7.1 together with performances of other modulation schemes. The value of a in Table 2.1 is taken as $\sqrt{2}$ to make the average transmitted energy of OOK identical with the other modulation schemes. Equations for BPSK and orthogonal PPM imply that SNRs in both schemes decrease in equal proportions, conserving the 3dB power efficiency of the former scheme to the latter irrespective of the timing jitter.

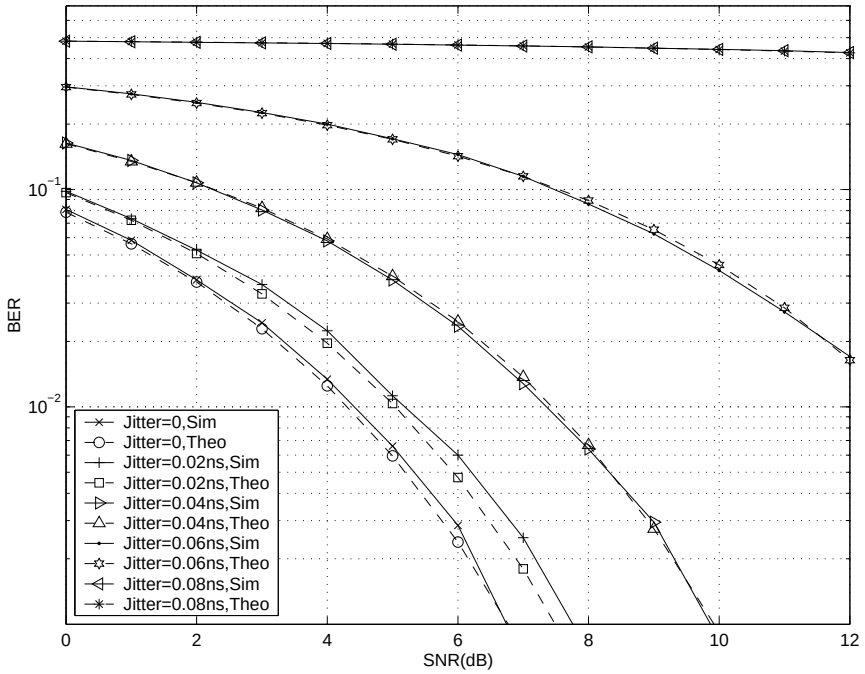

Figure 7.3 BER performance of BPSK with constant jitter in AWGN channel ($T_c = T_h = 0.8ns, N_s = 1$).

Knowing the PDF of timing jitter, the calculated BER expressions can be integrated over all possible jitter values to evaluate the average performance. Assuming that timing jitter is uniformly distributed between $(-\epsilon_0, \epsilon_0)$ the BER performance can be evaluated as follows

$$P_{avg}(\Gamma, \epsilon_0) = \int_{-\epsilon_0}^{\epsilon_0} P_b(\Gamma, \epsilon_j) p(\epsilon_j) d\epsilon_j \ , \tag{7.14}$$

where Γ denotes the SNR of the received signal, $P_{avg}(\Gamma)$ denotes the average BER corresponding to a certain jitter distribution at a certain SNR, $P_b(\Gamma, \epsilon_j)$ denotes the BER at a certain SNR and a fixed value of timing jitter as given in Table 7.1, and $p(\epsilon_j)$ is the probability density function of jitter, which is for uniform distribution given by

$$p(\epsilon_j) = \frac{1}{2\epsilon_0} \ . \tag{7.15}$$

The integral in (7.14) can be evaluated semi-analytically to average the BER performance over all possible jitter values. Theoretical and simulation results for BPSK in AWGN channel are depicted in Fig. 7.3 for a fixed value of timing jitter and in Fig. 7.4 for jitter uniformly distributed between

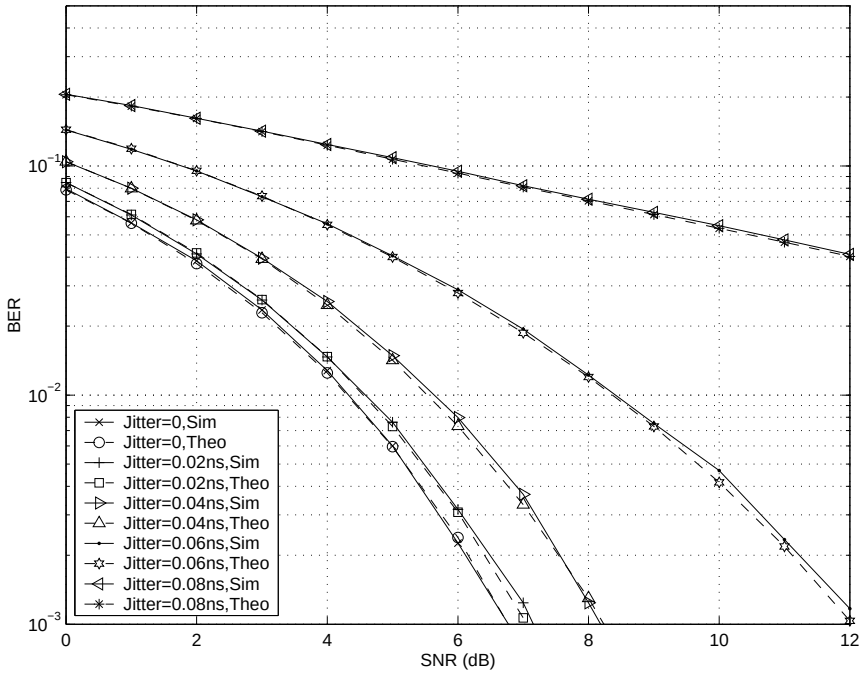

Figure 7.4 BER performance of BPSK with uniform distributed jitter in AWGN channel ($T_c = T_h = 0.8ns, N_s = 1$).

$\pm\epsilon_0$. Note that when the fixed value of jitter is $80ps$, accuracy of the detection is close to %50 since the SNR after the correlator output becomes very close to zero. Fig. 7.5 compares the performances of the four modulation schemes when jitter is uniformly distributed between $\pm\epsilon_0$, where it is seen that the gap between OOK and orthogonal PPM increases for larger values of timing jitter.

7.3.2 BER Performances in One-tap Rayleigh Fading Channel

In one-tap Rayleigh fading channels, the received signal has a complex amplitude γ_l that has a Rayleigh distribution. In such environments, the probability of error is found by integrating the BER over all possible instantaneous SNR values [52]

$$P_{rayl}(\Gamma) = \int_0^\infty P_b(\Gamma, \gamma) p(\gamma) dA, \tag{7.16}$$

where γ is the instantaneous SNR of the received signal given by $\gamma_l^2 \frac{N_s A E_p}{N_0}$, Γ is the average SNR, $P_{rayl}(\Gamma)$ is the bit error probability at a certain average SNR, and $p(\gamma)$ is the PDF of the instantaneous SNR values characterized by a chi-square distribution with two degrees of freedom which can

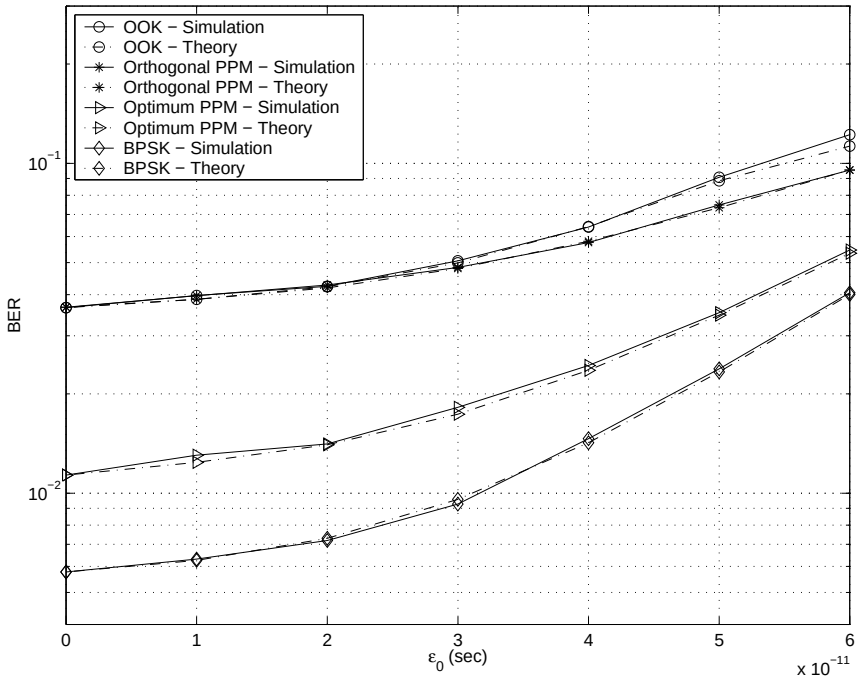

Figure 7.5 Effect of the fixed value of timing jitter on the BER performances of different modulation schemes ($SNR = 5dB, T_c = T_h = 0.8ns, N_s = 1$).

be written as

$$p(\gamma) = \frac{1}{\Gamma} exp\left(-\frac{\gamma}{\Gamma}\right) \ . \tag{7.17}$$

Plugging the error probabilities for different modulation schemes from Table 2.1 in (7.16), the closed form solution for the BER in Rayleigh fading channel is evaluated as

$$P_{rayl}(\Gamma) = \frac{1}{2}\left(1 - \sqrt{\frac{\Gamma'}{2+\Gamma'}}\right) \ , \tag{7.18}$$

where $\Gamma' = \Gamma$ for orthogonal PPM, $\Gamma' = 2\Gamma$ for BPSK, and $\Gamma' = \Gamma(1 - R(\delta))$ for optimum PPM. For a fixed value of timing jitter, the SNR values will be multiplied with the corresponding autocorrelation values as summarized in Table 7.2.

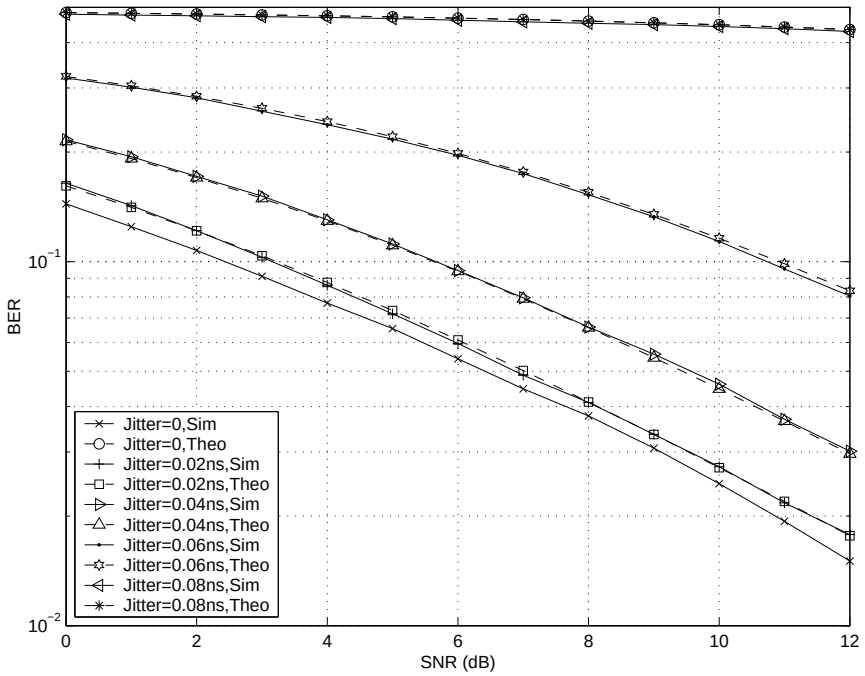

Figure 7.6 BER performance of BPSK with constant jitter in Rayleigh fading channel ($T_c = T_h = 0.8ns, N_s = 1$).

For uniformly distributed timing jitter, BER in Rayleigh fading channel can be evaluated by a numerical integration of expressions in Table 7.2 over all possible jitter values as

$$P_{avg}(\Gamma, \epsilon_0) = \int_{-\epsilon_0}^{\epsilon_0} P_{rayl}(\Gamma, \epsilon_j) p(\epsilon_j) d\epsilon_j \ . \tag{7.19}$$

Performance results for BPSK in Rayleigh fading channel for a fixed value of jitter and for uniformly distributed jitter are depicted in Figs. 7.6 and 7.7. Similar comments as in AWGN channel can be repeated, together with an observation of overall performance degradation for all jitter scenarios due to fading.

7.3.3 BER Performances in Dispersive Channel

Due to reflection, diffraction and scattering effects, the transmitted signal arrives at the receiver through multiple paths with different delays. The received signal from an N-tap channel can be

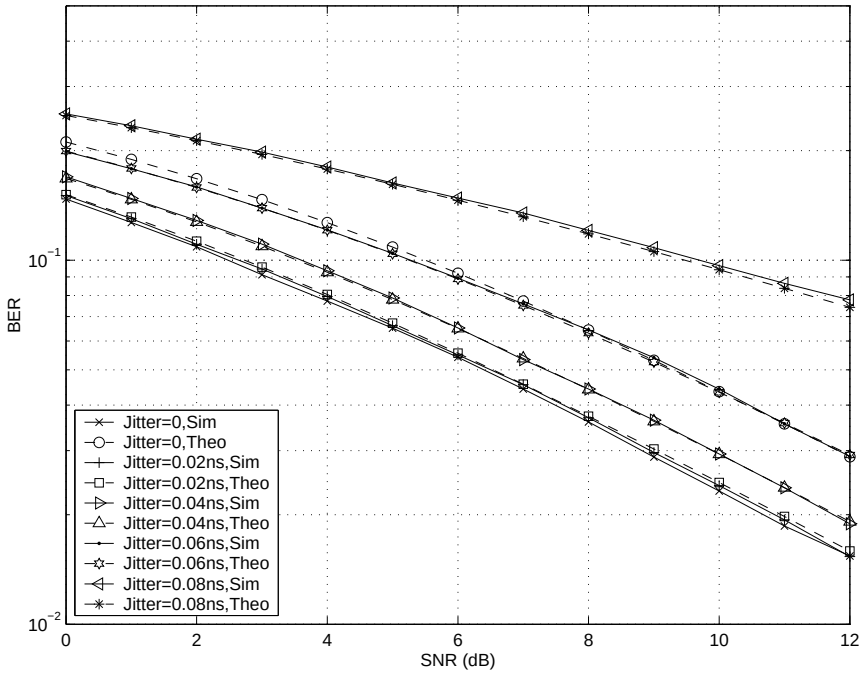

Figure 7.7 BER performance of BPSK with uniform distributed jitter in Rayleigh fading channel ($T_c = T_h = 0.8ns, N_s = 1$).

written as follows

$$r_{mp}(t) = \sum_{l=1}^{N} \gamma_l s^{(k)}(t - \tau_l) + n(t) \ , \tag{7.20}$$

where γ_l is the tap attenuation for the lth tap arriving at time τ_l and $s^{(k)}(t)$ is the transmitted signal from (2.1).

By using Rake receivers, it is possible to collect the energy at the delayed taps. *All-Rake*, *selective Rake*, or *partial Rake* receivers are all feasible approaches to collect all, strongest, or first arriving resolvable multipath components respectively [69]. Optimal combining of the multipath components is achieved by maximal ratio combining (MRC) in white noise, where the finger weights are designed based on the channel tap weights to maximize the output SNR. A reduced complexity combining technique that does not require the estimates of the fading amplitudes is equal gain combining (EGC), where all the multipath components are weighted equally.

Table 7.2 BER performances of UWB modulation schemes in Rayleigh fading channel and in the presence of timing jitter.

Modulation	BER
Orthogonal PPM	$\frac{1}{2}\left(1-\sqrt{\frac{\Gamma R^2(\epsilon_j)}{2+\Gamma R^2(\epsilon j)}}\right)$
Optimum PPM	$\frac{1}{2}\left(1-\sqrt{\frac{\Gamma R_{opt}}{2+\Gamma R_{opt}}}\right)$, $R_{opt}=\frac{[R(\epsilon_j)-R(\delta_{opt}-\epsilon_j)]^2}{1-R(\delta_{opt})}$
BPSK	$\frac{1}{2}\left(1-\sqrt{\frac{\Gamma R^2(\epsilon_j)}{1+\Gamma R^2(\epsilon j)}}\right)$

The PDF of the instantaneous SNR when using MRC is given by [52]

$$p(\gamma) = \sum_{k=1}^{N} \frac{\pi_k}{\Gamma_k} e^{-\frac{\gamma}{\Gamma_k}} , \tag{7.21}$$

$$\pi_k = \prod_{i=1, i\neq k}^{N} \frac{\Gamma_k}{\Gamma_k - \Gamma_i} , \tag{7.22}$$

where Γ_k is the average SNR for the kth tap. Knowing the PDF of the SNR, BER equation for AWGN can be conditioned on the instantaneous SNR and the average BER performance can be evaluated through integration over all possible SNR values. For example for BPSK, average performance using MRC in the presence of fixed timing jitter is given by

$$P_{mpath}(\Gamma, \epsilon_j) = \int_0^\infty p(\gamma) \frac{1}{2} \text{erfc}\left(\sqrt{\gamma R^2(\epsilon_j)}\right) d\gamma , \tag{7.23}$$

where it is assumed that all multipath taps are subject to same amount of timing jitter. This formulation can again be integrated over the PDF of timing jitter to find the average performance in the presence of uniformly distributed jitter

$$P_{avg}(\Gamma, \epsilon_0) = \int_{-\epsilon_0}^{\epsilon_0} P_{mpath}(\Gamma, \epsilon_j) p(\epsilon_j) d\epsilon_j . \tag{7.24}$$

Performance results for BPSK using MRC Rake receivers for a fixed value of jitter and for uniformly distributed jitter are shown in Figs. 7.8 and 7.9. A four tap Rayleigh fading channel profile with exponentially distributed average tap weights is assumed, and a Rake receiver with four fingers is employed, which assumes a perfect knowledge of the channel. Notice how the performance is improved compared to one-tap Rayleigh fading channel when using maximal ratio diversity combining. Different channel models (such as the channel measurements presented in [94], or IEEE 802.15

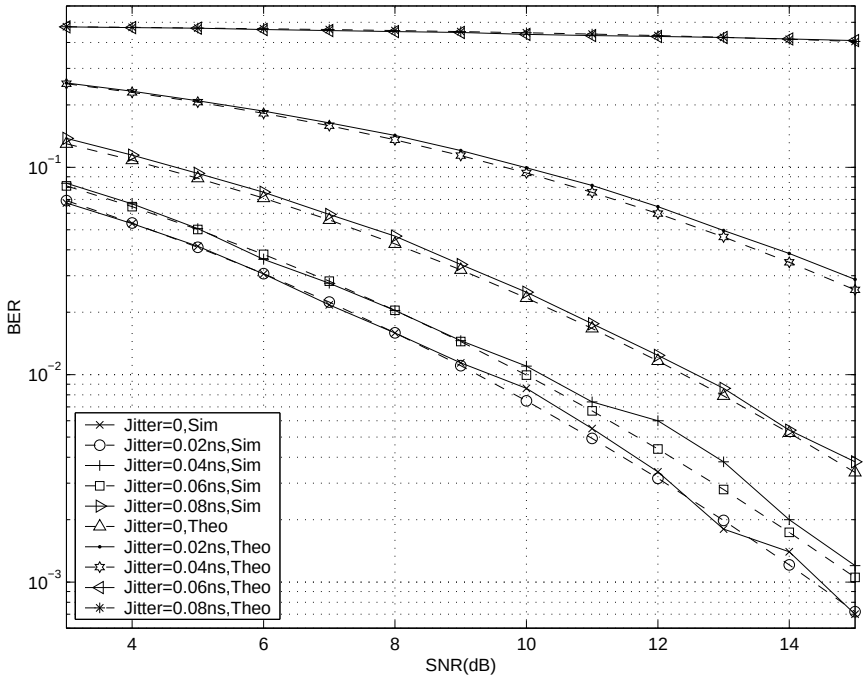

Figure 7.8 BER performance of BPSK with constant jitter in 4-tap multipath fading channel (exponential power delay profile) using MRC Rake receiver ($T_c = T_h = 0.8ns, N_s = 1$).

channel model [2]) can be easily integrated to the formulation outlined above, since the performance is a function of average tap weights.

7.4 Effect of Timing Jitter Distribution on System Performance

In the previous section it is assumed that timing jitter is uniformly distributed. Sources of timing jitter can be numerous, and therefore jitter can have different distributions. Sometimes, the timing jitter can be characterized by its range and RMS value only, where an upper bound for system performance is helpful to evaluate the worst case performance. In this section, first, jitter due to finger estimation error is introduced and its PDF is obtained using simulations. Later, effect of jitter PDF on system performance is analyzed and a worst case distribution given the variance and the range of the timing jitter is presented.

7.4.1 Jitter Due to Finger Estimation

Due to UWB delay resolution, Rake receivers have been widely proposed in order to exploit time diversity in multipath channels. Rake receiver requires the knowledge of the path delays to be able

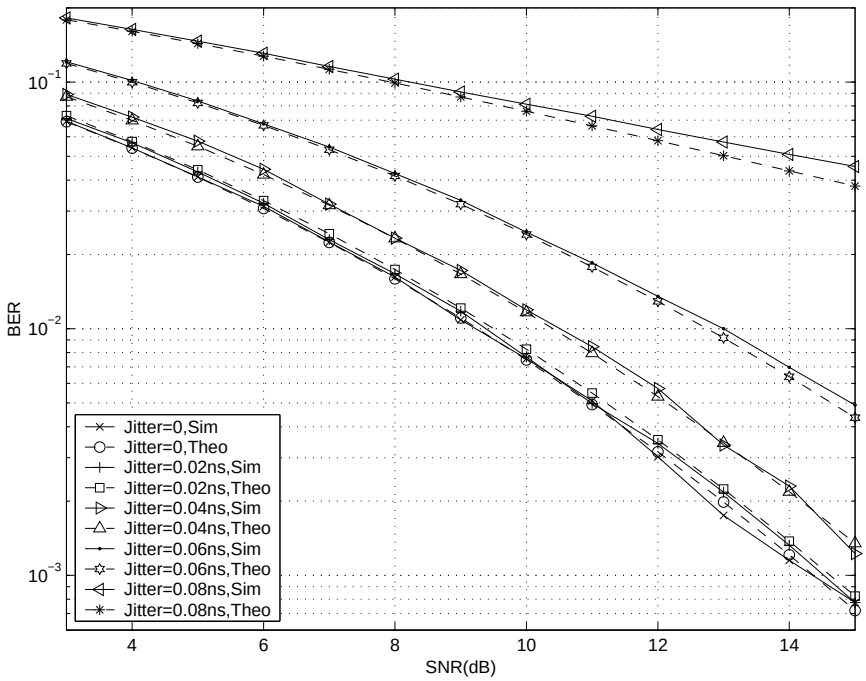

Figure 7.9 BER performance of BPSK with uniform distributed jitter in 4-tap multipath fading channel (exponential power delay profile) using MRC Rake receiver ($T_c = T_h = 0.8ns, N_s = 1$).

to lock on each correlator (finger) and coherently add the energy, increasing SNR. As explained in [57], finding the path locations is not an easy task due to pulse shaping. For each arriving path to the receiver, the pulse shape observed after correlation contains many components with non-zero energy. Finger estimation maximizes this correlation function in order to pick up the component with more energy. In the presence of noise, autocorrelation function may be maximized at times other than the actual position of the finger, which yields a finger estimation error. The timing jitter due to such an impairment may be on the order of the pulse width T_c and depends on the SNR value.

Jitter due to transceiver impairments are commonly modeled as Gaussian or uniform, but these models are no longer valid for finger estimation error. In order to find the appropriate model, finger estimation error is simulated for different SNR scenarios to obtain a histogram of resulting timing jitter. PDFs for different SNR values in Fig. 7.10 show that when SNR is low, the PDF is similar to the autocorrelation function of the first derivative of the monopulse, and finger locations are estimated between zero and T_c. For larger SNR, the PDF converges to an impulse function located at the actual position of the finger.

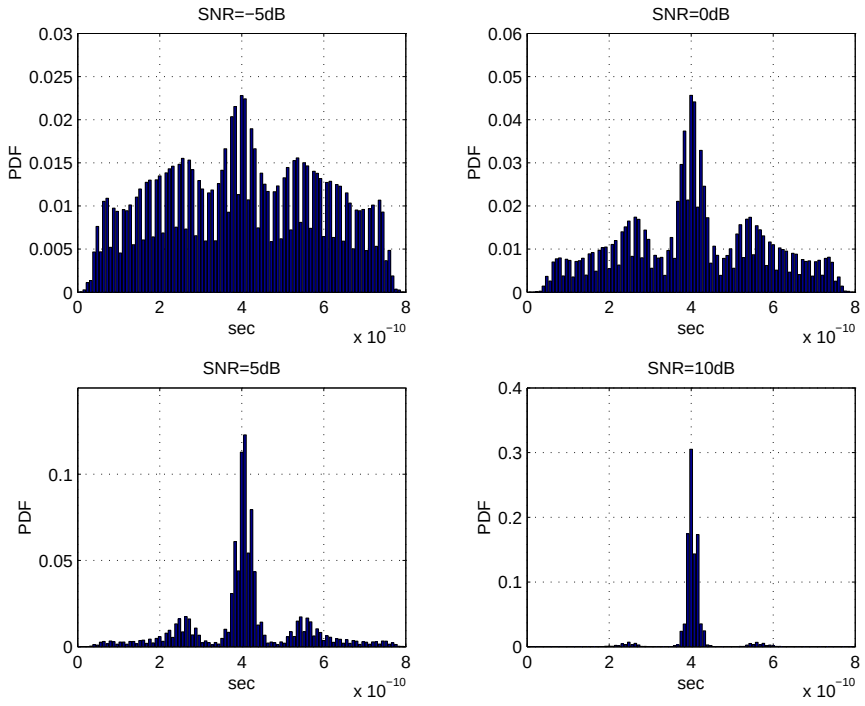

Figure 7.10 Probability densities of finger estimation errors ($T_c = T_h = 0.8ns$).

7.4.2 Effect of Jitter PDF on the BER Performance

It is shown in the previous section that in order to estimate the effect of timing jitter on the BER performance, PDF of timing jitter has to be known. Note that obtaining PDF would be difficult in many cases, instead statistics like RMS value and range (minimum and maximum jitter values) can be measured [224]. Given the variance, σ_ϵ^2, and the range, r_ϵ, of timing jitter, a worst case distribution (WCD) that will cause the largest degradation in system performance is given as [224, 225]

$$p(\epsilon_j) = \frac{\sigma_\epsilon^2}{2r_\epsilon^2}\left[\delta_D(\epsilon_j - r_\epsilon) + \delta_D(\epsilon_j + r_\epsilon)\right] + \left(1 - \frac{\sigma_\epsilon^2}{r_\epsilon^2}\right)\delta_D(\epsilon_j)\ , \tag{7.25}$$

where δ_D denotes the Dirac delta function. Given the range and the variance of the timing jitter, this PDF yields an upper bound for the system performance irrespective of the jitter distribution that has the same range and variance. Note that one can easily change the variance of the WCD without modifying its range.

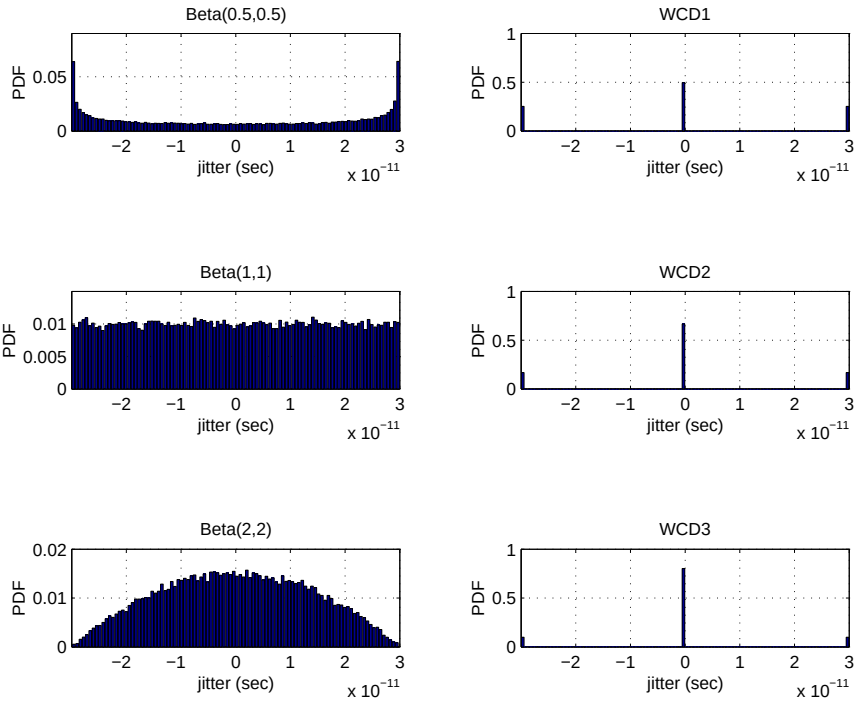

Figure 7.11 Histograms for the timing jitter used in the simulations and the corresponding worst case distributions that have the same variance and the range.

In order to compare the BER performances using different jitter distributions, random timing jitter are constructed using the Beta probability distribution with different parameters, given by [240]

$$p(\epsilon_j, p, q) = \frac{\epsilon_j^{p-1}(1-\epsilon_j)^{q-1}}{B(p,q)} \ , 0 \leq \epsilon_j \leq 1 \ , \tag{7.26}$$

$$B(p,q) = \int_0^1 t^{p-1}(1-t)^{q-1}dt \ , \tag{7.27}$$

The PDFs for the three different Beta distributions characterized by the parameters $(p,q) = (2,2)$ to represent a bounded Gaussian-like distribution, $(p,q) = (1,1)$ which corresponds to the uniform distribution, and $(p,q) = (0.5, 0.5)$ that has largest probability at the edges of the distribution are depicted in Fig. 7.11. All the three distributions are scaled so that the range of the timing jitter is $\pm 30ps$, which can be used as a typical margin for UWB systems [62]. For each Beta distribution, a worst case distribution with the same variance and range is evaluated, and obtained jitter samples are used in computer simulations. Performance results in Fig. 7.12 for BPSK show that WCD indeed yields an upper bound for another distribution that has the same variance and

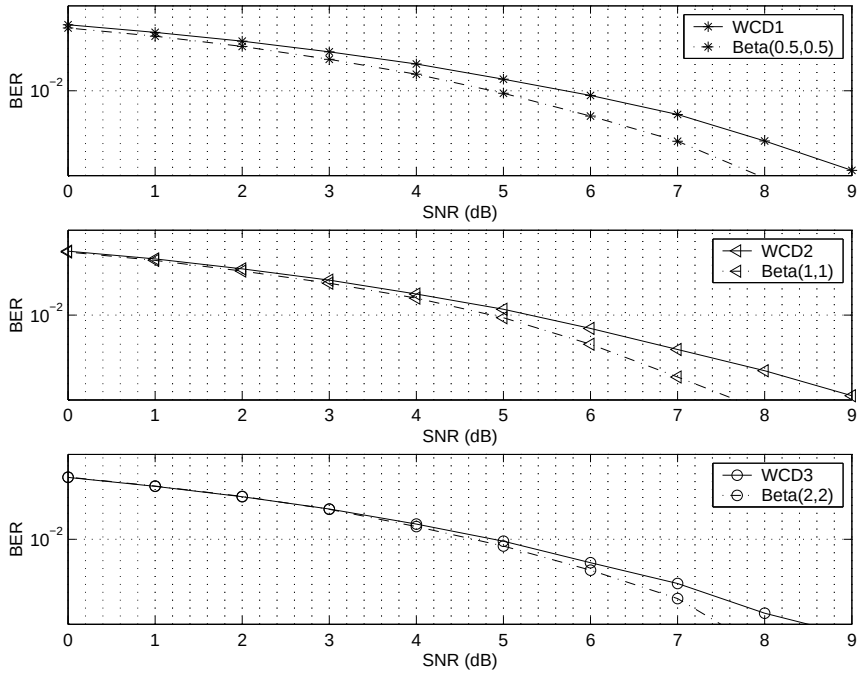

Figure 7.12 BER performance of BPSK for different jitter distributions in AWGN channel ($T_c = T_h = 0.8ns, N_s = 1$).

range. Beta distribution with $(p, q) = (0.5, 0.5)$ yields the worst performance compared to other Beta distributions, since it resembles to the WCD with the peaks at the edges of the distribution. Bounded Gaussian-like distribution has the best performance, because as mentioned in the previous section, performance degradation for small jitter values is negligible. Tightness of the worst case bound increases from the former to the latter.

7.5 Effect of Timing Jitter on the Performance of Systems With Different Pulse Shapes

As shown in Section 7.3 (Tables 7.1, 7.2), autocorrelation function of the employed pulse shape for a certain jitter value is a direct measure of the system performance. If the autocorrelation function decays faster, UWB performance will be more affected from timing jitter. In this section, effect of timing jitter on the performances of multiband [71] and modified Hermite polynomial based [241] UWB schemes are investigated.

Multiband UWB scheme is achieved by dividing UWB spectrum into a number of frequency bands by using a different pulse shape at each band. In order to adjust the central frequency of

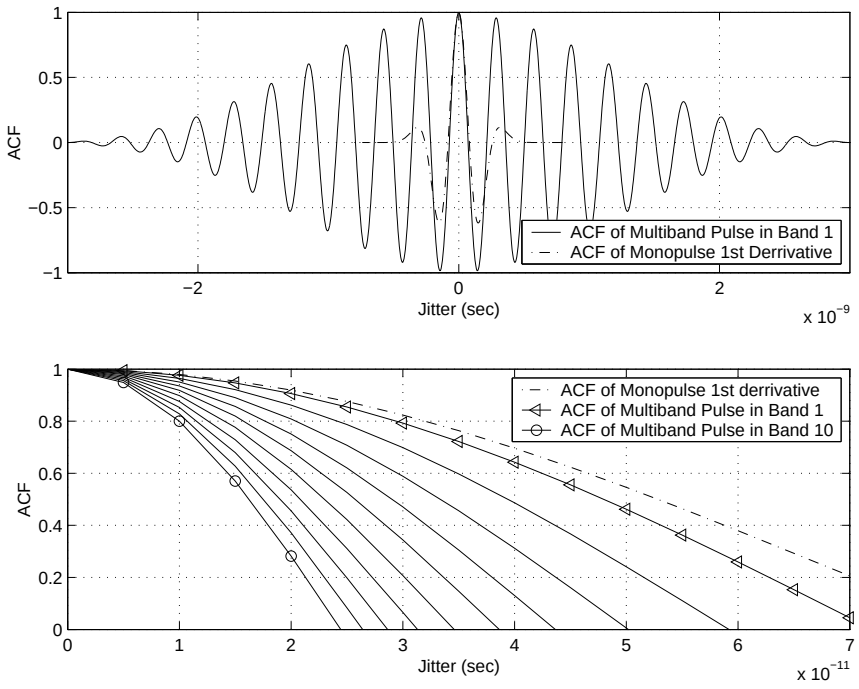

Figure 7.13 Comparison of autocorrelation functions of derivative of mono-cycle vs. pulse used in band-1 of multiband scheme, and comparison of the autocorrelations of the pulses used in all bands.

each band, pulses used at higher order bands have larger frequencies. This approach has a number of advantages, such as mitigating interference by not transmitting at the band(s) that are occupied by other technologies, or adjusting the data rate by using desired number of bands. In spite of these advantages, multiband scheme is more susceptible against timing jitter for higher order bands since the autocorrelation function of pulses used at these bands decay faster. In order to see the effect of timing jitter, a sample multiband scheme is constructed by dividing the $3.1 - 10.6$ GHz band into ten bands of 750 MHz each. The autocorrelation functions of the pulse used in band-1 (3.1-3.85 GHz) of multiband scheme and the pulse in (2.3) which is used in standard UWB scheme are compared in Fig. 7.13. It is seen that since the central frequencies of both systems are close, similar degradation will be observed in the performances. Fig. 7.13 also compares the autocorrelation functions of the pulses used in different bands of the multiband scheme with respect to the fixed timing jitter value that ranges from 0 to $70ps$. It is observed that degradation due to timing jitter when using multiband scheme will be worse for higher order bands.

A similar analysis can be repeated for UWB schemes that employ modified Hermite polynomial based pulses [241]. Using these polynomials, it is possible to construct a new pulse that is orthogonal

to the previous pulses by using certain transformations. Such higher order pulses have larger number of zero crossings and their autocorrelation functions decay faster, implying less robustness against timing jitter [239].

7.6 Conclusion

In this chapter, a framework that enables evaluation of the performances of different UWB modulation schemes in the presence of timing jitter is presented. It is observed that the performances of BPSK and PPM are degraded similarly, while OOK yields biased decisions towards zero. The PDF of timing jitter due to finger estimation error is presented using simulations. It is shown that the PDF depends on the employed pulse shape and the SNR. A worst case distribution that minimizes the system performance is also given and compared with other distributions that have the same variance and range. It is shown that for a given jitter range and variance, the worst case distribution provides an upper bound regardless of the jitter distribution. Dependency of the BER performance on the employed pulse shape is analyzed, and it is concluded that if the autocorrelation function of the employed pulse decays faster, the UWB system is more susceptible against timing jitter. Finally, the effect of timing jitter on the recently proposed multiband scheme is evaluated, where the higher bands are observed to be more susceptible against timing jitter as the pulses corresponding to those bands have narrower main lobes. As a result, users have to use time-frequency hopping codes so that every user benefits/suffers equivalently from all the bands.

CHAPTER 8

BER PERFORMANCES OF IR-UWB TRANSCEIVER TYPES AT SUB-NYQUIST SAMPLING RATES

8.1 Introduction

Despite the growing amount of technical contribution in the literature, successful deployment of *practical* IR-UWB networks still requires facing the challenges that arise at larger bandwidths and under practical operating scenarios. Due to very short duration of pulses, UWB receivers are capable of observing individual multipath components, which may be on the order of hundreds. When Nyquist rate sampling is possible, Rake receivers are the optimal receivers that can capture a large portion of the received energy [242], which is made possible with accurate synchronization to individual multipath components, and with exact knowledge of received pulse shapes. However, extremely large bandwidths of UWB signals make it challenging, complex, and costly to sample them at Nyquist rate to have all-digital implementation. Required high resolution analog to digital converters (ADC) are typically difficult to design even with most modern process technologies, and are power hungry [243]. Instead, the received signals may have to be sampled at lower rates. Since perfect matched-filtering no longer becomes possible at sub-Nyquist sampling due to 1) imperfect synchronization to individual replicas, and 2) the difficulty of estimating the *received* pulse shapes at different multipath components, suboptimal receiver techniques become of practical interest.

Performances of different transceiver types have been investigated before in the literature with the assumption of Nyquist-rate sampling. Rake reception for IR-UWB (as well as other wide-band) systems using different combining schemes have been analyzed in the literature [244]-[248]. Effect of imperfect tap weights [249, 250], and imperfect channel delay estimates [251] on the Rake performance were also investigated. Effects of template quantization noise on the channel estimation error was discussed in [252], frequency-dependent distortion effects and its implications on the receiver design was addressed in [253], and optimal/sub-optimal correlator template designs were covered in [254, 255]. Performances of Rake and transmitted-reference (TR) receivers were compared

in [256], where imperfect channel fading coefficient estimates, and perfect finger synchronization were assumed. Comparison of coherent, differentially coherent, and non-coherent transceivers under ideal scenarios was made in [257] using simulations. Energy detection (ED) and TR has been also analyzed individually in the literature as alternative UWB signal reception schemes [258]-[260]. A channel estimation technique which estimates the sample-spaced *projection* of the received multipath components was discussed before in [261], which recognizes the need for sub-optimal (but practical) algorithms for IR-UWB systems that operate at low rate samples. However, theoretical comparison of different transceiver architectures in realistic sampling constraints and different scenarios has not been addressed in the literature to the best knowledge of the authors.

In this chapter, three transceiver architectures that operate at low rate samples (e.g. chip-rate) are analyzed. In particular, bit error rate (BER) performances of stored-reference (SR), TR, and ED schemes are presented for various modulation schemes both in additive White Gaussian noise (AWGN) and multipath channels, and using Gaussian approximations (GA). The main contribution of the chapter is presenting a unified (semi-analytic) performance analysis framework for SR (with different combining options), TR, and ED receivers, which are based on histograms of the collected energies at sub-Nyquist sampling rates. Various trade-offs between different transceiver types are investigated, and issues such as channel estimation and effects of correlator template are discussed. Semi-analytical results are compared with simulations in IEEE802.15.4a channel models [3]. While SR enjoys the advantage brought by the clean correlator templates, its energy capture capability drops significantly as the sampling rate decreases.

8.2 System Model

8.2.1 Received UWB Signals

While the transmitted signals are (typically) the same for SR and ED receivers, TR includes delayed version of the same signal, and therefore yields a slightly different transmitted signal model. Let the received UWB multipath signal for the former schemes be represented as

$$r(t) = b_{\lfloor j/N_s \rfloor} r_s\big(t - a_{\lfloor j/N_s \rfloor}\delta\big) + n(t) \ , \tag{8.1}$$

$$r_s(t) = \sum_{j=-\infty}^{\infty} d_j \omega_{mp}\big(t - jT_f - c_j T_c - \tau_{toa}\big) \ , \tag{8.2}$$

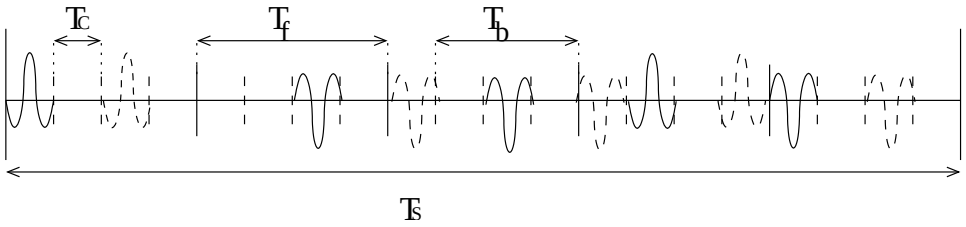

Figure 8.1 Illustration of transmitted IR-UWB pulses in a symbol, where $(N_s, N_h) = (5, 4)$, $T_b = 3T_c$, and $(\{c_j\}, \{d_j\}) = (\{0, 2, 1, 1, 0\}, \{+1, -1, -1, +1, -1\})$. The pulses with solid lines correspond to ED and SR. Dashed pulses can be included for TR (after appropriate energy scaling) with $D = 2T_c$.

while for the TR case the received signal is modeled by

$$\tilde{r}(t) = \frac{1}{\sqrt{2}}\Big(r_s(t) + b_{\lfloor j/N_s \rfloor} r_s\big(t - a_{\lfloor j/N_s \rfloor}\delta - D\big)\Big) + n(t) \ , \tag{8.3}$$

where frame index and frame duration are denoted by j and T_f, N_s represents the number of pulses per symbol, T_c is the chip duration, T_s is the symbol duration, τ_{toa} is the time of arrival (TOA) of the received signal, and N_h is the possible number of chip positions per frame, given by $N_h = T_f/T_c$. Effective pulse after the channel impulse response is given by $\omega_{mp}(t) = \sqrt{E_p}\sum_{l=1}^{L} \alpha_l \omega_l(t - \tau_l)$, where $\omega_l(t)$ is the received UWB pulse with unit energy, $E_p = \frac{E_b}{N_s}$ is the pulse energy, E_b is the bit energy, and α_l and τ_l are the fading coefficients and delays of the multipath components, respectively. Additive white Gaussian noise (AWGN) with zero-mean and double-sided power spectral density $\mathcal{N}_0/2$ and variance σ^2 is denoted by $n(t)$. The delay between the data and reference signals is denoted by D, and energy is appropriately scaled so that energy per symbol is identical for all cases. In order to avoid catastrophic collisions, and smooth the power spectral density of the transmitted signal, time-hopping codes $c_j^{(k)} \in \{0,\ 1, ..., N_h - 1\}$ are assigned to different users. Moreover, pseudo-random polarity codes $d_j \in \{\pm 1\}$ are used to introduce additional processing gain for the detection of desired signal, and smooth the signal spectrum (see Fig. 8.1).

Modulation can be binary phase shift keying (BPSK) or higher order $\mathcal{M}$-ary pulse amplitude modulation (PAM) for SR or TR schemes, where $b_{\lfloor j/N_s \rfloor} = (2m - 1 - \mathcal{M})$ and $a_{\lfloor j/N_s \rfloor} = 0\ \forall j$, $m \in \{1, 2, ..., \mathcal{M}\}$[1]. On the other hand, binary or $\mathcal{M}$-ary pulse position modulation (PPM) can be implemented for all three schemes using $a_{\lfloor j/N_s \rfloor} \in \{0,\ 1,\ ..., \mathcal{M} - 1\}$ and $b_{\lfloor j/N_s \rfloor} = 1\ \forall j$. The modulation index δ can be selected as multiples of chip-width, or it can be adjusted appropriately

[1]Note that $\mathcal{M}$-ary PAM may also be possible for ED if strictly positive amplitudes are used. However, received amplitudes will depend on the noise level, complicating the detection.

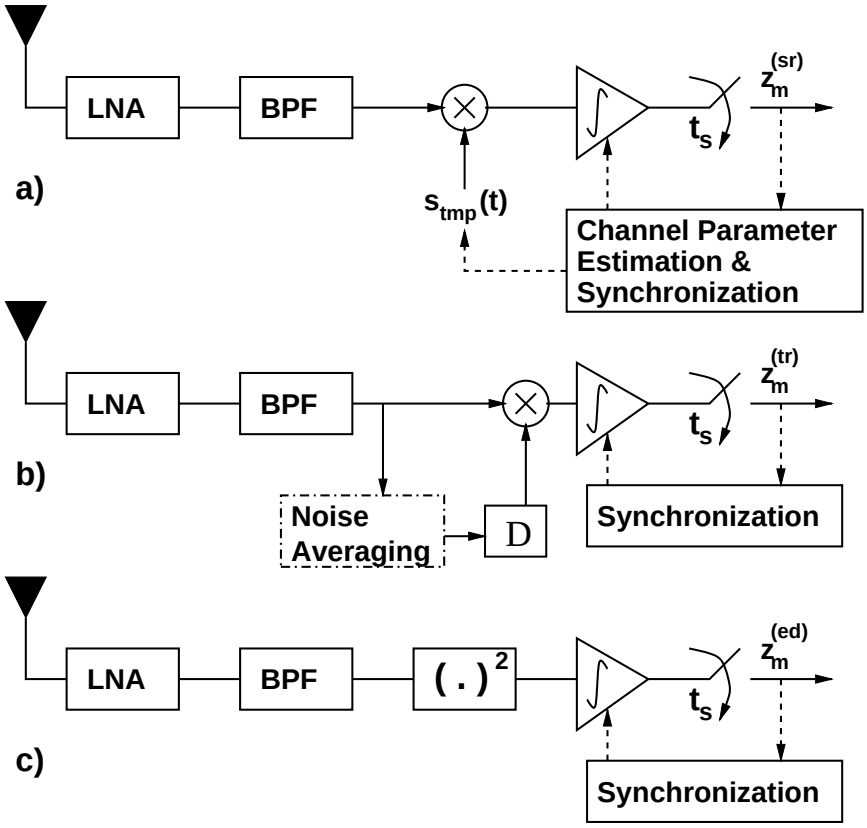

Figure 8.2 Different transceiver types for IR-UWB signaling: a) Stored-reference, b) Transmitted-reference, and c) Energy detection. We assume that t_s is on the order of chip duration. Also, $s_{tmp}(t)$ has to be estimated in practice.

to increase the Euclidean distance between the symbols for improving the performance of SR or TR [11]. On the other hand, it is better for TR and ED to be on the order of maximum excess delay to minimize multipath effects. On-off keying (OOK), where $b_{\lfloor j/N_s \rfloor} \in \{0, 1\}$ and $a_{\lfloor j/N_s \rfloor} = 0 \; \forall j$, can be used with all the three schemes, which requires estimation of a threshold, and practical threshold estimation techniques will be discussed in the upcoming sections. Bi-orthogonal modulations that are combinations of $\mathcal{M}$-ary PAM and $\mathcal{M}$-ary PPM are also possible for SR and TR. In the sequel, we consider only the binary modulation schemes when carrying out the performance analysis.

8.2.2 Receiver Analog Front-End Processing

Different approaches for collecting the energy are possible *before* sampling the signal in (8.1) or (8.3). Sampling can be achieved after correlating a locally generated template with the received

signal for SR (Fig. 8.2a), after a delay-and-correlate process (via delay lines in analog) for TR (Fig. 8.2b), and after a square law device for ED (Fig. 8.2c). In order to formulate the energy capture and corresponding decision statistics, consider the received waveforms in (8.1) and (8.3), and assume that the receiver is accurately synchronized to the leading edge of the received signal within a timing ambiguity determined by the sampling rate. In other words, the TOA is assumed to be estimated perfectly within the sampling granularity, i.e. $\hat{\tau}_{toa} = \left\lfloor \frac{\tau_{toa}}{t_s} \right\rfloor t_s$, where t_s denotes the sampling time. For all receiver types, the energy is collected within an integration window of length $T_{int} = N_{int} t_s$, which is smaller than the maximum excess delay of the channel[2]. Then, the decision statistics for the three transceiver types can be obtained as follows.

8.2.2.1 Stored Reference

For the case of SR, a sample-spaced correlator template can be defined as

$$s_{tmp}(t) = \sum_{j=\kappa N_s}^{(\kappa+1)N_s-1} \sum_{i=0}^{N_{int}-1} d_j \gamma_i \omega\left(t - jT_f - c_j T_c - it_s\right) , \tag{8.4}$$

where κ is the symbol index. The samples after correlating the received signal in (8.1) with the above template are given by

$$z_\kappa^{(sr)} = \int_{\kappa N_s T_f + \hat{\tau}_{toa}}^{(\kappa+1)N_s T_f + \hat{\tau}_{toa}} r(t) s_{tmp}\left(t\right) dt , \tag{8.5}$$

respectively, where γ_i is the combining coefficient for the ith pulse within the template window. In this chapter, we consider three different combining schemes for implementing a Rake receiver. For MRC and EGC, we have

$$\gamma_i = \begin{cases} \tilde{\alpha}_i^* , & \text{if MRC} , \\ e^{-j\angle\tilde{\alpha}_i} , & \text{if EGC} , \end{cases} \tag{8.6}$$

where $\tilde{\alpha}_i$ are the sample-spaced projected channel coefficients [261], and $*$ denotes the complex conjugate operation. Note that both in MRC and EGC, all the sample-spaced paths within the integration window are considered. While MRC requires the exact knowledge of fading amplitudes,

[2] Optimality of the integration window length for TR and ED was analyzed in the literature (e.g. [42] and references therein), and will not be discussed further here.

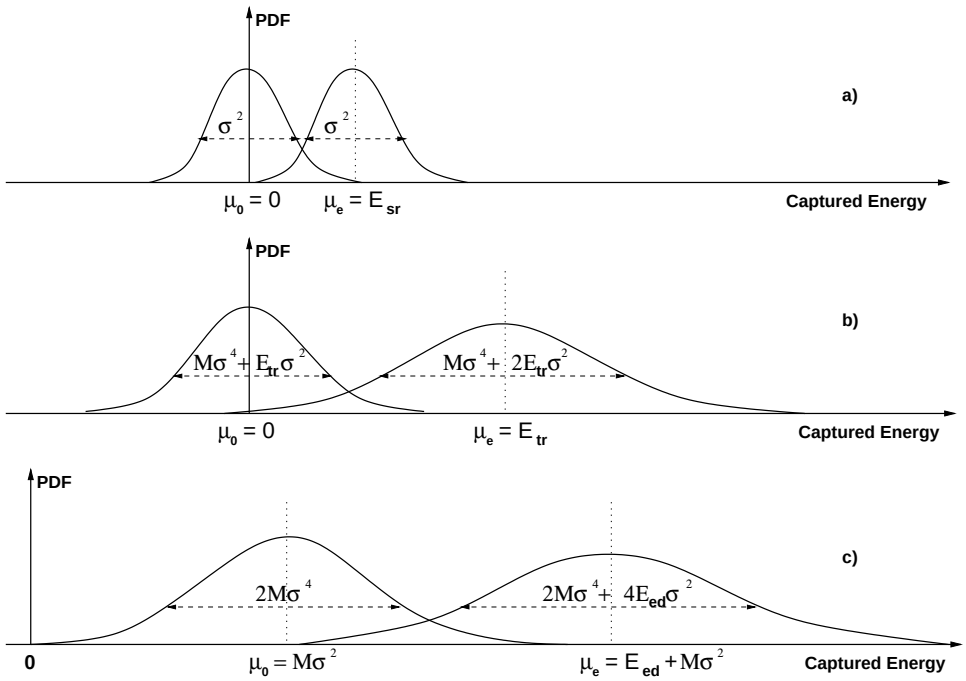

Figure 8.3 Comparison of mean and variance statistics of the sampled received signal in the presence and absence of signal energy within a certain sampling interval: a) Stored-reference (perfect template and channel estimates), b) Transmitted-reference (noisy template), and c) Energy detection.

EGC only requires the phases[3] and is thus more practical than the MRC. On the other hand, for selective combining (SC), only the strongest multipath component is used for detection, which considerably decreases the receiver complexity for a suboptimal performance. The mathematical representation for SC coefficients can be defined as

$$\gamma_i = \begin{cases} \tilde{\alpha}^*_{i'} \ , & \text{if } i' = \underset{i}{\text{argmax}} \left|\tilde{\alpha}_i\right| \ , \\ 0 \ , & \text{otherwise} \ . \end{cases} \tag{8.7}$$

The decision statistic in (8.5) depends on the captured energy under a particular sampling rate, integration interval, and channel realization. Letting E_{sr} to denote the captured energy for SR receiver when a signal is present and using a particular combining scheme, the decision statistics for

[3]For a carrier-less UWB signal, EGC only requires the polarities, since the phases are either 0 or π.

two different symbol hypothesis are as follows

$$z_{\kappa}^{(sr)} \sim \begin{cases} \mathcal{N}\left(E_{sr}, \sigma^2\right) , & \text{signal} , \\ \mathcal{N}\left(0, \sigma^2\right) , & \text{no signal} . \end{cases} \tag{8.8}$$

8.2.2.2 Transmitted Reference

For TR, the samples after correlating (8.3) with the delayed version of itself is formulated as

$$z_{\kappa}^{(tr)} = \sum_{j=\kappa N_s}^{(\kappa+1)N_s-1} \int_{jT_f+c_jT_c+\hat{\tau}_{toa}}^{jT_f+c_jT_c+T_{int}+\hat{\tau}_{toa}} \tilde{r}(t)\tilde{r}(t-D)dt , \tag{8.9}$$

which assumes accurate delay lines. It is also possible to clean the reference pulse employed in TR for a better performance [262].

If we denote E_{tr} to be the captured energy using a TR receiver, the statistics of the decision variable can be formulated as

$$z_{\kappa}^{(tr)} \sim \begin{cases} \mathcal{N}\left(E_{tr}, M\sigma^4 + 2E_{tr}\sigma^2\right) , & \text{signal} , \\ \mathcal{N}\left(0, M\sigma^4 + E_{tr}\sigma^2\right) , & \text{no signal} . \end{cases} \tag{8.10}$$

It is also possible to optimally combine the samples of a TR receiver for enhanced performance, as discussed in [263]-[266].

8.2.2.3 Energy Detection

Finally, the sample values for ED at the output of the square-law device are given by

$$z_{\kappa}^{(ed)} = \sum_{j=\kappa N_s}^{(\kappa+1)N_s-1} \int_{jT_f+c_jT_c+\hat{\tau}_{toa}}^{jT_f+c_jT_c+T_{int}+\hat{\tau}_{toa}} |r(t)|^2 dt . \tag{8.11}$$

With E_{ed} being the captured energy for ED receiver, the decision statistics are

$$z_{\kappa}^{(ed)} \sim \begin{cases} \mathcal{N}\left(M\sigma^2 + E_{ed}, 2M\sigma^4 + 4E_{ed}\sigma^2\right) , & \text{signal} , \\ \mathcal{N}\left(M\sigma^2, 2M\sigma^4\right) , & \text{no signal} . \end{cases} \tag{8.12}$$

Again, similar to TR case, a weighted ED receiver yields better performance as discussed in [267].

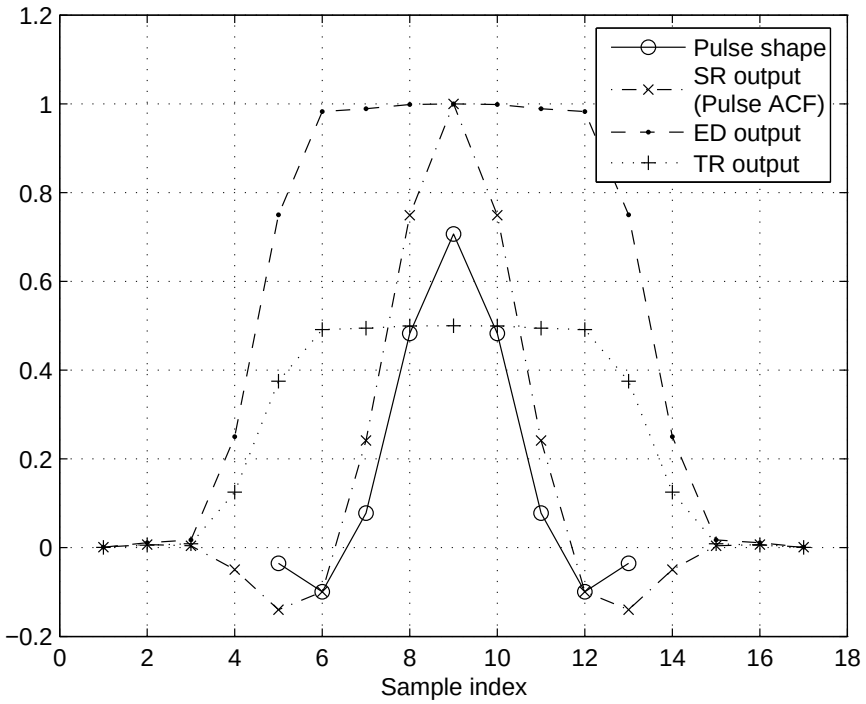

Figure 8.4 Received *normalized* pulse shape, and the sampled outputs corresponding to SR, ED, and TR for different timing offsets (1ns pulse is sampled at 8GHz, and energy is collected within 1ns windows and different offsets). The ED and TR outputs will scale with E, while SR output will scale with $\sqrt{E}$ for different E_b/N_0.

The statistics of the decision variables in the presence and absence of a useful signal for SR, TR, and ED are depicted in Fig. 8.3.

8.3 Trade-offs Between Different Transceivers and Channel Parameter Estimation

8.3.1 Energy Capture Characteristics vs. Noise Effects

When perfect synchronization is assumed (possible with Nyquist rate sampling), and with perfect pulse shape and channel estimates, the captured energies E_{sr}, E_{tr}, and E_{ed} will be identical. However, when low-rate samples are considered, the energy capture characteristics of the three transceiver types will be significantly different. In particular, any small timing mismatches will yield significant correlation losses for SR due to extremely short pulse durations, while TR and ED are more robust against timing mismatches. While pulse-shape estimation and synchronization to

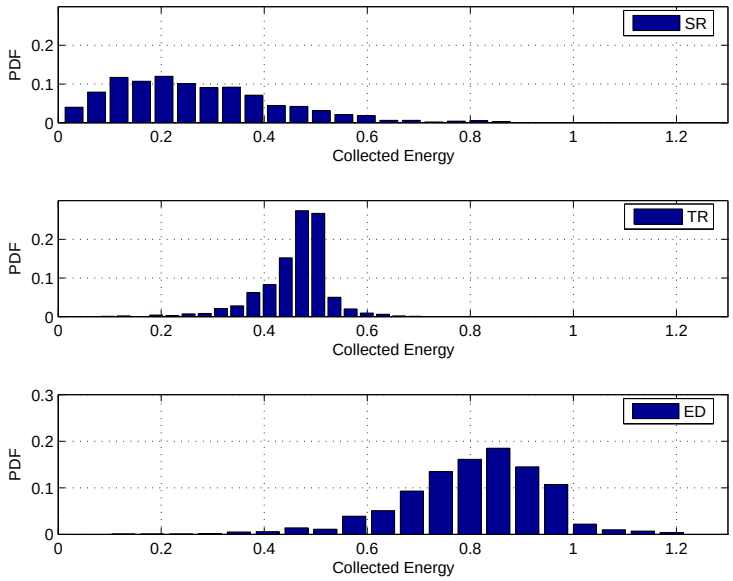

Figure 8.5 PDFs of captured energies for SR, TR, and ED in CM1, and for $t_s = 1$ns, $T_c = 1$ns, and $T_{int} = 40$ns. MRC is used for SR.

individual multipath components is very difficult at low rate samples[4], TR and ED becomes more advantageous in terms of energy capture when sub-Nyquist sampling is considered. This is more clearly demonstrated in Fig. 8.4, where an example pulse shape, and the captured energies from this pulse using the three transceiver types (at different delays) are depicted. With sampling durations on the order of pulse duration, it is very difficult to capture the correlation peak for SR, while ED and TR has a larger time support for a strong energy capture. Note that the existence of the transmitted-reference pulse yields a 3dB energy loss compared with the other two schemes (for the case when number of data and reference pulses are the same).

Due to sampling rate limitations, similar concepts will apply in multipath channels. Using certain channel models [3], it is possible to evaluate the PDF of the captured energy for the purpose of comparing the performances of different transceiver types and combining schemes. Energy capture of the three transceiver types are investigated in Fig. 8.5, where PDFs of the energies collected in 40ns windows are presented (see Section 8.5 for the details of the selected parameters). The timing offsets within the first sample ($t_s = 1$ns) are included, 1000 channel realizations with normalized total

[4]At Nyquist rate sampling, it may be possible to estimate the received pulse shapes and use them as a template for all-digital implementation [268].

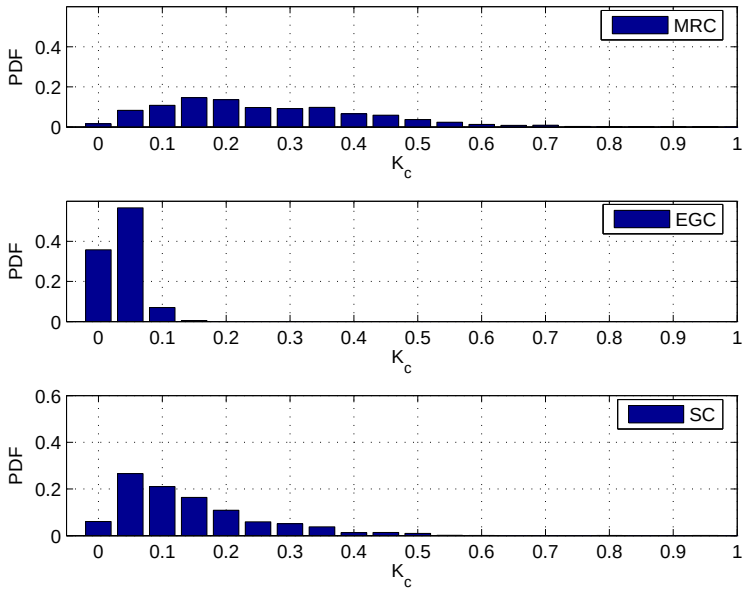

Figure 8.6 PDFs of K_c for MRC, EGC, and SC (1-Rake) in CM1, and for $t_s = 1$ns, using $T_{int} = 40$ns.

energy are used, and MRC combining is considered for SR. While ED has the best energy capture, TR has a 3dB degradation due to reference pulse employed[5]. Similar PDFs can be obtained for different combining schemes in SR, as presented in Fig. 8.6 (parameter K_c to be defined in Section 8.4.2.1). Figure shows that MRC has the best energy capture, which comes at a cost of higher complexity. On the other hand, EGC has worse energy capture compared with the other two, which is due to the fact that all the samples within the integration window are combined (regardless of whether there is signal or not) after removing their phases. Alternatively, a thresholding technique to discard the branches with low SNR may also have been carried out, which would have considerably improved the performance of EGC [269]. It is worth to mention that all the PDFs will change for a different set of system parameters (i.e., pulse shape, pulse duration, channel model, sampling rate, integration interval, bandwidth etc.). Higher sampling rates will enable better synchronization and energy capture for SR, with only yielding slight improvements for TR and ED.

[5]Note that the captured energy PDFs are obtained for identical received pulse shapes at different multipath components, which is also same with the correlator pulse shape. In the case of pulse shape mismatch or imperfect channel estimates, energy collection capability of SR will further degrade, with the TR and ED schemes being non-affected.

On the other hand, it is observed that the effect of noise is worse for the TR and ED approaches[6]. In particular, noise-square terms for the ED, and noise-cross-noise terms for TR degrade the detection performance. Therefore, even though TR and ED outperform SR at high SNR due to better energy capture (with moderate sampling rates), they have poor performance when the noise variance is large. While exact analysis of TR and ED require Chi-square statistics to be used; in this chapter, we consider Gaussian approximation to the Chi-square statistics, which becomes valid under certain cases, and allows a unified analysis of the three transceiver schemes. The critical parameter that determines the performance of both the TR and ED is the degree of freedom $M \approx 2Bt_s$. Smaller M values (i.e. smaller bandwidths, or smaller integration intervals) imply less degradation caused by noise. On the other hand, GA becomes valid for large M values.

8.3.2 Channel Parameter Estimation

Accurate channel parameter estimation is a required part of all wireless communication systems for successful demodulation of the symbols. For coherent signal reception, the arrival times, amplitudes, and sometimes the pulse shapes of individual multipath components are critical parameters to be estimated. For differentially-coherent or non-coherent receivers, such channel parameters are available; however, optimal integration start/stop points (or the threshold when OOK is employed) are important parameters that have to be estimated, and can be considered under the scope of channel parameter estimation[7]. Since the channel changes with time, the channel parameter estimation needs to be repeated every once in a while.

The fact that UWB receivers are able to observe individual multipath components (due to increasing bandwidths) requires high sampling rates to resolve these components, even though such high sampling rates might not be necessary for symbol demodulation. Typically, symbol-rate sampling is sufficient to demodulate the bits; however, channel parameter estimation for individual multipath components requires much higher sampling rates. Such high sampling rates can be possibly achieved in different ways: 1) Using high speed ADCs, 2) Using multiple low-rate parallel ADCs, 3) Using appropriately designed training symbols to increase the effective sampling rate.

Lemma 8.3.2.1: Let $t_s = \frac{T_s}{\beta}$ be the desired sampling rate, where T_s is the symbol duration. Then, with symbol-spaced sampling, β training symbols can be used to increase the effective sampling

[6]In fact, a parallel problem exists as well for SR at low SNR, since channel estimates will become more noisy.
[7]For weighted TR or ED, further parameters may need to be estimated for enhanced performance.

duration to t_s. To decrease the noise variance of the channel estimate, the estimates can be further averaged over N_t training symbols.

Proof: See Appendix of [23].

Note that using a channel estimation as discussed above may significantly decrease the ADC requirements (as we can achieve *both* the channel parameters estimation and symbol demodulation using symbol-rate samples). However, it requires the symbol duration and maximum excess delay of the channel to be sufficiently small, so that the channel is stationary over a large number of symbols.

8.3.3 Effect of Imperfect Correlation Template on Performance

The performance analysis for IR-UWB in the literature usually assumes that the correlator template shape perfectly matches to the received pulse shape(s)[8]. If only lower sampling rates are possible during channel estimation, it is apparent from (8.5) that SR will not be able to collect sufficient energy from the received multipath arrivals due to the timing and pulse-shape mismatches between the stored template signal and the received waveform. The shape mismatch between the received pulses and the template waveform is quantized using the fidelity metric in the literature before [270]-[272]. In this section, we shortly analyze the effect of imperfect receiver template on the performance for under-sampled SR systems. For the sake of modeling the imperfect template, we add Gaussian noise to the template, and then normalize the energy so that the noisy template has a unit energy. In other words, the imperfect correlator template $\omega_{imp}(t)$ is given by

$$\omega_{imp}(t) = \frac{\omega(t) + n_{tmp}(t)}{\sqrt{\int_{-\infty}^{\infty} \left|\omega(t) + n_{tmp}(t)\right|^2 dt}} , \tag{8.13}$$

where $n_{tmp}(t) \sim \mathcal{N}(0, \sigma_{tmp}^2)$ denotes the template noise, and σ_{tmp}^2 is the template noise variance (which depends on the template estimation algorithm). An example realization for the imperfect templates, and cross-correlation functions (CCF) between the original pulse-shape and these imperfect templates is given in Fig. 8.7. As the template distortion increases, it is seen that the correlation peak decreases. However, due to low-rate sampling of the signal, the correlation peak may not always be captured using SR. Also at particular delays, it is seen that an imperfect template may capture a larger amount of energy compared to the perfect template (e.g. at sample 6 for $\sigma_{tmp}^2 = -15$dB).

[8] At Nyquist rate sampling, it may be possible to estimate the received pulse shape(s) and use them as a template for all-digital implementation [268].

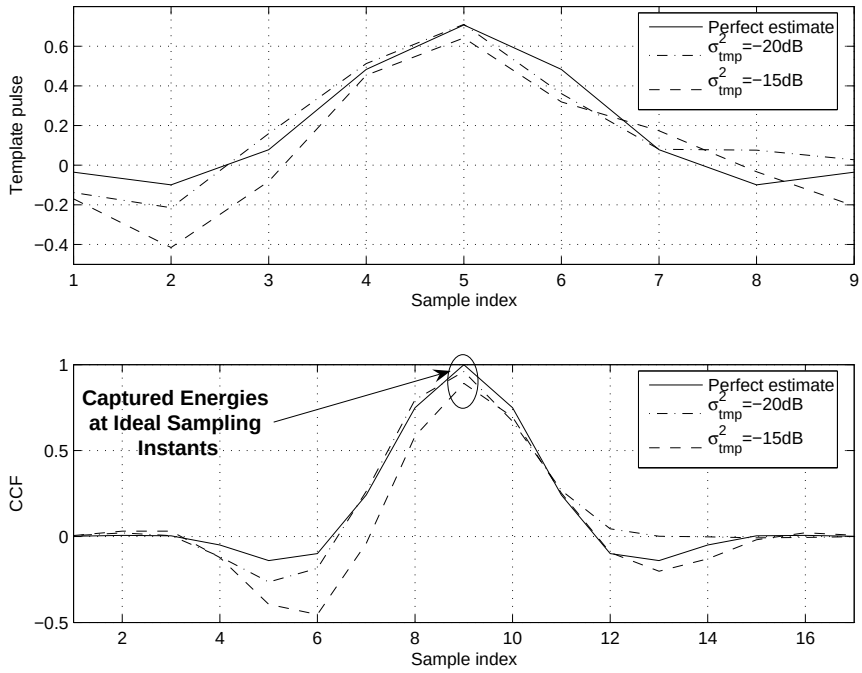

Figure 8.7 a) Correlator template shapes for different σ^2_{tmp}, b) CCFs of the correlator template with the original pulse shape for different σ^2_{tmp}.

8.3.4 Effect of Timing Jitter on the Performance

It is worth to briefly discuss the effects of timing jitter on the low rate SR scheme being considered. For ideal Rake receivers, where the receiver is perfectly synchronized with different multipath components, even very small amount of timing jitter seriously degrades the performance [20]. However, when low-rate samples are considered, the receiver is not synchronized to individual multipath components, and collects only the energy projections at sample-spaced intervals. This implies that the correlator outputs are already jittered. Therefore, it can be said that as long as the timing jitter is less than the sampling time, it will not seriously degrade the system performance.

8.4 Symbol Detection

In this section, first, BER expressions in AWGN channel are presented in terms of the *energy per bit*, with the assumption of perfect synchronization. Later, extending these results, more realistic multipath channels are considered, and BER performances of BPSK, OOK, and PPM modulations are analyzed.

8.4.1 BER Performance Analysis in AWGN Channel

Consider a multipath-free UWB channel first for the sake of theoretical analysis, where the receiver is perfectly synchronized with the received signal. Then, BERs for different modulation schemes can be evaluated as follows.

8.4.1.1 BPSK

The BER for SR will be given by (using a unit pulse energy template)

$$P_b^{(sr)} = Q\left(\frac{N_s\sqrt{E_p}}{\sqrt{N_s\sigma^2}}\right) = Q\left(\sqrt{\frac{E_b}{\sigma^2}}\right) \ , \tag{8.14}$$

while for TR, we have

$$P_b^{(tr)} = Q\left(\frac{N_s E_p/2}{\sqrt{N_s(M\sigma^4 + 2\sigma^2 E_p/2)}}\right) = Q\left(\frac{E_b/2}{\sqrt{MN_s\sigma^4 + \sigma^2 E_b}}\right) \ . \tag{8.15}$$

For ED, BPSK modulation is not applicable.

8.4.1.2 OOK

The OOK requires the estimation of a threshold for symbol detection, which is, for all three transceiver architectures, taken to be at the intersection of probability density functions (PDFs) corresponding to either binary hypothesis [42]. The means μ_0, μ_1 and variances σ_0^2, σ_1^2 corresponding to symbols 0 and 1 can be estimated via transmitting training symbols. Then, equating the PDF expressions, taking the natural logarithm of both sides and rearranging the terms, one obtains

$$C_1\xi^2 + C_2\xi + C_3 = 0 \ , \tag{8.16}$$

where the coefficients are given by [42]

$$\begin{aligned} &C_1 = \sigma_1^2 - \sigma_0^2 \ , \quad C_2 = -2\left(\mu_0\sigma_1^2 - \mu_1\sigma_0^2\right) \ , \\ &C_3 = \sigma_1^2\mu_0^2 - \sigma_0^2\mu_1^2 - 2\sigma_0^2\sigma_1^2\ln\left(\sigma_1/\sigma_0\right) \ , \end{aligned} \tag{8.17}$$

with the equation being a second order polynomial that can be easily solved for ξ (only larger of the roots is appropriate). Note that ξ is the threshold corresponding to the *collected energy per symbol*.

Table 8.1 Comparison of BERs for different UWB transceiver architectures.

Modulation	BPSK	OOK	PPM
SR	$Q\left(\sqrt{\frac{E_{sr}}{\sigma^2}}\right)$	$Q\left(\sqrt{\frac{\xi}{\sigma^2}}\right), \quad \xi = \frac{E_{sr}}{2}$	$Q\left(\sqrt{\frac{E_{sr}}{2\sigma^2}}\right)$
TR	$Q\left(\frac{E_{tr}}{\sqrt{M\sigma^4+2\sigma^2 E_{tr}}}\right)$	$\frac{1}{2}\left[Q\left(\frac{\xi}{\sqrt{M\sigma^4+\sigma^2 E_{tr}}}\right)+Q\left(\frac{E_{tr}-\xi}{\sqrt{M\sigma^4+2\sigma^2 E_{tr}}}\right)\right]$	$Q\left(\frac{E_{tr}}{\sqrt{2M\sigma^4+3\sigma^2 E_{tr}}}\right)$
ED	N/A	$\frac{1}{2}\left[Q\left(\frac{\xi-M\sigma^2}{\sqrt{2M\sigma^4}}\right)+Q\left(\frac{M\sigma^2+E_{ed}-\xi}{\sqrt{2M\sigma^4+4\sigma^2 E_{ed}}}\right)\right]$	$Q\left(\frac{E_{ed}}{\sqrt{4M\sigma^4+4\sigma^2 E_{ed}}}\right)$

By estimating the threshold as discussed above, the BER for SR is given by (using a unit pulse energy template)

$$P_b^{(sr)} = Q\left(\frac{\xi}{\sqrt{N_s\sigma^2}}\right) = Q\left(\frac{N_s\sqrt{\bar{E}_p}}{2\sqrt{N_s\sigma^2}}\right) = Q\left(\sqrt{\frac{E_b}{2\sigma^2}}\right) \ , \tag{8.18}$$

where $\bar{E}_p = \bar{E}_b/N_s$ is the pulse energy (when received bit is 1), and the optimal threshold is given by $\frac{\sqrt{\bar{E}_b}}{2}$ (since the noise variances for bit-0 and bit-1 are identical for SR). Also, since no energy is transmitted for bit-0 (as opposed to PPM and BPSK), we have $\bar{E}_b = 2E_b$ (i.e. $\bar{E}_p = 2E_p$) to equate the *average* power consumption for all modulation schemes.

On the other hand, for TR and ED, noise statistics corresponding to bits 0 and 1 are different, preventing closed-form expressions that depends on a single Q-function. For TR, BER becomes

$$\begin{aligned} P_b^{(tr)} &= \frac{1}{2}\left[Q\left(\frac{\xi}{\sqrt{N_s(M\sigma^4+\sigma^2\frac{\bar{E}_p}{2})}}\right)+Q\left(\frac{\bar{E}_b/2-\xi}{\sqrt{N_s(M\sigma^4+2\sigma^2\frac{\bar{E}_p}{2})}}\right)\right] \\ &= \frac{1}{2}\left[Q\left(\frac{\xi}{\sqrt{N_sM\sigma^4+\sigma^2E_b}}\right)+Q\left(\frac{E_b-\xi}{\sqrt{N_sM\sigma^4+2\sigma^2E_b}}\right)\right] \end{aligned} \tag{8.19}$$

and for the case of ED, BER is

$$\begin{aligned} P_b^{(ed)} &= \frac{1}{2}\left[Q\left(\frac{\xi-N_sM\sigma^2}{\sqrt{N_s2M\sigma^4}}\right)+Q\left(\frac{N_sM\sigma^2+\bar{E}_b-\xi}{\sqrt{N_s(2M\sigma^4+4\sigma^2\bar{E}_p)}}\right)\right] \\ &= \frac{1}{2}\left[Q\left(\frac{\xi-N_sM\sigma^2}{\sqrt{2N_sM\sigma^4}}\right)+Q\left(\frac{N_sM\sigma^2+2E_b-\xi}{\sqrt{2N_sM\sigma^4+8\sigma^2E_b)}}\right)\right] \end{aligned} \tag{8.20}$$

8.4.1.3 PPM

The BER for SR will be given by (using a unit pulse energy template)

$$P_b^{(sr)} = Q\left(\frac{N_s\sqrt{E_p}}{\sqrt{2N_s\sigma^2}}\right) = Q\left(\sqrt{\frac{E_b}{2\sigma^2}}\right) \ , \tag{8.21}$$

while for TR, we have

$$P_b^{(tr)} = Q\left(\frac{N_s E_p/2}{\sqrt{N_s(2M\sigma^4 + 3\sigma^2 E_p/2)}}\right) = Q\left(\frac{E_b/2}{\sqrt{2MN_s\sigma^4 + \frac{3}{2}\sigma^2 E_b}}\right) \ , \tag{8.22}$$

and for the case of ED, BER becomes

$$P_b^{(ed)} = Q\left(\frac{N_s E_p}{\sqrt{N_s(4M\sigma^4 + 4\sigma^2 E_p)}}\right) = Q\left(\frac{E_b}{2\sqrt{MN_s\sigma^4 + \sigma^2 E_b}}\right) \ . \tag{8.23}$$

As the BER expressions imply, using $N_s > 1$ for TR and ED degrades the performance as opposed to SR. Processing gain N_s can be also considered as a coefficient to (and can be folded into) the degree of freedom M, which increases the noise variance. Therefore, using fewer pulses per symbol (keeping the symbol energy same) is more favorable for TR and ED. On the other hand, employing multiple pulses per symbol is useful as it maintains user separation, and smoothes the power spectral density for all schemes. Also, using accurate delay lines (which considerably increases hardware complexity), the performance degradation in TR and ED can be mitigated by coherently summing the energies over multiple frames before delay/correlate device and square-law device, respectively.

8.4.2 BER Performance Analysis in Multipath Channel

When realistic channels are considered, the theoretical analysis depends on the channel model and sampling rate, as well as other assumed system parameters (combining scheme, integration interval etc.). In here, we follow a semi-analytic approach for performance analysis, where we consider the energy capture of the different combining schemes at sub-Nyquist rates, and we characterize the captured energies corresponding to these combining schemes.

8.4.2.1 Stored Reference

The BERs obtained in the previous section for the three modulation schemes in SR can be given in a more generalized form for multipath channels

$$P_b^{(mp)} = Q\left(\sqrt{\frac{K_c E_b}{\sigma^2} K_m}\right) \ , \tag{8.24}$$

where K_c is due to different combining schemes, and K_m is due to different modulation options ($K_m = 1$ for BPSK, and $K_m = 0.5$ for PPM or OOK). Depending on which combining scheme is used, K_c takes different values as follows

$$K_c = \begin{cases} \sum_{i=0}^{N_{int}-1} |\tilde{\alpha}_i|^2 & , \text{ if MRC,} \\ \left[\sum_{i=0}^{N_{int}-1} |\tilde{\alpha}_i|\right]^2 / N_{int} & , \text{ if EGC,} \\ |\tilde{\alpha}_{max}|^2 & , \text{ if SC,} \end{cases} \tag{8.25}$$

where $\tilde{\alpha}_{max}$ is the projected channel coefficient with the maximum absolute value (a 1-Rake receiver is considered for SC).

The energy capture of a particular combining scheme is characterized by the parameter K_c. Depending on the channel model, employed pulse shape (and duration), sampling rate, and the combining scheme, the PDF of this energy capture parameter can be obtained to carry out a semi-analytic analysis.Alternatively, instead of using all the projected paths, a thresholding technique to discard the branches with low SNR may also have been carried out, which would have considerably improved the performance of EGC [269]. Having obtained the PDFs $p(K_c)$ for different combining schemes as in Fig. 8.6, the average BER for different modulations and combining schemes can be evaluated by averaging over the PDF of K_c as follows

$$P_b^{(avg)} = \int_0^\infty P_b(\tilde{K}_c) p(\tilde{K}_c) d\tilde{K}_c \ , \tag{8.26}$$

where $\tilde{K}_c$ is for an instantaneous channel realization.

8.4.2.2 Transmitted Reference

Following an approach similar to discussed for the case of SR, the BER performances that correspond to an instantaneous captured energy for TR can be easily obtained. The average BER can then be evaluated by conditioning the BER on the instantaneous collected energy, and averaging over its PDF as follows

$$P_b^{(avg)} = \int_0^\infty P_b(E_{tr}) p(E_{tr}) dE_{tr} \ . \tag{8.27}$$

8.4.2.3 Energy Detection

Similar to TR case, the BER for ED can be obtained by averaging the collected energy over its PDF as

$$P_b^{(avg)} = \int_0^\infty P_b(E_{ed}) p(E_{ed}) dE_{ed} \ . \tag{8.28}$$

8.5 Simulation Results

Computer simulations are performed to evaluate and compare the three transceiver architectures in 802.15.4a CM1 channels [3], which has a maximum excess delay on the order of 100ns. The following parameters are employed in all the simulations: $T_c = 1$ns, $B = 4$GHz, $D = 60$ns, $N_s = 1$. A raised-cosine pulse with parameter 0.25 is used, and sampled with 0.125ns intervals in the simulations, which is the same rate that the channel is sampled (note that this is different than *receiver* sampling rate t_s, and is just for simulation purposes).

Before presenting performances under multipath, in order to serve as a benchmark for the latter results, the AWGN performances of BPSK, OOK, and PPM, and the effects of imperfect correlation template and timing jitter on the BER are depicted in Fig. 8.8. The timing jitter is uniformly distributed in $(-0.25\text{ns}, 0.25\text{ns})$, and σ_{tmp}^2 is selected as -15db and -20dB (with respect to the normalized template energy). The timing jitter effects are seen to be disastrous, and timing mismatches on the order of quarter the pulse duration may seriously hurt the detection performance.

For multipath simulations, the same integration interval and sampling granularity as in energy capture analysis in Section 8.3.1 is used. Simulations are performed to evaluate the BER performances of different transceiver architectures and modulation schemes, and they are compared with

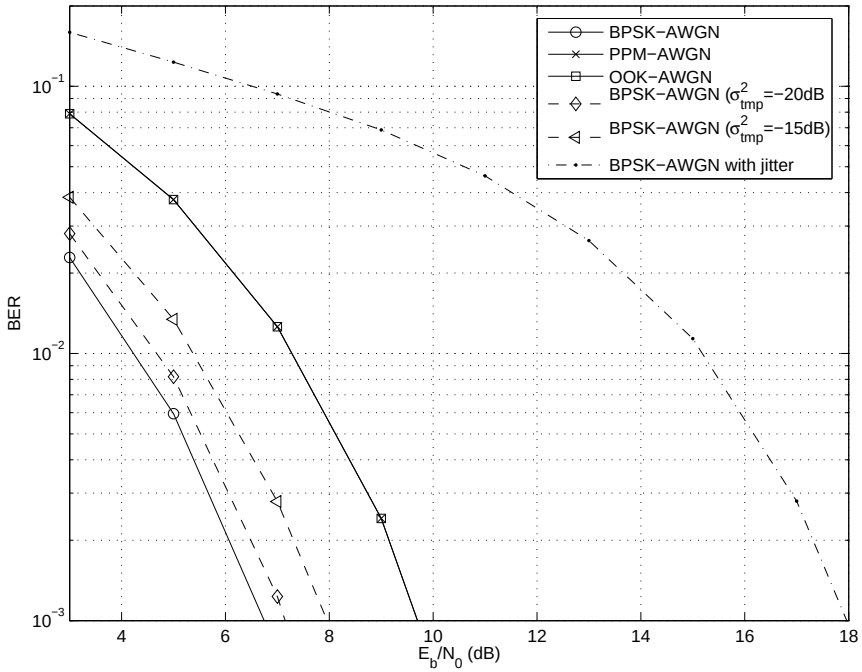

Figure 8.8 BER of BPSK, PPM, and OOK in AWGN channel, and with different imperfections (timing jitter is uniformly distributed within (−0.25ns,0.25ns)).

semi-analytical results. Threshold ξ for OOK is calculated assuming perfect noise mean and variance estimates, and using the GA outlined before. For PPM, both $\delta = 10$ns and $\delta = 100$ns cases are considered to demonstrate the cross-modulation interference (CMI) effects [273] for different transceivers. Simulations are performed over 1000 different channel realizations, and are further averaged over 200 trials. The theoretical (semi-analytical) curves are obtained by using the analysis in Table 8.1, and averaging over the PDFs of collected energies in Figs. 8.5,8.6.

The results in Figs. 8.9-8.11 show general agreement between simulations and the semi-analytic analysis. While clean templates employed with SR make them more favorable at low E_b/N_0, better energy collection capabilities of TR and ED dominate as E_b/N_0 increases. Also, PPM is seen to be applicable to TR and ED only for δ values on the order of maximum excess delay of the channel, while SR is much less affected from CMI due to clean templates employed. Finally, PPM and OOK modulations have identical performance for the case of SR; however, their performances are no longer the same when they are used with ED and TR, as also implied by Table 8.1.

In Fig. 8.12 simulations and semi-analytical results are used to analyze the performance of SR with BPSK and with different combining algorithms. As expected, MRC is seen to perform the best

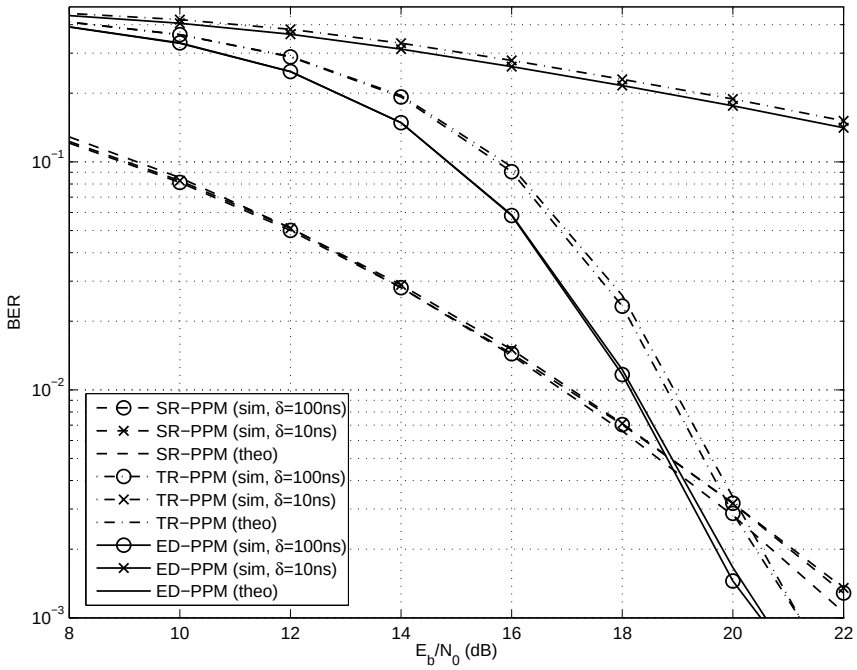

Figure 8.9 BER of PPM with with SR, TR, and ED in 802.15.4a CM1 channel model (T_{int} = 40ns, B = 4GHz, T_c = 1ns).

compared to the other algorithms. Also, timing jitter effects (distributed uniformly in (−1ns,1ns)), and effects of the imperfect correlation template (with $\sigma^2_{tmp} = -15$dB) are simulated in Fig. 8.13. Even for the timing mismatches on the order of pulse duration, the degradation is seen to be insignificant due to the reasons discussed before.

Lastly, effect of integration interval on the performance of TR, ED, and SR with MRC and EGC is investigated in Fig. 8.14. While the performance of SR with MRC always improves with integration interval (with the assumption of perfect channel estimates), it is seen that there exists an optimal integration interval for TR, ED, and SR with EGC. It should be noted that MRC will observe a similar optimum integration interval if the noisy channel estimates are to be used.

8.6 Conclusion

In this chapter, stored reference, transmitted reference, and energy detector transceivers are compared and analyzed semi-analytically and with simulations. Generic and unified performance analysis models that exploit the collected energies under sampling rate constraints are presented for different transceiver types.

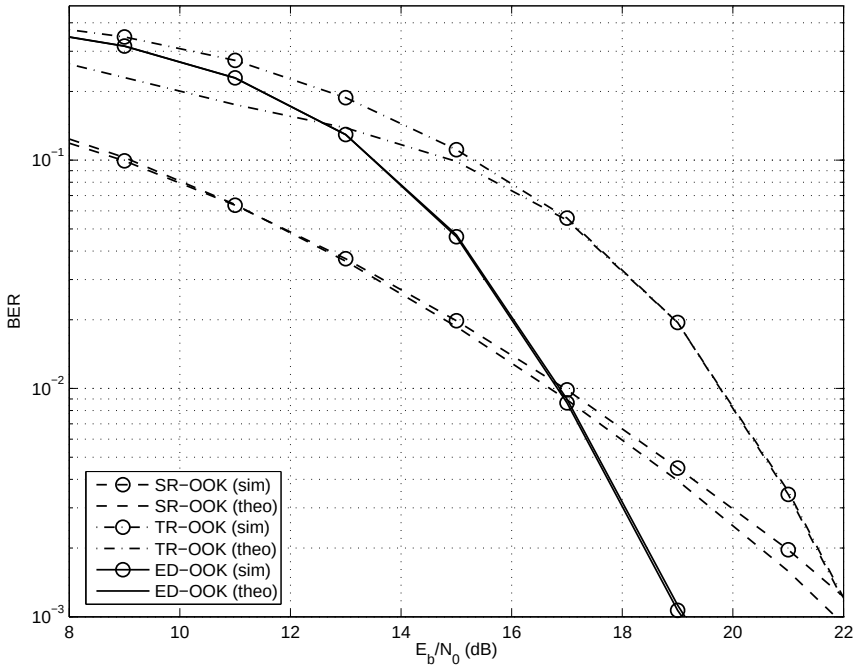

Figure 8.10 BER of OOK with SR, TR, and ED in 802.15.4a CM1 channel model (T_{int} = 40ns, B = 4GHz, T_c = 1ns).

The sub-optimal (due to sub-Nyquist sampling) Rake reception technique that collects the energies at regular timing instants is shown to have much less energy capture compared with TR and ED. However, low-rate SR is less affected from system imperfections (which may arise frequently in practice) such as template shape mismatch and timing jitter. Also, it is very suitable for implementing an interference rejection combining receiver (such as using generalized Rake receivers [274, 275]) due to regular placement of the fingers irrespective of signal existence. Lastly, larger N_s values is shown to degrade the performance of TR and ED, while not affecting the performance of SR.

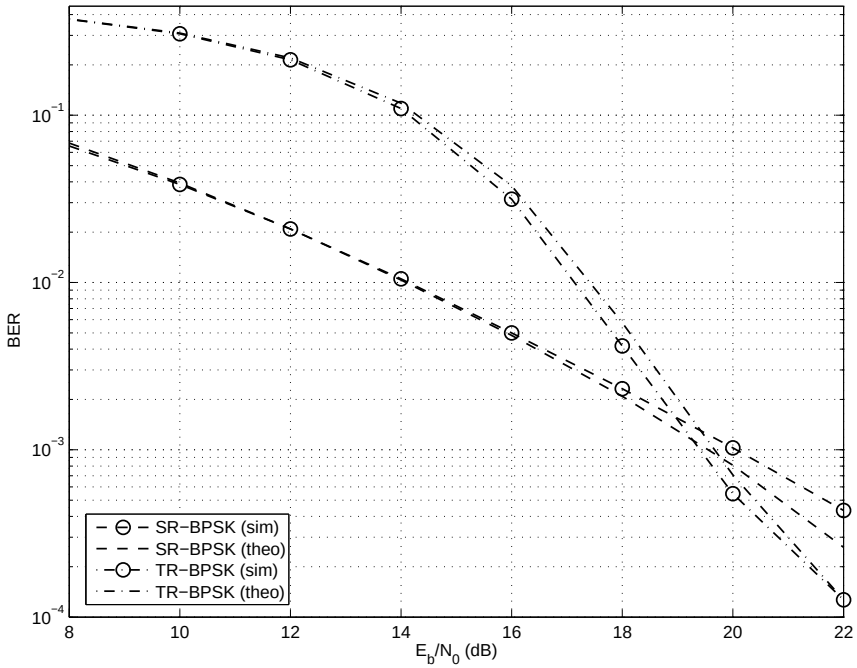

Figure 8.11 BER of BPSK with SR and TR in 802.15.4a CM1 channel model and using MRC ($T_{int} = 40$ns, $B = 4$GHz, $T_c = 1$ns).

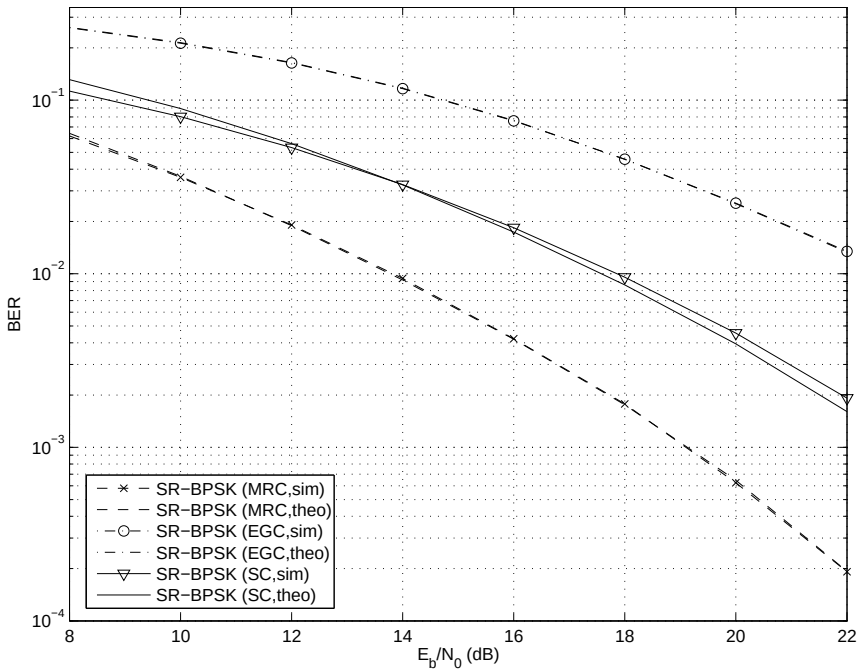

Figure 8.12 BERs of BPSK with SR and different combining schemes in 802.15.4a CM1 channel model ($T_{int} = 40$ns, $B = 4$GHz, $T_c = 1$ns).

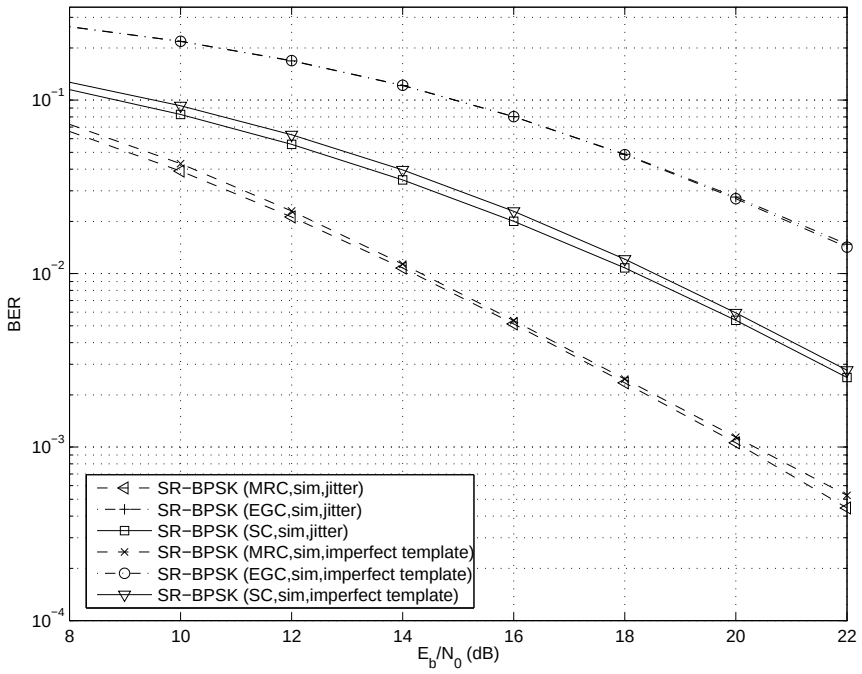

Figure 8.13 BER of BPSK with SR and different combining schemes in 802.15.4a CM1 channel model and in the presence of timing jitter of imperfect templates ($T_{int} = 40$ns, $B = 4$GHz, $T_c = 1$ns).

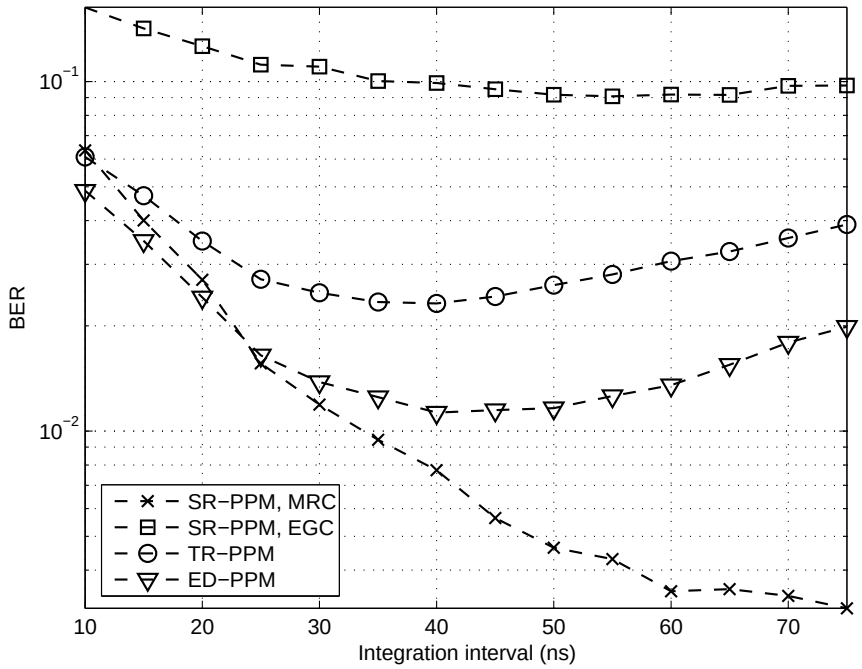

Figure 8.14 BER of PPM with respect to integration interval for different transceiver types and combining schemes in 802.15.4a CM1 channel model ($E_b/N_0 = 18$dB, $B = 4$GHz, $T_c = 1$ns).

CHAPTER 9

RANGING WITH IR-UWB RADIOS AT LOW-RATE SAMPLING

9.1 Introduction

Time of arrival (TOA) estimation and ranging using impulse radio (IR) ultrawideband (UWB) systems require accurate detection of the leading edge path of a received signal, which may not be the strongest [276]. Since Nyquist rate sampling is practically challenging for IR-UWB systems due to extremely large bandwidths, the leading edge detection may have to be achieved at low-rate samples. This can be realized by using energy blocks and processing the signal with a square-law device before sampling it [27]. Such a method considerably decreases the complexity of the receiver, and relaxes the *a priori* knowledge requirements such as the optimal template waveform.

Accurate (and unbiased) ranging algorithm design is a very difficult task due to unknown channel parameters that may show great deviations depending on the path that the signal traverses. One of the possible methods for identification of the leading edge is searching it back from the strongest (or an earlier locked [277]) sample position. In [24, 27, 30, 277], two different kinds of searchback schemes are discussed for finding the leading edge. To our best knowledge, an IR-UWB ranging algorithm design that jumps backward to a prior sample, and starts searching for the leading edge in the *forward* direction (using a threshold comparison) is first mentioned in [277] with samples collected directly from the received signal. A similar algorithm is investigated in [27], where the samples are collected after an energy detector, and a more theoretical treatment of the estimation performance is attempted. On the other hand, in [30], a second type of searchback algorithm searches the samples one by one in the *backward* direction starting from the strongest sample, and taking into account possible clusterings of the multipath components. The various parameters (such as the searchback window length, threshold etc.) for these different approaches can be adjusted based on the statistics of a particular channel model [3]. Comparison of these two types of algorithms from different aspects is presented in [24].

In either approaches, determination of an appropriate threshold for leading edge identification carries significant importance for the ranging accuracy. The threshold is set based only on the noise floor in [277, 30] due to lack of full knowledge of channel parameters. However, this is a sub-optimal threshold setting, since the threshold decision is made independent of the received signal energy. An alternative normalized-thresholding technique that does not require noise-level estimation is discussed in [27], which implicitly exploits both the signal and noise statistics, however in a sub-optimal and heuristic way. It is shown in [29] that the Kurtosis of the received signal samples may be exploited for improving the accuracy using normalized-threshold selection.

In this chapter, our contribution is on the analysis of the optimality of the threshold selection for the first searchback algorithm (using an energy detector). We also formulate a generic error analysis approach which can be considered for different ranging algorithms. First, an additive white Gaussian noise (AWGN) channel is considered, and with the assumption of perfectly known channel parameters, the optimal threshold is investigated so that the probability of detection of the arriving signal is maximized. Later, for multipath channels, it is shown that the optimality metric should be changed so as to minimize the mean absolute error (MAE). Performance differences between the theoretically-optimum threshold setting and the noise-based threshold setting are demonstrated to be insignificant within certain signal to noise ratio (SNR) ranges for appropriate selection of system parameters.

9.2 System Model

9.2.1 Signal Model

Let the received time-hopping IR-UWB multipath signal be represented as

$$r(t) = \sum_{j=-\infty}^{\infty} d_j \omega_{mp}(t - jT_f - c_j T_c - \tau_{toa}) + n(t) \tag{9.1}$$

where τ_{toa} is the TOA of the received signal, frame index and frame duration are denoted by j and T_f, and each pulse is transmitted within a chip of duration T_c. The time-hopping codes and random polarity codes are denoted by $c_j \in \{0,\ 1, ..., N_h - 1\}$ and $d_j \in \{\pm 1\}$, respectively, where $N_h = T_f/T_c$ is the possible number of chip positions within a frame. While time hopping (TH) sequence design with a good zero correlation zone and effects of imperfect autocorrelation characteristics are research areas by themselves [30], we consider no time-hopping in this chapter. Also, no modulation is considered

for the ranging process, and a single pulse per symbol is used ($T_s = T_f$). The effective pulse after the multipath channel is given by $\omega_{mp}(t) = \sqrt{E}\sum_{l=1}^{L} \alpha_l \omega(t - \tau_l)$, where $\omega(t)$ is the received UWB pulse with unit energy, E is the pulse energy (which is equal to bit energy E_b for single pulse per bit), α_l and τ_l are the fading coefficients and delays of the multipath components, respectively. The AWGN with zero-mean and double-sided power spectral density $\mathcal{N}_0/2$ and variance σ^2 is denoted by $n(t)$. In the sequel, we assume that $\tau_{toa} \sim \mathcal{U}(0, T_f)$, where $\mathcal{U}(.)$ denotes the uniform distribution.

The signal arriving at the receiver antenna is first passed through a band-pass filter of bandwidth B, processed with a square-law device, and finally fed to an integrate and dump device with a sampling duration of t_s. The samples are further averaged over N_t symbols to improve the ranging accuracy, thanks to the long preambles dedicated for accurate ranging. The integrator output samples can be expressed as

$$z[n] = \frac{1}{N_t}\sum_{j=1}^{N_t} \int_{(j-1)T_f+(n-1)t_s}^{(j-1)T_f+nt_s} |r(t)|^2 dt \ , \tag{9.2}$$

where n denotes the sample index. Note that for a single symbol, $z[n]$ has a centralized Chi-square distribution for noise-only samples, and a non-centralized Chi-square distribution for signal plus noise samples. However, since we consider a large N_t, from the central limit theorem, distribution of $z[n]$ can be conveniently approximated as

$$z[n] \sim \mathcal{N}\left(M\sigma^2 + E_n, \frac{2M\sigma^4 + 4E_n\sigma^2}{N_t}\right) = \mathcal{N}(\mu_n, \sigma_n^2) \ , \tag{9.3}$$

where the degree of freedom is given by $M \approx 2Bt_s$, and the (noise-free) waveform energy that falls within the nth sample is denoted by E_n.

9.2.2 TOA Estimation Model

In order to estimate the leading edge sample, we assume that the the receiver is accurately synchronized to the peak sample, which would typically be a valid assumption due to large N_t (i.e. averaged noise effects). Let n_{max} denote the sample index for the peak sample, n_{le} the index for the leading edge sample, D_{max} the difference between the peak sample and the leading edge sample, and W_{sb} the searchback window length (in samples) extending backwards from n_{max}. The first sample within the window has an index n_{sb}, and the number of noise-only samples prior to the leading edge

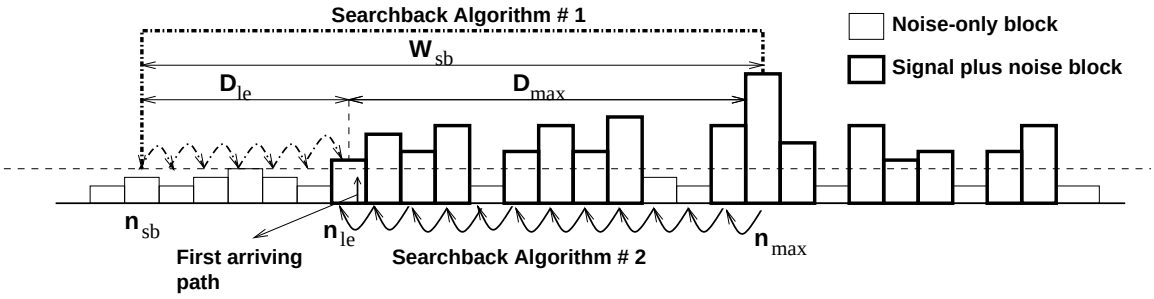

Figure 9.1 Illustration of two kinds of searchback schemes.

sample is given by $D_{le} = W_{sb} - D_{max} = n_{le} - n_{sb}$. Note that the statistics of D_{le} can be obtained from the realizations of different channel models. These notations are depicted in Fig. 9.1.

In order to set a threshold based on the noise level, we assume that the noise variance is already estimated. We define the probability of false alarm to be the probability of detecting a (single) noise-only sample as a signal-plus-noise sample. Then, given a certain P_{fa}, the threshold that is based solely on the noise level can be defined as[1] $\xi = \tilde{\sigma}^2 Q^{-1}(P_{fa}) + \tilde{\mu}$, where the mean and the variance of noise-only samples are given by $\tilde{\mu} = M\sigma^2$, and $\tilde{\sigma} = 2M\sigma^4/N_t$, respectively, as implied by (9.3).

9.2.3 Searchback Schemes

For TOA estimation purposes, we assume that the receiver is already locked to the strongest sample, and it identifies the leading edge by searching back the samples prior to this strongest sample. In below, we review two such searchback schemes that were discussed in the literature. An illustration of these algorithms is presented in Fig. 9.1.

9.2.3.1 Searchback Algorithm-1 (SBA1)

In the first searchback scheme, the algorithm jumps backwards from the peak index to the beginning of the searchback window [27]. Then, it searches for the leading edge in the forward direction, and picks the first threshold-exceeding sample as the leading edge. More mathematically, the leading edge sample is estimated as $\hat{n}_{sb1} = \min\{n | z[n] > \xi\}$, where $n \in \{n_{max} - W_{sb}, n_{max} - W_{sb} + 1, \cdots, n_{max}\}$. In the next sections, sub-optimal selection of the threshold based only on the noise level will be discussed, and will be compared when the threshold is selected in an optimal way.

[1] We define P_{fa} to be the probability of a single noise sample being larger than a certain threshold.

Before this discussion, for completeness, an alternative searchback scheme is explained below, whose performance will be compared with SBA1 via simulations.

9.2.3.2 Searchback Algorithm-2 (SBA2)

In the second searchback scheme, the algorithm searches back the samples backwards one by one starting from the peak sample by comparing each sample with the threshold [30]. A challenge that this algorithm faces is that there may be multiple clusters of multipath components prior to the peak sample in a typical UWB channel realization (see Fig. 9.1). This implies that there may be noise-only samples in between different clusters, and the algorithm should continue searching back the leading edge even if certain samples are below the threshold. It is therefore proposed in [30] to allow a number of consecutive occurrences of noise-only samples while continuing the backward search to handle the clustering problem. The threshold when K consecutive noise-only samples exist is given as $\xi = \tilde{\sigma} Q^{-1}\left(1-(1-P_{fa})^{\frac{1}{K}}\right) + \tilde{\mu}$, where the optimum threshold is now a function of K. Note that K may be obtained (approximately) from average channel statistics.

9.2.4 A Generic Error Analysis Approach

It is possible to formulate a *generic* error analysis framework that can be applied to any leading edge estimation algorithm. The key idea is calculating the probability of estimating a particular sample as the leading edge when a certain algorithm is employed. Then, the MAE of the TOA estimate can be calculated by using the detection probability of a particular sample to weight the *average* timing error corresponding to that sample, i.e.

$$e^{(MAE)}(\mathbf{E}_\lambda, D_{le,\lambda}) = \sum_{i\in\{1,2,\cdots,n_{max}\}} P_D(i|\lambda) \times e_i \ , \tag{9.4}$$

where $\mathbf{E}_\lambda = [E_{1,\lambda}, E_{2,\lambda}, \cdots, E_{n_{max},\lambda}]$ is a vector of waveform energies falling within different samples ($E_{i,\lambda} = 0$ for $i < n_{le}$), λ indicates the channel realization number, $P_D(i|\lambda)$ is the probability of detecting the ith sample as the leading edge sample (depends on the TOA estimation algorithm and the channel realization λ), and average timing error for choosing block i is *approximately* given

by [30]

$$e_i = \begin{cases} |n_{le} - i| t_s & \text{if } i \neq n_{le}, \\ 0.25 t_s & \text{if } i = n_{le}. \end{cases} \tag{9.5}$$

9.2.4.1 Average MAE Performance With A-priori Knowledge of Channel

In order to assess the average MAE performance of an algorithm for a particular channel model, consider that a total of Λ realizations of the channel model are available. The MAE for each channel realization can be obtained using (9.4) with the knowledge of $\mathbf{E}_\lambda$. Then, the average MAE can be expressed as

$$e_{avg1}^{(MAE)} = \frac{1}{\Lambda} \sum_{\lambda=1}^{\Lambda} e^{(MAE)}(\mathbf{E}_\lambda, D_{le,\lambda}) \ . \tag{9.6}$$

9.3 Optimal Threshold Selection for SBA1

Determination of the threshold carries significant importance for accurate estimation of the leading edge path. If the threshold is too small, it results in early false alerts; on the other hand, a too large threshold results in missed detection of the leading edge. Accurate setting of the threshold requires knowledge of the channel parameters, *which is usually not available during ranging.* In particular, in order to optimally set a threshold, the energy vector $\mathbf{E}_\lambda$ has to be known[2]. Since such *a-priori* knowledge is not available in reality, it is not possible to use the theoretically optimal threshold. However, it is important to know how worse a certain sub-optimal threshold selection technique performs when compared with the optimal threshold selection.

In this section, we analyze and compare the accuracy of SBA1 using optimal and sub-optimal threshold values. First, AWGN channels are considered for simplicity, where the optimal threshold is defined as the one that maximizes the probability of detection of the arriving signal. Then, multipath channel analysis is presented, where the optimality metric is changed to minimizing the MAE in TOA estimation.

[2]In fact, this also implies the knowledge of the TOA, since $E_i = 0$ for $i < n_{le}$.

9.3.1 Optimality of the Leading Edge Detection Threshold for AWGN Channel

Consider an AWGN channel, where all the signal energy is concentrated within the leading edge sample (i.e. $E_i = E_b$ if $i = n_{le}$, and $E_i = 0$ if otherwise), and the algorithm jumps D_{le} samples backwards from this sample to initiate a threshold comparison (in forward direction). Then, the three critical parameters that determine the optimal threshold value are: 1) Number of noise-only blocks tested prior to hitting the leading edge sample (D_{le}), 2) Noise variance (σ^2), and 3) Energy of the leading edge sample, which is equal to energy per bit for AWGN case (E_b). Given an arbitrary threshold ξ, the probability of detection of the leading edge sample is given by

$$P_D(n_{le}|\xi, D_{le}, E_b, \sigma^2) = \left[1 - Q\Big(\frac{\xi - \tilde{\mu}}{\tilde{\sigma}}\Big)\right]^{D_{le}} Q\Big(\frac{\xi - \tilde{\mu}_e}{\tilde{\sigma}_e}\Big) \ , \tag{9.7}$$

where $\mu_e = \tilde{\mu} + E_b$ and $\sigma_e = \sqrt{\tilde{\sigma}^2 + 4E_b\sigma^2/N_t}$ are the mean and standard deviation of the leading edge sample. If the (D_{le}, E_b, σ^2) tuple is assumed known, then the optimal detection threshold satisfies

$$\frac{dP_d(n_{le}|\xi, D_{le}, E_b, \sigma^2)}{d\xi} = 0 \ . \tag{9.8}$$

Lemma 9.3.1.1: In an AWGN channel, the threshold that maximizes the probability of detection is *approximately* given by the following

$$\xi_{opt} = \frac{-\mathcal{B} + \sqrt{\mathcal{B}^2 - 4\mathcal{A}\mathcal{C}}}{2\mathcal{A}} \ , \tag{9.9}$$

where $\mathcal{A} = \sigma_e^2 - \tilde{\sigma}^2$, $\mathcal{B} = 2\mu_e\tilde{\sigma}^2 - 2\tilde{\mu}\sigma_e^2$, and $\mathcal{C} = \tilde{\mu}^2\sigma_e^2 - \mu_e^2\tilde{\sigma}^2 - \tilde{\sigma}^2\sigma_e^2 \ln\Big(\frac{\sigma_e D_{le}}{\tilde{\sigma}}\Big)$.

Proof: See Appendix of [25].

Note that the threshold given in (9.9) is only an approximation, which is not tight as will be demonstrated later. In order to calculate the optimal threshold more accurately, a brute-force threshold search can be performed via simulations so that the theoretical expression in (9.7) is maximized, and the optimal threshold is given by

$$\xi_{opt} = \underset{\xi}{\text{argmax}}\Big\{P_D(n_{le}|\xi, D_{le}, E_b, \sigma^2)\Big\} \ , \tag{9.10}$$

where we test the threshold values $\tilde{\mu} \le \xi \le \mu_e$.

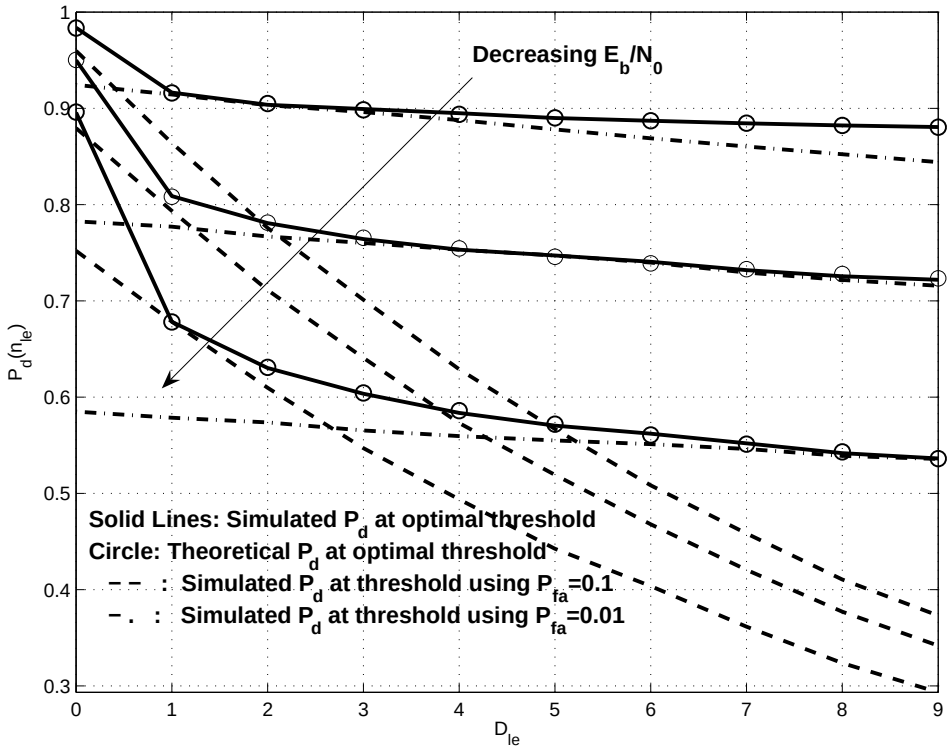

Figure 9.2 Probability of detections of the leading energy sample in AWGN channel using the optimum and noise-based thresholds at $E_b/N_0 \in \{6, 8, 10\}$dB with respect to D_{le}.

As an alternative to the optimal threshold setting, since the D_{le} and E_b values are typically not known, one can set the threshold based solely on the noise variance σ^2 (which can be estimated a-priori), and using a certain P_{fa}.

Computer simulations are done to evaluate the probability of detections of the leading edge using two types of thresholds (optimal vs. sub-optimal) discussed above in AWGN channels, and the results are compared with theory. Noise variance σ^2 is set to unity, and E_b is scaled to obtain different E_b/N_0 values. Also, we set $N_t = 1$, $t_s = 4$ns and $B = 500$MHz, yielding $\tilde{\mu} = M\sigma^2 = 4$.

In Fig. 9.2, theoretical and simulated[3] probability of detections for both optimum and P_{fa} based threshold settings are shown. Results show that if D_{le} is large, using smaller P_{fa} values (i.e. larger thresholds) is more beneficial since it increases the P_d; this is because larger thresholds decrease the chances of early false-alerts. On the other hand, as D_{le} decreases, it becomes more desirable to use larger values of P_{fa} for setting the threshold. The P_d curves obtained using the

[3]Thresholds are obtained using the brute-force search in (9.10) for both the theoretical and simulated P_d.

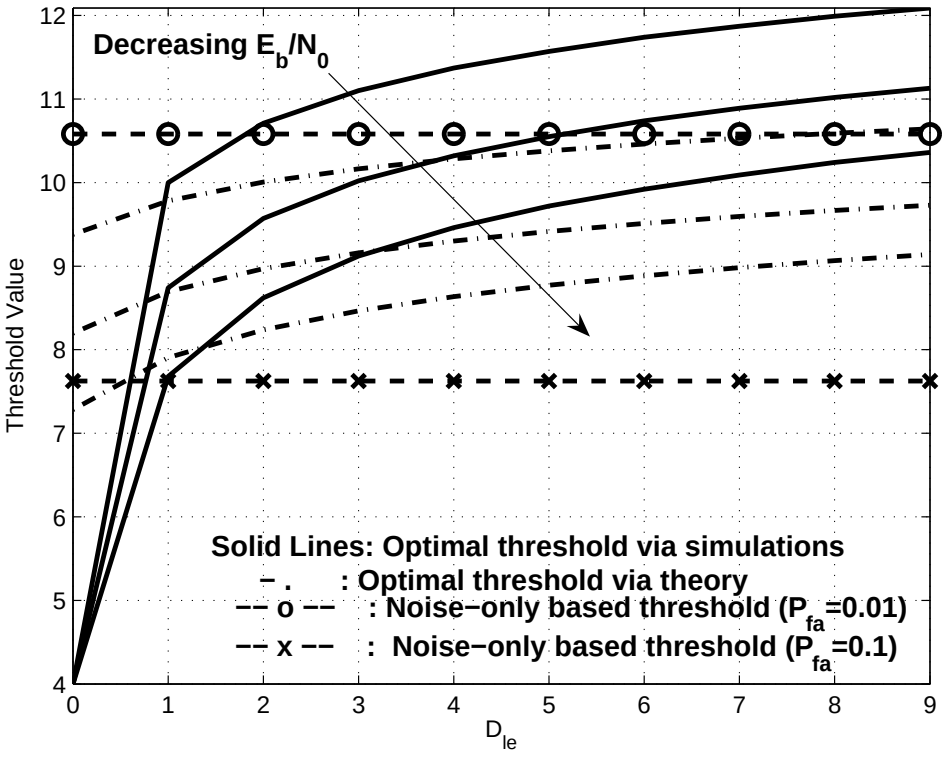

Figure 9.3 Optimum and noise-based thresholds in AWGN channel at $E_b/N_0 \in \{6, 8, 10\}$dB with respect to D_{le}.

noise-based thresholds are seen to be tangential with the optimal P_d curves only for certain D_{le} values. The corresponding optimal and noise-based threshold values and the approximations to the optimal threshold at different E_b/N_0 are presented in Fig. 9.3. The optimal threshold values are seen to increase with D_{le} and E_b/N_0, and approximation in (9.9) is not tight (but well models the behavior).

9.3.1.1 Variable D_{le} Case

In multipath channels, the D_{max} changes depending on the environment and the dispersiveness of the channel. While D_{max} tends to be small for line-of-sight (LOS) situations, it is typically larger for non-line-of-sight (NLOS) cases. The D_{le} can be easily obtained from D_{max} with the knowledge of W_{sb}. Using the available channel models [3], the PDF of the D_{le} can be captured for a particular channel model based on a large number of channel realizations from that model [30].

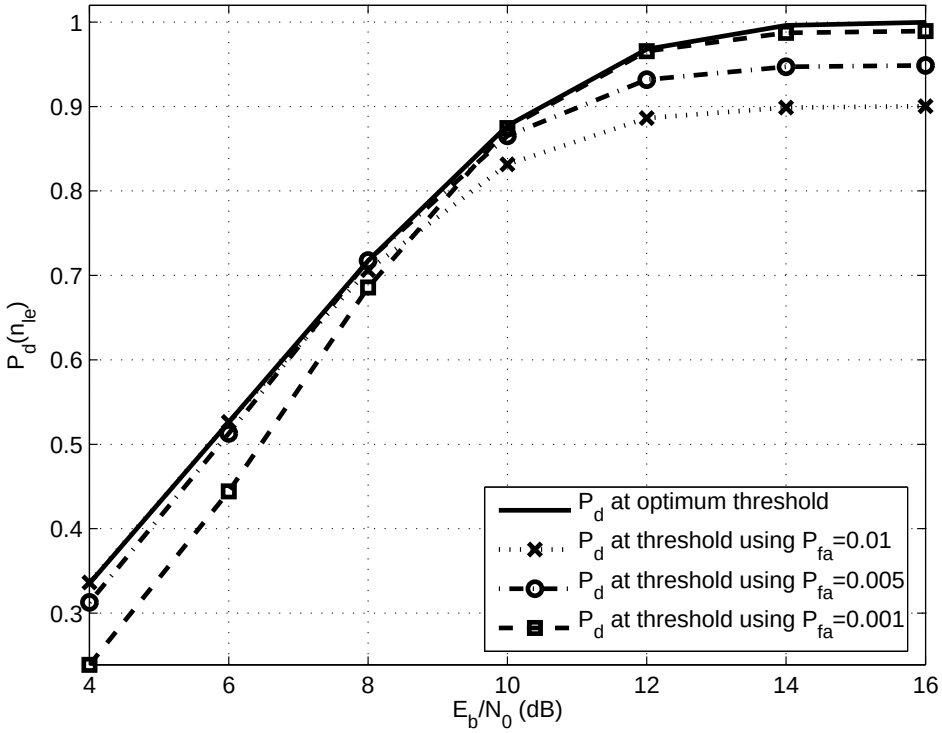

Figure 9.4 Simulated average probability of detections of the leading energy sample in AWGN channel using the optimum and noise-based thresholds with respect to E_b/N_0.

We can incorporate the PDF of D_{le} for AWGN case to show its average effect. The optimal threshold will then be the one that maximizes the average probability of detection, given by

$$P_D^{(avg)}(n_{le}|\xi, E_b, \sigma^2) = \int_{D_{le}} P_D(n_{le}|\xi, D_{le}, E_b, \sigma^2) p(D_{le}) dD_{le} \ , \tag{9.11}$$

and the threshold that maximizes (9.11) can be again found by using a brute-force search.

The probability of detection versus E_b/N_0 is plotted in Fig. 9.4 for different threshold settings. The thresholds are obtained using a brute-force search so as to maximize (9.11), and the simulated P_d results are verified via theory (only simulations are shown for brevity). The PDF of D_{max} given in [30] for CM1 channel model of [3] is used to average the probability of detection using a W_{sb} of 15 (corresponding to 60ns for t_s = 4ns). The results show that for a fixed P_{fa}, noise-based threshold curve is tangential with the optimal threshold curve at a certain E_b/N_0 value. At high E_b/N_0, the P_d becomes flat at a larger value for smaller P_{fa}; this is because the leading edge energy becomes sufficiently large, and it becomes possible to detect it using larger thresholds (avoiding false-alerts in

the searchback). However, higher P_{fa} values may become more desirable if E_b/N_0 is not sufficiently large.

9.3.2 Optimality of the Leading Edge Detection Threshold for Multipath Channel

Now consider the more realistic multipath channels as presented in the system model in Section 9.2.1. The leading edge sample energy in multipath channels may be very weak depending on the LOS/NLOS characteristics of the channel, and where the arriving path may fall only partially within the leading energy sample. Therefore, maximization of the probability of detection of the leading edge does not necessarily yield the best ranging accuracy (since detecting a latter sample may be much easier for certain channel realizations). Hence, for multipath channels, we choose the optimal threshold so as to minimize the MAE of the TOA estimate[4].

In order to find the optimal threshold, we assume that the $(D_{le}, \mathbf{E}_\lambda, \sigma^2)$ tuple is known. Then, the MAE of the TOA estimate can be calculated after weighting the average timing error corresponding to each block with the probability of detecting that block

$$e^{(MAE)}(n_{le}|\xi, D_{le}, \mathbf{E}_\lambda, \sigma^2) = \sum_{i=n_{sb}}^{n_{le}+n_{med}-1} P_D(i|\xi, D_{le}, \mathbf{E}_\lambda, \sigma^2) e_i \ , \tag{9.12}$$

where we consider that the set of samples between n_{sb} and $n_{le}+n_{med}-1$ may all be estimated using the searchback algorithm, and average timing error for choosing block i is given by (9.5). The energy vector $\mathbf{E}_\lambda$ captures the instantaneous signal energies at different sample indices. The probability of detection of the ith sample is given by

$$P_D(i|\xi, D_{le}, \mathbf{E}_\lambda, \sigma^2) = \left[\prod_{j=1}^{i-1} \left(1 - Q\Big(\frac{\xi - \mu_j}{\sigma_j}\Big)\right)\right] Q\Big(\frac{\xi - \mu_i}{\sigma_i}\Big) \ , \tag{9.13}$$

where μ_j and σ_j are as in (9.3), and the optimal threshold satisfies

$$\frac{de^{(MAE)}(n_{le}|\xi, D_{le}, \mathbf{E}_\lambda, \sigma^2)}{d\xi} = 0 \ . \tag{9.14}$$

Again, the evaluation of (9.14) is analytically intractable, and it is possible to find the threshold that minimizes (9.12) using a brute-force search $\xi_{opt} = \underset{\xi}{\text{argmin}}\Big\{e^{(MAE)}(n_{le}|\xi, D_{le}, \mathbf{E}_\lambda, \sigma^2)\Big\}$.

[4]Note that this is not the only performance metric, and other performance metrics, such as the confidence level of a certain timing accuracy, may also be defined [30].

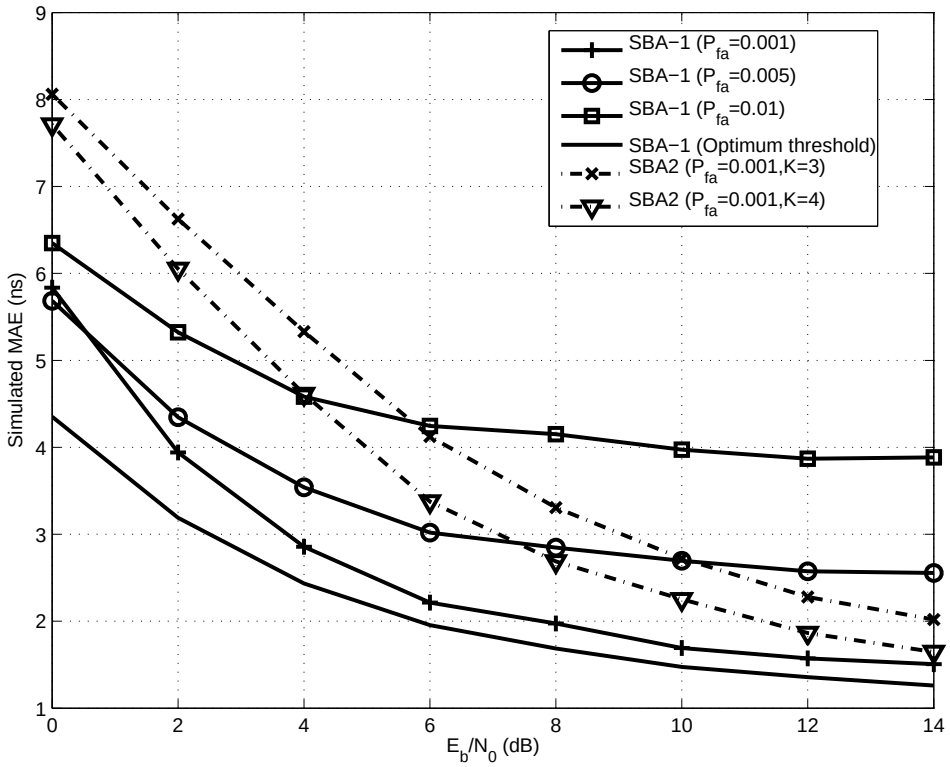

Figure 9.5 Simulated MAE performances for different algorithms, and when using the optimal threshold that minimizes the MAE.

It is important to note that there may be certain channel realizations where it becomes preferable to detect a latter sample rather than the leading edge sample, since the leading edge path(s) may be very weak. In such cases, the optimal threshold that minimizes the MAE may be larger than the leading edge energy value(s). In other words, since setting the threshold to a very small value may yield early false alerts, the MAE may be minimized by the detection of a latter stronger sample (using a larger threshold).

9.3.2.1 Simulation Results

The CM1 channel model of 802.15.4a in [3] is used to simulate the MAE performance of the optimal and noise-based thresholds (1000 different realizations), and compare them with theory. Again, noise variance σ^2 is set to unity, E_b is scaled to obtain different E_b/N_0, $t_s = 4$ns, $W_{sb} = 15$ (corresponding to 60ns), and $B = 500$MHz, yielding $\tilde{\mu} = M\sigma^2 = 4$. The number of averaging symbols is set to $N_t = 10^3$ in order to decrease the noise floor.

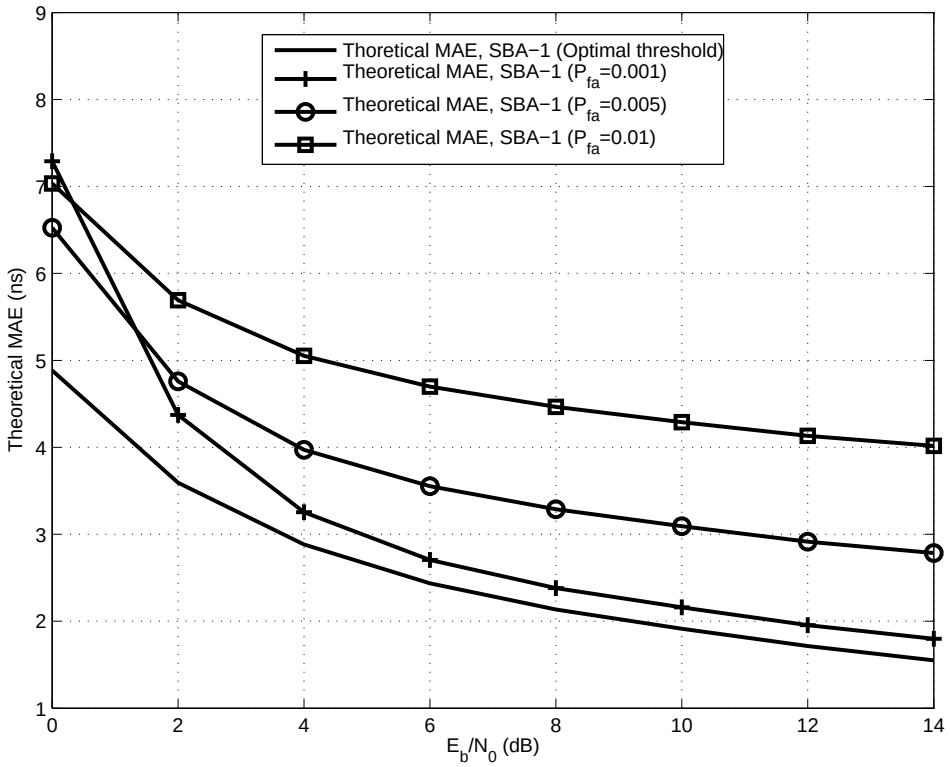

Figure 9.6 Theoretical MAE performances for SBA1 at different threshold settings, and when using the optimal threshold that minimizes the MAE.

In Fig. 9.5, the simulated MAEs of SBA1 when using noise-based thresholds are shown for $P_{fa} \in \{0.001, 0.005, 0.01\}$, along with optimal threshold result (thresholds calculated using brute-force search). For comparison purposes, simulation results for SBA2 are also presented for two different values of K, and for $P_{fa} = 0.001$. It is seen that when the noise-only based threshold is used with $P_{fa} = 0.001$, the MAE is on the order of fraction of a nano-second close to the optimal MAE for sufficiently high E_b/N_0 (for the given N_t value). On the other hand, as E_b/N_0 (or N_t) decreases, choosing a larger P_{fa} becomes more desirable. The performance of SBA2 is seen to improve considerably as E_b/N_0 increases.

The MAEs obtained using the expression (9.12) for SBA1 are plotted in Fig. 9.6 for different threshold settings (again averaged over 1000 channel realizations). The results are slightly worse compared to simulated performances, which is due to the approximation in (9.5) [30]. They are seen to be closer to the simulations for larger P_{fa} values.

9.4 Conclusion

In this chapter, a theoretical error analysis is carried out for a particular searchback algorithm (SBA1) to be used in UWB ranging. Optimality of the threshold for AWGN and multipath channels have been investigated. It is shown that in multipath channels, it is more desirable to choose the threshold so as to minimize the MAE of the TOA estimate, rather than maximizing the probability of detection of the leading edge. Theoretical and simulation results show that the practical approach of setting the threshold based only on the noise-level may give very close results when compared with the optimal threshold setting. This requires appropriate selection of the parameters such as P_{fa} and N_t based on the typical operating E_b/N_0 range.

CHAPTER 10

CONCLUSION AND FUTURE WORK

In this dissertation, we have addressed a number of transceiver design issues in impulse radio UWB systems. Practical implementation aspects such as sampling rate limitations (which are commonly neglected in the literature), timing jitter, and MAI are considered in different chapters. Some of the more significant issues that were reported (to our best knowledge) the first time in the literature are as follows

- Adaptation of two different types of processing gains in UWB systems and its analysis,
- Unified theoretical performance evaluation of UWB transceiver types (SR, TR, ED) at low-rate samples using the energy capture statistics of different transceivers,
- Development of a generic framework for theoretical performance evaluation (using the mean absolute errors) of different TOA estimation algorithms using non-coherent receivers,
- Characterization of the effects of timing jitter on the BER of IR-UWB for different scenarios.

Different parts of the work in this dissertation have been recognized by the wireless research community and cited by various journal papers (e.g. [278]-[285]), conference papers (e.g. [154, 273, 286]-[302]), and books/thesis/dissertations (e.g. [303]-[309]).

Below, we first present a list of specific contributions in different chapters of the dissertation. Then, possible extensions of the work done are discussed.

10.1 List of Specific Contributions

- UWB modulation options
  - This chapter is a unified and stand-alone reference for different UWB modulation options. We compared the trade-offs between these modulation types, such as the spectral

characteristics, power efficiencies, implementation complexities, multipath, multiuser interference, and timing jitter.

- Multiple accessing and time hopping sequence design
  - Presented a unified description of possible multiple access options for UWB systems. Namely, CDMA, FDMA, TDMA, time-hopping and frequency-hopping are discussed from UWB perspective.
  - Presented an adaptive code construction for centralized UWB systems (synchronous communications); the codewords of different users are adapted based on the number of users in the system and the maximum excess delay of the channel, and aims to minimize interference due to multipath.
  - For asynchronous communications, reviewed the correlation characteristics of code constructions based on congruence equations and finite field theory. Between other options, quadratic congruence codes have best combination of autocorrelation and cross-correlation characteristics.
  - Presented a BER performance analysis technique by capturing the statistics of the MAI using hit histograms.
- Adaptation of multiple access parameters for IR-UWB
  - Proposed a novel adaptive *downlink* signaling scheme (e.g. in cluster-based wireless sensor networks) that adapts the number of pulses per symbol based on the QoS requirements, and at the same time provides orthogonal signals for all the users.
  - For asynchronous communications, adaptation of two kinds of multiple access parameters are considered: number of pulses per symbol and number of pulse positions per frame. Based on the interference level in the system, appropriate set of parameters are selected for each user so that the desired QoS levels are achieved.
  - Two different cases are considered. For fixed frame duration case, the goal is to increase the average throughput depending on the interference level. For fixed symbol duration, the goal is to minimize battery consumption and maximize the network lifetime, again based on the interference level.

  - Validity of Gaussian approximation used in the above analysis is investigated using the KL distance; it is shown to be more valid for larger number of pulses per symbol, and smaller frame durations.

- Channel estimation at different sampling rates and under MAI
  - Investigated the UWB channel estimation performance with symbol-spaced, frame-spaced, and chip-spaced sampling scenarios and under multiple access interference.
  - For symbol-spaced sampling, proposed to use an absolute value based channel estimator, which is a semi-blind approach. It considerably decreases the number of training bits required to estimate the channel with slight performance loss at high SNR.
  - For frame-spaced sampling, proposed a simple pulse-discarding receiver to mitigate multiuser interference effects in strong near/far scenarios. The proposed estimator is different than previously proposed pulse discarding receivers, since no channel estimate knowledge is assumed.
  - A chip-spaced LS channel estimation model is introduced, which estimates a projection of the actual channel impulse response on the chip-spaced samples.

- Review of multiple access interference cancellation algorithms for UWB systems
  - Presented a unified and comprehensive review of multiple access interference mitigation and cancellation algorithms for UWB systems.
  - Emphasized the unique aspects of IR-UWB multiuser interference cancellation different than that of techniques used for CDMA systems.
  - Classified various algorithms under the following groups: 1) Transmitter-side interference avoidance techniques, 2) ML algorithms, 3) Linear receivers, 4) Subtractive/iterative interference cancellation, 5) Blind/adaptive techniques, 6) Other approaches.

- Effects of timing jitter on the performance of IR-UWB
  - Derived the BERs of various modulation options under timing jitter in AWGN, 1-tap Rayleigh fading, and multipath fading channels. Verified theoretical BER results with simulations.

- Treated finger estimation error as timing jitter, and obtained its PDF using simulations. The PDF is shown to depend on pulse shape and SNR, and converge to a unit impulse function as SNR increases.
- Investigated the effect of the jitter distribution on the BER performance. A worst case jitter distribution that gives an upper bound on the system performance is presented and compared with other distributions.
- Timing jitter effects on the performance of different pulse shapes, and on multiband UWB is investigated. It is shown that timing jitter effects are much harsher for higher-order bands in a multiband scheme, since the main lobe of the pulse autocorrelation functions start decaying faster.

• BER performances of IR-UWB transceiver types under sub-Nyquist sampling rates

- Provided a generic and unified model for performance evaluation of three different UWB transceiver types: Stored-reference receivers, transmitted-reference receivers, and energy detectors.
- Considered PPM, OOK, and BPSK modulations with each transceiver and derived the BERs in AWGN and multipath channels.
- For multipath channels, considered the effects of sub-Nyquist sampling rates, and provided a framework for energy capture analysis at low-rate sampling for all the three transceiver types. This is then used for semi-analytic BER evaluations.
- For Rake receivers, MRC, EGC, and SC types of combining algorithms are compared at low-rate samples.
- Effects of timing jitter, template pulse shape mismatch, and integration interval on the BER performance are analyzed under low-rate sampling assumption.

• Threshold selection for two different types of searchback schemes for ranging using IR-UWB

- Two types of threshold-based ranging algorithms are compared for UWB systems which use a searchback from the strongest sample to identify the leading edge path.
- Optimal threshold selection that maximizes the probability of detection of the leading edge sample is derived for AWGN channels.

- For multipath channels, the optimality metric is changed to be the minimization of the mean absolute error of the TOA estimate, since maximization of the probability of detection of the leading edge does not necessarily maximize ranging accuracy.
- The ranging accuracy with optimal threshold is compared with noise-only based threshold. It is shown that the performance loss is insignificant as long as appropriate number of averaging symbols is used based on the operating SNR range.

10.2 Possible Future Work

Following extensions of the work presented in this dissertation might be possible:

- Performance comparison of UWB and multicarrier modulations
  - Individual multipath components in UWB systems have low fading margins due to short-duration pulses, which is a distinct advantage when compared with narrowband systems. However, due to same reason, Rake receivers with large number of fingers might be required to capture the energy, which may considerably increase the complexity.

    In multicarrier systems (such as OFDM), on the other hand, the receiver *observes* only a single (or very few) multipath component(s) for each carrier, which has a large fading margin. Therefore, the channel at each carrier has to be estimated occasionally, and the complexity increases with the number of carriers.

    To our best knowledge, there is not a unified study that investigates the trade-offs between UWB and multicarrier modulations; such a study can be particularly interesting when considering the time varying channel characteristics (fading levels vs. dispersiveness of the channels) and their impacts on the system-level design (optimal bandwidth selection, optimal transmission rate of training symbols, complexity trade-offs etc.).
- Channel estimation at different sampling rates and under MAI
  - Subspace [146] and power of R [310] based UWB channel estimation techniques have been proposed in the literature. However, they either require matrix inversion, or eigendecomposition, both of which are computationally costly. A blind channel estimation technique that does not require either of the costly operations was proposed for CDMA systems

in [311], and similar lower-complexity techniques can be considered for UWB channel estimation and at the same time exploit its unique signaling scheme.

  - We have proposed a pulse-discarding receiver (prior to channel estimation) in Chapter 5 using a heuristic threshold selection. A more theoretical framework can be developed for optimal threshold selection based on the *a-priori* information assumptions.

- Multiple access interference cancellation algorithms for IR-UWB

  - In Chapter 6, various techniques for MAI cancellation were discussed. Neural networks, per survivor processing, Kalman filters, and genetic algorithms are some of the techniques that were applied to CDMA systems, and can as well be considered for UWB.

  - Blind subspace techniques might be particularly appropriate for UWB systems where the number of pulses per symbol is much larger than the number of users in the system (e.g. in low-rate wireless sensor networks). By projecting the signal subspace onto a lower-dimensional subspace, considerable complexity reductions can be obtained.

  - UWB interference cancellation techniques are commonly discussed for coherent receivers in the literature. However, interference cancellation techniques for more practical receiver types (such as TR receivers) have not been investigated in detail (other than [173]), and would be an interesting topic to dig into.

- BER performances of IR-UWB transceiver types under sub-Nyquist sampling rates

  - Even though we have shown the effect of chip-spaced sampling on the detection performance of different transceiver types in Chapter 8, we have not investigated the effects of various different sampling rates on the performance. It might be interesting to see how SR will start out-performing the TR and ED as the sampling rate increases (with the assumption of perfect channel estimates).

- TOA Estimation and Ranging using IR-UWB

  - The two searchback schemes introduced in Chapter 9 can be further improved using an iterative optimization technique. Upon estimating an initial value for the TOA, this may be used as an *a-priori* knowledge, and the estimate can be enhanced in an iterative manner.

- In practical systems that use time-hopping, multipath interference from the autocorrelation sidelobes ruins the performance of the searchback scheme. Time hopping codes with zero correlation zones alleviate the problem to some extent as long as maximum excess delay is kept smaller than the zero correlation zone [30]. However, such a design may not be always possible. Ternary codes with optimal autocorrelation characteristics do not have such a problem; however, due to the correlator template used in such systems, the resulting noise variance after pulse combining is twice that of noise variance in time-hopping systems. Therefore, techniques that handle the sidelobe interference in time-hopping based searchback schemes will be useful, such as using the CLEAN algorithm [312], or using an adaptive threshold selection.
- Investigation of how increasing sampling rates will improve the ranging accuracy is an interesting issue that should be further analyzed.
- Effects of timing jitter on the MAE performance and the real-time implementation complexities of different ranging algorithms are other practical issues that can be looked into.

REFERENCES

[1] K. Siwiak and D. McKeown, *Ultra-wideband Radio Technology.* 1st ed. West Sussex, UK: John Wiley & Sons Ltd., 2004.

[2] J. Foerster, "IEEE P802.15 working group for wireless personal area networks (WPANs), channel modeling sub-committee report - final," Mar., 2003. [Online]. Available: http://www.ieee802.org/15/pub/2003/Mar03/.

[3] A. F. Molisch, K. Balakrishnan, C. C. Chong, S. Emami, A. Fort, J. Karedal, J. Kunisch, H. Schantz, U. Schuster, and K. Siwiak, "IEEE 802.15.4a channel model - final report," Sept., 2004. [Online]. Available: http://www.ieee802.org/15/pub/TG4a.html.

[4] "UWB link hits 667Mbits/s data rate," WirelessWeb, Feb. 2005. [Online]. Available: http://wireless.iop.org/articles/news/6/2/8/1.

[5] M. C. O'Connor, "FCC certifies Ubisense's UWB," RFID Journal, Dec. 13 2004. [Online]. Available: http://www.rfidjournal.com/article/articleview/1285/1/1/.

[6] "The RFID revolution starts now! sapphire DART ultra wideband precision asses location system," Multispectral Solutions, Inc., 2005. [Online]. Available: http://www.multispectral.com/pdf/Sapphire-Revolution.pdf.

[7] J. R. Foerster, E. Green, S. Somayazulu, and D. Leeper, "Ultra-wideband technology for short- or medium-range wireless communications," *Intel Technology Journal*, Apr. Q2, 2001.

[8] "Ultrawideband (UWB technology)," White Paper, Intel Corporation, 2005. [Online]. Available: http://www.intel.com/technology/uwb/download/Ultra-Wideband.pdf.

[9] "Cellonics technology," Technical White Paper, Cellonics, Inc., October 2001. [Online]. Available: http://www.cellonics.com/tech/art/CellonicsTWP.zip.

[10] "XS110 UWB solution for media-rich wireless applications," Fact Sheet, Freescale Semiconductor, Inc., 2004. [Online]. Available: http://www.freescale.com/microcontrollers/doc/fact-sheet/MOTUWBFS.pdf.

[11] I. Guvenc and H. Arslan, "On the modulation options for UWB systems," in *Proc. IEEE Military Commun. Conf. (MILCOM)*, vol. 2, Boston, MA, Oct. 2003, pp. 892–897.

[12] H. Arslan, I. Guvenc, and S. Ahmed, *UWB Modulation Options.* John Wiley and Sons, 2006, in Ultra Wideband Wireless Communication.

[13] I. Guvenc and H. Arslan, "Design and performance analysis of time hopping sequences for UWB-IR systems," in *Proc. IEEE Wireless Commun. Networking Conf. (WCNC)*, vol. 2, Atlanta, GA, Mar. 2004, pp. 914–919.

[14] ——, "TH sequence construction for centralised UWB-IR systems in dispersive channels," *IEE Electronics Lett.*, vol. 40, no. 8, pp. 491–492, Apr. 2004.

[15] I. Guvenc, H. Arslan, S. Gezici, and H. Kobayashi, "Adaptation of multiple access parameters in time hopping UWB cluster based wireless sensor networks," in *Proc. IEEE Mobile Ad-hoc and Sensor Systems Conf. (MASS)*, Ft. Lauderdale, FL, Oct. 2004, pp. 235–244.

[16] ——, "Adaptive multiple accessing for UWB-IR wireless sensor networks," *To Appear in IEE Proceedings on Commun.*, Mar. 2006.

[17] I. Guvenc and H. Arslan, "A semi-blind channel estimator and multiuser receiver for UWB systems," in *Proc. Wireless and Microwave Conference (WAMICON)*, Clearwater, FL, Apr. 2004.

[18] ——, "UWB channel estimation with various sampling rate options," in *Proc. IEEE Sarnoff Symposium*, Princeton, NJ, Apr. 2005, pp. 229–232.

[19] ——, "A review on multiple access interference cancellation and avoidance for IR-UWB," *To be submitted to Eurasip Journal on Wireless Communications and Networking*, Mar. 2006.

[20] ——, "Performance evaluation of UWB systems in the presence of timing jitter," in *Proc. IEEE Ultrawideband Syst. Technol. (UWBST)*, Reston, VA, Nov. 2003, pp. 136–141.

[21] ——, "Performance analysis of UWB systems in the presence of timing jitter," *Journal on Communications and Networks (JCN)*, vol. 6, pp. 182–191, June 2004.

[22] ——, "Bit error rates of IR-UWB transceiver types at sub-nyquist sampling rates," to Appear in IEEE Wireless Commun. Networking Conf. (WCNC), Las Vegas, NV, Apr. 2006.

[23] ——, "On the transceiver types of IR-UWB systems at sub-Nyquist sampling rates," *Submitted to IEEE Trans. Vehic. Technol.*, Feb. 2006.

[24] ——, "Comparison of two searchback schemes for non-coherent TOA estimation in IR-UWB systems," to appear in IEEE Sarnoff Symposium, Princeton, NJ, Mar. 2006.

[25] ——, "Optimality of searchback threshold selection for TOA estimation in IR-UWB systems," *Submitted to IEEE Trans. Wireless Commun.*, Jan. 2006.

[26] I. Guvenc and Z. Sahinoglu, "Multiscale energy products for TOA estimation in IR-UWB systems," in *Proc. IEEE Global Telecommun. Conf. (GLOBECOM)*, vol. 1, St. Louis, MO, Dec. 2005, pp. 209–213.

[27] ——, "Threshold-based TOA estimation for impulse radio UWB systems," in *Proc. IEEE Int. Conf. UWB (ICU)*, Zurich, Switzerland, Sept. 2005, pp. 420–425.

[28] I. Guvenc, Z. Sahinoglu, and H. Arslan, "Multiscale energy products and normalized threshold selection for TOA estimation in IR-UWB systems," *Submitted to IEEE Trans. Vehic. Technol.*, Oct. 2005.

[29] I. Guvenc and Z. Sahinoglu, "Threshold selection for UWB TOA estimation based on kurtosis analysis," *IEEE Commun. Lett.*, vol. 9, no. 12, pp. 1025–1027, Dec. 2005.

[30] I. Guvenc, Z. Sahinoglu, A. F. Molisch, and P. Orlik, "Non-coherent TOA estimation in IR-UWB systems with different signal waveforms," in *Proc. IEEE Int. Workshop on Ultrawideband Networks (UWBNETS)*, Boston, MA, Oct. 2005, pp. 245–251, (invited paper).

[31] ——, "Waveform design and threshold selection for non-coherent IR-UWB ranging," *Submitted to IEEE Trans. Vehic. Technol.*, Aug. 2005.

[32] I. Guvenc and Z. Sahinoglu, "TOA estimation with different IR-UWB transceiver types," in *Proc. IEEE Int. Conf. UWB (ICU)*, Zurich, Switzerland, Sept. 2005, pp. 426–431.

[33] I. Guvenc, Z. Sahinoglu, and P. Orlik, "TOA estimation for IR-UWB systems with different transceiver types," to Appear in IEEE Trans. Microwave Theory and Techniques (Special Issue on Ultrawideband), Apr. 2005.

[34] Z. Sahinoglu and I. Guvenc, "Multiuser interference mitigation in non-coherent UWB ranging via nonlinear filtering," Submitted to IEEE Int. Conf. Ultrawideband (ICUWB), Waltham, MA, Sep. 2006.

[35] ——, "Multiuser interference mitigation for ToA based ranging via non-coherent ultrawideband radios," *Submitted to EURASIP J. Wireless Commun. Networking*, Sept. 2006.

[36] I. Guvenc and Z. Sahinoglu, "Simulations on non-coherent ranging," IEEE802.15 Working Group for Wireless Personal Area Networks (WPANs), June 2005, (standards contribution).

[37] Z. Sahinoglu and I. Guvenc, "Simulations on non-coherent ranging - II," IEEE802.15 Working Group for Wireless Personal Area Networks (WPANs), July 2005, (standards contribution).

[38] Z. Sahinoglu, I. Guvenc, and A. F. Molisch, "Method and system for estimating time of arrival of signals using multiple different time scales," Filed, MERL Patent No:1682, 2005.

[39] A. F. Molisch, I. Guvenc, and Z. Sahinoglu, "Method and receiver for identifying a leading edge time period in a received radio signal," Filed, MERL Patent No:1715, 2005.

[40] I. Guvenc and Z. Sahinoglu, "A method for time of arrival estimation using kurtosis analysis," Filed, MERL Patent, 2005.

[41] Z. Sahinoglu and I. Guvenc, "Filtering and multiple hypothesis testing for time of arrival estimation," Filed, MERL Patent, 2005.

[42] M. E. Sahin, I. Guvenc, and H. Arslan, "Optimization of energy detector receivers for UWB systems," in *Proc. IEEE Vehic. Technol. Conf. (VTC)*, vol. 2, Stockholm, Sweden, June 2005, pp. 1386–1390.

[43] ——, "Joint parameter estimation for UWB energy detectors using OOK," *Submitted to Springer J. Wireless Personal Commun.*, Dec. 2005.

[44] H. Celebi, I. Guvenc, and H. Arslan, "On the statistics of channel models for UWB ranging," to appear in IEEE Sarnoff Symposium, Princeton, NJ, Mar. 2006.

[45] S. Yarkan, I. Guvenc, and H. Arslan, "Location-aided opportunistic spectrum usage in wireless communication systems," Submitted to IEEE Int. Conf. Cognitive Radio Oriented Wireless Networks and Commun. (CROWNCOM), Mykonos Islan, Greece, June 2006.

[46] N. Brown, J. Tucker, I. Guvenc, and H. Arslan, "A flexible hardware platform for ultrawideband communication research," Wireless and Microwave Conference (WAMICON), Clearwater, FL, Apr. 2004, (poster presentation).

[47] I. Guvenc and H. Arslan, "System design issues in ultrawideband communications," Wireless and Microwave Symposium, Tampa, FL, Apr. 2003, (poster presentation).

[48] ——, "Multiuser transceiver design for time hopping ultrawideband impulse radio systems," Wireless and Microwave Conference (WAMICON), Clearwater, FL, Apr. 2004, (poster presentation).

[49] H. Celebi, M. E. Sahin, I. Guvenc, T. S. Price, and H. Arslan, "Low complexity UWB impulse radio," Wireless and Microwave Conference (WAMICON), Clearwater, FL, Apr. 2005, (poster presentation).

[50] M. Win and R. A. Scholtz, "Ultra-wide bandwidth time-hopping spread-spectrum impulse radio for wireless multiple-access communications," *IEEE Trans. Commun.*, vol. 48, no. 4, pp. 679–689, Apr. 2000.

[51] X. Huang and Y. Li, "Performances of impulse train modulated ultra-wideband systems," in *Proc. IEEE Int. Conf. Commun. (ICC)*, vol. 2, New York, Apr. 2002, pp. 758–762.

[52] J. G. Proakis, *Digital Communications*, McGraw-Hill, New York, 1995.

[53] J. McCorkle, "Why such uproar over ultra-wideband?" *Communication Systems Design Magazine*, March 2002.

[54] M. Welborn, "System considerations for ultra-wideband wireless networks," in *Proc. IEEE Radio and Wireless Conf. (RAWCON)*, Boston, MA, Aug. 2001, pp. 5–8.

[55] J. R. Foerster, "The performance of a direct-sequence spread ultra-wideband system in the presence of multipath, narrowband interference, and multiuser interference," in *Proc. IEEE Conf. UWB Syst. Technol. (UWBST)*, vol. 3, Baltimore, MD, May 2002, pp. 87–91.

[56] L. Ge, G. Yue, and S. Affes, "On the BER performance of pulse-position-modulation UWB radio in multipath channels," in *Proc. IEEE Conf. UWB Syst. Technol. (UWBST)*, vol. 3, Baltimore, MD, May 2002, pp. 231–234.

[57] H. Arslan, S. Gupta, G. Bottomley, and S. Chennakeshu, "New approaches to adjacent channel interference suppression in FDMA/TDMA mobile radio systems," *IEEE Trans. Veh. Technol.*, vol. 49, no. 4, pp. 1126–1139, July 2000.

[58] V. S. Somayazulu, "Multiple access performance in UWB systems using time hopping vs. direct sequence spreading," in *Proc. Wireless Commun. Networking Conf. (WCNC)*, vol. 2, Orlando, USA, Mar. 2002, pp. 522–525.

[59] M. Iacobucci and M. G. Benedetto, "Multiple access design for impulse radio communication systems," in *Proc. IEEE Int. Conf. Commun. (ICC)*, vol. 2, New York, Apr. 2002, pp. 817–820.

[60] M. Hamalainen, R. Tesi, J. Iinatti, and V. Hovinen, "On the performance comparison of different UWB data modulation schemes in AWGN channel in the presence of jamming," in *Proc. IEEE Radio and Wireless Conf. (RAWCON)*, Boston, MA, Aug. 2002, pp. 83–86.

[61] L. Zhao and A. M. Haimovic, "Performance of ultra-wideband communications in the presence of interference," *IEEE Jour. Sel. Areas Commun.*, vol. 20, no. 9, pp. 1684–1691, Dec. 2002.

[62] W. M. Lovelace and J. K. Townsend, "The effects of timing jitter and tracking on the performance of impulse radio," *IEEE J. Select. Areas Commun.*, vol. 20, no. 9, pp. 1646–1651, Dec. 2002.

[63] L. B. Michael, M. Ghavami, and R. Kohno, "Effect of timing jitter on Hermite function based orthogonal pulses for ultra wideband communication," in *Proc. Int. Symp. on Wireless Pers. Multimedia Commun.*, Aalborg, Denmark, Sept. 2001, pp. 441–444.

[64] E. Fishler and H. V. Poor, "On the tradeoff between two types of processing gain," in *Proc. 40th Annual Allerton Conf. on Commun. Control Computing*, Monticello, IL, Oct. 2002.

[65] Y. P. Nakache and A. F. Molisch, "Spectral shape of UWB signals-influence of modulation format, multiple access scheme and pulse shape," *Technical Report (TR2003-40)*, May 2003.

[66] G. R. Aiello, L. Taylor, and M. Ho, "A UWB architecture for wireless video networking," in *Proc. IEEE Int. Conf. Consumer Elect. (ICCE)*, Jun. 2001.

[67] G. Cariolaro, T. Erseghe, and L. Vangelista, "Exact spectral evaluation of the family of digital pulse interval modulated signals," *IEEE Trans. Inform. Theory*, vol. 47, no. 7, pp. 2983–2992, Nov. 2001.

[68] J. M. M. Romano and A. Haimovich, "Biorthogonal modulation for suppresing ultra-wideband spectral lines," Technical Report, 2003. [Online]. Available: http://web.njit.edu/jmr2224/research/biorthogonalmodulation.pdf.

[69] D. Cassioli, M. Z. Win, F. Vatalaro, and A. F. Molisch, "Performance of low-complexity RAKE reception in a realistic UWB channel," in *Proc. IEEE Int. Conf. Commun. (ICC)*, vol. 2, New York, Apr. 2002, pp. 763–767.

[70] S. Gezici, H. Kobayashi, H. V. Poor, and A. F. Molisch, "Performance evaluation of impulse radio UWB systems with pulse-based polarity randomization in asynchronous multiuser environments," in *Proc. IEEE Wireless Commun. Networking Conf. (WCNC)*, vol. 2, Atlanta, GA, Mar. 2004, pp. 908–913.

[71] G. R. Aiello and G. D. Rogerson, "Ultra-wideband wireless systems," *IEEE Microwave Magazine*, vol. 4, no. 2, pp. 36–47, Jun. 2003.

[72] L. Piazzo and J. Romme, "Spectrum control by means of the TH code in UWB systems," in *Proc. (IEEE) Vehic. Technol. Conf. (VTC)*, Jeju, Korea, Apr. 2003.

[73] H. Arslan, "Multiaccess interference cancellation receiver for time-hopping ultra-wideband communication," in *Proc. IEEE Int. Conf. Commun. (ICC)*, vol. 6, Paris, France, June 2004, pp. 3394–3398.

[74] J. R. Foerster, "The performance of a direct-sequence spread ultra-wideband system in the presence of multipath, narrowband interference, and multiuser interference," in *Proc. IEEE Conf. UWB Syst. Technol. (UWBST)*, vol. 3, Baltimore, USA, May 2002, pp. 87–91.

[75] L. L. Yang and L. Hanzo, "Residue number system assisted fast frequency-hopped synchronous ultra-wideband spread-spectrum multiple-access: a design alternative to impulse radio," *IEEE J. Select. Areas Commun.*, vol. 20, no. 9, pp. 1652–1663, Dec. 2002.

[76] S. Kim, K. H. Park, S. Yang, H. S. Kim, and Y. Shin, "Time hopping sequences based on pseudo random codes for ultra wideband impulse radio systems," in *Proc. Int. Technical Conf. Circuits/Systems Computers Commun.*, Phuket, Thailand, July 2002.

[77] C. M. Canadeo, M. A. Temple, R. O. Baldwin, and R. A. Raines, "Code selection for enhancing UWB multiple access communication performance using TH-PPM and DS-BPSK modulations," in *Proc. IEEE Wireless Commun. Networking Conf. (WCNC)*, vol. 1, New Orleans, LU, Mar. 2003, pp. 678–682.

[78] ——, "UWB multiple access performance in synchronous and asynchronous networks," *IEE Electronics Lett.*, vol. 39, no. 11, pp. 880–882, May 2003.

[79] C. Muller, S. Zeisberg, H. Seidel, and A. Finger, "Spreading properties of time hopping codes in ultra wideband systems," in *IEEE Int. Symp. Spread-Spectrum Tech. Appl.*, Prague, Czech Republic, Sept. 2002, pp. 64–67.

[80] S. V. Maric and E. L. Titlebaum, "A class of frequency hop codes with nearly ideal characteristics for use in multiple-access spread-spectrum communications and radar and sonar systems," *IEEE Trans. Commun.*, vol. 40, no. 9, pp. 1442–1447, Sept. 1992.

[81] ——, "Frequency hop multiple access codes based upon the theory of cubic congruences," *IEEE Trans. Aerospace Electron. Syst.*, vol. 26, no. 6, pp. 1035–1039, Nov. 1990.

[82] S. V. Maric, E. L. Titlebaum, and Z. Kostic, "Address assignment for multiple-access systems based upon the theory of congruence equations," in *Proc. IEEE Global Telecommunications Conf. (GLOBECOM)*, vol. 1, Nov. 1989, pp. 283–287.

[83] O. Moreno and S. V. Maric, "A new family of frequency-hop codes," *IEEE Trans. Commun.*, vol. 48, no. 8, pp. 1241–1244, Aug. 2000.

[84] G. C. Yang and W. C. Kwong, *Prime Codes with applications to CDMA optical and wireless networks*, 1st ed. Norwood, MA: Artech House, Inc., 2002.

[85] Z. Zhang, F. Zeng, and L. Ge, "Correlation properties of time-hopping sequences for impulse radio," in *Proc. IEEE Int. Conf. Acoustics, Speech, Sig. Processing (ICASSP)*, vol. 4, Hong Kong, Apr. 2003, pp. 141–144.

[86] M. S. Iacobucci and M. G. D. Benedetto, "Multiple access design for impulse radio communication systems," in *Proc. IEEE Int. Conf. Commun. (ICC)*, vol. 2, New York City, NY, May 2002, pp. 817–820.

[87] ——, "Time hopping codes in impulse radio multiple access communication systems," in *Proc. Int. Workshop 3G Infrastructure Services*, Athens, Greece, July 2001, pp. 171–175.

[88] S. Ratti and M. S. Iacobucci, "Cell search in ultra wide band time hopping asynchronous networks," in *Proc. Int. Workshop Mobile Wireless Commun.*, Stockholm, Sweden, Sept. 2002, pp. 282–285.

[89] T. Erseghe, "Time-hopping patterns derived from permutation sequences for ultra-wideband impulse-radio applications," in *Proc. WSEAS Int. Conf. Commun.*, vol. 1, Crete, July 2002, pp. 109–115.

[90] T. K. Woo, "Optimal time-hopping scheme for CDMA air interface in broad-band wireless systems," *IEEE J. Select. Areas Commun.*, vol. 18, no. 1, pp. 53–61, Jan. 2000.

[91] L. Bin, "One-coincidence sequences with specified distance between adjacent symbols for frequency-hopping multiple access," *IEEE Trans. Commun.*, vol. 45, no. 4, pp. 408–411, Apr. 1997.

[92] M. Welborn, T. Miller, J. Lynch, and J. McCorkle, "Multi-user perspectives in UWB communications networks," in *Proc. IEEE Conf. UWB Syst. Technol. (UWBST)*, vol. 3, Baltimore, MD, May 2002, pp. 271–275.

[93] L. Yang and G. B. Giannakis, "Multistage block-spreading for impulse radio multiple access through ISI channels," *IEEE J. Select. Areas Commun.*, vol. 20, no. 9, pp. 1767–1777, Dec. 2002.

[94] M. Z. Win and R. A. Scholtz, "Characterization of ultra-wide bandwidth wireless indoor channels: A communication theoretic view," *IEEE J. Select. Areas Commun.*, vol. 20, no. 9, pp. 1613–1627, Dec. 2002.

[95] P. Fan, "New direction in spreading sequence design and the related theoretical bounds," in *IEEE Int. Conf. Commun. Circuits Syst.*, no. 1, Jul. 2002, pp. 43–48.

[96] W. Ye and P. Fan, "Two classes of frequency hopping sequences with no hit zone," in *Proc. Int. Symp. Commun. Theo. Appl. (ISCTA)*, Cumbria, UK, August 2003.

[97] G. Durisi and S. Benedetto, "Performance evaluation of TH-PPM UWB systems in the presence of multiuser interference," *IEEE Commun. Lett.*, vol. 7, no. 5, pp. 224–226, May 2003.

[98] M. Z. Win and R. A. Scholtz, "Impulse radio: How it works," *IEEE Commun. Letters*, vol. 2, no. 2, pp. 36–38, Feb. 1998.

[99] W. M. Lovelace and J. K. Townsend, "Adaptive rate control with chip discrimination in UWB networks," in *Proc. IEEE Ultrawideband Systems Technol. (UWBST)*, Reston, VA, Nov. 2003, pp. 195–199.

[100] H. Arslan, *Adaptation Techniques and the Enabling Parameter Estimation Algorithms for Wireless Communication Systems.* Book Chapter, Signal Processing Communications Handbook, CRC Press, 2004.

[101] J. Y. L. Boudec, R. Merz, B. Radunovic, and J. Widmer, "A MAC protocol for UWB very low power mobile ad-hoc networks based on dynamic channel coding with interference mitigation," EPFL Technical Report ID: IC/2004/02, Lausanne, Switzerland, Tech. Rep., Jan. 2004.

[102] G. Giancola, L. D. Nardis, M. G. D. Benedetto, and E. Dubuis, "Dynamic resource allocation in time varying ultra wideband channels," in *Proc. IEEE Int. Conf. Commun. (ICC)*, vol. 6, Paris, France, June 2004, pp. 3581–3585.

[103] W. Chung and D. Ha, "An accurate ultra wideband (UWB) ranging for precision asset location," in *Proc. IEEE Conf. Ultrawideband Syst. Technol. (UWBST)*, Reston, VA, Nov. 2003, pp. 389–393.

[104] H. Zhang and R. Kohno, "Soft-spectrum adaptation in UWB impulse radio," in *Proc. IEEE Personal Indoor Mobile Radio Commun. (PIMRC)*, vol. 1, Beijing, China, Sep. 2003, pp. 289–293.

[105] S. S. Kolenchery, J. K. Townsend, J. A. Freebersyser, and G. Bilbro, "Performance of local power control in peer-to-peer impulse radio networks with bursty traffic," in *Proc. IEEE Global Telecommun. Conf.*, vol. 2, Phoenix, AR, Nov. 1997, pp. 910–916.

[106] S. J. Oh and K. M. Wasserman, "Adaptive resource allocation in power constrained cdma mobile networks," in *Proc. IEEE Wireless Commun. Networking Conf. (WCNC)*, vol. 1, New Orleans, LA, Sept. 1999, pp. 510–514.

[107] D. Kim, "Rate-regulated power control for supporting flexible transmission in future CDMA mobile networks," *IEEE J. Select. Areas Commun.*, vol. 17, no. 5, pp. 968–977, May 1999.

[108] L. C. Yun and D. G. Messerschmitt, "Variable quality of service in CDMA systems by statistical power control," in *Proc. IEEE Int. Conf. Commun.*, vol. 2, Seattle, WA, June 1995, pp. 713–719.

[109] F. Berggren and S. L. Kim, "Energy-efficient control of rate and power in DS-CDMA systems," *IEEE Trans. Wireless Commun.*, vol. 3, no. 3, pp. 725–733, May 2004.

[110] J. Diaz and Y. Bar-ness, "Adaptive transmission for UWB impulse radio communications," in *Proc. Conf. on Information Sciences Syst. (CISS)*, Baltimore, MD, Mar. 2003.

[111] G. Giancola, L. D. Nardis, and M. G. D. Benedetto, "Multi user interference in power-unbalanced ultra wide band systems: Analysis and verification," in *Proc. IEEE Ultrawideband Syst. Technol. Conf. UWBST*, Reston, VA, Nov. 2003, pp. 325–329.

[112] H. Yomo, P. Popovski, C. Wijting, I. Z. Kovacs, N. Deblauwe, A. F. Baena, and R. Prasad, "Medium access techniques in ultra-wideband ad hoc networks," in *Proc. 6th National Conf. of Society for Electronic, Telecommun., Automatics, and Informatics (ETAI)*, Ohrid, Macedonia, Sep. 2003.

[113] F. Cuomo, C. Martello, A. Baiocchi, and F. Capriotti, "Radio resource sharing for ad hoc networking with UWB," *IEEE J. Select. Areas Commun.*, vol. 20, no. 9, pp. 1722–1732, Dec. 2002.

[114] H. Zu and A. Ganz, "A radio resource control method in UWB MAC protocol design," in *Proc. IEEE Military Commun. Conf. (MILCOM)*, vol. 2, Boston, MA, Oct. 2003, pp. 886–891.

[115] T. Minn and K. Y. Siu, "Dynamic assignment of orthogonal variable-spreading-factor codes in W-CDMA," *IEEE J. Select. Areas Commun.*, vol. 18, no. 8, pp. 1429–1440, Aug. 2000.

[116] W. R. Heinzelman, A. Chandrakasan, and H. Balakrishnan, "Energy efficient communication protocol for wireless microsensor networks," in *Proc. Annual Hawaii International Conferance on System Sciences*, Hawaii, Jan. 2000, pp. 3005–3013.

[117] "Federal Communications Commision: Revision of part 15 of the commision's rules regarding ultra-wideband transmission system," First Report and Order, ET Docket 98-153, FCC 02-48, April 2002.

[118] S. Gezici, H. Kobayashi, H. V. Poor, and A. F. Molisch, "Performance evaluation of impulse radio UWB systems with pulse-based polarity randomization," *IEEE Trans. Sig. Processing*, vol. 53, no. 7, pp. 2537–2549, July 2005.

[119] N. He and C. Tepedelenlioglu, "Adaptive synchronization for non-coherent uwb receivers," in *Proc. IEEE International Conference on Acoustics, Speech, and Signal Processing (ICASSP'04)*, vol. 4, Montreal, Quebec, Canada, May 2004, pp. 517–520.

[120] S. Kullback, *Information theory and statistics*. Wiley, New York, 1959.

[121] V. Lottici, A. D'Andrea, and U. Mengali, "Channel estimation for ultra-wideband communications," *IEEE J. Select. Areas Commun.*, vol. 20, no. 9, pp. 1638–1645, Dec. 2002.

[122] R. Dilmaghani, M. Hernandez, M. Ghavami, and R. Kohno, "Optimum sequence design and performance evaluation of channel estimation techniques for ultra-wideband systems," *IEE Proceedings on Commun.*, vol. 152, no. 2, pp. 241–245, Apr. 2005.

[123] L. Huang and C. C. Ko, "Performance of maximum-likelihood channel estimator for UWB communications," *IEEE Commun. Lett.*, vol. 8, no. 6, pp. 356–358, June 2004.

[124] L. Yang and G. B. Giannakis, "Optimal pilot waveform assisted modulation for ultrawideband communications," *IEEE Trans. Wireless Commun.*, vol. 3, no. 4, pp. 1236–1249, July 2004.

[125] L. T. Son and K. M. Ahmed, "Performance of coherent direct sequence ultra wideband receiver with iterative channel estimation and detection," in *Proc. IEEE Int. Symp. Commun. and Information Technol. (ISCIT)*, vol. 2, Sapparo, Japan, Oct. 2004, pp. 1218–1223.

[126] Y. Li, X. G. Xia, R. Yao, and W. Zhu, "Coding assisted iterative channel estimation for impulse radio ultra-wide band communication systems," in *Proc. IEEE Int. Conf. Acoustics, Speech and Signal Processing (ICASSP)*, vol. 3, Philadelphia, PA, Mar. 2005, pp. 329–332.

[127] B. Mielczarek, M. O. Wessman, and A. Svensson, "Performance of coherent UWB rake receivers with channel estimators," in *Proc. IEEE Vehic. Technol. Conf. (VTC)*, vol. 3, Orlando, FL, Oct. 2003, pp. 1880–1884.

[128] H. Sato and T. Ohtuski, "Frequency domain channel estimation and equalisation for direct sequence ultra wideband (DS-UWB) system," *IEE Proceedings on Commun.*, vol. 153, no. 1, pp. 93–98, Feb. 2006.

[129] I. Maravic, M. Vetterli, and K. Ramchandran, "Channel estimation and synchronization with sub-Nyquist sampling and application to ultra-wideband systems," in *Proc. IEEE Int. Symp. Circuits and Syst. (ISCAS)*, vol. 5, Vancouver, Canada, May 2004, pp. 381–384.

[130] A. M. Tonello and R. Rinaldo, "A time-frequency domain approach to synchronization, channel estimation, and detection for DS-CDMA impulse radio systems," *IEEE Trans. Wireless Commun.*, vol. 4, no. 6, pp. 3018–3030, Nov. 2005.

[131] K. Haneda and J. I. Takada, "An application of SAGE algorithm for UWB channel estimation," in *Proc. IEEE Ultrawideband Syst. Technol. (UWBST)*, Reston, VA, Nov. 2003, pp. 483–487.

[132] J. Cai, X. Shen, J. W. Mark, H. Liu, and T. D. Todd, "Semiblind channel estimation for pulse-based ultra-wideband wireless communication systems," *IEEE Trans. Vehic. Technol.*, vol. 55, no. 1, pp. 95–103, Jan. 2006.

[133] C. Carbonelli, U. Mengali, and U. Mitra, "Synchronization and channel estimation for UWB systems," in *Proc. IEEE Global Telecommun. Conf. (GLOBECOM)*, vol. 2, San Francisco, CA, Dec. 2003, pp. 764–768.

[134] P. Liu and Z. Xu, "POR-based channel estimation for UWB communications," *IEEE Trans. Wireless Commun.*, vol. 4, no. 6, pp. 2968–2982, Nov. 2005.

[135] Z. Wang and X. Yang, "Blind channel estimation for ultra wide-band communications employing pulse position modulation," *IEEE Signal Processing Lett.*, vol. 12, no. 7, pp. 520–523, July 2005.

[136] Y. Zeng and Z. Zhou, "A swept sampling channel estimator for UWB system," in *Proc. IEEE Int. Symp. Commun. Information Technol. (ISCIT)*, vol. 1, Beijing, China, Oct. 2005, pp. 664–667.

[137] L. Ke, H. Yin, and P. Xu, "A novel channel estimation method for ultra-wideband communications based on OSCR receiver," in *Proc. IEEE Int. Conf. Commun. Circuits Syst.*, vol. 1, Beijing, China, May 2005, pp. 432–436.

[138] P. Liu, Z. Xu, and J. Tang, "Mean and covariance based estimation of multiple access uwb channels," in *Proc. IEEE Ultrawideband Systems and Technol. (UWBST)*, Reston, VA, Nov. 2003, pp. 458–462.

[139] R. Dilmaghani, M. Ghavami, and H. Aghvami, "Channel estimation technique for ultra-wideband pulse transmitters," *IEE Electronics Lett.*, vol. 40, no. 21, pp. 1348–1350, Oct. 2004.

[140] Z. Xu, J. Tang, and P. Liu, "Blind channel estimation for multiple access UWB communications based on periodic time hopping and pulse rate modeling," in *Proc. IEEE Topical Conference on Wireless Communication Technology*, Honolulu, HA, Oct. 2003, pp. 27–29.

[141] C. Carbonelli and U. Mitra, "Clustered channel estimation for UWB signals," in *Proc. IEEE Int. Conf. Commun. (ICC)*, vol. 4, Paris, France, June 2004, pp. 2432–2436.

[142] W. M. Lovelace and J. K. Townsend, "Chip discrimination for large near-far power ratios in UWB networks," in *Proc. IEEE Military Commun. Conf. (MILCOM)*, vol. 2, Boston, MA, Oct. 2003, pp. 868–873.

[143] S. Gezici, H. Kobayashi, and H. V. Poor, "A comparative study of pulse combining schemes for impulse radio UWB systems," in *Proc. IEEE Sarnoff Symp.*, Princeton, NJ, Apr. 2004, pp. 7–10.

[144] E. Fishler and H. V. Poor, "Low complexity multi-user detectors for time hopping implse radio systems," *IEEE Trans. Sig. Processing*, vol. 52, no. 9, pp. 2561–2571, Sep. 2004.

[145] ——, "Iterative (turbo) multiuser detectors for impulse radio systems," *Submitted to IEEE Trans. Commun.*, 2002.

[146] P. Liu, Z. Xu, and J. Tang, "Subspace multiuser receivers for UWB communication systems," in *Proc. IEEE Ultrawideband Systems and Technol. (UWBST)*, Reston, VA, Nov. 2003, pp. 116–120.

[147] S. Verdu, *Multiuser Detection.* 1st ed. Cambridge, UK: Cambridge University Press, 1998.

[148] L. Yang and G. B. Giannakis, "Multistage block-spreading for impulse-radio multiple access through ISI channels," *IEEE J. Select. Areas Commun. (JSAC)*, vol. 20, no. 9, pp. 1767–1777, Dec. 2002.

[149] C. J. L. Martret and G. B. Giannakis, "All-digital impulse radio with multiuser detection for wireless cellular systems," *IEEE Trans. Commun.*, vol. 50, no. 9, pp. 1440–1450, Sep. 2002.

[150] M. Chen and X. Li, "Transmitter-based channel equalization and MUI suppression for UWB systems," in *Proc. IEEE Int. Conf. Modern Problems of Radio Engineering, Telecommun., and Computer Science*, Lviv-Slavasko, Ukraine, Feb. 2004, pp. 501–504.

[151] I. Guvenc and H. Arslan, "Design and performance analysis of time hopping sequences for UWB-IR systems," in *Proc. IEEE Wireless Commun. Networking Conf. (WCNC)*, vol. 2, Atlanta, GA, Apr. 2004, pp. 914–919.

[152] G. M. Maggio, N. Rulkov, and L. Reggiani, "Pseudo-chaotic time hopping for UWB impulse radio," *IEEE Trans. Circuits and Syst.*, vol. 48, no. 12, pp. 1424–1435, Dec. 2001.

[153] Y. Tang, B. Vucetic, and Y. Li, "An FFT-based multiuser detection for asynchronous block-spreading CDMA ultrawideband communication systems," in *Proc. IEEE Int. Conf. Commun. (ICC)*, vol. 5, Seoul, Korea, May 2005, pp. 2872–2876.

[154] Z. Zhang, F. Zeng, and L. Ge, "Time-hopping sequences construction with few-hit zone for quasi-synchronous THSS-UWB systems," in *Proc. IEEE Vehic. Technol. Conf. (VTC)*, vol. 3, Stockholm, Sweden, May 2005, pp. 1998–2002.

[155] M. Cha, X. K. Kwak, J. Lee, and C. Lee, "Novel interference-cancelled ZCD-UWB system for WPAN," in *Proc. IEEE Int. Conf. Commun. (ICC)*, vol. 1, Paris, France, June 2004, pp. 95–99.

[156] S. Kuno, T. Yamazato, M. Katayama, and A. Ogawa, "A study on quasi-synchronous CDMA based on selected PN signature sequences," in *Proc. IEEE Spread Spectrum Techniques Applications*, vol. 2, Jul. 1994, pp. 479–483.

[157] V. DaSilva and E. S. Sousa, "Performance of orthogonal CDMA codes for quasi-synchronous communication systems," in *Proc. 2nd Int. Conf. Universal Personal Commun.*, vol. 2, Oct. 1993, pp. 995–999.

[158] A. Muqaibel, B. Woerner, and S. Riad, "Application of multi-user detection techniques to impulse radio time hopping multiple access systems," in *Proc. IEEE Ultrawideband Syst. Technol. (UWBST)*, Baltimore, MD, May 2002, pp. 169–173.

[159] Y. C. Yoon and R. Kohno, "Optimum multi-user detection in ultra-wideband (UWB) multiple-access communication systems," in *Proc. IEEE Int. Conf. Commun.*, vol. 2, New York City, NY, May 2002, pp. 812–816.

[160] Y. Zhang, W. S. Lu, and T. A. Gulliver, "Recursive multiuser detection for DS-UWB systems," in *Proc. IEEE Pacific Rim Conf. on Commun. Computers and Sig. Processing (PACRIM)*, Victoria, BC, Canada, Aug. 2005, pp. 534–537.

[161] X. Zhangliang and X. Quanshi, "A novel multi-user detector in UWB communication systems," in *Proc. IEEE Workshop on Sensor Array and Multichannel Signal Processing*, Sitges, Spain, July 2004, pp. 129–132.

[162] A. M. Tonello and R. Rinaldo, "Frequency domain multiuser detection for impulse radio systems," in *Proc. IEEE Vehic. Technol. Conf. (VTC)*, vol. 2, Stockholm, Sweden, May 2005, pp. 1381–1385.

[163] R. Lupas and S. Verdu, "Linear multiuser detectors for synchronous code-division multiple access channels," *IEEE Trans. Info. Theory*, vol. 35, no. 1, pp. 123–136, Jan. 1989.

[164] S. Moshavi, "Multiuser detection for DS-CDMA communications," *IEEE Commun. Mag.*, vol. 34, pp. 124–137, Oct. 1996.

[165] A. D. Hallen, J. Holtzman, and Z. Zvonar, "Multiuser detection for CDMA systems," *IEEE Personal Commun.*, vol. 2, no. 2, pp. 46–58, Apr. 1995.

[166] R. M. Buehrer, N. S. Correal-Mendoza, and B. D. Woerner, "A simulation comparison of multiuser receivers for cellular CDMA," *IEEE Trans. Vehic. Technol*, vol. 49, no. 4, pp. 1065–1085, July 2000.

[167] S. Im and E. J. Powers, "An iterative decorrelating receiver for DS-UWB multiple access systems using biphase modulation," in *Proc. IEEE Workshop on Sig. Processing Syst. (SIPS)*, Austin, TX, Oct. 2004, pp. 59–64.

[168] H. V. Poor, "Probability of error in MMSE multiuser detection," *IEEE Trans. Info. Theory*, vol. 43, no. 3, pp. 858–871, May 1997.

[169] Q. Li and L. A. Rusch, "Multiuser receivers for DS-CDMA UWB," in *Proc. IEEE Ultrawideband Sytstems and Technol. (UWBST)*, Baltimore, MD, May 2002, pp. 163–167.

[170] Q. Li and L. Rusch, "Multiuser detection for DS-CDMA UWB in the home environment," *IEEE J. Select. Areas Commun.*, vol. 20, no. 9, pp. 1710–1711, Dec. 2002.

[171] S. Gezici, H. Kobayashi, H. V. Poor, and A. F. Molisch, "Optimal and suboptimal linear receivers for time-hopping impulse radio systems," in *Proc. IEEE Ultrawideband Syst. Technol. (UWBST)*, Kyoto, Japan, May 2004, pp. 11–15.

[172] S. Gezici, M. Chiang, H. V. Poor, and H. Kobayashi, "A genetic algorithm based finger selection scheme for UWB MMSE receivers," in *Proc. IEEE Int. Conf. Ultra-wideband (ICU)*, Zurich, Switzerland, Sep. 2005, pp. 164–169.

[173] C. Steiner and K. Witrisal, "Multiuser interference modeling and suppression for a multichannel differential IR-UWB system," in *Proc. IEEE Int. Conf. Ultra-wideband (ICU)*, Zurich, Switzerland, Sep. 2005, pp. 667–672.

[174] J. Choi, "A framework for multiuser detection in time-hopping UWB with random sign repetition," in *Proc. IEEE Int. Conf. Commun. Syst. (ICCS)*, Singapore, Sep. 2004, pp. 11–15.

[175] ——, "Random sign repetition time-hopping UWB with multiuser detection," *Eurasip J. Wireless Commun. Networking*, vol. 5, no. 4, pp. 590–598, Sep. 2005.

[176] Z. Xu, J. Tang, and P. Liu, "Frequency domain estimation of multiple access ultra-wideband signals," in *Proc. IEEE Workshop on Statistical Signal Processing*, St. Lois, Missoiri, Sept. 2003, pp. 65–68.

[177] S. Morosi and T. Bianchi, "Frequency domain multiuser detectors for ultra-wideband short-range communications," in *Proc. IEEE Int. Conf. Acoustics, Speech, Signal Processing (ICASSP)*, vol. 3, Mar. 2004, pp. 637–640.

[178] G. Weeks, J. K. Townsend, and J. A. Freeberseyer, "Performance of hard decision detection for impulse radio," in *Proc. IEEE Military Commun. Conf. (MILCOM)*, vol. 2, Atlantic City, NJ, Nov. 1999, pp. 1201–1206.

[179] E. Baccarelli and M. Biagi, "A simple adaptive coding scheme for multiuser interference suppression in ultra-wideband radio transmissions," *IEEE Trans. Commun.*, vol. 53, no. 8, pp. 1283–1287, Aug. 2005.

[180] L. Son, K. M. Ahmed, J. A. Cooper, G. Brodin, and D. M. A. Walsh, "Direct sequence UWB receiver with iterative channel estimation and detection," in *Proc. Int. Conf. Mobile Wireless Commun. Networks (MWCN)*, Marrakech, Morocco, Sept. 2005.

[181] H. V. Poor, "Iterative multiuser detection," *IEEE Sig. Processing Mag.*, vol. 21, no. 1, pp. 81–88, Jan. 2004.

[182] ——, "Turbo multiuser detection: An overview," in *Proc. IEEE Int. Symp. Spread Spectrum Tech. & Appl.*, New Jersey, USA, Sept. 2000, pp. 583–587.

[183] J. Hagenauer, "The turbo principle: Tutorial introduction and state of the art," in *Proc. IEEE Int. Symp. Turbo Codes*, Brest, France, Sept. 1997, pp. 1–11.

[184] A. Bayesteh and M. N. Kenari, "Iterative interference cancellation and decoding for coded UWB-TH-CDMA systems in AWGN channel," in *Proc. IEEE Int. Symp. on Spread-Spectrum Tech. Appl.*, Prague, Czech Republic, Sept. 2002, pp. 263–267.

[185] T. Li and B. Y. Wang, "Low-complexity iterative multiuser detector for time-hopping impulse radio systems," in *Proc. IEEE Wireless Commun. Networking Conf. (WCNC)*, vol. 1, New Orleans, LA, Sept. 2005, pp. 377–380.

[186] N. Boubaker and K. B. Letaief, "Combined multiuser successive interference cancellation and partial RAKE reception for ultra-wideband wireless communications," in *Proc. IEEE Vehic. Technol. Conf. (VTC)*, vol. 2, Los Angeles, CA, Sep. 2004, pp. 1209–1212.

[187] S. Han, C. C. Woo, and D. Hong, "UWB interference cancellation receiver in dense multipath fading channel," in *Proc. IEEE Vehic. Technol. Conf. (VTC)*, vol. 2, Milan, Italy, May 2004, pp. 1233–1236.

[188] U. Madhow and M. L. Honig, "MMSE interference suppression for direct-sequence spread-spectrum CDMA," *IEEE Trans. Commun.*, vol. 42, no. 12, pp. 3178–3188, Dec. 1994.

[189] P. B. Rapajic and B. S. Vucetic, "Adaptive receiver structures for asynchronous CDMA systems," *IEEE Trans. Commun.*, vol. 12, no. 4, pp. 685–697, May 1994.

[190] S. Y. Jung and D. J. Park, "Multi-user detection using hidden training sequence for DS-CDMA UWB system," in *Proc. IEEE Vehic. Technol. Conf. (VTC)*, vol. 3, Los Angeles, CA, Sep. 2004, pp. 1924–1928.

[191] S. Verdu, "Adaptive multiuser detection," in *Proc. IEEE Spread Spectrum Techniques and Applications*, vol. 1, Oulu, Finland, July 1994, pp. 43–50.

[192] X. Wang and H. V. Poor, "Blind multiuser detection: A subspace approach," *IEEE Trans. Info. Theory*, vol. 44, no. 2, pp. 677–690, Mar. 1998.

[193] M. L. Honig and J. S. Goldstein, "Adaptive reduced-rank interference suppression based on the multistage Wiener filter," *IEEE Trans. Commun.*, vol. 50, no. 6, pp. 986–994, June 2002.

[194] X. Cai, H. Ge, and A. N. Akansu, "Low-rank MMSE detector for synchronous DS-CDMA," in *Proc. IEEE Asilomar Conference on Signals, Systems, and Computers*, vol. 2, Monterey, CA, Oct. 1999, pp. 940–944.

[195] M. L. Honig, "A comparison of subspace adaptive filtering techniques for DS-CDMA interference suppression," in *Proc. IEEE Military Commun. Conf. (MILCOM)*, vol. 2, Monterey, CA, Nov. 1997, pp. 836–840.

[196] Z. Xu, P. Liu, and J. Tang, "A subspace approach to blind multiuser detection in ultra-wideband channels," *EURASIP J. Applied Signal Processing: Special Issue on UWB - State of the Art (in press)*, 2004.

[197] S. H. Wu, U. Mitra, and C. C. J. Kuo, "Multistage MMSE receivers for ultra-wide bandwidth impulse radio communications," in *Proc. IEEE Ultrawideband Syst. Technol. (UWBST)*, Kyoto, Japan, May 2004, pp. 16–20.

[198] Z. Tian, H. Ge., and L. L. Scharf, "Low-complexity multiuser detection and reduced-rank Wiener filters for ultra-wideband multiple access," in *Proc. IEEE Int. Conf. Acoustics, Speech, and Signal Processing (ICASSP)*, vol. 3, Philadelphia, PA, Mar. 2005, pp. 621–624.

[199] P. Liu, Z. Xu, and J. Tang, "Minimum variance multiuser detection for impulse radio UWB systems," in *Proc. IEEE Ultrawideband Systems and Technol. (UWBST)*, Reston, VA, Nov. 2003, pp. 111–115.

[200] Z. Xu, P. Liu, and X. Wang, "Blind multiuser detection: From MOE to subspace methods," *IEEE Trans. Signal Processing*, vol. 52, no. 2, pp. 510–524, Feb. 2004.

[201] C. M. Chang and K. C. Chen, "Frequency-domain approach to DS-CDMA multiuser detection over frequency-selective slowly fading channels," in *Proc. IEEE Personal Indoor and mobile Radio Commun. (PIMRC)*, vol. 3, Lisbon, Portugal, Sept. 2002, pp. 1280–1284.

[202] ——, "Frequency-domain approach to multiuser detection in DS-CDMA communications," *Proc. IEEE Personal Indoor and mobile Radio Commun. (PIMRC)*, vol. 3, pp. 1280–1284, Sept. 2002.

[203] T. J. Lim, K. Rasmussen, and H. Sugimoto, "An asynchronous multiuser CDMA detector based on the Kalman filter," *IEEE J. Select. Areas Commun.*, vol. 16, no. 9, pp. 1711–1722, Dec. 1998.

[204] T. J. Lim and Y. Ma, "The Kalman filter as the optimal linear minimum mean-squared error multiuser CDMA detector," *IEEE Trans. Info. Theory*, vol. 46, no. 7, pp. 2561–2566, Nov. 2000.

[205] B. P. Flanagan and J. Dunyak, "A steady state decoupled kalman filter technique for multiuser detection," in *Proc. IEEE Military Commun. Conf.*, vol. 1, Boston, MA, Oct. 2003, pp. 347–352.

[206] J. F. Liao, C. L. Tsai, and B. S. Chen, "Robust adaptive channel estimation and multiuser detection for ultra wideband in a realistic indoor channel," in *Proc. IEEE Int. Conf. Commun. (ICC)*, vol. 4, Seoul, Korea, May 2005, pp. 2845–2851.

[207] B. Aazhang, B. P. Paris, and G. C. Orsak, "Neural networks for multiuser detection in code-division multiple access communications," *IEEE Trans. Commun.*, vol. 40, no. 7, pp. 1212–1222, July 1992.

[208] N. Wang, W. P. Zhu, and B. Zheng, "Blind multiuser detection for DS-CDMA systems: A neural network approach," in *Ninth DSP Workshop*, vol. 5, Orlando, FL, May 1999, pp. 603–606.

[209] G. Kechriotis and E. S. Manolakos, "A hybrid digital signal processing-neural network CDMA multiuser detection scheme," *IEEE Trans. Circuits Syst.:Analog and Digital Signal Processing*, vol. 43, no. 2, pp. 96–104, Feb. 1996.

[210] M. G. Shayesteh, M. Menhaj, and H. Amindavar, "Computational intelligence techniques for multiuser detection of DS/CDMA signals," in *Proc. IEEE Computationan Intelligence in Robotics and Automation*, vol. 1, Taipei, Taiwan, July 2003, pp. 390–395.

[211] M. J. Juntti, T. Schlosser, and J. O. Lilleberg, "Genetic algorithms for multiuser detection in synchronous CDMA," in *Proc. IEEE Int. Symp. Commun. Theory*, Ulm, Germany, June 1997, p. 492.

[212] L. Dong, X. Youyun, S. Wentao, L. Hanwen, and L. Xingzhao, "Genetic algorithms based multiuser detection for CDMA systems," in *Proc. IEEE Symp. on Emerging Technologies: Mobile and Wireless Commun.*, vol. 1, Shanghai, China, June 2004, pp. 321–324.

[213] K. Yen and L. Hanzo, "Genetic algorithm assisted multiuser detection in asynchronous CDMA communications," *IEEE Trans. Vehic. Technol.*, vol. 53, no. 5, pp. 1413–1422, Sept. 2004.

[214] C. Ergun and K. Hacioglu, "Multiuser detection using a genetic algorithm in CDMA communications systems," *IEEE Trans. Commun.*, vol. 48, no. 8, pp. 1374–1383, Aug. 2000.

[215] Z. Xie, C. K. Rushforth, R. T. Short, and T. K. Moon, "Joint signal detection and parameter estimation in multiuser communications," *IEEE Trans. Commun.*, vol. 41, no. 7, pp. 1208–1216, Aug. 1993.

[216] B. L. Yeap, F. Guo, E. L. Kuan, H. Wei, and L. Hanzo, "Blind per-survivor processing based multiuser detection for channel coded multicarrier DS-CDMA systems," in *Proc. IEEE Vehic. Technol. Conf. (VTC)*, vol. 3, Milan, Italy, May 2004, pp. 1376–1380.

[217] E. L. Kuan and L. Hanzo, "Turbo-coded blind per-survivor processing multiuser detection cdma," in *Proc. IEEE Personal Indoor Mobile Radio Commun. (PIMRC)*, vol. 1, London, UK, Sept. 2000, pp. 746–750.

[218] I. Guvenc and H. Arslan, "Th sequence construction for centralised UWB-IR systems in dispersive channels," *IEE Electronics Lett.*, vol. 40, no. 8, pp. 491–492, Apr. 2004.

[219] P. R. Trischitta and E. L. Varma, *Jitter in Digital Transmission Systems*, 1st ed. Norwood, MA: Artech House Inc., 1989.

[220] S. Haykin, *Communication Systems.* 3rd ed. New York: John Wiley and Sons, Inc., 1994, pp. 461–465.

[221] C. Duff, "Jitter analysis techniques," Agilent Technologies, p. 1, 2002. [Online]. Available: http://www.agilent.com.

[222] J. Sun, M. Li, and J. Wilstrup, "A demonstration of deterministic jitter (DJ) deconvolution," in *Proc. IEEE Instrumentation Measurement Technol. Conf. (IMTC)*, vol. 1, Anchorage, AK, May 2002, pp. 293–298.

[223] "Application note, HFAN-4.0.3: Jitter in digital communication systems, part 1," Maxim High-Frequency/Fiber Communications Group, pp. 2–6, Sep. 2001. [Online]. Available: http://pdfserv.maxim-ic.com/arpdf/AppNotes/5hfan403.pdf.

[224] K. Schumacher and J. J. O'reily, "Distribution free bound on the performance of optical communication systems in the presence of jitter," *IEE Proceedings*, vol. 136J, no. 2, pp. 129–136, Apr. 1989.

[225] Z. Nikolic, M. Stefanovic, and N. Stojanovic, "Upper bound of error probability in the presence of intersymbol interference and jitter," *IEE Electron. Lett.*, vol. 30, no. 5, pp. 389–390, Mar. 1994.

[226] L. Tomba and W. A. Krzymien, "Performance enhancement of multicarrier CDMA systems impaired by chip timing jitter," in *Proc. IEEE Int. Symp. Spread Spectrum Techniques Appl.*, vol. 1, Sept. 1996, pp. 22–25.

[227] B. Kaushik, R. Ganesh, and R. Sadhu, "Modeling delay jitter distribution in voice over IP," Jan. 2003, unpublished. [Online]. Available: http://arxiv.org/pdf/cs.PF/0301005.

[228] S. Shenghe, G. Shize, and L. Chunming, "An adaptive deconvolution method for eleminating the effect of the time jitter," in *Proc. IEEE Instrumentation Measurement Technol. Conf. IMTC*, vol. 3, Hamamatsu, Japan, May 1994, pp. 1140–1142.

[229] M. P. Li, J. Wilstrup, R. Jessen, and D. Petrich, "A new method for jitter decomposition through its distribution tail fitting," in *Proc. IEEE Int. Test Conf. (ITC)*, Atlantic City, NJ, Sept. 1999, pp. 788–794.

[230] C. Mailhes and B. Lacaze, "Jitter effects in a multipath environment," in *Proc. IEEE Int. Conf. Acoustics Speech Sig. Processing (ICASSP)*, vol. 6, Salt Lake City, UT, May 2001, pp. 3905–3908.

[231] M. Shimanouchi, "An approach to consistent jitter modelling for various jitter aspects and measurement methods," in *Proc. IEEE Int. Test Conf. (ITC)*, Baltimore, MD, Nov. 2001, pp. 848–857.

[232] Y. Takasaki, *Digital Transmission Design and Jitter Analysis*, Artech House Inc., 1991.

[233] D. Kelly, S. Reinhardt, R. Stanley, and M. Einhorn, "Pulson second generation timing chip: enabling UWB through precise timing," in *Proc. IEEE Conf. UWB Syst. Technol. (UWBST)*, Baltimore, MD, May 2002, pp. 117–121.

[234] G. Durisi and S. Benedetto, "Performance evaluation and comparison of different modulation schemes for UWB multiaccess systems," in *Proc. IEEE Int. Conf. Commun. (ICC)*, vol. 3, Anchorage, AK, May 2003, pp. 2187–2191.

[235] M. Z. Win, "A unified spectral analysis of generalized time-hopping spread-spectrum signals in the presence of timing jitter," *IEEE J. Select. Areas Commun.*, vol. 20, no. 9, pp. 1664–1676, Dec. 2002.

[236] ——, "Spectral density of random time-hopping spread-spectrum UWB signals with uniform timing jitter," in *Proc. IEEE Mil. Commun. Conf. MILCOM*, vol. 2, Atlantic City, NJ, Nov. 1999, pp. 1196–1200.

[237] ——, "Spectral density of random UWB signals," *IEEE Commun. Lett.*, vol. 6, no. 12, pp. 526–528, Dec. 2002.

[238] Y. Shin and J. Ahn, "Effect of timing jitter in an ultra wideband impulse radio system," in *Proc. IEEE Int. Symp. on Intelligent Signal Processing and Commun. Syst. (ISPACS)*, Hawaii, Nov. 2000, pp. 502–505.

[239] L. B. Michael, M. Ghavami, and R. Kohno, "Effect of timing jitter on Hermite function based orthogonal pulses for ultra wideband communication," in *Proc. 4th Int. Symp. Wireless Personal Multimedia Commun.*, Aalborg, Denmark, Sept. 2001, pp. 441–444.

[240] "NIST/SEMATECH e-Handbook of statistical methods," Jun. 2003. [Online]. Available: http://www.itl.nist.gov/div898/handbook/.

[241] M. Ghavami, L. B. Michael, and R. Kohno, "Hermite function based orthogonal pulses for for ultra wideband communication," in *Proc. 4th Int. Symp. Wireless Personal Multimedia Commun.*, Aalborg, Denmark, Sept. 2001, pp. 437–440–1651.

[242] M. Z. Win and R. A. Scholtz, "Energy capture vs. correlator resources in ultra-wide bandwidth indoor wireless communication channels," in *Proc. IEEE Military Commun. Conf. (MILCOM)*, vol. 3, Monterey, CA, Nov. 1997, pp. 1277–1281.

[243] P. P. Newaskar, R. Blazquez, and A. R. Chandrakasan, "A/D precision requirements for an ultra-wideband radio receiver," in *Proc. IEEE Workshop on Signal Processing Syst. (SIPS)*, San Diego, CA, Oct. 2001, pp. 270–275.

[244] F. Rajwani and N. C. Beaulieu, "Simplified bit error rate analysis of PAPM-UWB with MRC and EGC in lognormal fading channels," in *Proc. IEEE Int. Conf. Commun. (ICC)*, vol. 5, Seoul, Korea, May 2005, pp. 2886–2889.

[245] J. D. Choi and W. E. Stark, "Performance analysis of RAKE receivers for ultra-wideband communications with PPM and OOK in multipath channels," in *Proc. IEEE Conf. Commun. (ICC)*, vol. 3, New York, NY, Apr. 2002, pp. 1969–1973.

[246] ——, "Performance of ultra-wideband communications with suboptimal receivers in multipath channels," *IEEE J. Select. Areas Commun.*, vol. 20, no. 9, pp. 1754–1766, Dec. 2002.

[247] M. K. Simon and M. S. Alouini, "A unified approach to the performance analysis of digital communication over generalized fading channels," *Proceedings of the IEEE*, vol. 86, no. 9, pp. 1860–1877, Sept. 1998.

[248] A. Rajeswaran, V. S. Somayazulu, and J. R. Foerster, "RAKE performance for a pulse based UWB system in a realistic UWB indoor channel," in *Proc. IEEE Int. Conf. Commun. ICC*, vol. 4, Anchorage, Alaska, May 2003, pp. 2879–2883.

[249] J. D. Choi and W. Stark, "Performance of UWB communications with imperfect channel estimation," in *Proc. IEEE Military Commun. Conf. (MILCOM)*, vol. 2, Boston, MA, Oct. 2003, pp. 915–920.

[250] H. Niu, J. A. Ritcey, and H. Liu, "Performance UWB RAKE receivers with imperfect tap weights," in *Proc. IEEE Conf. on Acoustics, Speech, and Signal Processing (ICASSP)*, vol. 4, Hong Kong, Apr. 2003, pp. 125–128.

[251] H. Sheng, R. You, and A. M. Haimovich, "Performance analysis of ultra-wideband Rake receivers with channel delay estimation errors," in *Proc. Conf. on Information Sciences and Syst. (CISS)*, Princeton, NJ, Mar. 2004, pp. 921–926.

[252] M. S. W. Chen and R. W. Brodersen, "The impact of a wideband channel on UWB system design," in *Proc. IEEE Military Commun. Conf. (MILCOM)*, Monterey, CA, Oct. 2004.

[253] R. C. Qiu, "A generalized time domain multipath channel and its application in ultra-wideband (UWB) wireless optimal receiver design: System performance analysis," in *Proc. Wireless Commun. Networking Conf. (WCNC)*, vol. 2, Atlanta, GA, Apr. 2004, pp. 901–907.

[254] R. D. Wilson and R. A. Scholtz, "Template estimation in ultra-wideband radio," in *Proc. IEEE Asilomar Conf. Signals, Systems, Computers*, vol. 2, Pacific Grove, CA, Nov. 2003, pp. 1244–1248.

[255] K. Taniguchi and R. Kohno, "Design and analysis of template waveform for receiving UWB signals," in *Proc. IEEE Conf. on Ultrawideband Syst. Technol. (UWBST)*, Kyoto, Japan, May 2004, pp. 125–129.

[256] M. H. Chung and R. A. Scholtz, "Comparison of transmitted- and stored-reference systems for ultra-wideband communications," in *Proc. IEEE Military Commun. Conf. (MILCOM)*, vol. 1, Monterey, CA, Oct. 2004, pp. 521–527.

[257] G. Durisi and S. Benedetto, "Comparison between coherent and non-coherent receivers for UWB communications," *Eurosip J. Applied Sig. Processing*, vol. 3, pp. 359–368, 2005.

[258] S. Paquelet, L. M. Aubert, and B. Uguen, "An impulse radio asynchronous transceiver for high data rates," in *Proc. Ultrawideband Syst. Technol. (UWBST)*, Kyoto, Japan, May 2004, pp. 1–5.

[259] L. Yang, G. B. Giannakis, and A. Swami, "Noncoherent ultra-wideband radios," in *Proc. IEEE Military Commun. Conf. (MILCOM)*, vol. 2, Monterey, CA, Oct. 2004, pp. 786–791.

[260] Y. L. Chao and R. A. Scholtz, "Multiple access performance of ultra-wideband transmitted reference systems in multipath environments," in *Proc. Wireless Commun. Networking Conf. (WCNC)*, Atlanta, GA, Apr. 2004, pp. 1788–1793.

[261] Z. Tian and V. Lottici, "Efficient timing acquisition in dense multipath for UWB communications," in *Proc. IEEE Vehic. Technol. Conf. (VTC)*, vol. 2, Orlando, FL, Oct. 2003, pp. 1318–1322.

[262] X. Wu, L. Wu, and Z. Tian, "Performance analysis of UWB impulse radios with noisy template reception," in *Proc. IEEE Asilomar Conf. Signals, Systems, Computers*, vol. 2, Pacific Grove, CA, Nov. 2004, pp. 1501–1505.

[263] G. Leus and A. J. Van-Der-Veen, "A weighted autocorrelation receiver for transmitted reference ultra wideband communications," in *Proc. IEEE Signal Processing Advances in Wireless Communications (SPAWC)*, June 2005, pp. 965–969.

[264] Y. L. Chao and R. A. Scholtz, "Weighted correlation receivers for ultra-wideband transmitted reference systems," IEEE Global Telecommun. Conf. (GLOBECOM), pp. 66–70, Dec. 2004.

[265] J. Romme and G. Durisi, "Transmit reference impulse radio systems using weighted correlation," in *Proc. IEEE Ultrawideband Syst. Technol. (UWBST)*, Kyoto, Japan, May 2004, pp. 141–145.

[266] J. Romme and K. Witrisal, "On transmitted-reference UWB systems using discrete- time weighted autocorrelation," in *Proc. IEEE Vehic. Technol. Conf. (VTC)*, Stockholm, Sweden, May 2005.

[267] Z. Tian and B. M. Sadler, "Weighted energy detection for ultra-wideband signals," in *Proc. IEEE Signal Processing Advances in Wireless Communications (SPAWC)*, New York City, NY, June 2005, pp. 1069–1072.

[268] A. M. Orndorff, "Transceiver design for ultra-wideband communications," Master's thesis, Virginia Polytechnic Institute and State University, Blacksburg, VA, May 2004.

[269] A. Anamalai, G. Deora, and C. Tellambura, "Unified analysis of generalized selection diversity with normalized threshold test per branch," in *Proc. IEEE Wireless Commun. Networking Conf. (WCNC)*, vol. 2, New Orleans, LA, Mar. 2003, pp. 752–756.

[270] T. Wang, Z. N. Chen, and K. Chen, "Effect of selecting antenna and template on ber performance in pulsed UWB wireless communication systems," in *Proc. IEEE Int. Workshop on Antenna Technology (IWAT)*, Marina Mandarin, Singapore, Mar. 2005, pp. 446–449.

[271] Z. N. Chen, X. H. Wu, H. F. Li, N. Yang, and M. Y. W. Chia, "Considerations for source pulses and antennas in UWB radio systems," *IEEE Trans. Antennas and Propagation*, vol. 52, no. 7, pp. 1739–1748, July 2004.

[272] D. M. Shan, Z. N. Chen, and X. H. Wu, "Signal optimization for UWB radio systems," *IEEE Trans. Antennas and Propagation*, vol. 53, no. 7, pp. 2178–2184, July 2005.

[273] H. Celebi and H. Arslan, "Cross-modulation interference for pulse position modulated UWB signals," in *Proc. IEEE Military Commun. Conf. (MILCOM)*, Atlantic City, NJ, Oct. 2005, pp. 1–7.

[274] G. E. Bottomley, T. Ottosson, and Y. P. E. Wang, "A generalized RAKE receiver for interference suppression," *IEEE J. Select. Areas Commun.*, vol. 18, no. 8, pp. 1536–1545, Aug. 2000.

[275] I. Bergel, E. Fishler, and H. Messer, "Narrowband interference suppression in time-hopping impulse radio systems," in *Proc. IEEE Conf. Ultrawideband Syst. Technol. (UWBST)*, Baltimore, MD, May 2002, pp. 303–307.

[276] J.-Y. Lee and R. A. Scholtz, "Ranging in a dense multipath environment using an UWB radio link," *IEEE J. Select. Areas Commun.*, vol. 20, no. 9, pp. 1677–1683, Dec. 2002.

[277] R. A. Scholtz and J. Y. Lee, "Problems in modeling UWB channels," in *Proc. IEEE Asilomar Conf. Signals, Syst. Computers*, vol. 1, Monterey, CA, Nov. 2002, pp. 706–711.

[278] S. R. Aedudodla, S. Vijaykumaran, and T. F. Wong, "Timing acquisition in ultra-wideband communication systems," *IEEE Trans. Vehic. Technol.*, vol. 54, no. 5, pp. 1570–1583, Sept. 2005.

[279] R. C. Qiu, H. Liu, and X. Shen, "Ultra-wideband for multiple access communications," *IEEE Commun. Mag.*, vol. 43, no. 2, pp. 80–87, Feb. 2005.

[280] G. Giancola, C. Martello, F. Cuomo, and M. G. D. Benedetto, "Radio resource management in infrastructure-based and ad hoc networks," *Wiley Wireless Commun. and Mobile Computing Journal*, vol. 5, no. 5, pp. 581–597, Aug. 2005.

[281] M. G. D. Benedetto and B. Vojcic, "Ultra-wideband (UWB) wireless communications: A tutorial," *Journal on Communications and Networks*, vol. 5, no. 4, pp. 290–302, Dec. 2003.

[282] G. Giancola and M. G. D. Benedetto, "A novel approach for estimating multi user interference in impulse radio UWB networks: the pulse collusion model," *EURASIP Signal Processing Journal - Special Issue on Signal Processing in UWB Communications*, Oct. 2005.

[283] D. Domenicali, G. Giancola, M. G. D. Benedetto, and L. D. Nardis, "Fluid coding and coexistence in ultra wide band networks," *ACM/Springer Journal on Mobile Networks and Applications - Special Issue on Ultra-Wideband for Sensor Networks*, 2005.

[284] M. G. D. Benedetto and L. D. Nardis, "Tuning UWB signals by pulse shaping: Towards context-aware wireless networks," *EURASIP Signal Processing Journal - Special Issue on Signal Processing in UWB Communications*, Oct. 2005.

[285] N. V. Kokkalis, P. T. Mathiopoulus, G. K. Karagiannidis, and C. S. Koukourlis, "Performance analysis of M-ary PPM TH-UWB systems in the presence of MUI and timing jitter," *IEEE J. Select Areas Commun.*, 2006.

[286] H. Sheng, R. You, and A. M. Haimovich, "Performance analysis of ultra-wideband rake receivers with channel delay estimation errors," in *Proc. IEEE Conf. Information Sciences and Systems (CISS)*, Princeton, NJ, Mar. 2004, pp. 921–926.

[287] B. Q. Ruiz, A. A. vazquez, M. L. Rubio, and J. L. G. Garcia, "Impulse radio UWB system architecture for smart wireless sensor networks," in *Proc. IEEE Int. Workshop on Networking with UWB*, Rome, Italy, July 2005, pp. 35–39.

[288] T. C. Wong, J. W. Mark, and K. C. Chua, "Capacity region of a multi-code DS-UWB system supporting variable bit rate multiclass services," in *Proc. IEEE Int. Conf. Commun. (ICC)*, vol. 4, Seoul, Korea, May 2005, pp. 2857–2861.

[289] ——, "Capacity region of a multi-time-hopping PPM UWB system supporting video services," in *Proc. IEEE Vehic. Technol. Conf. (VTC)*, vol. 1, Dallas, TX, Sep. 2005, pp. 53–57.

[290] Z. Zhang, F. Zeng, and L. Ge, "Two-stage time-hopping sequences with zero correlation zone for quasi-synchronous THSS-UWB systems," in *Proc. IEEE Int. Conf. Acoustics, Speech, and Signal Processing (ICASSP)*, vol. 3, Philadelphia, PA, Mar. 2005, pp. 609–612.

[291] W. Hu and G. Zheng, "Orthogonal Hermite pulses used for UWB M-ary communication," in *Proc. IEEE Int. Conf. Information Technology: Coding and Computing (ITCC)*, vol. 1, Las Vegas, NV, Apr. 2005, pp. 97–101.

[292] T. C. Wong, J. W. Mark, and K. C. Chua, "Performance analysis of variable bit rate multiclass services in a multi-time-hopping pulse position modulation UWB system," in *Proc. IEEE Wireless Commun. Networking Conf. (WCNC)*, vol. 1, New Orleans, LA, Mar. 2005, pp. 651–656.

[293] H. Huang, H. Yin, G. Wei, and J. Zhu, "The structure and performance on an orthogonal sinusoidal correlation receiver of impulse radio," in *Proc. IEEE Vehic. Technol. Conf. (VTC)*, vol. 2, Los Angeles, CA, Sep. 2004, pp. 1192–1196.

[294] R. Merz and J. Y. L. Boudec, "Effect of interfering users on the modulation order and code rate for UWB impulse-radio bit-interleaved coded M-ary PPM," in *Proc. IEEE Int. Workshop on Ultrawideband Wireless Networking (UWBNETS)*, Boston, MA, Oct. 2005, pp. 233–239.

[295] Z. Tian and B. M. Sadler, "Weighted energy detection of ultra-wideband signals," in *Proc. IEEE Signal Processing Advances in Wireless Commun. (SPAWC)*, vol. 2, New York, NY, May 2005, pp. 1068–1072.

[296] H. Wymeersch, F. Simoens, H. Bruneel, and M. Moeneclaey, "Multi-dimensional modulation for UWB communications," in *Proc. IEEE Signal Processing Advances in Wireless Commun. (SPAWC)*, vol. 2, New York, NY, May 2005, pp. 42–46.

[297] M. E. Sahin and H. Arslan, "Inter-symbol interference in high data rate UWB communications using energy detector receivers," in *Proc. IEEE Int. Conf. UWB (ICU)*, Zurich, Switzerland, Sep. 2005, pp. 176–179.

[298] Z. Zhang, F. Zeng, and L. Ge, "Family of time-hopping sequences with no-hit zone and few-hit zone for quasi-synchronous THSS-UWB systems," in *Proc. IEEE Int. Conf. UWB (ICU)*, Zurich, Switzerland, Sep. 2005, pp. 43–48.

[299] W. Zhang, Z. Bai, H. Shen, W. Liu, and K. S. Kwak, "A novel timing jitter resist method in UWB systems," in *Proc. IEEE Int. Symp. Commun. Information Technol. (ISCIT)*, vol. 2, Beijing, China, Oct. 2005, pp. 833–836.

[300] J. Schroeder, S. Galler, and K. Kyamakya, "A low-cost experimental ultra-wideband positioning system," in *Proc. IEEE Int. Conf. UWB (ICU)*, Zurich, Switzerland, Sep. 2005, pp. 632–637.

[301] Q. Li and W. S. Wong, "A novel timing jitter robust UWB impulse radio system," in *Proc. IEEE Military Commun. Conf. (MILCOM)*, Atlantic City, NJ, Oct. 2005, pp. 1–6.

[302] G. Giancola and M. G. D. Benedetto, "Evaluating BER in sparse IR UWB networks under the pulse collusion model," in *Proc. IEEE WirelesCom Conf.*, Maui, Hawaii, June 2005.

[303] M. G. D. Benedetto and G. Giancola, *Understanding Ultra Wide Band Fundamentals.* Prentice Hall PTR, 2004.

[304] H. Arslan, Z. N. Chen, and M. G. D. Benedetto, Eds., *Ultra Wideband Wireless Communications.* John Wiley & Sons, 2005.

[305] J. R. Ward, "Chip discrimination for UWB impulse radio networks in multipath channels," Master's thesis, North Carolina State University, Raleigh, NC, Aug. 2005.

[306] A. H. Jodar, "On the coexistence of ultra wideband (UWB) wireless communication systems with narrowband interference," Master's thesis, Simon Fraser University, Burnaby, BC, Canada, July 2005.

[307] H. Sheng, "Transceiver design and system optimization for ultra-wideband communications," Ph.D. dissertation, New Jersey Institute of Technology, Newark, NJ, May 2005.

[308] V. Venkatesan, "Performance of a binary pulse position modulated ultra-wideband system with direct sequence spreading for multiple access," Master's thesis, Oregon State University, Corvallis, OR, Jan. 2004.

[309] A. Nezirovic, "Optimization of parameters in UWB radio for single-user scenario," Master's thesis, Royal Instutute of Technology, Stockholm, Sweden, Jun. 2005.

[310] P. Liu and Z. Xu, "POR channel estimation for UWB communications," in *Proc. IEEE CAS Symposium on Emerging Technologies*, vol. 1, Shanghai, China, June 2004, pp. 25–28.

[311] O. Ozdemir and M. Torlak, "Blind channel estimation without eigendecomposition," in *Proc. IEEE Int. Conf. Commun. (ICC)*, vol. 5, Paris, France, June 2004, pp. 2621–2625.

[312] J. Tsao and B. D. Steinberg, "Reduction of sidelobe and speckle artifacts in microwave imaging: the CLEAN technique," *IEEE Tran. Antennas and Propagation*, vol. 36, no. 4, pp. 543–556, Apr. 1988.

ABOUT THE AUTHOR

Ismail Guvenc received his B.S. from Electrical and Electronics Department, Bilkent University, Turkey, in 2001, and M.S. from Electrical and Computer Engineering, University of New Mexico, NM, in 2002, with a thesis on indoor geolocation and tracking in wireless local area networks. He is expecting his Ph.D. degree in May 2006 from University of South Florida in Electrical Engineering. He worked in Mitsubishi Electric Research Labs between January and August, 2005, with special focus on UWB ranging and positioning techniques. His research interests are broadly in wireless communications and signal processing. In particular, he has worked significantly on different aspects of UWB systems, such as ranging, adaptive system design, transceiver types, channel parameter estimation, and multiuser aspects. Moreover, he is interested in cognitive radio, wireless sensor networks, OFDM systems, and MIMO systems. He has published more than 20 conference and journal papers, and co-authored a book chapter on UWB modulation options. He has 4 pending US patent applications.